



RCSI

UNIVERSITY
OF MEDICINE
AND HEALTH
SCIENCES

Royal College of Surgeons in Ireland

repository@rcsi.com

Development of a Chemoablative, Thermoresponsive Hydrogel as a Drug Delivery Platform for Lung Cancer Applications

AUTHOR(S)

Seóna Rossi

CITATION

Rossi, Seóna (2018): Development of a Chemoablative, Thermoresponsive Hydrogel as a Drug Delivery Platform for Lung Cancer Applications. Royal College of Surgeons in Ireland. Thesis.
<https://doi.org/10.25419/rcsi.10803329.v1>

DOI

[10.25419/rcsi.10803329.v1](https://doi.org/10.25419/rcsi.10803329.v1)

LICENCE

CC BY-NC-SA 4.0

This work is made available under the above open licence by RCSI and has been printed from <https://repository.rcsi.com>. For more information please contact repository@rcsi.com

URL

https://repository.rcsi.com/articles/thesis/Development_of_a_Chemoablative_Thermoresponsive_Hydrogel_as_a_Drug_Delivery_Platform_for_Lung_Cancer_Applications/10803329/1

Development of a Chemoablative, Thermoresponsive Hydrogel as a Drug Delivery Platform for Lung Cancer Applications

Submitted to the Royal College of Surgeons in Ireland in
partial fulfilment of the requirements for the degree of

Doctor of Philosophy

August 2018



RCSI

Seóna M Rossi B.Sc. (Pharm), MPharm, MPSI

School of Pharmacy, RCSI, Dublin

Supervisors:

Dr Helena Kelly

Dr Ben Ryan

Declaration

I declare that this thesis, which I submit to RCSI for examination in consideration of the award of a higher degree of Doctor of Philosophy is my own personal effort. Where any of the content presented is the result of input or data from a related collaborative research programme this is duly acknowledged in the text such that it is possible to ascertain how much of the work is my own. I have not already obtained a degree in RCSI or elsewhere on the basis of this work. Furthermore, I took reasonable care to ensure that the work is original, and, to the best of my knowledge, does not breach copyright law, and has not been taken from other sources except where such work has been cited and acknowledged within the text.

Signed _____

Student Number _____

Date _____

Abstract

Systemic chemotherapy has long been the mainstay of cancer chemotherapy treatment for all cancer types. The lack of specificity, and subsequent destructive off-target side-effects, has prompted alternative delivery methods to be considered, in particular for solid tumour cancers. Direct injection of chemotherapeutics into solid tumours can increase local concentrations and reduce off-site toxicity, but such an approach is challenged by rapid clearance of the drug, resulting in inaccurate and unpredictable dosing. Attention has, therefore, turned to the development of drug delivery platforms, which can facilitate improved retention and sustained release of chemotherapeutics after direct intratumoural injection. Thermoresponsive hydrogels are amenable to intratumoural administration as they are liquids at room temperature and undergo gelation at a characteristic temperature. Drug-loading of thermoresponsive hydrogels creates an *in situ*-forming drug delivery platform. Lung cancer is the leading cause of cancer-related death worldwide, with current systemic treatment strategies failing to address this large, unmet clinical need. Locoregional administration of thermoresponsive hydrogels to lung cancer can be achieved using interventional oncology techniques, which employs image guidance to perform minimally invasive procedures. The overall aim of this thesis was to develop and characterise a chemoablative, thermoresponsive hydrogel as a drug delivery platform for intratumoural administration in a lung cancer application.

Formulation optimisation of the blank thermoresponsive hydrogel was undertaken to adjust the sol-gel transition temperature to within clinically relevant parameters. A dual drug-loaded thermoresponsive hydrogel was successfully formulated with “gold-standard” chemotherapeutics, cisplatin and paclitaxel. *In vitro* disintegration and release profiles of the lead blank and drug-loaded formulations were determined over 28 and 10 days respectively, with the drug-loaded thermoresponsive hydrogel demonstrating sustained release of both chemotherapeutics.

An *in vitro* cytotoxicity assessment of the lead blank and drug-loaded thermoresponsive hydrogels was undertaken in a non-small cell lung cancer cell line, A549, which demonstrated a dose-dependent cytotoxicity of both formulations at all doses evaluated. A non-cancerous fibroblast cell line, Balb/c 3T3 clone A31, was used to assess *in vitro* cytotoxicity of the blank thermoresponsive hydrogel in

non-target tissue, which revealed that it was biocompatible at lower doses. A 3D *in vitro* model of lung cancer was established to create a biomimetic model for IT injection of ChemoGel. The cytotoxic capacity of the lead blank and drug-loaded thermoresponsive hydrogels was subsequently confirmed in the 3D model over 14 days.

In order to facilitate clinical intra-procedural imaging of administration, a radiopaque variation of the lead thermoresponsive hydrogel was formulated with the addition of an iodinated contrast agent, Visipaque®. Rheological behaviour, radiopacity and injectability of the lead radiopaque formulation was assessed. Distribution of the injected thermoresponsive hydrogel in an *ex vivo* tissue model was assessed. *In vitro* cytotoxicity of the radiopaque formulations was confirmed using the 3D *in vitro* lung cancer model previously developed in this thesis. Sterilisation of the lead formulations was evaluated using pharmacopoeial methods, and ethylene oxide gas sterilisation was identified as the most suitable method. Thermoresponsivity, disintegration and release profiles were evaluated post-sterilisation, and it was confirmed that ethylene oxide sterilisation did not negatively impact the behaviour of the lead thermoresponsive hydrogels.

Lead radiopaque thermoresponsive hydrogels were assessed in a murine lung cancer xenograft model, using A549-luciferase cells. Retention of intratumourally administered blank and drug-loaded thermoresponsive hydrogels at the site of injection was confirmed using *in vivo* and *ex vivo* fluorescent imaging over 14 days. Efficacy of treatment was monitored using physical tumour volume measurements and bioluminescent imaging. Tumour volume increase was determined to be statistically significantly reduced following blank and drug-loaded thermoresponsive hydrogel treatment, compared to saline treatment for at least 14 days. 100% survival of treated mice was observed at Day 14. No statistically significant difference observed between selected welfare indicators following intratumoural administration of the blank or drug-loaded thermoresponsive hydrogel compared to saline.

Presented in this thesis is the development and optimisation of a chemoablative thermoresponsive hydrogel, which can be dual drug-loaded with chemotherapeutics intended for the treatment of lung cancer.

Table of Contents

Declaration.....	1
Abstract	2
Table of Contents.....	4
Acknowledgements.....	10
Patents, prizes and presentations.....	11
List of Tables	14
List of Figures.....	15
List of Equations.....	19
List of Abbreviations.....	20

Chapter 1

Literature Review.....	24
1.1 Introduction	26
1.2 Thermoresponsive hydrogels as drug delivery platforms.....	26
1.2.1 Hydrophilic polymers	26
1.2.2 Stimuli responsive hydrogels	28
1.2.3 Thermoresponsive hydrogels	30
1.2.3.1 <i>Rheological characterisation of thermoresponsive hydrogels</i>	32
1.2.3.2 <i>Thermoresponsive hydrogels as drug delivery platforms</i>	34
1.3 Lung Cancer	37
1.3.1 Gross anatomy of the lung.....	37
1.3.1.1 <i>Pathophysiology of tumour tissue in the lung</i>	38
1.3.2 Incidence and mortality of lung cancer.....	39
1.3.3 Diagnosis and staging of lung cancer	41
1.3.4 Lung cancer treatment strategies	45
1.3.4.1 <i>Traditional chemotherapeutics</i>	45
1.3.4.2 <i>Precision treatment options</i>	47
1.3.4.3 <i>Current treatment regimens</i>	50
1.3.4.4 <i>Pharmacoeconomics</i>	51
1.4 Interventional Oncology and Intratumoural Drug Delivery	51
1.4.1 Ablative procedures	52
1.4.2 Embolisation procedures	54
1.4.3 Intratumoural administration	56
1.4.4 Pre-clinical investigations of thermoresponsive hydrogels for intratumoural administration	57
1.4.5 Clinical investigations of thermoresponsive hydrogels for intratumoural administration ...	58
1.5 Aim and objectives.....	61

Chapter 2

Development and optimisation of a thermoresponsive hydrogel as a drug delivery platform..... 62

2.1 Introduction	64
2.1.1 Poloxamer 407	64
2.1.1.1 <i>Physicochemical properties</i>	64
2.1.1.2 <i>Biological properties</i>	66
2.1.2 2-Hydroxypropyl- β -Cyclodextrin	67
2.1.2.1 <i>Physicochemical properties</i>	67
2.1.2.2 <i>Biological properties</i>	68
2.1.3 Chitosan.....	68
2.1.3.1 <i>Physicochemical properties</i>	68
2.1.3.2 <i>Biological properties</i>	69
2.1.4 Genipin	70
2.1.4.1 <i>Physicochemical properties</i>	70
2.1.4.2 <i>Biological properties</i>	70
2.1.5 ChemoGel formulation	72
2.1.6 Aim and objectives	73
2.2 Materials and Methods	74
2.2.1 Formulation optimisation	74
2.2.1.1 <i>Preparation of a blank thermoresponsive hydrogel</i>	74
2.2.1.2 <i>Preparation of a paclitaxel-Cyclodextrin complex</i>	74
2.2.1.3 <i>Preparation of a dual drug-loaded thermoresponsive hydrogel</i>	75
2.2.2 Material characterisation	78
2.2.2.1 <i>Rheological assessment</i>	78
2.2.2.2 <i>Scanning Electron Microscopy</i>	80
2.2.2.3 <i>Differential Scanning Calorimetry</i>	80
2.2.2.4 <i>Macroscopic inspection of thermogelation</i>	81
2.2.2.5 <i>Disintegration studies</i>	81
2.2.3 Analytical determination of chemotherapeutics.....	81
2.2.3.1 <i>High-performance liquid chromatography determination of paclitaxel</i>	81
2.2.3.2 <i>Inductively coupled plasma mass spectrometry determination of platinum</i>	82
2.2.3.3 <i>Analysis of paclitaxel content in paclitaxel/HP-β-CD complex</i>	83
2.2.3.4 <i>Chemotherapeutic release studies</i>	83
2.3 Results	84
2.3.1 Assessment of rheological properties of the blank thermoresponsive hydrogel	84
2.3.2 Assessment of the effect of cisplatin-loading on the thermoresponsive hydrogel	85
2.3.3 Formulation and characterisation of the paclitaxel-Cyclodextrin complex	87
2.3.3.1 <i>Material characterisation of the paclitaxel-Cyclodextrin complex</i>	87
2.3.3.2 <i>Quantification of paclitaxel in the paclitaxel/HP-β-CD complex</i>	88
2.3.4 Assessment of the effect of paclitaxel-loading on thermoresponsive hydrogel	89
2.3.5 Characterisation of blank ChemoGel and drug ChemoGel formulations	92
2.3.5.1 <i>Rheological characterisation</i>	92
2.3.5.2 <i>Disintegration studies</i>	95
2.3.5.3 <i>Release of chemotherapeutics from dual drug-loaded formulations</i>	97

2.4 Discussion	98
2.5 Conclusion	104
Chapter 3	
<i>In vitro</i> evaluation of ChemoGel formulations	105
3.1 Introduction	107
3.1.1 Cancer biology.....	107
3.1.2 <i>In vitro</i> lung cancer cell culture.....	108
3.1.3 <i>In vitro</i> fibroblast cell culture	108
3.1.4 2D and 3D <i>in vitro</i> cell culture models.....	108
3.1.4.1 3D <i>in vitro</i> models of lung cancer	110
3.1.5 <i>In vitro</i> cytotoxicity assessment of thermoresponsive hydrogels in 2D and 3D models ...	111
3.1.6 Aim and objectives	112
3.2 Materials and Methods	113
3.2.1 Cell culture and subculturing of cell lines	113
3.2.2 2D <i>in vitro</i> cell viability assays.....	114
3.2.2.1. Cell Counting Kit-8 assay	114
3.2.2.2 LIVE/DEAD Viability/Cytotoxicity assay	115
3.2.3 Assessment of cytotoxicity of blank and drug ChemoGel	115
3.2.4 Apoptosis analysis	116
3.2.5 Assessment of cytotoxicity of degradation products from blank ChemoGel	117
3.2.6 Assessment of cytotoxicity of the individual excipients of ChemoGel formulation	117
3.2.7 Development of 3D <i>in vitro</i> model of lung cancer.....	118
3.2.7.1 Scaffold fabrication	118
3.2.7.2 <i>In vitro</i> cell culture of A549 cells in 2D and 3D	119
3.2.8 Comparison of A549 cell proliferation in 2D and 3D cell culture	119
3.2.9 Assessment of viability/cytotoxicity of A459 cells in 2D and 3D culture	120
3.2.10 Assessment of migration of A549 cells in a collagen scaffold	120
3.2.11 Assessment of cytotoxicity of blank and drug ChemoGel in a 3D <i>in vitro</i> model of lung cancer	121
3.2.12 Statistical analysis.....	122
3.3 Results	123
3.3.1 Assessment of cytotoxicity of blank and drug ChemoGel in a human lung cancer cell line.....	123
3.3.1.1 Impact of seeding density on cytotoxicity of blank ChemoGel.....	123
3.3.1.2 Dose-dependant cytotoxicity of blank ChemoGel	124
3.3.1.3 Dose-dependant cytotoxicity of drug ChemoGel.....	125
3.3.1.4 Cytotoxicity of lead ChemoGel formulations.....	126
3.3.2 Apoptosis analysis	128
3.3.3 Assessment of cytotoxicity of ChemoGel in a non-cancerous murine cell line.....	130
3.3.4 Assessment of cytotoxicity of the individual excipients of ChemoGel formulation	131
3.3.5 Development of an <i>in vitro</i> 3D lung cancer model.....	132
3.3.5.1 Proliferation of A549 cells in 2D and 3D over 21 days.....	132
3.3.5.2 Viability of A459 cells in 2D and 3D over 21 days.....	134
3.3.5.3 Migration of A549 cells through 3D environment	135

3.3.5.4 Assessment of blank and drug ChemoGel cytotoxicity in 3D model of lung cancer.....	136
3.4 Discussion.....	138
3.5 Conclusion	145

Chapter 4

Translational reality of ChemoGel – assessment of relevant factors	146
4.1 Introduction	148
4.1.1 Imaging in Interventional Oncology	148
4.1.2 Injectability	150
4.1.3 Sterilisation.....	152
4.1.4 Aim and Objectives	155
4.2 Materials and Methods	156
4.2.1 Formulation of radiopaque ChemoGel	156
4.2.1.1 Rheological assessment of thermoresponsivity of Visipaque® labelled ChemoGel formulation	156
4.2.1.2 Measurement of the radiopacity of a Visipaque® labelled ChemoGel formulation	156
4.2.1.3 Assessment of contrast release from Visipaque® labelled ChemoGel	156
4.2.1.4 Assessment of distribution of Visipaque® labelled ChemoGel in ex vivo animal tissue	157
4.2.2 Injectability of ChemoGel.....	157
4.2.2.1 Rheological assessment of shear thinning properties of lead thermoresponsive hydrogels	157
4.2.2.2 Injection force assessment	158
4.2.3 In vitro cytotoxicity evaluation of blank and drug Visipaque® ChemoGel	159
4.2.4 Freeze-drying and rehydration of ChemoGel.....	160
4.2.5 Sterilisation of freeze-dried ChemoGel	160
4.2.5.1 Dry heat sterilisation.....	160
4.2.5.2 Gamma-irradiation sterilisation.....	160
4.2.5.3 Ethylene Oxide sterilisation.....	161
4.2.6 Disintegration studies	161
4.2.7 In vitro release studies of Visipaque® ChemoGel and sterilised ChemoGel formulations	161
4.2.8 Statistical analysis.....	162
4.3 Results	163
4.3.1 Assessment of the radiopacity of ChemoGel.....	163
4.3.1.1 Rheological assessment of thermoresponsivity of Visipaque® labelled ChemoGel.....	163
4.3.1.2 Measurement of radiopacity of Visipaque® labelled ChemoGel.....	164
4.3.2 Injectability of ChemoGel.....	166
4.3.3 Assessment of the cytotoxicity of blank and drug Visipaque® ChemoGel in a 3D model of lung cancer.....	169
4.3.4 Assessment of freeze-drying and sterilisation on the material properties of ChemoGel formulations	171
4.3.4.1 Freeze-drying and rehydration of ChemoGel	171
4.3.4.2 Sterilisation of ChemoGel.....	171
4.3.5 Disintegration studies	174

4.3.6. Release studies	175
4.4 Discussion.....	178
4.5 Conclusion	186

Chapter 5

<i>In vivo</i> assessment of Visipaque® ChemoGel formulations in a murine xenograft model of Lung Cancer	187
5.1 Introduction	189
5.1.1 Pre-clinical murine cancer models	189
5.1.2 In vivo imaging of animal models	192
5.1.3 Aim and Objectives	194
5.2 Materials and Methods	195
5.2.1 Blank and drug Visipaque® ChemoGel preparation.....	195
5.2.2 Cell culture	195
5.2.3 Animal procedures	196
5.2.3.1 <i>Animal maintenance</i>	196
5.2.3.2 <i>Anaesthesia</i>	196
5.2.3.3 <i>Tumour xenograft establishment</i>	196
5.2.3.4 <i>Intratumoural injection</i>	197
5.2.4 Xenograft monitoring	198
5.2.4.1 <i>Physical tumour volume measurement</i>	198
5.2.4.2 <i>Bioluminescence monitoring</i>	198
5.2.4.3 <i>Fluorescence monitoring</i>	199
5.2.5 Post-experiment analysis.....	200
5.2.5.1 <i>Ex vivo analysis of blood serum</i>	200
5.2.5.2 <i>Ex vivo analysis of tumour and organs</i>	201
5.2.6 Statistical analysis.....	201
5.3 Results	202
5.3.1 <i>In vitro</i> evaluation of fluorescent Visipaque® ChemoGel	202
5.3.2 <i>In vitro</i> and <i>in vivo</i> evaluation of bioluminescent A549-luc cell line.....	202
5.3.3 Assessment of localisation and retention of blank and drug Visipaque® ChemoGel following intratumoural administration	203
5.3.4 <i>Ex vivo</i> analysis of retention of blank and drug Visipaque® ChemoGel	204
5.3.5 Assessment of effect of intratumoural administration of blank and drug Visipaque® ChemoGel on tumour volume.....	206
5.3.6 Assessment of effect of blank or drug Visipaque® ChemoGel on tumour bioluminescence	207
5.3.7 Assessment of acute off-site toxicity following intratumoural administration of blank and drug Visipaque® ChemoGel	209
5.4 Discussion.....	211
5.5 Conclusion	217

Chapter 6

Final Conclusions	218
6.1 Overview	220
6.2 Chapter 2: Development and optimisation of a thermoresponsive hydrogel as a drug delivery platform	222
6.3 Chapter 3: <i>In vitro</i> evaluation of ChemoGel formulations.....	223
6.4 Chapter 4: Translational reality of ChemoGel – assessment of relevant factors	225
6.5 Chapter 5: <i>In vivo</i> assessment of Visipaque® ChemoGel formulations in a murine xenograft model of Lung Cancer.....	227
6.6 Future work	230
6.7 Overall conclusion	232

Chapter 7

Appendices	233
Appendix 1. High-performance liquid chromatography determination of paclitaxel.....	234
Appendix 2. Inductively coupled plasma mass spectrometry determination of platinum...235	
Appendix 3. Assessment of the effect of cisplatin-loading on thermoresponsive hydrogel.....	236
Appendix 4. Determination of the linear viscoelastic region of blank and drug ChemoGel	238
References	239

Acknowledgements

Firstly, I would like to express my sincere thanks to my supervisor Dr Helena Kelly. I honestly don't know how anyone does a Ph.D. without a supervisor like you! I am so grateful for all the support and guidance that you have given me during my time in RCSI. Your patience with my perfectionism is something to be admired. I would also like to thank my co-supervisor Dr Ben Ryan, who made my last bout of experimental work so enjoyable, which is something I thought I would never say about an *in vivo* study! Your enthusiasm and expertise was so appreciated.

I would like to thank all the staff in the School of Pharmacy, who welcomed me so warmly, and offered assistance whenever I needed it. A particular thanks to the technical team, Colin, Jim, Peter and Eoin, for putting up with my many requests and always lightening the mood. An extra big thanks to Danielle, who always went above and beyond. Thanks to Anatomy and Chemistry technical staff, Johnny, Vinny and Emmet for all the help and crisis management over the years.

Thanks to Prof. John Cassidy for use of the ICP-MS in DIT, and to Prof. Garry Duffy and Mr. David Monahan for carrying out H & E staining in NUIG. In particular, thanks to Dr Tim Murray and Prof. Michael Lee who gave such fantastic clinical insight into the ChemoGel project, and were always so pleasant and helpful to deal with. In RCSI, thanks to Dr Joanne Ramsey, Dr Cian O'Leary and Dr Caroline Curtin for all the technical advice over the years. Big thanks to the other two members of team ChemoGel Niall and Kevin for giving a new boost of energy to the project, just when I was starting to get tired!

I could not have made it through the last three and half years without all the support I received from so many fantastic research staff in RCSI. Between TERG and Pharmacy there's far too many people to name, but thanks to everyone, past and present, for all the laughs and good times, which made the long days and late nights much more doable! Thanks, in particular, to Fatemah, Lauren, Rachel G, Tati, David, Alice Mc and Fajer for always brightening my day. A special thanks to Emily and Tony for keeping me company in the library over the last few months – you got this!

I am so lucky to have made an amazing bunch of friends in RCSI. Thanks to Christina, Laura, Gemma and Alice for the constant supply of gossip and scientific knowledge in equal measure. Joanne, bringer of chocolate and wisdom, I couldn't

have made it through these last few months without you and your never ending energy. A special thanks also to Eimear, who was the best surrogate post-doc ever!

To all my non-Ph.D. friends, who wondered what I was doing for the last few years, thank you for putting up with me. I am so grateful for my Clontarf friends, who are always there for me. In particular Jessica, Audrey and Louise, thanks for all the love and support and looking forward to lots of good times in the future. To my Pharmacy friends, I don't know what I would have done without you, especially the Pembroke princesses, Fiona, Sorcha and Sarah. Your constant encouragement and support has meant so much to me, and I know that I wouldn't have made it through without you guys cheering me on the whole time. I will never be able to express my thanks to Tina as elegantly as she would, but the lunches we shared during our mutual time in RCSI kept me going. Thanks for being such a special friend, you are an inspiration and are going to make the most fantastic clinician one day soon. To the Bostonians, Jackie and Caroline, our adventures are some of my fondest memories of the last few years and I look forward to many more travels in the future.

To my family, words can't even begin to describe how unbelievably essential you were to this Ph.D., and to life in general! Thanks to Cillian and Conor for always reminding me I'm the stupidest smart person they know, but always being there for me when I needed a pick-me-up. I am so grateful to my Mom for instilling such a strong work ethic in me, and leading by example to teach me what it is to be strong, smart and generous woman. To my Dad, my hero, thanks for being my daily inspiration to keep going – your unending positivity is incredible and infectious. This is the last bit of “study season stress” I will inflict on you all, I promise!

Finally, to Leo, who tried so hard to understand what I did every day, but only ever learnt the words “cisplatin” and “HPLC”; your never-ending belief that doing a Ph.D. was the best thing I have done, and unrelenting encouragement, has seen me through. A special thanks for all the lifts, and understanding that “five more minutes” meant I would still be in the lab for another half an hour. I am so grateful for all the amazing times we've had, and can't wait to get started on life post-Ph.D.

Funding sources

I gratefully acknowledge my funding sources which allowed me to complete my PhD, the Enterprise Ireland Commercialisation Fund and the bursary provided by the School of Pharmacy, RCSI.

Patents, prizes and presentations

Patents filed

H.M. Kelly, G.P. Duffy, **S.M. Rossi**, C.L. Hastings. A thermo-responsive hydrogel for intratumoral administration as a treatment in solid tumor cancers. P12389EP00. RCSI.

Prizes

Best Oral Presentation (2018): United Kingdom & Ireland Controlled Release Society Annual Meeting. 4th – 5th June 2018, School of Pharmacy, Queen's University, Belfast, Northern Ireland.

Shortlist for Best Poster (2017): Irish Association for Cancer Research 53rd Annual Meeting. 22nd – 24th February 2017, Newpark Hotel, Kilkenny, Ireland.

Scholarships awarded

James M Flaherty Research Scholarship (2017/2018): Awarded €7,000 to complete a six week scholarship visit to the laboratory of Prof. Christine Allen, Faculty of Pharmacy, University of Toronto, Toronto, Canada.

Clement Archer Scholarship (2014): Awarded bursary from School of Pharmacy, RCSI to undertake fully-funded Ph.D. in Pharmaceutics.

Presentations

S.M. Rossi, T.E. Murray, M.J. Lee, B.K. Ryan, H.M Kelly. Development of a radiopaque thermoresponsive hydrogel for intratumoural administration to solid tumours. United Kingdom & Ireland Controlled Release Society Annual Meeting. 4th – 5th June 2018, School of Pharmacy, Queen's University, Belfast, Northern Ireland.

Oral presentation

S.M. Rossi & H.M. Kelly. ChemoGel – A thermoresponsive drug delivery platform for intratumoral delivery of chemotherapeutics in pancreatic cancer. Medtech Strategist Innovation Summit Pre-conference Technology Showcase. 16th April 2018. RCSI, Dublin, Ireland. *Oral presentation*

S.M. Rossi, B.K. Ryan, H.M. Kelly. *In vivo* study of a novel chemoablative, thermoresponsive hydrogel for intratumoural administration in a murine A549

List of Tables

Table 1.1 Total number of publications from a Web of Science database search for thermoresponsive hydrogels in cancer applications.	37
Table 1.2 Classification of subtypes of lung cancer.	42
Table 1.3 Chemotherapeutics used in the treatment of lung cancer.	46
Table 1.4 Targeted therapies for common genetic mutations and immune-oncology drugs approved for treatment of non-small cell lung cancer.	49
Table 2.1 Formulation composition of preparations evaluated for thermoresponsivity.	76
Table 2.2 Oscillatory experimental parameters for rheological characterisation of lead formulations, blank ChemoGel and drug ChemoGel.	80
Table 2.3 Analytical parameters employed in detection of paclitaxel using high performance liquid chromatography.	82
Table 2.4 Analytical parameters employed in detection of platinum using inductively coupled plasma mass spectrometry.	82
Table 2.5 Sol-gel transition temperatures and varying crosslinking procedures.	85
Table 2.6 Analytical quantification of paclitaxel in paclitaxel/HP-β-CD complex	89
Table 2.7 Sol-gel transition temperatures and stabilities of paclitaxel-loaded thermoresponsive hydrogel formulations.	90
Table 2.8 Sol-gel transition temperatures and stabilities of paclitaxel-loaded thermoresponsive hydrogel formulations.	93
Table 3.1 Cell culture requirements of A549 and Balb/c 3T3 clone A31 cells.	114
Table 3.2 Concentrations of individual excipients evaluated for cytotoxicity.	118
Table 4.1 Functions of image guidance in interventional oncology procedures	149
Table 4.2 Approved sterilisation methods	153
Table 4.3 Summary of medical devices used in injectability testing of various ChemoGel formulations	158
Table 4.4 Radiopacity of ChemoGel formulations with varying concentrations of Visipaque®	164
Table 4.5 Evaluation of the effect of compendial sterilisation methods on thermoresponsivity of blank ChemoGel.	172
Table 4.6 Sol-gel transition temperatures and stabilities of paclitaxel-loaded thermoresponsive hydrogel formulations.	173
Table 5.1 Imaging parameters used for bioluminescent and fluorescent image acquisition on the IVIS® Spectrum In Vivo Imaging System.	200
Table A.1 Formulation composition of preparations evaluated for thermoresponsivity.	238

List of Figures

Figure 1.1 <i>Hydrophilic polymers; source and interactions.</i>	27
Figure 1.2 <i>Examples of stimuli responsive hydrogels.</i>	28
Figure 1.3 (A) <i>Phase diagram of upper and lower critical solution temperature polymers.</i> (B) <i>Schematic of lower critical solution temperature thermoresponsive hydrogels at different temperatures.</i>	31
Figure 1.4 (A) <i>Drug-loaded thermoresponsive hydrogel at room temperature in an injectable liquid state, and at body temperature (37°C) in the gel state.</i> (B) <i>In-situ gelation facilitates moulding to the target tissue.</i>	35
Figure 1.5 <i>Mechanism of drug release from hydrogels.</i>	36
Figure 1.6 (A) <i>Diagram of the upper and lower respiratory tract.</i> (B) <i>Weibel's airway generations.</i>	38
Figure 1.7 <i>Cancer (A) incidence and (B) mortality rates predicted until 2030.</i>	41
Figure 1.8 <i>Summary of staging of lung cancer according to the TNM staging classification 8th edition.</i>	44
Figure 1.9 <i>Oncogenetic driver mutations of non-small cell lung cancer adenocarcinoma.</i>	45
Figure 1.10 <i>Summary of National Institute for Health and Care Excellence guidance pathway for treatment of non-small cell lung cancer.</i>	50
Figure 2.1 <i>Pluronic solutions (left) undergo micellisation (centre) and gelation (right) at characteristic concentration dependent temperatures.</i>	65
Figure 2.2 (A) <i>Truncated cone shape of cyclodextrins, which can complex with hydrophobic drug molecules.</i> (B) <i>Chemical structure of 2-Hydroxypropyl-β-Cyclodextrin.</i>	68
Figure 2.3 <i>Chemical structure of Chitosan</i>	69
Figure 2.4 <i>Chemical structure of Genipin (left) and Genipin crosslinked Chitosan chains (right).</i> ..	71
Figure 2.5 <i>Overview of optimisation process of blank and drug-loaded thermoresponsive hydrogel.</i>	75
Figure 2.6 <i>Formulation protocol for the blank and dual drug-loaded thermoresponsive hydrogel.</i> ..	78
Figure 2.7 <i>Rheogram of temperature sweep of GF7 from 20°C-40°C.</i>	86
Figure 2.8 <i>Rheogram of temperature sweep of GF18 from 20°C-40°C.</i>	86
Figure 2.9 (A - D) <i>Scanning electron microscopy qualitatively demonstrated the formation of a paclitaxel/HP-β-CD inclusion complex.</i>	87
Figure 2.10 <i>Overlay of representative Differential Scanning Calorimetry thermograms of HP-β-CD, paclitaxel and paclitaxel/HP-β-CD complex.</i>	88
Figure 2.11 <i>Rheogram of temperature sweep of formulations to determine impact of addition of cisplatin (GF18), paclitaxel (GF20) and cisplatin and paclitaxel (GF21) to the blank hydrogel formulation (GF6).</i>	91
Figure 2.12 <i>Rheogram of temperature sweeps of blank and drug-loaded thermoresponsive hydrogel formulations without (GF21) and with (GF22) free powder incorporated.</i>	92
Figure 2.13 (A) <i>Representative image of ChemoGel, at room temperature, in liquid state (left) and following incubation at 37°C, in gelled state (right).</i> (B) <i>Rheogram of oscillatory temperature sweeps of blank and drug ChemoGel at 20°C and 37°C over a 60 min period.</i> (C) <i>Rheograms of oscillatory time sweeps of blank and drug ChemoGel at 20°C and 37°C over a 60 min period.</i> (D) <i>Rheograms of</i>	

oscillatory time sweeps of blank and drug ChemoGel with varying temperatures of 20°C and 37°C.	94
Figure 2.14 (A) Disintegration profile of Poloxamer 407 17% w/w, blank ChemoGel without Genipin, blank ChemoGel or drug ChemoGel over 28 days. (B) Representative images of blank ChemoGel exposed to PBS for predetermined timepoints.....	96
Figure 2.15 (A) Cumulative percentage of loaded platinum and paclitaxel released over a 10 day period (240 h). (B) Quantity of platinum and paclitaxel released (µg/ml) measured at each timepoint over a 10 day period (left). Total quantity of platinum and paclitaxel released over a 10 day period (right).	97
Figure 3.1 Schematic of experimental set up for 3D in vitro cytotoxicity evaluation of blank and drug ChemoGel.	121
Figure 3.2 (A) Relative viability of A549 cells at different seeding densities after exposure to 0 or 20 µL of blank ChemoGel for 24 h. (B) Representative images of Live/Dead staining of increasing A549 cell densities treated with (i) 0 µL or (ii) 20 µL of blank ChemoGel for 24 h.	123
Figure 3.3 (A) Relative viability of A549 cells treated with 0 . 30 µL of blank ChemoGel for 24 and 48 h. (B) Representative images of Live/Dead staining of A549 cells treated with (i) 0 µL, (ii) 10 µL, (iii) 20 µL or (iv) 30 µL of ChemoGel for 24 and 48 h.	124
Figure 3.4 (A) Relative viability of A549 cells treated with 0 . 30 µL of drug ChemoGel for 24 and 48 h. (B) Representative images of Live/Dead staining of A549 cells exposed to (i) 0 µL, (ii) 10 µL, (iii) 20 µL or (iv) 30 µL of drug ChemoGel for 24 (top) and 48 (bottom) h.	125
Figure 3.5 (A) Relative viability of A549 cells treated with 30 µL of cisplatin/paclitaxel solution, blank ChemoGel or drug ChemoGel for 24 and 48 h. (B) Representative images of Live/Dead staining of A549 cells exposed to (i) Medium, (ii) cisplatin/paclitaxel solution, (iii) blank ChemoGel or (iv) drug ChemoGel for 24 (top) and 48 (bottom) h.	127
Figure 3.6 Flow cytometric analysis of apoptosis using Annexin-V-APC and PI staining of (A) Medium, (B) cisplatin/paclitaxel solution, (C) blank ChemoGel and (D) drug ChemoGel treated A549 cells for 24 h in vitro. (E) Proportion of live, early apoptotic, late apoptotic/necrotic cells treated with Medium, cisplatin/paclitaxel solution, blank ChemoGel and drug ChemoGel	129
Figure 3.7 (A) Relative viability of Balb/c 3T3 clone A31 cells treated with 0 . 30 µL of ChemoGel for 24 and 48 h. (B) Relative viability of Balb/c 3T3 clone A31 cells treated with disintegration products of ChemoGel (extract) for 24 h.	131
Figure 3.8 Relative viability of (A) A549 cells and (B) Balb/c 3T3 A31 cells following treatment with Poloxamer 407, Chitosan, 2-Hydroxypropyl-β-Cyclodextrin or Genipin for 24 and 48 h.	132
Figure 3.9 dsDNA content of A549 cells seeded at 100,000 or 200,000 cells per well and cultured in (A) 2D monolayers and (B) 3D Collagen-Hyaluronic acid scaffolds over 21 days. (C) Fold change in dsDNA of A549 cells at two seeding densities seeded in 2D or 3D over 21 days.	133
Figure 3.10 Representative images of Live/Dead staining of A549 cells cultured in 2D and 3D at two seeding densities (100,000 or 200,000 cells per well or scaffold) over 21 days.	134
Figure 3.11 Representative images of H&E staining of A549 cells seeded at 100,000 (left) or 200,000 (right) cells per scaffold at Day 1, 7 and 14.	135
Figure 3.12 (A) Representative images of intra-scaffold injection of Medium or ChemoGel over time. (B) Relative viability of A549 cells cultured on a 3D scaffold following intra-scaffold injection of Medium, cisplatin/paclitaxel solution, blank ChemoGel or drug ChemoGel. (C) Representative	

<i>images of Live/Dead staining of A549-seeded scaffolds treated with Medium, cisplatin/paclitaxel solution, blank ChemoGel or drug ChemoGel over time.</i>	<i>137</i>
<i>Figure 4.1 European Medicines Agency decision tree for selection of sterilisation methods for non-aqueous liquids, semi-solids or dry powder products.</i>	<i>154</i>
<i>Figure 4.2 Representative image of injectability set up using a Zwick mechanical testing machine.</i>	<i>159</i>
<i>Figure 4.3 Rheogram of the oscillatory temperature sweeps from 20°C - 40°C of ChemoGel formulations containing different concentrations of Visipaque® solution.</i>	<i>163</i>
<i>Figure 4.4 Visipaque® release from ChemoGel with 20% w/w Visipaque® over 24 h.....</i>	<i>165</i>
<i>Figure 4.5 Representative (A & B) US and (C & D) CT images of ChemoGel with 20%w/w Visipaque® distribution in an ex vivo tissue model. (E) CT images of radiopaque ChemoGel spreading through vascular and biliary channels.</i>	<i>166</i>
<i>Figure 4.6 Rheograms of steady state flow procedure on blank and drug ChemoGel and ChemoGel with Visipaque® (0 . 30% w/w).....</i>	<i>167</i>
<i>Figure 4.7 Determination of the maximum force required to inject 500 µL of (A) blank ChemoGel or dH2O through an 18G needle of 7cm length or 2.9Fr catheter of 130cm length at 2 ml/min or 1 ml/min (B) blank ChemoGel, ChemoGel with 20% w/w Visipaque® and dH2O through an 18G needle of 7cm length at a rate of 2 ml/min. (C) ChemoGel with 20% w/w Visipaque® through a range of clinically relevant needles/catheters at a rate of 2 ml/min.</i>	<i>168</i>
<i>Figure 4.8 (A) Relative viability of A549 cells cultured on a 3D scaffold following intra-scaffold injection of Medium, blank Visipaque® ChemoGel or drug Visipaque® ChemoGel. (B) Live/Dead staining of A549-seeded scaffolds post treatment with Medium, blank Visipaque® ChemoGel or drug Visipaque® ChemoGel over time.</i>	<i>170</i>
<i>Figure 4.9 (A) Representative image of front (top) and side (bottom) view of ChemoGel wafer produced after freeze-drying. (B) Rheogram of oscillatory temperature sweep from 20°C - 40°C of ChemoGel pre- and post- freeze-drying and rehydration.</i>	<i>171</i>
<i>Figure 4.10 Rheogram of oscillatory temperature sweep from 20°C - 40°C of ChemoGel pre- and post- EtO sterilisation.</i>	<i>172</i>
<i>Figure 4.11 Rheogram of steady state flow procedure of ChemoGel formulations post-sterilisation</i>	<i>174</i>
<i>Figure 4.12 Disintegration profile of (A) unsterilised blank or drug Visipaque® ChemoGel and (B) blank or drug ChemoGel or Visipaque® ChemoGel post-ethylene oxide sterilisation over 28 days.....</i>	<i>175</i>
<i>Figure 4.13 (A) Cumulative amount of platinum and paclitaxel detected in release buffer over 10 days as a percent of original quantity of platinum and paclitaxel respectively loaded in drug Visipaque® ChemoGel. (B) Quantity of platinum and paclitaxel detected in release buffer at each timepoint measured up to 10 days (left) and total quantity of platinum and paclitaxel detected in release buffer over 10 days (right).</i>	<i>176</i>
<i>Figure 4.14 (A & C) Cumulative amount of platinum and paclitaxel detected in release buffer over 10 days as a percent of original quantity of platinum and paclitaxel respectively loaded in EtO sterilised drug ChemoGel and drug Visipaque® ChemoGel respectively. (B & D) Quantity of platinum and paclitaxel detected in release buffer at each timepoint measured up to 10 days (left)</i>	

and total quantity of platinum and paclitaxel detected in release buffer over 10 days (right) in EtO sterilised drug ChemoGel and drug Visipaque® ChemoGel respectively.	177
Figure 5.1 Murine models of cancer	189
Figure 5.2 Example of intratumoural injection on anesthesised mouse.	197
Figure 5.3 Schematic of experimental set up for in vivo experiments in Chapter 5.	198
Figure 5.4 Representative in vitro (A) fluorescent and (B) bioluminescent images of fluorescently labelled Visipaque® ChemoGel.....	202
Figure 5.5 (A & B) A549-luc cells in vitro demonstrate a linear bioluminescent signal between 2,000 and 64,000 cells. (C) In vivo bioluminescent imaging of A549-luc tumours 10 . 30 min after D-Luciferin administration.	203
Figure 5.6 (A) Representative overlay images of bioluminescent A549-luc cells post-intratumoural administration of 100 µL of fluorescently tagged blank Visipaque® ChemoGel (left) or drug Visipaque® ChemoGel (right) at Day 0. (B) Representative fluorescent images at Day 0 (top) and Day 14 (bottom) post-intratumoural administration of Saline (left), blank Visipaque® ChemoGel (centre) or drug Visipaque® ChemoGel (right).	204
Figure 5.7 (A) Representative images (greyscale photograph [left], fluorescent signal [centre] and overlay [right]) of Saline (top), blank Visipaque® ChemoGel (centre) or drug Visipaque® ChemoGel (bottom) treated tumours excised on Day 14 post-intratumoural administration. (B) Representative images of kidneys (left hand side of image) and liver (right hand side of image) excised at Day 14 from mice treated with Saline (left), blank Visipaque® ChemoGel (centre) or drug Visipaque® ChemoGel (right).	205
Figure 5.8 (A) Tumour volume (mm ³) following intratumoural administration of 100 µL of Saline, blank Visipaque® ChemoGel or drug Visipaque® ChemoGel at Day 0. (B) Representative images of excised tumours at Day 14 following intratumoural administration of Saline (left), blank Visipaque® ChemoGel (centre) or drug Visipaque® ChemoGel (right).	207
Figure 5.9 (A) Fold change in bioluminescent signal (total flux, photons/s) since Day 0, at Day 14 post-intratumoural administration of saline, blank Visipaque® ChemoGel or drug Visipaque® ChemoGel. (B) Representative images of bioluminescent signal from A549-luc tumours in vivo at Day 0 (left) and Day 14 (right) following intratumoural administration of Saline (top), blank Visipaque® ChemoGel (centre) or drug Visipaque® ChemoGel (bottom).	208
Figure 5.10 A549-luc tumour bearing mice treated with Saline, blank Visipaque® ChemoGel or drug Visipaque® ChemoGel did not show any significant alterations in (A) body weight, (B) white blood cell count or (C) blood serum levels of Aspartate transaminase (AST) (left) and Urea (right).	210
Figure A.1 (A) paclitaxel calibration curve and (B & C) representative HPLC peaks	235
Figure A.2 Platinum calibration curve	236
Figure A.3 Rheograms of oscillatory stress sweeps from 1 to 100 Pa at (A) 20°C (B) 37°C.	239

List of Equations

$$G' = G \cos(\delta)$$

(Equation 1)

$$G'' = G \sin(\delta)$$

(Equation 2)

$$\tan(\delta) = G''/G'$$

(Equation 3)

(Equation 4)

(Equation 5)

(Equation 6)

(Equation 7)

List of Abbreviations

ALK	Anaplastic lymphoma kinase
ANOVA	Analysis of variance
AST	Aspartate Aminotransferase
ATCC	American Type Culture Collection
ATP	Adenosine triphosphate
BCS	Biopharmaceutical Classification System
BLI	Bioluminescence imaging
BP	British Pharmacopoeia
CCK-8	Cell counting kit 8
CD	Cyclodextrin
CHyA	Collagen-Hyaluronic acid
cm²	Centimetre squared
CMC	Critical Micelle Concentration
COPD	Chronic Obstructive Pulmonary Disorder
CS	Chitosan
CT	Computed Tomography
cTACE	Conventional transarterial chemoembolisation
CTLA-4	Cytotoxic T-lymphocyte antigen 4
Ctr1	Copper transporter 1
DD	Degree of Deacetylation
DEB	Drug-eluting bead
DEB-TACE	Drug-eluting bead transarterial chemoembolisation
dH₂O	Deionised water
DHT	Dehydrothermal
DMEM	Dulbecco's Modified Eagles Medium
DMSO	Dimethyl Sulfoxide
DNA	Deoxyribonucleic acid
DSC	Differential Scanning Calorimetry
dsDNA	Double stranded deoxyribonucleic acid
EBUS	Endobronchial ultrasound
ECM	Extracellular matrix
EDAC	N-(3-Dimethylaminopropyl)-N'-ethylcarbodiimide hydrochloride
EGFR	Epidermal growth factor receptor
EMA	European Medicines Agency
EO	Ethylene oxide
EU	European Union
FACS	Fluorescence-activated cell sorting
FBS	Fetal bovine serum
FDA	United States Food and Drug Administration
FITC	Fluorescein isothiocyanate
FLI	Fluorescence imaging
FNAB	Fine-needle-aspiration biopsy
g	Gram
G	Gauge

G''	Loss modulus
G'	Storage modulus
GF	Gel Formulation
GFP	Green fluorescent protein
GP	Genipin
GRAS	Generally Recognised As Safe
h	hour
HCC	Hepatocellular carcinoma
HIF1α	Hypoxia-inducible factor 1-alpha
HLB	Hydrophile-Lipophile Balance
HPLC	High-performance liquid chromatography
HPRA	Health Products Regulatory Authority
HP-β-CD	2-Hydroxypropyl-Beta-Cyclodextrin
HTS	High throughput screening
HU	Hounsfield units
HyA	Hyaluronic acid
Hz	Hertz
ICP-MS	Inductively coupled plasma mass spectrometry
IM	Intramuscular
IO	Interventional oncology
IP	Intraperitoneal
IRE	Irreversible electroporation
ISO	International Organization for Standardization
IT	Intratumoural
IV	Intravenous
IVIS	In Vivo Imaging System
L	Litre
LC	Lung cancer
LCST	Lower critical solution temperature
luc	Luciferase
LVR	Linear viscoelastic region
M	Molar
MFA	Microwave frequency ablation
mg	Milligram
min	minute
ml	Millilitre
mm	Millimetre
mM	Millimolar
mm³	Millimetre cubed
MMC	Mitomycin C
MRI	Magnetic Resonance Imaging
mTorr	Millitorr
mV	Millivolts
MW	Molecular weight
NBCS	New born calf serum
NBF	Neutral Buffered Formalin
NCI	National Cancer Institute

NDA	New Drug Application
NHS	National Health Service
NHS	N-Hydroxysuccinimide
NICE	The National Institute for Health and Care Excellence
nm	nanometre
NME	New molecular entity
NSCLC	Non-small cell lung cancer
NSCLC NOS	Non-small cell lung cancer not otherwise specified
OS	Overall survival
P407	Poloxamer 407
Pa	Pascal
Pa.s	Pascal second
PACE	Pulmonary arterial chemoembolisation
PBS	Phosphate Buffered Sodium
PD-1	Programmed cell death protein 1
PDL-1	Programmed death ligand 1
PEG	Poly(ethylene glycol)
PEO	Poly(ethylene oxide)
PET	Positron Emission Tomography
pH	potential Hydrogen
PI	Propidium iodide
PLGA	Poly(lactic-co-glycolic acid)
PNAGA	Poly(N-acryloyl glycinamide)
pNiPAAm	Poly(N-isopropylacrylamide)
PO	Propylene oxide
PPO	Poly(propylene oxide)
ppm	Parts per million
Pt	Platinum
QALY	Quality-adjusted life year
RFA	Radiofrequency ablation
ROI	Region of interest
ROS	Reactive Oxygen Species
rpm	Revolutions per minute
s	second
SAL	Sterility Assurance Level
SC	Subcutaneous
SCLC	Small cell lung cancer
SEM	Scanning Electron Microscopy
SEM	Standard error of the mean
sol-gel	Solution-gel
SPC	Summary of Product Characteristics
SPECT	Single-photon emission computed tomography
SPF	Specific Pathogen Free
TACE	Transarterial chemoembolisation
TAE	Transarterial embolisation
TBNA	Transbronchial needle aspiration
TKI	Tyrosine kinase inhibitor

TME	Tumour Microenvironment
TNM	Tumour-Node-Metastasis
TPP	Sodium tripolyphosphate
TRITC	Tetramethylrhodamine
UCP2	Uncoupling Protein 2
UCST	Upper critical solution temperature
US	Ultrasound
US	United States
UTUC	Upper tract urothelial carcinoma
UV	Ultraviolet
v/v	volume/volume (ml/100 ml)
VEGF	Vascular endothelial growth factor
w/v	weight/volume (g/100 ml)
w/w	weight/weight (g/100 g)
WBC	White blood cell
WST-8	Water-soluble tetrazolium salt 8
X	Magnification
%	Percentage
°C	Degrees Celsius
µg	Microgram
µL	Microlitre
2D	Two dimensional
3D	Three dimensional

č. 23/2016 Sb. (R)

Žijí v ČR ± 1 & 2 3

1.1 Introduction	26
1.2 Thermo-responsive hydrogels as drug delivery platforms	26
1.2.1 Hydrophilic polymers	26
1.2.2 Stimuli responsive hydrogels	28
1.2.3 Thermo-responsive hydrogels	30
1.2.3.1 Rheological characterisation of thermo-responsive hydrogels	32
1.2.3.2 Thermo-responsive hydrogels as drug delivery platforms	34
1.3 Lung Cancer	37
1.3.1 Gross anatomy of the lung	37
1.3.1.1 Pathophysiology of tumour tissue in the lung	38
1.3.2 Incidence and mortality of lung cancer	39
1.3.3 Diagnosis and staging of lung cancer	41
1.3.4 Lung cancer treatment strategies	45
1.3.4.1 Traditional chemotherapeutics	45
1.3.4.2 Precision treatment options	47
1.3.4.3 Current treatment regimens	50
1.3.4.4 Pharmacoeconomics	51
1.4 Interventional Oncology and Intratumoural Drug Delivery	51
1.4.1 Ablative procedures	52
1.4.2 Embolisation procedures	54
1.4.3 Intratumoural administration	56
1.4.4 Pre-clinical investigations of thermo-responsive hydrogels for intratumoural administration	57
1.4.5 Clinical investigations of thermo-responsive hydrogels for intratumoural administration ...	58
1.5 Aim and objectives	61

1.1 Introduction

This thesis will focus on the formulation and *in vitro* and *in vivo* evaluation of a novel thermoresponsive hydrogel as a locoregional drug delivery platform. The development process of the final thermoresponsive hydrogel contained in this thesis was underpinned by the following:

1. Thermoresponsive hydrogels as drug delivery platforms
2. Lung cancer (LC) as the proof of concept application
3. Interventional oncology (IO) and intratumoural (IT) drug delivery

An overview of these topics will be provided in this literature review.

1.2 Thermoresponsive hydrogels as drug delivery platforms

1.2.1 Hydrophilic polymers

Hydrogels are 3D networks of hydrophilic polymers, which can swell and absorb large quantities of water, up to thousands of times their dry weight (1, 2). Water is imbibed into the hydrogel as a result of interactions with the hydrophilic groups on the polymeric backbone (3). The structure and function of each hydrogel is determined by the chemical composition, and the type of polymeric crosslinking. Hydrogels can be formulated from natural or synthetic polymers, with physical or chemical crosslinks (Fig. 1.1). Natural polymers commonly used in the formulation of hydrogels include chitosan, collagen and hyaluronic acid. Poly(ethylene oxide)-b-poly(propylene oxide)-b-poly(ethylene oxide) (PEO-PPO-PEO), poly(ethylene glycol)-b-(dl-lactic acid-co-glycolic acid)-b-ethylene glycol (PEG-PLGA-PEG) and poly(N-isopropylacrylamide) (pNiPAAm) are examples of some common synthetic polymer-based hydrogels (1). Physical crosslinking mechanisms are reversible, and include physical entanglements of the polymers or physical interactions via hydrogen bonding, ionic interactions or hydrophobic interactions. Chemical crosslinking is brought about via covalent bonding, which produces irreversible crosslinks. Small molecules can be added to hydrogel formulations to increase physical or chemical crosslinking. The crosslinked nature of hydrogels creates a porous structure, which can be utilised for drug-loading, and subsequent delivery of the therapeutic payload in a localised, sustained manner. The structure and porosity of hydrogels can be manipulated by controlling the functional groups on the polymeric backbone and crosslinker density (4). Increased crosslinking in a

hydrogel structure imparts a stronger physical integrity and can render it insoluble in physiological conditions, thereby slowing rates of degradation. The degree of crosslinking can also influence the rate of drug release (5). Simple hydrogels have a wide range of applications, including use in contact lenses, wound dressings, hygiene products, tissue engineering and drug delivery (4). Advanced drug delivery using hydrogels is a widely researched topic, but the volume of research has not resulted in an equivalent rate of translation into clinically approved products (4, 6).

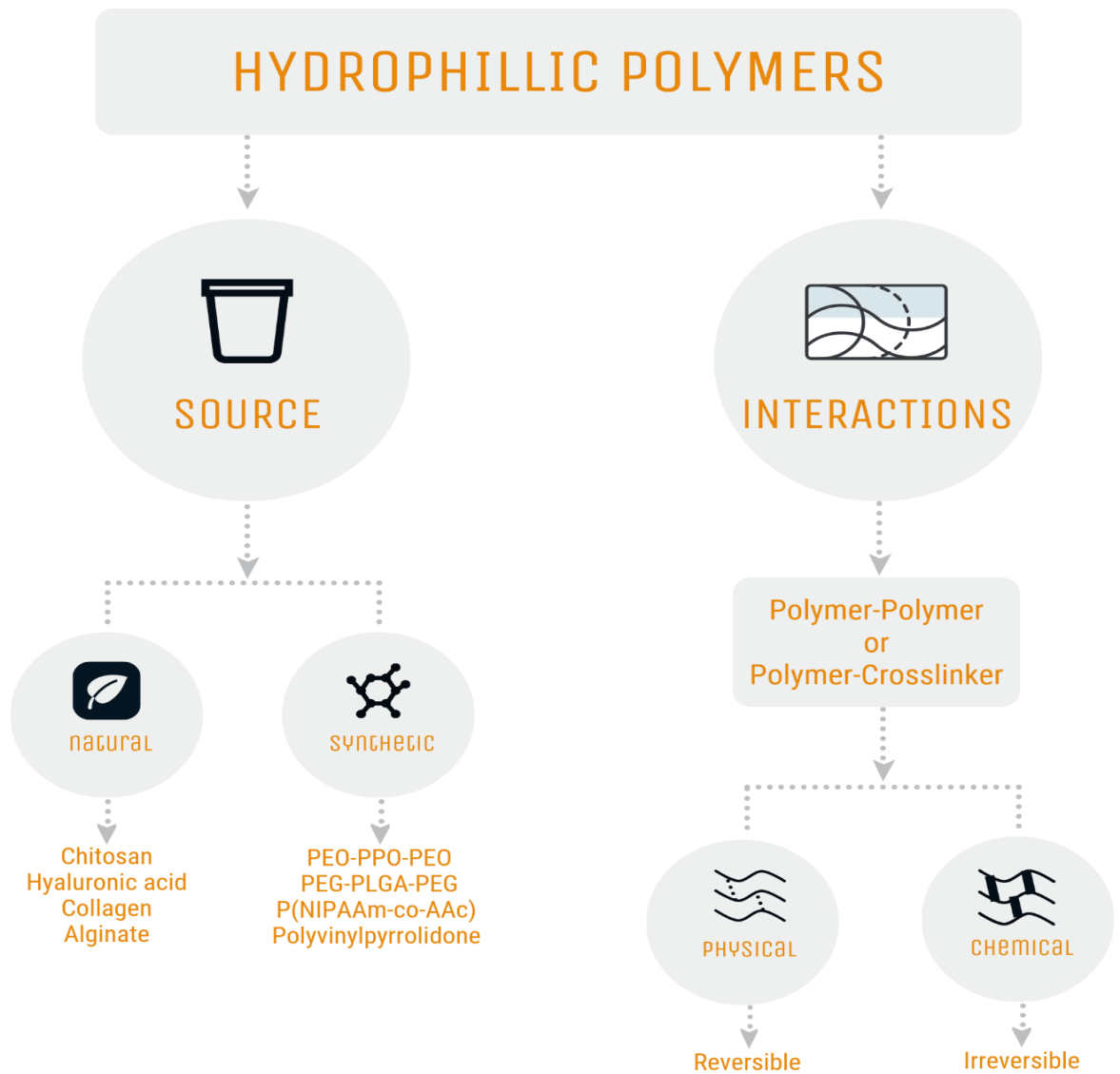


Figure 1.1 *Hydrophilic polymers; source and interactions.*

1.2.2 Stimuli responsive hydrogels

The range of polymers that can be used in the formulation of hydrogels has progressed since the early 1960's, when they were defined as "simple, water-swollen macromolecular networks" (7). The subsequent discovery of polymers that form hydrogels with the ability to respond to stimuli in their environment provided an opportunity to develop sustained release drug delivery platforms. Environmental fluctuations, such as physiological cues or application of external stimuli, induce structural alterations in these "smart" hydrogels (8). They are highly sensitive to small deviations in their environment, undergoing a sharp physical or chemical change in response to pH, irradiation (electric, magnetic, UV, light), glucose concentration or temperature (Fig. 1.2) (9).

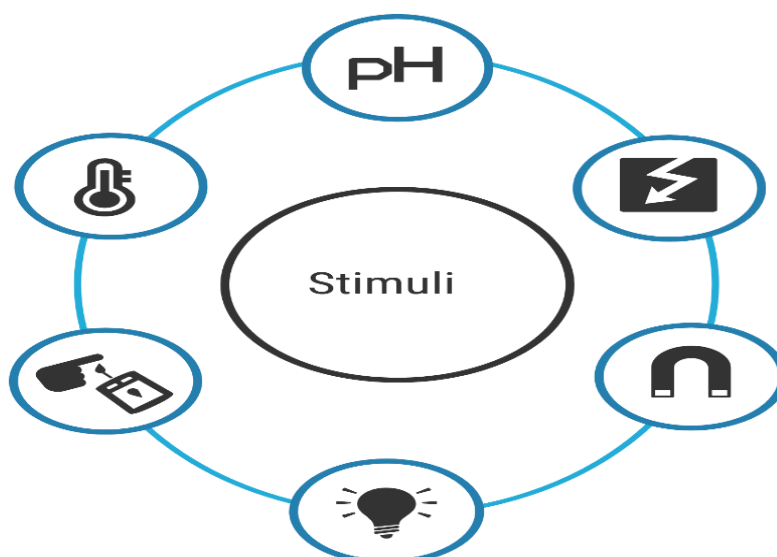


Figure 1.2 *Examples of stimuli responsive hydrogels.*

pH responsive polymers can be employed in a variety of ways to aid drug delivery in oral and parenteral dosage forms. Commercially available oral drug delivery systems commonly make use of pH responsive polymers to facilitate targeted drug delivery. Such polymers are used in enteric coatings, and allow the encapsulated drug to pass through the acidic environment of the stomach intact, before solubilising in the colon where the drug is released (10). pH responsive hydrogels can also be formulated to undergo a structural change at physiological pH to facilitate release of the loaded drug at the target site (11). Carbopol® is a commonly used mucoadhesive hydrophilic polymer that is pH responsive. It is made up of crosslinked chains of poly(acrylic acid) and is available in a range of viscosities,

controlled by the degree of crosslinking (12). Increasing concentrations of Carbopol® increases the acidity of the polymer solution, which may be harmful to patients, and therefore additional excipients such as hydroxypropyl-methylcellulose can be added to increase the pH of the solution slightly, while still allowing for gelation to occur at physiological pH (13). Carbopol® pH responsive hydrogels are commonly used for a wide range of local delivery applications, including vaginal, ocular, nasal and enteric delivery (14).

A number of pH responsive hydrogel formulations are the focus of pre-clinical research into locoregional delivery to tumours. As tumours are more acidic than healthy tissue, pH responsive hydrogels can respond to this pH change to selectively release their chemotherapeutic payload when they come in contact with the tumour site. A glycol-chitosan and benzaldehyde capped poly(ethylene glycol)-block-poly(propylene glycol)-block-poly(ethylene glycol) pH responsive hydrogel was formulated to encapsulate paclitaxel and doxorubicin. *In vitro* release data revealed that drug release was increased at lower pH for both of the encapsulated drugs, due to changes in the structure of the hydrogel at acidic pH (15).

Magnetic-field sensitive hydrogels are hydrogels which contain micro- or nano-magnetic particles embedded in the hydrogel structure. These hydrogels are sensitive to change in magnetic fields, which can be controlled by an external stimulus, to induce mechanical and thermal changes within the hydrogel (16, 17). Potential applications of magnetic responsive hydrogels include tissue engineering and drug delivery (16). The mechanical changes have also been harnessed to improve resolution during magnetic resonance imaging (MRI) (18). The thermal changes induced by applying an alternating magnetic field can also be used to induce local hyperthermia, which can be used in the treatment of cancer as either a direct method of inducing cell death, or to sensitise cancer cells in advance of radiation or chemotherapy. The possibility of co-delivery of chemotherapeutics in the magnetic responsive hydrogels has also been investigated (19). It is recognised, however, that these interactions can be challenging to execute in a selective manner, without incurring damage to surrounding non-target tissue.

Glucose sensitive hydrogels can be designed to respond to high levels of glucose, often by conjugating an enzyme on to the hydrogel structure. This can be used in the treatment of diabetes, in which a threshold level of glucose would trigger release of insulin loaded into the 3D hydrogel structure. An enzymatic reaction occurs between the glucose (substrate) and the enzyme on the hydrogel, causing a drop

in pH which induces a collapse in the hydrogel structure and release of insulin (20). Another mechanism of insulin release from glucose responsive hydrogels was proposed with the development of a PEG-phenylboronic acid-based hydrogel. This was formulated by conjugating the PEG-containing phenylboronic acid macromonomer with a PEG macromonomer containing a glucose-like diol, and loading it with insulin. The insulin was subsequently released *in vitro* in response to exposure to glucose containing media, and it was hypothesised that competitive binding of the free glucose to the PEG-phenylboronic acid would induce structural changes in the hydrogel, thereby releasing insulin in a controlled manner (21).

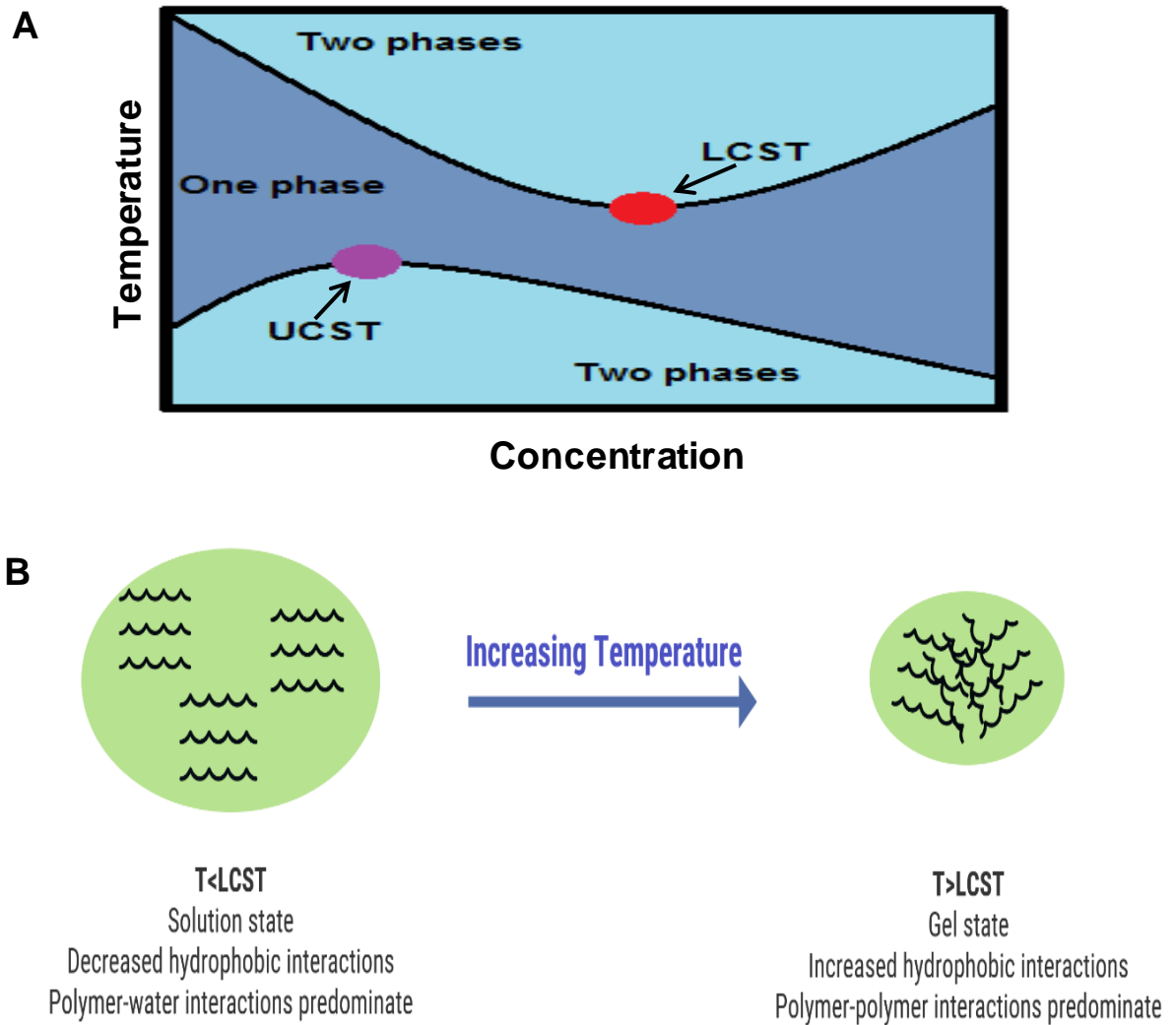
1.2.3 Thermoresponsive hydrogels

Some of the most extensively researched stimuli responsive hydrogels are those which respond to temperature (22). Temperature responsive polymers can be sensitive to a 1°C change in environmental temperature. The response to the stimulus is relatively large and alters the conformation of the hydrogel in a characteristic manner.

Based on their phase diagram, thermoresponsive hydrogel polymers have either an upper critical solution temperature (UCST) or a lower critical solution temperature (LCST) (Fig. 1.3 A). Three types of interaction exist for thermoresponsive hydrogels:

1. Polymer-polymer interactions
2. Polymer-water interactions
3. Water-water interactions

LCST polymers undergo gelation above a characteristic temperature, termed the sol-gel transition temperature. Below the sol-gel transition temperature of LCST hydrogels, the polymers are swollen in solution form. In this temperature range the polymer-water interactions tend to predominate, and the hydrogel exists as a solution. As temperature increases, these interactions become less favourable and hydrophobic interactions begin to dominate. At the transition temperature, the polymers will contract abruptly, resulting in the formation of an increasing number of polymer-polymer interactions, leading to gelation of the hydrogel (Fig. 1.3 B) (23). If the hydrogel is thermoreversible, the hydrophobic interactions become less dominant when the temperature is decreased, and the polymer chains begin to interact with the water molecules again, returning the hydrogel to solution form (24, 25).



Thermoresponsive hydrogels based on pNiPAAm polymers are the most extensively researched. pNiPAAm hydrogels undergo a sharp thermoresponse at 32°C, transitioning from coil conformation to aggregated globules in aqueous solution upon gelation (26). Another commonly used excipient in the formulation of LCST thermoresponsive hydrogels is the tri block copolymer, poly(ethylene oxide)-b-poly(propylene oxide)-b-poly(ethylene oxide) (PEO-PPO-PEO, Pluronic) (27-30). Pluronic can form micelles, which have a hydrophilic coat (PEO) and a hydrophobic core (PPO). The creation of a hydrophobic core promotes the use of Pluronic as a solubiliser for drugs with poor aqueous solubility. Gelation occurs due to the packing arrangement of these micelles and micelle entanglement, once

sufficient polymer concentration and external temperature has been reached (31, 32). Aqueous solutions of Poloxamer 407 (P407) exhibit thermoreversible properties at concentrations of 20% w/w and above (33). The disintegration rate of Poloxamer-based thermoresponsive hydrogels has, however, limited their usefulness in the clinical setting. The fast disintegration rate of these hydrogels *in vivo* is due to low mechanical strength and high permeability (1, 25). The use of physical or chemical crosslinkers can dramatically change the disintegration rate. The physicochemical interactions between the polymers and additional formulation excipients can be highly concentration-dependent, with each excipient influencing the structure and thermoresponse of the final formulation. Poloxamer-based hydrogels will be discussed in greater detail in Chapter 2.

UCST polymers are less clinically useful, as they exist as a liquid above their characteristic phase transition temperature and undergo gelation below this temperature. This would require storage and administration of the hydrogel at elevated temperatures, to ensure that gelation would occur at body temperature. Poly(N-acryloyl glycinamide) (PNAGA) is an example of a UCST polymer (34).

Altering the hydrophilic/lipophilic balance of the hydrogel formulation has a large impact on the gelation temperature. Surfactants and co-solvents can impact the hydrophilic/lipophilic balance of the formulation and thus, the gelation temperature. Salt concentration also impacts gelation temperature (35). All excipients in the formulation must be tightly controlled to ensure that a hydrogel with a reproducible sol-gel transition temperature is produced. Increasing the hydrophobic content of the hydrogel will result in the polymer-water interactions becoming less favourable. Polymer-polymer interactions will then predominate at lower temperatures, resulting in a lower sol-gel transition temperature. Conversely, increasing the hydrophilic content of the hydrogel allows for an increased LCST, thus the sol-gel transition temperature can be tailored, as required (25).

1.2.3.1 Rheological characterisation of thermoresponsive hydrogels

Rheology is the study of the deformation and flow of matter, and makes use of the relationship between stress and strain to characterise a material (36). Stress can be defined as the force applied per unit area, measured in Pascals (Pa). Stress can also take into account the direction in which the force is applied; shear stress is most commonly used in rheological measurements and results from a parallel applied force. Strain is a unitless measure of deformation in response to stress applied, and is more complicated to measure than stress. Purely viscous materials

undergo irreversible deformation in response to stress applied. A perfectly elastic material will deform instantly to a defined point, within its elastic limits, under stress. When the stress is removed, a perfectly elastic material will recover almost immediately to its original state.

In reality, very few materials are purely viscous or elastic. Rather, they display a blend of both characteristics, and are deemed viscoelastic materials. Under constant stress, viscoelastic materials will dissipate some energy through flow (viscous behaviour), and store the remainder (elastic behaviour). Hydrogels are viscoelastic materials, and oscillatory rheology can be used to characterise the viscoelasticity of the formulation. It can also characterise its behaviour under different conditions including, but not limited to, varying stress, temperature or time (37). Oscillatory rheology uses a geometry to apply a sinusoidal stress to a sample loaded onto a peltier plate and measures the resulting strain. Depending on the material properties, the resulting strain waves generated will lag behind the stress waves applied by the phase angle, δ , which is used to calculate the elastic and viscous proportions of the material (38). The storage modulus (G') is the elastic component of the hydrogel. The loss modulus (G'') is a measure of the viscous component of the hydrogel. When G'' predominates over G' the material is defined as a viscoelastic liquid, and when G' is greater than G'' the material is defined as a viscoelastic solid or semi-solid. This can be used to track the transition of thermoresponsive hydrogels over a temperature range. Below the sol-gel transition temperature $G'' > G'$; the temperature at which $G' = G''$ is defined as the sol-gel transition temperature and gelation occurs at this temperature. G' and G'' are calculated by the software and are derived from the complex shear modulus (G^*), as outlined below.

$$G' = G^* \cos(\delta) \quad \text{(Equation 1)}$$

$$G'' = G^* \sin(\delta) \quad \text{(Equation 2)}$$

$$\tan(\delta) = G''/G' \quad \text{(Equation 3)}$$

G' provides a measure of the strength of the hydrogel, but not necessarily its robustness, which is why other material characterisation methods, such as disintegration testing, should also be carried out in conjunction with rheology to fully characterise a hydrogel.

Rotational rheology is used to calculate the viscosity of a material. Viscosity, defined as the resistance to flow, is calculated by dividing the shear stress by the

shear rate, and is measured in Pa.s. In these measurements, the geometry rotates fully to apply the shear stress to the material, in comparison to the sinusoidal movements in oscillatory rheology (39). A benefit of using a rotational rheometer over a simple viscometer is that the viscosity of a material can be calculated over a range of applied shear stresses.

1.2.3.2 Thermoresponsive hydrogels as drug delivery platforms

Thermoresponsive hydrogels are commonly employed as delivery platforms for a range of applications, including the delivery of small molecules, proteins, steroids, genes and other therapeutics or cells (25, 26, 40). They can be formulated as inert drug delivery depots or exert pharmacological effects in their own right to augment the therapeutic payload. Local or systemic delivery is achievable using thermoresponsive hydrogels, which can be administered via topical (41), ocular (42), nasal (43), vaginal (44) or parenteral routes (45, 46).

The non-invasive nature of parenteral administration via injection is seen as a major advantage, as the patient does not require surgical implantation of the drug delivery system (Fig. 1.4 A) (24). Physically crosslinked hydrogels are disintegrable due to their reduced stability, arising from the hydrophobic interactions between polymer chains or weak bonds which can be broken down by hydrolysis (40, 47, 48). This means that hydrogels do not have to be surgically removed from the patient once the drug load has been delivered, further reducing the invasiveness of the procedure for the patient. The rate of degradation of the hydrogel can be tailored by modifying the nature and degree of crosslinking. The temperature-induced conformational change following administration of the thermoresponsive hydrogel means that no external stimulus e.g. magnetisation, need be applied. This increases the simplicity and safety of the procedure, as only injection is required (49). The *in situ* gelation offers the opportunity for the hydrogel to mould to the target tissue, facilitating a better fit than the preformed implants (7), and allows for sustained release of the drug at the required site of action in the body (Fig. 1.4 B) (22, 50).

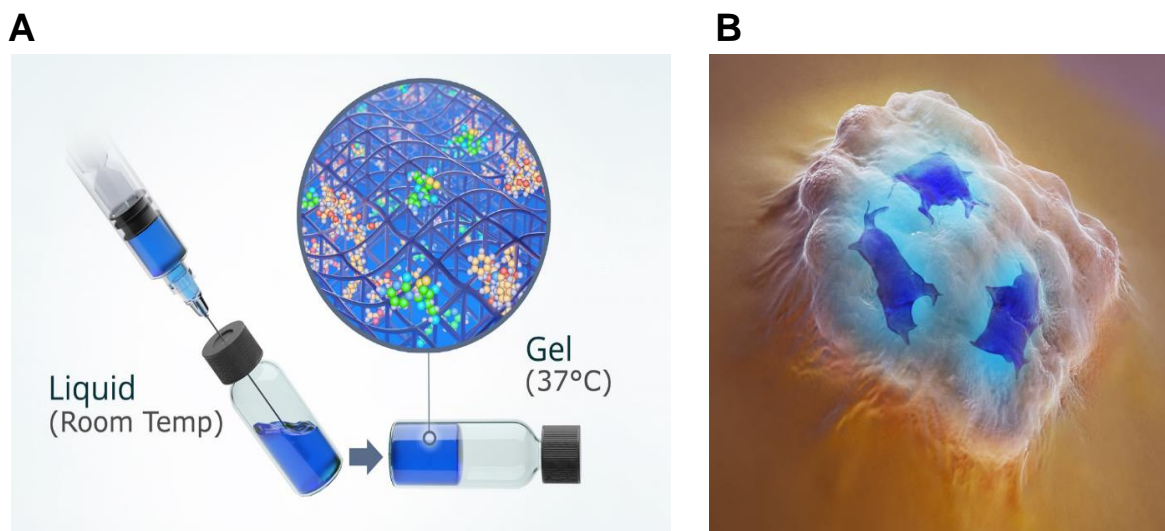


Figure 1.4 (A) Drug-loaded thermoresponsive hydrogel at room temperature in an injectable liquid state, and at body temperature (37°C) in the gel state. **(B)** In-situ gelation facilitates moulding to the target tissue.

The rate of release of drugs from thermoresponsive hydrogels is dependent on a number of factors related to the material properties of the hydrogel, the physicochemical characteristics of the drug encapsulated, and the nature of the surrounding fluid. In general for hydrogels, rate of release is affected by the viscosity of the hydrogel carrier, with more viscous hydrogels demonstrating slower release (2). The mechanism of drug release from hydrogels determines the release rate, with diffusion controlled release being the most common mechanism seen in hydrogels. Swelling controlled or chemically controlled/erosion release is also seen in hydrogel-based controlled release (Fig. 1.5) (50, 51). The nature of the drug encapsulated within the hydrogel can also affect release rate. Hydrophobic drugs tend to undergo slower diffusion rates through the hydrogel than hydrophilic drugs, resulting in slower release rates (24). Release from hydrogels frequently involves a blend of two or more of the above mechanisms, and can be tailored by altering the chemical structure of the hydrogel to ensure effective drug delivery to the target site (50). *In vitro* assessment of release from thermoresponsive hydrogels presents a number of challenges, due to the phase changes exhibited affecting mathematical modelling of drug release. *In situ* gelation of thermoresponsive hydrogels, and subsequent *in situ* crosslinking which may occur adds further complexity (51). Locoregional delivery commonly involves administration into tissue, which has a lower volume of surrounding fluid compared to systemic administration. Consideration of the local environment in the target application must be included in the design of *in vitro* release models (52, 53).

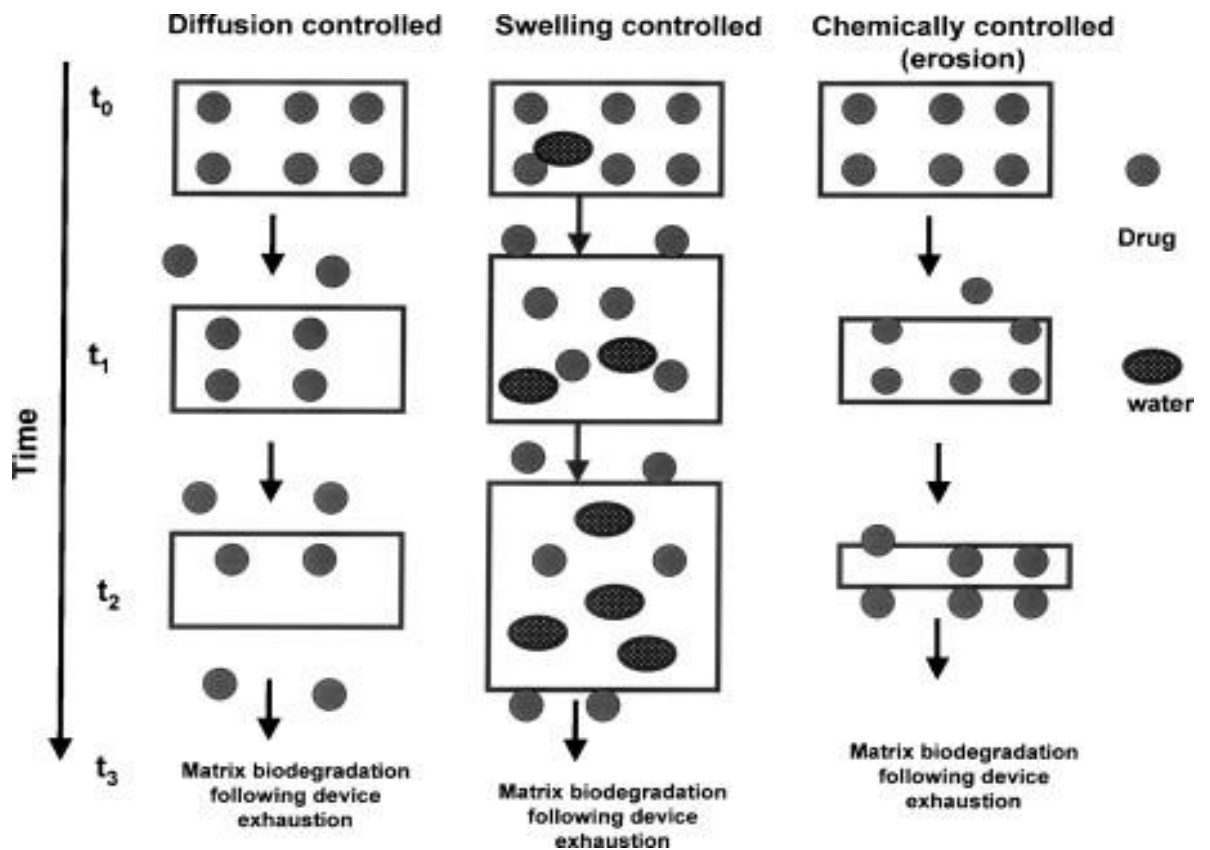


Figure 1.5 Mechanism of drug release from hydrogels. Taken from (50).

Thermoresponsive hydrogels employed as drug delivery platforms have been the focus of an increasing amount of pre-clinical research. From 1991 to May 2018, 1,314 publications were found to include the terms “thermoresponsive” and “gel*” in the Web of Science database. The growing interest in this area of research is reflected in the number of publications per year. Publications containing these terms have increased from 4 in 1991 to 154 publications in 2017. 39 of the papers published from 1992 to May 2018 contained the term “cancer”, all of which were published between 2008 and 2018. Other combination searches are shown in Table 1.1. The translation of thermoresponsive hydrogel technology to the clinic has been less successful (6), with only a handful of products progressing to the clinical trial stage, to varying degrees of success (54-56).

Table 1.1 Total number of publications from a Web of Science database search for thermoresponsive hydrogels in cancer applications.

Search term	Number of publications (1991- May 2018)	Number of publications in 2017	Number of publications in "cancer"
"Thermosensitive" "gel*"	2,037	163	173
"Thermoreversible" "gel*"	2,175	107	30
"Thermogel"	127	27	19

Systemic chemotherapy has long been the mainstay of cancer chemotherapy treatment for all cancer types. The lack of specificity and subsequent destructive off-target side-effects has in turn prompted alternative delivery methods to be considered, in particular for solid tumour cancers (8, 57). Thermoresponsive hydrogels for direct IT delivery in solid tumour treatment has been investigated in the pre-clinical and clinical setting. Chemotherapeutic delivery from IT administered thermoresponsive hydrogels has been proposed as a safer and more effective method of treatment for patients with solid tumours than traditional systemic administration (8, 22, 55, 56, 58-61). The potential for minimally invasive administration, localisation of chemical payload and reduction in off-target side-effects suggest that IT delivery via thermoresponsive hydrogels offers significant improvements to treatment efficacy and quality of life compared to current "gold-standard" systemic treatment.

A wide range of solid tumours have been assessed in the pre-clinical development of thermoresponsive hydrogels, including liver, bladder, breast, lung, pancreas, osteosarcoma, oesophageal and brain cancers (8, 58, 61-63). In particular, lung, pancreas and brain cancer are associated with very poor prognosis (64). This thesis will focus on the development of a thermoresponsive hydrogel for LC applications.

1.3 Lung Cancer

1.3.1 Gross anatomy of the lung

The lower respiratory tract consists of two lungs and the airways (trachea, bronchi, bronchioles and alveoli). The right lung consists of three lobes, and the left lung is

10 – 20% smaller, with two lobes (Fig. 1.6 A) (65). The airways are highly bifurcated structures, which consist of approximately 23 generations, according to Weibel's (1963) model of the airways (Fig. 1.6 B) (66). Each generation produces narrower, shorter airways, with increased branching. The airways culminate with the alveoli, which are highly vascularised, function for gaseous exchange and offer a surface area of 70 – 80 m² (65).

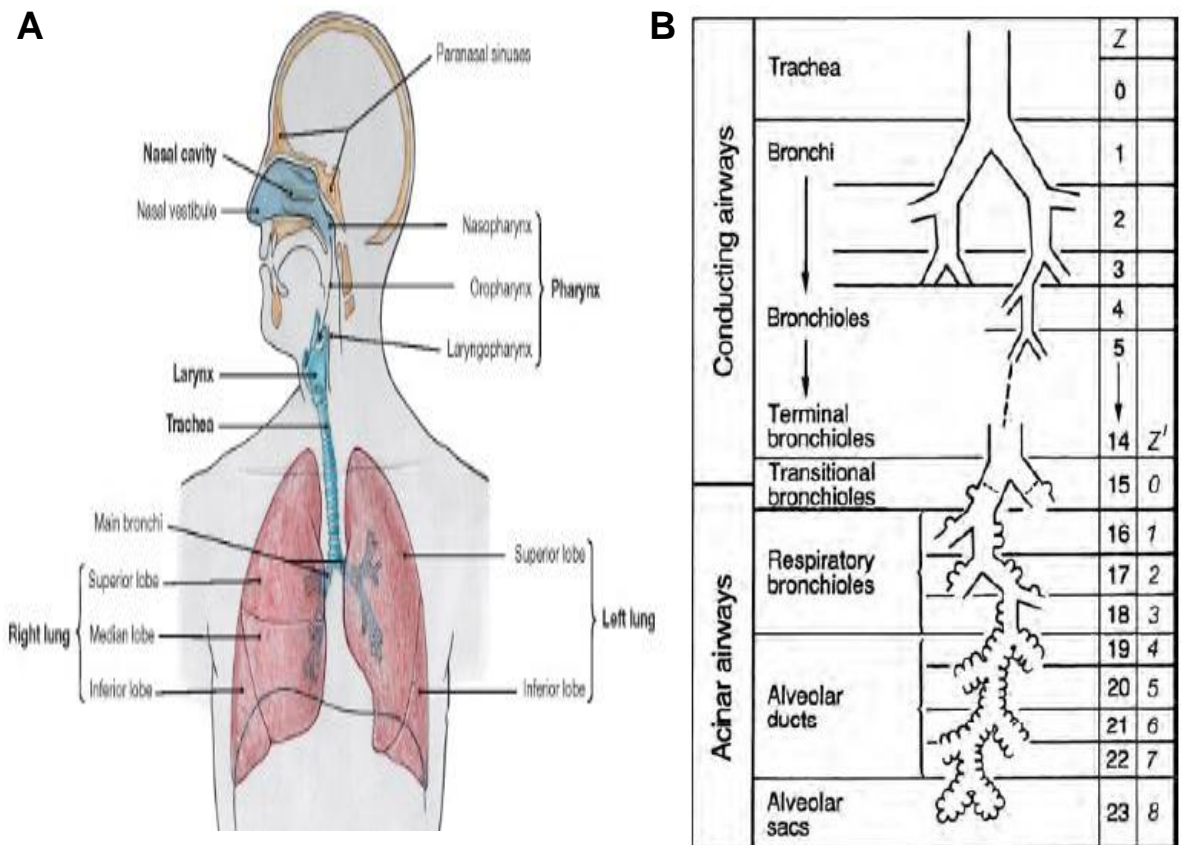


Figure 1.6 (A) Diagram of the upper and lower respiratory tract. Taken from (65). **(B)** Weibel's airway generations. Z and Z' are the number of airways in each generation.

1.3.1.1 Pathophysiology of tumour tissue in the lung

The large inter- and intra- tumour heterogeneity associated with LC tumours presents significant challenges for accurate diagnosis and treatment (68). Tumour masses cannot be viewed as individual entities which control their own lineage, phenotype and fate. Rather, the tumour growth and metastatic processes are influenced by the surrounding cells. The tumour microenvironment (TME) is made up of an altered extracellular matrix (ECM) and embedded cellular components, called tumour-associated stromal cells, which include cancer-associated fibroblasts and tumour-associated macrophages (69-71). The composition of the stromal cells and their interaction with tumour cells influence the progression of the malignancy

and development of distant site metastasis. The TME of LC has a variable composition depending on the stromal cells and cytokines present (72).

While healthy lung tissue is well vascularised, the same cannot be said for lung tumour tissue. The vasculature of the tumour is limited and leaky compared to normal tissue blood supply, and blood flow is unevenly distributed throughout the tumour mass (69). In a normal homeostatic environment vasculature is less than 10 μm away from cells, but tumour cells can be located 100 – 200 μm away from their closest capillary blood supply. Hypoxic areas develop in regions further from the vasculature, which the tumour can manipulate to increase survival by a number of mechanisms. Hypoxic conditions can drive the secretion of pro-angiogenic factors, such as vascular endothelial growth factor (VEGF) (73). This induces growth of new vasculature, which is highly inefficient, and struggles to control hypoxic levels in the tumour. Further angiogenesis is promoted, through the upregulation of factors such as hypoxia-inducible factor 1-alpha (HIF1 α), which subsequently upregulates VEGF production following binding with a receptor in the nucleus of the tumour cell, thus enabling survival of the tumour (74). Many chemotherapeutics rely on the production of free radicals to bring about DNA damage (69). The absence of oxygen in certain tumour regions, enables the tumour to become resistant to such mechanisms of action. Additionally, cancer cells favour the process of anaerobic glycolysis, even in the presence of sufficient oxygen. This results in surplus production of H⁺ ions as a by-product of the reaction. The ensuing acidic environment has been termed an “engineering niche”. This niche allows cancer cells to create an environment which is more favourable to their survival. The H⁺ ions induce cell death in healthy cells surrounding the tumour (75). They also act to degrade the ECM which allows for easier intravasation by cancer cells into the circulating bloodstream. The acidic nature of the TME further triggers angiogenesis in the tumour region, promoting hypoxia, and ultimately cancer cell survival, as outlined above.

1.3.2 Incidence and mortality

In 2012, there were 1.8 million new cases of LC reported worldwide (76). LC represents the second most commonly diagnosed cancer worldwide, after prostate and breast, for men and women respectively (76). 26,838 cases of LC were diagnosed in Ireland over a 14 year period (2000 – 2014) (77). Projected incidences for LC for both sexes are predicted to level off from 2020 to 2030 (Fig. 1.7 A), which can be attributed, in large part, to the anti-smoking policies adopted at a

governmental level in the western world. Incidence continues to rise in African and Asian countries, however, due to continued high rate of smoking and environmental carcinogens prevalent in these populations (78).

Smoking is positively correlated with the development of pulmonary tumours, with up to 80% of LC deaths attributable to cigarette smoke (79). Rates of smoking in women rose in 1930's due to promotion of the concept of a cosmopolitan woman smoker by tobacco companies. This has led to a delayed onset in increased incidence of LC in women. Subsequent smoking cessation policies in the western world have positively impacted the incidence of LC in men, but have not yet caught up with the inflated uptake of smoking in women (80). Other risk factors include, chronic obstructive pulmonary disorder (COPD), environmental exposure to toxic insults, such as radon and asbestos, and family history of LC (81, 82).

Mortality rates for the majority of cancers have decreased in recent years. This is mainly due to improved screening and treatment of cancer. Some cancers do not comply with this generalisation, and have seen an increase in mortality rates over the years, including liver, thyroid, pancreatic and uterine cancer. Lung and bronchus cancer are projected to be the leading cause of cancer-related deaths in 2018, accounting for 26% and 25% of cancer deaths for men and women respectively (83). The LC mortality rate is predicted to remain the highest up to 2030 (Fig. 1.7 B). While the mortality rate is expected to decrease slightly after 2020, it will still remain approximately 2.5 times the rate of pancreatic cancer, the second most common cause of cancer-related death predicted in 2030 (64). From 2000 to 2014, the average age-standardised 5-year net survival for LC patients in Ireland increased from 10.1% to 17.5%, which fell within the range of the majority of the 71 countries reviewed as part of the CONCORD-3 study (77). The high mortality rate associated with LC is indicative of a large unmet clinical need for more effective treatments and screening processes.

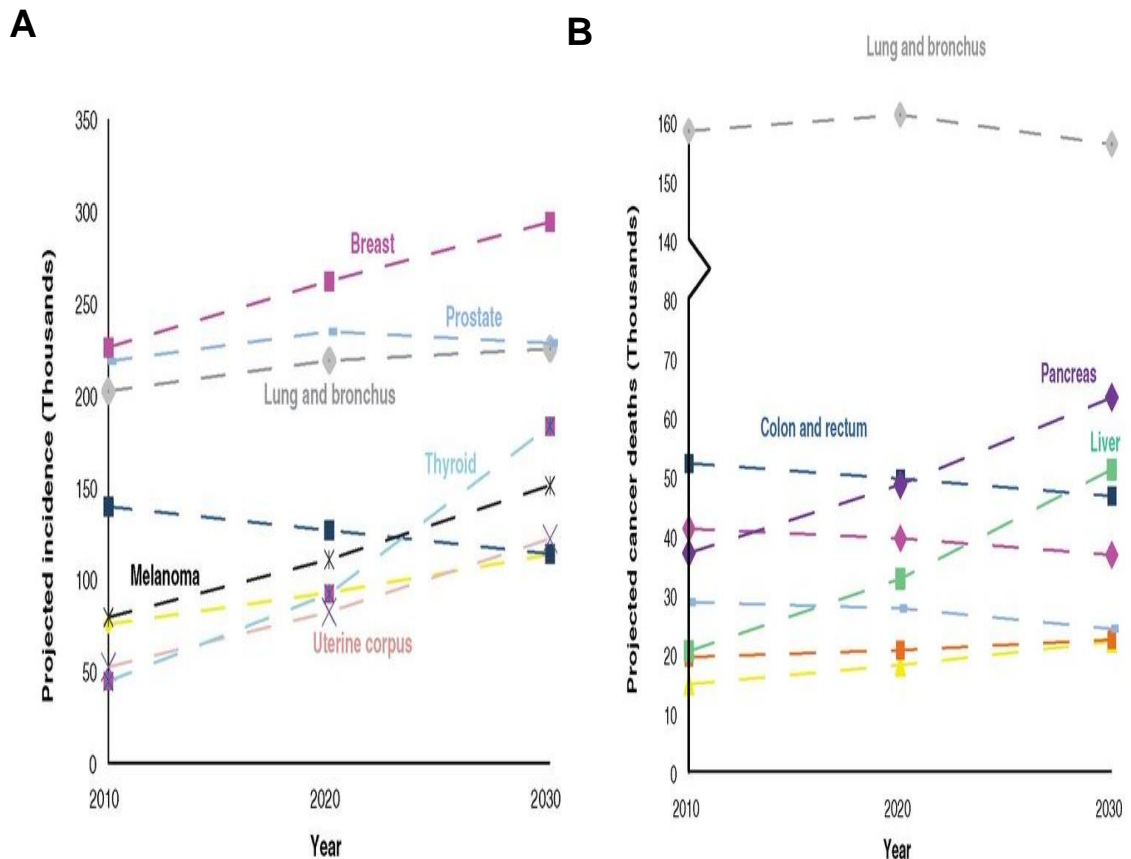


Figure 1.7 Cancer (A) incidence and (B) mortality rates predicted until 2030. Adapted from (64).

1.3.3 Diagnosis and staging of lung cancer

Early stage LC is a potentially curable disease. Unfortunately, the majority of LC patients present in later stages of the disease, with distant metastatic sites established (84). Symptomatic presentation of LC, which is the most common reason for diagnosis, is often indicative of late stage LC. The value and success associated with screening initiatives for LC remains unclear, with low dose computed tomography (CT) screening demonstrating the most promise, if appropriate “at risk” patient cohorts, multidisciplinary team expertise and supports are available (85).

Differential diagnosis is usually made based on chest X-Ray and contrast-enhanced CT scans of lower neck, thorax, and upper abdomen. Definitive diagnosis is then established using a variety of techniques including, but not limited to, sputum cytology, transthoracic needle aspiration, flexible bronchoscopy, electromagnetic navigation bronchoscopy, radial endobronchial ultrasound (EBUS) and transbronchial needle aspiration (TBNA) and Positron Emission Tomography (PET)-CT. (81, 86). Histological subtyping using immunohistochemical staining of biopsied tissue is used to define LC subtype and further sub-classifications. LC can

be broadly divided into non-small cell LC (NSCLC) and small cell LC (SCLC). NSCLC accounts for approximately 75 – 80% of cases of newly diagnosed LC. The main subtypes of LC are summarised in Table 1.2 (87-89).

Table 1.2 *Classification of subtypes of lung cancer.*

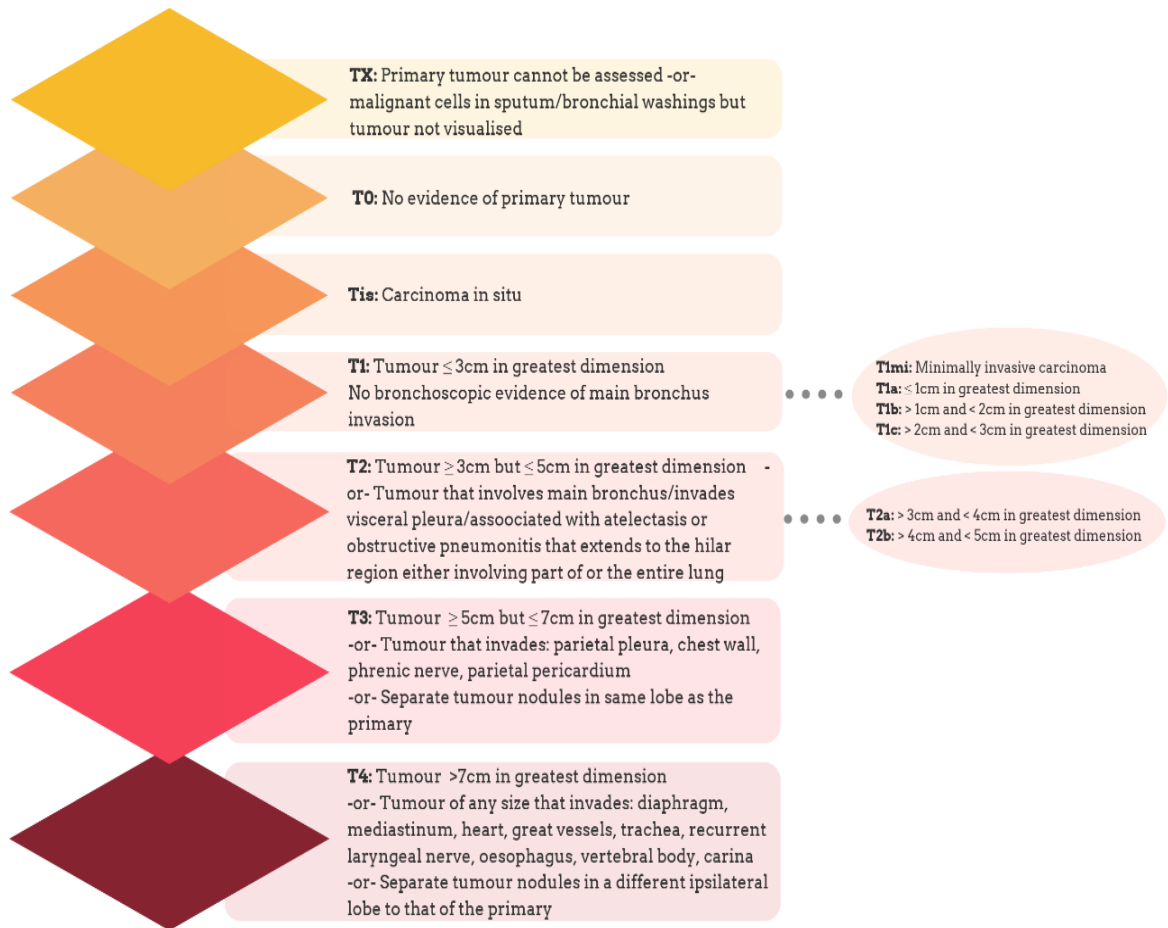
Subtype	Further sub-classification	Origin	Comments
NSCLC	Adenocarcinoma	Peripheral bronchi	40% of all LC
	Squamous cell carcinoma	Main bronchi	25-30% of all LC
	Adenocarcinoma in situ & Minimally invasive adenocarcinoma	Alveoli	Very good five year survival rate after resection (almost 100%)
	NSCLC not otherwise specified (NSCLC NOS)/ Large cell carcinoma		10% of NSCLC Rapid fatal spread
SCLC	-	Neuroendocrine	10-15% of all LC Most aggressive type of LC, poor prognosis
Carcinoid	-	Neuroendocrine	1-2% of all LC
Other	Mixture of subtypes	-	-

Correct diagnosis and staging of malignancy is important to establish optimal treatment strategies and prognostic evaluation (87). Staging of LC is carried out according to the 8th edition of the “Tumor-Node-Metastasis” (TNM) classification system, which takes into account the clinical information available prior to surgical resection, and the pathological information determined after surgical resection. The dimensions of the primary tumour (T), the involvement of regional lymph nodes (N) and development of distant site metastasis (M) are used to stage the tumour based on predetermined sub-classification criteria and determine prognosis (Fig. 1.8). The TNM classification is highly applicable to the staging of NSCLC, but its application in the staging of SCLC is more difficult. It is of note that the TNM classification

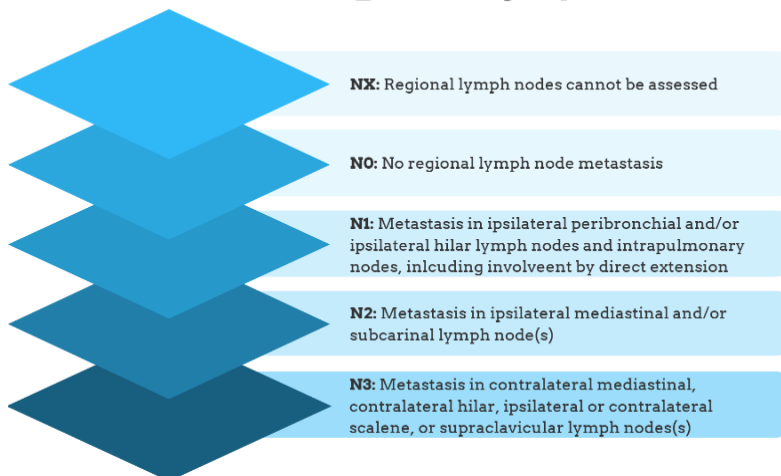
should only be used for staging and prognosis; treatment paradigms should be designed based on current clinical guidelines and best practice (87, 90, 91).

NSCLC is acknowledged to be a highly heterogeneous disease, with the histological subsets outlined in Table 1.2 also displaying wide-ranging genetic heterogeneity. Oncogenetic drivers commonly associated with LC, including Kras mutations, epidermal growth factor receptor (EGFR) mutation (with or without T790M mutation) and anaplastic lymphoma kinase (ALK) rearrangements, can be screened for using molecular testing in order to guide precision therapy. These aforementioned aberrant genetic drivers of NSCLC are the most common, with others mutations also included in Figure 1.9. Testing for programmed cell death protein 1 (PD1) and programmed death ligand 1 (PDL-1) protein expression in tumour samples is also used to guide appropriate prescribing of immune-oncology treatment (92, 93).

T: Primary Tumour



N: Regional Lymph Nodes



M: Distant Metastasis

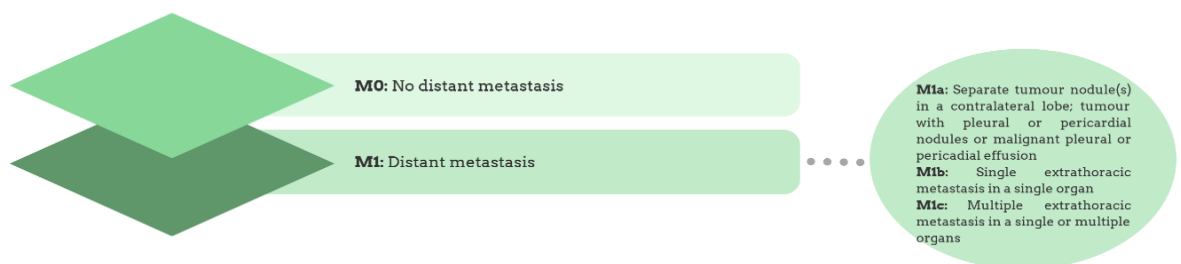


Figure 1.8 Summary of staging of lung cancer according to the TNM staging classification 8th edition. Adapted from (90).

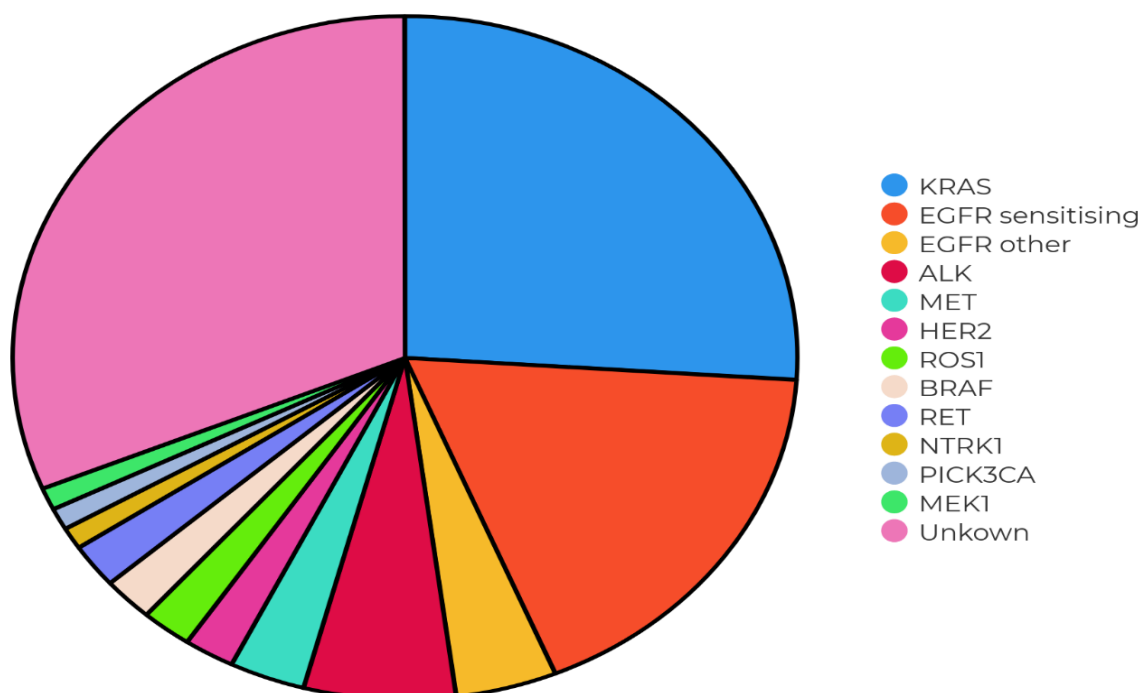


Figure 1.9 *Oncogenetic driver mutations of non-small cell lung cancer adenocarcinoma. Adapted from (94).*

1.3.4 Lung cancer treatment strategies

Traditional treatment of cancer is based around three pillars of therapy; surgery, chemotherapy and radiation. Depending on the stage of LC diagnosed, one or a combination of these treatments may be selected as directed by evidenced-based best practice associated with the histological and molecular definition of the tumour type.

1.3.4.1 Traditional chemotherapeutics

The use of systemic chemotherapy to treat cancer began in the 1940's with the use of Nitrogen Mustard, a non-specific DNA alkylating agent, to treat non-Hodgkin's lymphoma. Although treatment did not deliver long-term results, it marked the beginning of the explosion of drug discovery to treat cancer (95). Traditional chemotherapeutics target rapidly proliferating cells and interfere with this proliferation. They do not have cancer cell-specific toxicity, and can indiscriminately target any cell in the body, including bone marrow and hair, resulting in some of the common side-effects associated with treatment. Chemotherapy can be divided into a number of classes depending on the mechanism of action of the drug, most of which interfere with DNA or microtubule formation, with some examples of chemotherapeutics listed in Table 1.3.

Table 1.3 *Chemotherapeutics used in the treatment of lung cancer.*

Drug class	Mechanism of action	Drug indicated for NSCLC
Alkylating drugs	Damage DNA and interfere with cell replication	Not usually indicated for use in NSCLC
Anthracyclines	Multiple methods, primarily intercalation of DNA	Not usually indicated for use in NSCLC
Antimetabolites	Interfere with cell division and growth due to similar structure as essential cellular components	Gemcitabine, Pemetrexed,
Vinca alkaloids and etoposide	Antimitotic agents which bind to tubulin and prevent the formation of microtubules	Etoposide for SCLC
Platinum compounds	Forms DNA adducts to prevent replication	Cisplatin, Carboplatin
Taxanes	Antimitotic agents which stabilise microtubules	Paclitaxel, Docetaxel
Topoisomerase I inhibitors	Inhibits topoisomerase I which is involved in DNA synthesis	Topotecan for SCLC

In this thesis, the focus is on the use of the platinum-doublet regime, comprising of cisplatin and paclitaxel. Cisplatin is a platinum-based drug, which was first synthesised in 1844 (96). It is slightly soluble in aqueous media, and is normally administered via the intravenous (IV) route. It is indicated for treatment of a range of solid tumours, including lung, testicular, cervical, bladder, and head and neck cancer (97). A major drawback of cisplatin treatment is the toxicity associated with its administration, including severe nausea and vomiting, nephrotoxicity, ototoxicity, peripheral neuropathy and myelosuppression. Aggressive IV administration of fluids for hydration is required during cisplatin administration to minimise renal toxicity (97). Cisplatin-induced cellular apoptosis is mediated by the formation of DNA adducts. Uptake of cisplatin into the cell is facilitated by a copper transporter (Ctr1) present on the cellular membrane. Activation of the cisplatin molecule occurs following hydrolysis in the cytoplasm when water molecules replace the chloride atoms on the cisplatin structure. This enables binding of the electrophilic hydrolysed cisplatin to the nucleophilic purine residues on DNA. The subsequent damage to the DNA interferes with normal cell division processes, and induces apoptosis.

However, resistance to cisplatin treatment frequently develops with suggested mechanisms for this resistance including a reduction in the cellular uptake of cisplatin into the tumour cell due to cisplatin-induced degradation of the Ctr1 membrane transporter, and development of increasingly effective DNA adduct repair mechanisms by the tumour cell (96, 98).

Paclitaxel is an anti-mitotic agent, which was first isolated from the Pacific yew tree (*taxus brevifolia*) in the 1960's, and entered clinical trials in the 1980's, before being approved by the United States Food and Drug Administration (FDA) for use in NSCLC in 1999 (99). Paclitaxel is insoluble in water, which presents formulation and drug delivery challenges. To facilitate IV administration, paclitaxel is formulated in a polyoxyethylated castor oil and ethanol vehicle, known as Cremophor EL (100). Cremophor EL is associated with severe hypersensitivity reactions and toxicity, necessitating a pre-medication schedule consisting of an anti-histamine, a histamine H₂-receptor antagonist and a corticosteroid (97). Other side-effects of paclitaxel treatment include myelosuppression, peripheral neuropathy, cardiac conduction defects with arrhythmias, hair loss, muscle pain and mild to moderate nausea and vomiting. In an effort to overcome the hypersensitivity and toxicity risk associated with Cremophor EL, an albumin-bound paclitaxel nanoparticle formulation was developed, Abraxane, which was approved for use as second line treatment in defined circumstances of metastatic breast cancer, pancreatic cancer and NSCLC (97, 101). Paclitaxel's anti-tumour activity is exerted via microtubule stabilisation, which disrupts the normal process of mitosis in the G₂/M phase, and halts cellular division (102).

1.3.4.2 Precision treatment options

Modern LC treatment is a rapidly evolving field, with guidelines and recommendations changing at considerable pace. With a number of new small molecules and monoclonal antibodies approved for LC, and even more in clinical trials, the era of precision oncology has called for increased histological and molecular classification of LC tumours to screen for mutations and protein expression, which may allow for personalised medication regimes design. Although a number of these drugs have been integrated into first line therapy recommendations, conflicting and confusing clinical trial outcomes have led to uncertainty over the benefit inferred to the patient, especially when considering the cost associated (103). Overall, scientists and clinicians involved in LC research and treatment have called for the development of more robust and reliable biomarker

screening to improve selection of precision medicines, and ultimately clinical outcomes (104, 105).

Tyrosine kinase inhibitors (TKIs) are small molecule therapeutics, which have been successful as targeted treatments for oncogenetic drivers, such as EGFR mutations and ALK rearrangements. EGFR mutations and ALK rearrangements are more commonly found in NSCLC with adenocarcinoma as histological subtype, and never smokers (106, 107). Resistance to treatment has led to the development and licensing of multiple generations of these targeted therapies. Table 1.4 details some of the commonly used TKIs in NSCLC treatment.

In recent times, immune-oncology has come to the forefront of cancer therapy, whereby the altered immune response in cancer pathology is targeted. A number of inhibitory pathways, known as “immune checkpoints”, are integral to the function of the human immune system (108). These checkpoints ensure efficient and measured immune responses to stresses in the body. They can, however, also be manipulated by tumour cells in order to evade detection, and subsequent destruction, by immune cells. LC has a number of immune-evasive pathways, including induction of cytotoxic T-lymphocyte antigen-4 (CTLA-4) and overexpression of PD-L1 (109). Four immune-oncology therapeutics have been approved for the second line treatment of NSCLC (Table 1.4). More recent clinical trials have, however, highlighted the shortcomings associated with the use of these agents as a first line treatment, further reinforcing the need for more robust biomarkers to determine appropriate treatment pathways for patients (110). Combination therapy of immunotherapy drugs has been suggested as a means to improve progression-free survival rates, with a recent Phase III clinical trial (CheckMate 227, NCT02477826) supporting the combination use of a CTLA-4 and PD-1 inhibitor, ipilimumab and nivolumab, as first line treatment in patients with NSCLC and a high tumour mutational burden (111).

Table 1.4 Targeted therapies for common genetic mutations and immune-oncology drugs approved for treatment of non-small cell lung cancer. FDA, Food and Drug Administration. EGFR, Epidermal growth factor receptor. ALK, Anaplastic lymphoma kinase. PD-1, Programmed cell death protein 1. PD-L1, Programmed death ligand 1.

Mutation/Target	Treatment	FDA Approval	
		Initial	Current
Kras (112)	No effective targeted therapy available	-	-
EGFR (113-116)	<i>1st generation</i> - Gefitinib - Erlotinib	2003, 2004	1 st line monotherapy treatment of EGFR+ NSCLC tumours, which have EGFR exon 19 deletions or exon 21 (L858R) substitution mutations
	<i>2nd generation</i> - Afatinib	2013	
	<i>3rd generation</i> - Osimertinib	2017	
ALK (117-119)	<i>1st generation</i> - Crizotinib	2011	ALK+ NSCLC
	<i>2nd generation</i> - Ceritinib - Alectinib	2014, 2015	
PD-1 (120)	Nivolumab	2015	Second line metastatic NSCLC (progression with platinum-based chemotherapy)
PD-1 (121)	Pembrolizumab	2015	Second line metastatic NSCLC that has advanced on previous treatment, with PD-L1 expressing tumours
PD-L1 (122)	Atezolizumab	2016	Second line metastatic NSCLC (progression with platinum-based chemotherapy)
PD-L1 (123)	Durvalumab	2018	Advanced late stage NSCLC that has stabilised

1.3.4.3 Current treatment regimens

Clinical guidance for NSCLC treatment is undergoing frequent updates as new evidence comes to the fore (124). The National Institute for Health and Care Excellence (NICE) is a special health authority in the United Kingdom, which develops guidelines and standards to ensure quality health and social care for patients in the National Health Service (NHS), across most illness and disease states. Currently, NICE guidelines recommend an initial screening of LC patients by a thoracic oncologist and thoracic surgeon to establish the patients' suitability for multimodal treatment plan, which encompasses surgery, chemotherapy and radiation. There are five main options presented by the NICE guidelines as treatment pathways, which are detailed in Figure 1.10.



Figure 1.10 Summary of The National Institute for Health and Care Excellence (NICE) guidance pathway for treatment of non-small cell lung cancer (NSCLC). Adapted from (125).

1.3.4.4 Pharmacoeconomics

Pharmacoeconomics is the application of economic parameters to a drug treatment or healthcare intervention. Cost effectiveness considerations in selecting cancer treatment is given prominence in NICE guidelines. In 2009, LC accounted for the biggest proportion of cancer care costs in the European Union (EU). Approximately €18.8 billion of the EU cancer care budget was spent on the treatment of LC patients, equivalent to 15% of the total budget (126). The newer cancer treatments are commonly associated with considerably larger reimbursement costs. As different disease management pathways become available, the rising costs associated with treatment must be critically assessed against the clinical benefit to the patient.

NICE has determined that £30,000 is a reasonable cost to be associated per quality-adjusted life year (QALY) (127). In contrast, increasingly high development costs associated with bringing a new cancer therapy to market in the United States have been estimated to result in the new therapy costing \$2.7 million per life year saved. It has also been noted in an increasing number of instances that these inflated costs do not equate to increased patient safety outcomes (127). Evidently, new strategies need to be employed to reduce the cost of drug development and improve patient outcomes simultaneously.

1.4 Interventional Oncology and Intratumoural Drug Delivery

As previously stated in Section 1.3, standard chemotherapy regimens are delivered to the patient via IV infusion of cytotoxic substances. The reduction in quality of life during traditional chemotherapeutic treatment due to off-target side-effects is well documented, resulting in physical, psychological and social implications for the patient (128). Locoregional chemotherapeutic administration is emerging as a potential treatment pathway, which may improve rates of success, with concomitant reduction in side-effect profiles (129).

IO has developed as a new sub-specialty of interventional radiology. IO utilises image-guided techniques to perform minimally invasive procedures in the treatment of cancer. Imaging is used in the diagnostic, treatment and post-treatment stages of patient care (130, 131). Though a relatively new field, IO is a rapidly expanding area with the initial focus being directed towards hepatocellular carcinoma (HCC). Two-thirds of the IO related articles published between 1996 and 2008 were on the

topic of IO applications in liver cancer. IO in LC is particularly important in the field of diagnostics. Its therapeutic value is becoming more prominent with the advent of advanced imaging modalities and medical devices facilitating the minimally invasive procedures (132, 133). There are a range of procedures now in clinical practice which fall under this sub-specialty, including ablation and embolisation, which centre on direct treatment of the tumour under image guidance, and these will be discussed further below in Sections 1.4.1 – 1.4.3.

1.4.1 Ablative procedures

Ablative procedures can be divided between chemical and energy-based ablation. Chemical ablative procedures include the IT injection of absolute ethanol or acetic acid under image guidance. This technique is most commonly used in the treatment of liver cancer. Successful treatment of liver cancer using alcohol ablation has been reported for treatment of small tumours (less than 3 cm). Treatment schedules call for frequent dose administration, with up to four to eight sessions required once- or twice- weekly. Other limitations associated with alcohol ablation are uneven tumour distribution and a high recurrence rate (up to 43% of cases) (134). Alcohol ablation was recommended as the standard of care for interventional ablative treatment of liver cancer for many years but newer ablative techniques, such as radiofrequency ablation (RFA), are overtaking it as the ablative treatment of choice (135).

Energy-based ablative interventions were previously referred to as thermal ablation. This term had to be broadened to encompass newer technologies which do not utilise the application of extreme temperatures to the tumour site to achieve ablation, such as irreversible electroporation (IRE) (136). Thermal ablation procedures, using high (over 60°C) or low (less than -40°C) temperatures, are utilised to bring about tumour tissue destruction (137). RFA and microwave frequency ablation (MFA) are techniques which utilise heat to induce cell death. Initially, both techniques were developed for the treatment of liver carcinoma, but their application in LC is also being investigated (138). The use of RFA is restricted in certain tumours because it cannot be used to treat tumours close to vasculature. It is also associated with decreased efficacy in large tumours. RFA is suitable for the treatment of tumours located in the outer two-thirds of the lung parenchyma (139). MFA is more suited to treatment of a larger tumour mass due to greater ablation zones than RFA, but adoption of this technique into clinical guidance requires more clinical evaluation (139, 140). The aerated nature of the lung limits the conductivity of RFA, but improves the mechanism of MFA (141).

A prospective, intention-to-treat, single-arm, multicentre clinical trial evaluated the effectiveness of RFA treatment in LC patients (142). This clinical trial found that a complete tumour response was elicited in a high proportion of patients for the duration of a 2 year observation period following treatment. RFA has been proposed to be most successful for the treatment of lung tumours with a diameter of less than 3 cm (143). A retrospective study of 69 cases of MFA treatment of LC determined that its efficacy may also be limited by tumour size. This study concluded that tumours with a diameter of greater than 4 cm were more likely to continue to progress after MFA treatment (144). Both RFA and MFA treatment of lung tumours have excellent side effect profiles, with pneumothorax listed as the most common complication for both procedures (145, 146).

Percutaneous cryoablation employs freeze-thaw cycles to induce cell death and also relies on the recruitment of inflammatory cytokines to the treatment site (140). Cryoablation has been found to be effective in treatment of early stage NSCLC (77 – 88% survival after 3 years) and to improve overall survival (OS) rates in late stage LC when compared to palliative treatment (median OS: 14 months following cryoablation vs 7 months following palliative treatment) (147, 148).

IRE is a non-thermal energy-based ablation technique, which is proposed to improve tumour tissue selectivity and consistency of treatment, compared to thermal ablative procedures. Currently, IRE procedures are only recommended in the context of research by NICE guidelines. The guideline surrounding the procedure states that more evidence is needed to support the claim that IRE has improved tumour tissue selective targeting, compared to other ablative procedures (149). IRE involves the application of short electrical pulses to the tumour, which creates permanent nanopores in the cell membrane, thereby disrupting the cellular homeostasis, resulting in cell death (150). NanoKnife® system is a FDA cleared medical device which consists of an IRE generator, and up to six probes, with the procedure being carried out under CT or ultrasound (US) guidance. It has clearance for the ablation of soft tissue, but it is not specified for a particular condition (151).

To date, the studies conducted on thermal ablation techniques for LC applications have had small patient sample sizes, which limits the validity of results. Larger patient trials need to be conducted in order to determine the overall efficacy and safety of these treatments. A limitation of these techniques is the small tumour

dimensions required for success (3 – 4 cm). Thermal ablation treatment may not be appropriate for patients in the T2b and above categories based on the 8th edition of the TNM classification system, and therefore other treatments must be utilised. One study determined that approximately 45.7% of all patients included in the analysis (n=1272) had a tumour diameter of greater than 3 cm (152), indicating that a sizeable proportion of LC patients do not fall within the acceptable range for this procedure.

1.4.2 Embolisation procedures

Transarterial embolisation (TAE) is a technique commonly used in the treatment of HCC. It involves the placement of a catheter in the tumour-supplying arteries, which arise from the main hepatic artery. This is done with a view to delivering an embolic agent to cut off blood supply to the tumour mass, which will result in ischemia and cell death. The liver is well vascularised, and as such, other blood vessels can maintain adequate blood supply to the rest of the organ (153). This may be a limiting factor in the translation of this technique to other tumours, since a well vascularised organ is required to ensure that healthy tissue is not compromised. A modification of the TAE procedure is known as transarterial chemoembolisation (TACE). This involves the delivery of chemotherapeutics in a drug carrier, usually ethiodized oil, during the embolisation procedure (154).

Polymeric drug delivery platforms have been proposed to improve sustained release of locally administered chemotherapeutics (129). Drug eluting beads (DEB) are polymeric microparticles which can be delivered using the TACE procedure (DEB-TACE). Once delivered via catheter, the DEBs can act to block tumour-supplying blood vessels, while simultaneously delivering loaded chemotherapeutics (155). The DEB-TACE technique was developed in order to account for the inconsistent delivery of chemotherapeutics using conventional TACE (cTACE) procedures.

A number of commercially available drug-loaded microspheres have received CE marking in Europe, although none have been approved by the FDA. These include DC Bead (BTG, UK), HepaSphere™ (also known as QuadraSphere in US, Merit Medical, USA), LifePearl® (Terumo, Japan) and Embozene TANDEM (Boston Scientific, USA). These DEBs are available in a range of sizes, from 70µm – 800µm. DC Bead is the most commonly used chemoembolic used in clinical practice (156). DC Beads are composed of a polyvinyl alcohol hydrogel, which has

modified sulfonate groups. Drug-loading is achieved by ionic interaction of the positively charged chemotherapeutic drugs to the negatively charged sulfonate group on the DC Bead (157). Commercially available DC Beads range in size from 70µm – 700µm. The first clinical trials employed using DC Beads utilised the larger size range (500µm – 700µm) (158), with the smaller size range tending to be the preferred product in more recent years (159). The smaller size range is said to improve distal tumour penetration, without increasing the risk of off-target embolism, a side-effect which had previously been a limiting factor in the use of these smaller microspheres (160). Size of bead, chemotherapeutic chosen and dose of chemotherapeutic all affect loading times recommended by the manufacturer. Doxorubicin and irinotecan are the only drugs currently indicated for DEB-TACE treatment. A limitation of this loading method is that chemotherapeutics without a positive charge cannot be loaded into the beads under these conditions.

Many of the clinical studies involving DEB-TACE treatment compare efficacy and safety to cTACE. A Cochrane review concluded that cTACE did not improve health-related quality of life outcomes (153), and DEB-TACE seeks to improve on this through sustained release of the loaded therapeutics. The first results from clinical investigations involving DEBs were published in Europe (n=27) and Asia (n=15 Phase I, n=20 Phase II) in 2007 (158, 161) and in America in 2009 (n=20) (162). These three trials were small, single arm investigations into the safety, efficacy and technical feasibility of DEB-TACE treatment. In the period since these initial trials, single armed studies have continued to populate the clinical evidence gathered to support IO integration into clinical practice (163).

Application of chemoembolisation in LC is currently being evaluated. Vogl *et al.* (2005) conducted a small interventional study to evaluate the effectiveness of pulmonary arterial chemoembolisation (PACE) in LC metastases (n=23). They found that 8 patients had a reduction in tumour volume, 6 patients had no increase or decrease in tumour volume, and 9 patients had disease progression following treatment. This study was limited in sample size and lack of control group for comparison (164). The application of DEB-TACE requires more evaluation for efficacy and safety in LC models.

DEB-PACE was also assessed in a sheep model using Irinotecan-loaded DEBs (DC Bead®, 300-500µm). The irinotecan DEBs were administered to the descending right pulmonary artery of a healthy sheep lung via super-selective catheterisation. Various doses of Irinotecan-loaded DEBs were assessed and

compared to direct injection of irinotecan solutions to the pulmonary artery. A significant decrease in systemic drug concentrations following DEB-based administration was observed, compared to free irinotecan administration. The authors suggest that the embolisation of the pulmonary artery with DEBs prevented the released irinotecan from “wash-out” into the systemic circulation. The irinotecan solution did not have the same protection and, therefore, the drug solution was more easily carried to systemic circulation. None of the treatment-limiting toxicities normally associated with systemic irinotecan treatment in humans, such as severe diarrhoea and neutropenia, were observed in the DEB treated animals, which may be associated with the reduced systemic concentration (165). These studies demonstrate the feasibility of DEB-PACE in LC.

1.4.3 Intratumoural administration

Direct injection of the chemotherapeutics into the tumour mass is known as IT instillation. This technique aims to deliver the chemotherapeutics only to the site of action, thereby reducing the off-target side-effects commonly associated with traditional chemotherapy. *In vivo* animal studies have shown that direct IT instillation of chemotherapeutic solution can deliver more than 10 – 30 times the IV dose, with minimal side effects (57). Celikoglu *et al.* (2006) demonstrated that IT administration of up to 40 mg of cisplatin (4 mg/ml) was safe and feasible using endobronchial access to lung tumours as a debulking method prior to surgery (n=17) (166), or irradiation (n=23) (167). Subsequent to this, they published a detailed protocol on IT administration to lung tumours (57). 20 mg of cisplatin (1 mg/ml solution) was administered to patients with NSCLC (n=15) and determined to be a safe and feasible method of palliation of these tumours (168). Schmidt *et al.* (2013) demonstrated that IT administration of cisplatin to NSCLC tumours could also incorporate direct treatment of lymph nodes associated with the tumour (169). Treatment of lymph nodes is proposed to impact the metastatic processes of LC. Lymph nodes associated with the tumours may also benefit from the “non-direct treatment” following drainage of IT administered chemotherapeutics during clearance (170). 10 mg of cisplatin was also delivered in 20 – 30 ml of a 5% ethanol solution using 22G needles and percutaneous access to lung tumours in repeated cycles of weekly IT administration (171). The authors of this study indicated that IT treatment, combined with second line chemotherapy, suggested improved survival, although this conclusion should be interpreted with caution due to the small sample size (n=17). Treatment was also observed to be well tolerated. IT cisplatin (1 mg/ml)

was investigated in the treatment of isolated hilar and mediastinal recurrence of LC following radiation, with 69% of patients treated responding to treatment (n=35). A multi-centre trial (n=88) assessed the effects of IT administration of paratoluenesulfonamide in ethanol for palliation and debulking of severe malignant airway obstruction, and found it to prolong survival, with minor normal tissue damage (172). More recently, IT administration of viral-based treatments for LC has been assessed. A Phase I trial investigating IT administration of autologous dendritic cells transduced with an adenoviral vector expressing the CCL21 gene for LC patients observed that 25% of patients had stable disease after 56 days, although the small sample size once again limits the reliability of results (n=16) (173). IT administration of adenoviral p53 was also investigated in a Phase I clinical trial, and determined to be safe and feasible (n=15) (174).

While clinical investigations to date provide proof of concept, and support the safety and feasibility of the IT approach, the small sample sizes involved limit the conclusions that can be drawn with regards to efficacy. Another issue facing direct IT instillation of chemotherapeutic solutions is the rapid clearance of these drugs from the tumour site, which results in inaccurate and unpredictable dosing. Attention has turned to the development of drug delivery systems, which can facilitate sustained release of chemotherapeutics from inside the tumour. Thermoresponsive hydrogels are one such drug delivery platform suitable for IT administration (175). As outlined in Section 1.2.3, the *in situ* gelation of thermoresponsive hydrogels facilitates an increased retention time, allowing for sustained release of chemotherapeutics at the site of action.

1.4.4 Pre-clinical investigations of thermoresponsive hydrogels for intratumoural administration

Various studies have investigated the efficacy of IT delivery of drug-loaded thermoresponsive hydrogels in pre-clinical models of a variety of solid tumours. Single and multi-drug-loading of thermoresponsive hydrogels has been investigated, in order to ascertain the efficacy of locoregional sustained release of chemotherapeutics from within the tumour.

P407 thermoresponsive hydrogels are commonly employed as drug delivery platforms for IT administration to solid tumours, with the superiority of this treatment modality compared to systemic administration established in a number of pre-clinical models of solid tumours (176-179). Other thermoresponsive hydrogels have

also been investigated, including poly(ethylene glycol)-*b*-poly(caprolactone-co-lactide) diblock copolymer loaded with doxorubicin or 5-fluorouracil. A single IT injection of these drug-loaded thermoresponsive hydrogels resulted in greater or equivalent tumour growth suppression as repeated systemic administration of the same drug solution (180, 181). Preferential accumulation and retention of paclitaxel in tumour tissue following IT administration of a paclitaxel nanoparticle-loaded thermoresponsive hydrogel was observed *in vivo*, compared to the IT or systemically administered paclitaxel solution (182). IT delivery of dual drug-loaded thermoresponsive hydrogels has also reported improved efficacy and side-effect profiles (178, 183), with the challenge associated with multi-drug-loading well documented (52).

1.4.5 Clinical investigations of thermoresponsive hydrogels for intratumoural administration

A number of clinical trials involving IT delivery of thermoresponsive hydrogels have evaluated their potential in the treatment of solid tumours, although successful translation into clinical practice has not yet been established.

OncoGel™ (Protherics, Salt Lake City, USA) is a paclitaxel-loaded thermoresponsive hydrogel, based on the Regel polymer. ReGel is a triblock copolymer comprised of PLGA–PEG–PLGA. ReGel increases the solubilisation of hydrophobic drug molecules, like paclitaxel, due to formation of micelles with hydrophobic cores. In clinical studies, OncoGel™ was prepared for administration in a single-use syringe, with varying paclitaxel concentrations. Dose related toxicity was seen at the local site of administration but no systemic toxicity was reported (184). OncoGel™ was administered as an adjunct to radiotherapy in a Phase II clinical trial for treatment of patients with inoperable oesophageal cancer. Increasing doses of paclitaxel (0.48 – 2 mg of paclitaxel/tumour cm³) administered IT using OncoGel™ were well tolerated, and it was reported that, in conjunction with radiotherapy, OncoGel™ was clinically effective at reducing tumour burden (185). A Phase IIb clinical trial (NCT00573131), comparing local administration of OncoGel™ to oesophageal tumours prior to systemic chemotherapy and concurrent external beam radiation to the same treatment without OncoGel™, was prematurely terminated due to lack of improved efficacy in comparison to the control group. The authors of this study concluded that while locoregional delivery of OncoGel™ was feasible and safe, efficacy over current therapies could not be established (55).

MitoGel™ (Urogen Pharma Ltd., Israel) is a mitomycin C (MMC)-loaded thermoresponsive hydrogel, based on the RTgel (TC-3 gel) technology. This technology (proprietary information) has been developed for the treatment of bladder diseases, and has been loaded with other therapeutics, including Botulinum Toxin, for a number of indications. MitoGel™ is proposed for use in the treatment of low-grade, non-muscle invasive upper tract urothelial carcinoma (UTUC) (186). The technical feasibility and safety of MitoGel™ administration has been evaluated in a preclinical swine model (61). A pivotal, open-label, single-arm Phase 3 clinical trial, the OLYMPUS study, was commenced in April 2017 (NCT02793128). This clinical trial was approved by the FDA, based on findings submitted from the ongoing investigator-initiated compassionate use programme, in relation to the safety and efficacy of this technology (186). The compassionate use clinical trial is classified as an expanded access trial for an individual patient, between 76 and 77 years of age (NCT02701023). The total duration for this study was set at three months, and at date of writing no results have been released (56). Vesigel is another MMC-RTgel thermoresponsive hydrogel developed by Urogen™ with some initial clinical studies indicating its potential in the treatment of low grade non-muscle invasive bladder cancer.

A non-thermo-responsive injectable cisplatin/epinephrine purified bovine collagen gel (IntraDose®, Matrix Pharmaceuticals, CA, USA) designed for IT administration received orphan drug designation for treatment of recurrent squamous cell head and neck cancer in 2000. Human trials progressed to Phase III randomized, double-blind, placebo-controlled, multi-centre trials. The FDA, however, denied the “New Drug Application” (NDA) based on the lack of objective clinical efficacy. The experimental design was also called into question, as the statistical significance of the primary endpoint was determined from the pooling of data from two studies. The primary endpoint was “patient benefit” and the NDA reviewers were of the view that this was not well correlated with tumour response (54). Use of non-traditional primary endpoints is a common feature of IO clinical trials, and a significant challenge exists in demonstrating sufficient evidence to gain regulatory approval based on these alternative endpoints (163).

An excellent review by Franklin *et al.* (2014) explores the challenges facing clinical trials in IO. One of the most interesting points raised by the authors is the difference between efficacy, as measured by disease response to the intervention, and clinical effectiveness, which encompasses efficacy, but also takes into account the patient

benefit. They note that it is clinical effectiveness which prompts changes in clinical practice (163). The outcomes commonly selected in clinical trials for traditional oncology treatments are often not applicable in IO. Generally, OS is recognised as the most important primary endpoint in oncological clinical trials, but this may not be the most relevant measure of treatment success in IO trials. Local tumour response (e.g. time to tumour progression, and quality of life of patient undergoing treatment) may prove to identify the benefit of drug delivery using IO procedures, and locate the speciality more firmly in clinical practice. It has also been noted that clinical trials in IO are limited by small sample sizes, non-blinding of clinicians due to technical requirements of the procedure, and lack of control groups. Innovation is required in trial design and patient recruitment to ensure that robust, well designed clinical trials are carried out (187).

1.5 Aim and objectives

It was hypothesised that a chemoablative, thermoresponsive hydrogel could be formulated as a dual drug delivery platform for IT administration to LC.

The aim of this thesis was to develop, characterise and evaluate a novel dual drug-loaded thermoresponsive hydrogel for use as an IT drug delivery platform in LC.

The main objectives of this thesis were to:

Objective 1: Optimise and characterise a novel thermoresponsive hydrogel containing cisplatin and paclitaxel (*Chapter 2*)

Objective 2: Assess the *in vitro* cytotoxicity of the blank and drug-loaded thermoresponsive hydrogel in a 2D and 3D model of a human lung cancer cell line (A549 cell line), and in a non-cancerous cell line (3T3 Balb/c clone A31 cell line) (*Chapter 3*)

Objective 3: Evaluate the translational reality of thermoresponsive hydrogels for IO procedures, and modify the lead blank and drug-loaded formulations to address selected clinical adoption and regulatory hurdles (*Chapter 4*)

Objective 4: Evaluate the acute *in vivo* retention, efficacy and off-site toxicity profiles of IT administration of lead thermoresponsive hydrogel formulations in an A549 murine xenograft model of LC (*Chapter 5*)

2.1 Introduction	64
2.1.1 Poloxamer 407	64
2.1.1.1 <i>Physicochemical properties</i>	64
2.1.1.2 <i>Biological properties</i>	66
2.1.2 2-Hydroxypropyl- β -Cyclodextrin	67
2.1.2.1 <i>Physicochemical properties</i>	67
2.1.2.2 <i>Biological properties</i>	68
2.1.3 Chitosan	68
2.1.3.1 <i>Physicochemical properties</i>	68
2.1.3.2 <i>Biological properties</i>	69
2.1.4 Genipin	70
2.1.4.1 <i>Physicochemical properties</i>	70
2.1.4.2 <i>Biological properties</i>	70
2.1.5 ChemoGel formulation	72
2.1.6 Aim and objectives	73
2.2 Materials and Methods	74
2.2.1 Formulation optimisation	74
2.2.1.1 <i>Preparation of a blank thermoresponsive hydrogel</i>	74
2.2.1.2 <i>Preparation of a paclitaxel-Cyclodextrin complex</i>	74
2.2.1.3 <i>Preparation of a dual drug-loaded thermoresponsive hydrogel</i>	75
2.2.2 Material characterisation	78
2.2.2.1 <i>Rheological assessment</i>	78
2.2.2.2 <i>Scanning Electron Microscopy</i>	80
2.2.2.3 <i>Differential Scanning Calorimetry</i>	80
2.2.2.4 <i>Macroscopic inspection of thermogelation</i>	81
2.2.2.5 <i>Disintegration studies</i>	81
2.2.3 Analytical determination of chemotherapeutics	81
2.2.3.1 <i>High-performance liquid chromatography determination of paclitaxel</i>	81
2.2.3.2 <i>Inductively coupled plasma mass spectrometry determination of platinum</i>	82
2.2.3.3 <i>Analysis of paclitaxel content in paclitaxel/HP-β-CD complex</i>	83
2.2.3.4 <i>Chemotherapeutic release studies</i>	83
2.3 Results	84
2.3.1 Assessment of rheological properties of the blank thermoresponsive hydrogel	84
2.3.2 Assessment of the effect of cisplatin-loading on the thermoresponsive hydrogel	85
2.3.3 Formulation and characterisation of the Cyclodextrin-paclitaxel complex	87
2.3.3.1 <i>Material characterisation of the paclitaxel-Cyclodextrin complex</i>	87
2.3.3.2 <i>Quantification of paclitaxel in paclitaxel/HP-β-CD complex</i>	88
2.3.4 Assessment of the effect of paclitaxel-loading on the thermoresponsive hydrogel	89
2.3.5 Characterisation of blank ChemoGel and drug ChemoGel formulations	92
2.3.5.1 <i>Rheological characterisation</i>	92
2.3.5.2 <i>Disintegration studies</i>	95
2.3.5.3 <i>Release of chemotherapeutics from dual drug-loaded formulations</i>	97
2.4 Discussion	98
2.5 Conclusion	104

2.1 Introduction

Development of a baseline thermoresponsive hydrogel consisting of P407, 2-Hydroxypropyl- β -Cyclodextrin (HP- β -CD), Chitosan (CS) and Genipin (GP) had been previously undertaken in the Kelly lab (unpublished data). However, a full understanding of the impact of variations to the formulation had not been undertaken. This section provides an overview of the main constituents of the thermoresponsive hydrogel formulation, and their function in the final product.

Excipients in pharmaceutical formulations are often defined as “inert drug carriers” that only function to modify the physicochemical features of the formulation or to improve the patient acceptability of the final formulation. However, it is now recognised that newer hydrogels are formulated with multifunctional excipients, which have the potential to augment the overall therapeutic effect of the chemical payload they are delivering (188). These excipients can facilitate a range of actions including; increased drug delivery to the site of action using targeting mechanisms, increased cellular uptake at the site of action, and exerting a pharmacological effect at the site of action.

2.1.1 Poloxamer 407

2.1.1.1 Physicochemical properties

Poloxamer copolymers are composed of triblock arrangement of ethylene oxide (EO) and propylene oxide (PO). A general formula, $EO_x-PO_y-EO_x$, is applicable to the composition of all Poloxamer formulations. The ratio of x:y defines the physicochemical properties of the product, including its hydrophilic/lipophilic nature (32). P407 is commercially available as Pluronic F127, and is subject to pharmacopoeial standards. It has a molecular weight (MW) range of 9,840 to 14,600 Da, and the PEO:PPO ratio by weight is approximately 2:1, with a HLB value of between 18 and 23 (189, 190). P407 has been defined as an “inactive” ingredient by the FDA (32).

As previously mentioned in Chapter 1, aqueous solutions of P407 exhibit thermoreversible properties at concentrations of 20% w/w and above (33). P407 exists as a micellar solution at temperatures below the characteristic sol-gel transition temperature, with micelles consisting of an extended hydrophilic PEO corona and a hydrophobic PPO core (Fig. 2.1). The formation of micelles in solution occurs at very low P407 concentrations, and the critical micelle concentration

(CMC) is also affected by temperature; the CMC of P407 at 25°C is 0.7% w/v, and is reduced to 0.025% w/v at 35°C. P407 can function as a solubiliser as methyl groups on PPO in the hydrophobic core can interact with the desired hydrophobic drug molecule via Van der Waals forces, while the hydrophilic PEO corona forms hydrogen bonds with the surrounding water to improve aqueous solubility of these drugs (28, 189) .

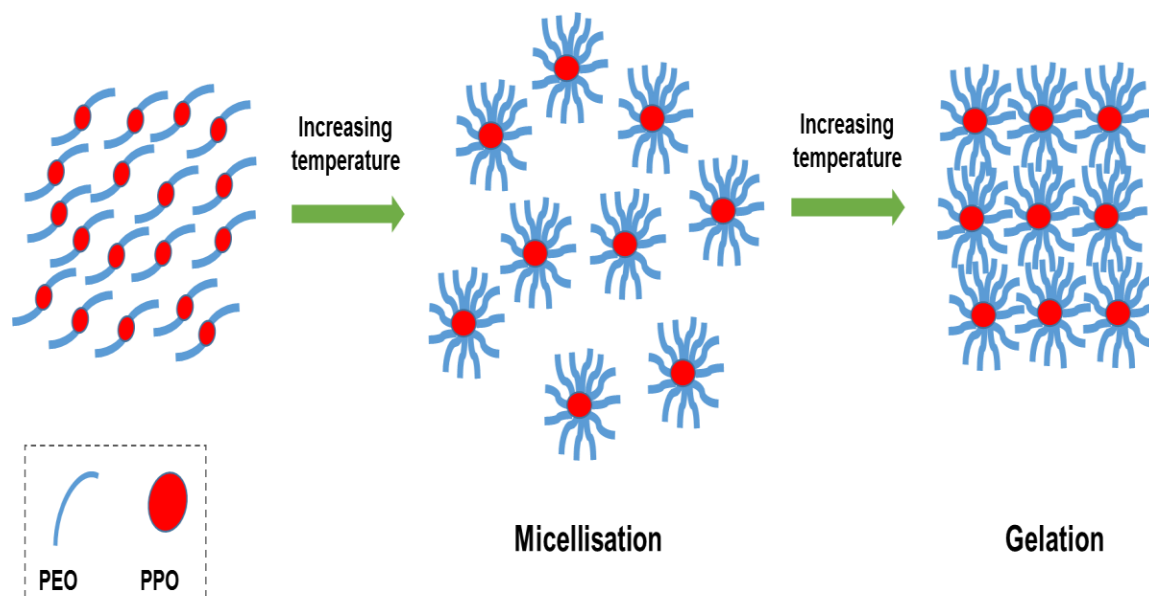


Figure 2.1 Poloxamer solutions (left) undergo micellisation (centre) and gelation (right) at characteristic concentration dependent temperatures. Adapted from (32).

P407 solutions undergo gelation as temperatures increase past the sol-gel transition temperature to form a closely packed micellar hydrogel (Fig. 2.1) (191). Increased concentrations of P407 produce higher viscosity formulations with lower sol-gel transition temperatures (30). The viscosity of the P407 formulations in the liquid state is highly dependent on both temperature and concentration, but in the gel state, the viscosity is seen to be independent of these variables (31). In general, P407 produces low viscosity formulations, and this imparts poor mechanical strength to the hydrogel, which results in fast disintegration rates *in vivo* (25). The addition of a crosslinked interpenetrating agent can be utilised to increase the strength of Poloxamer-based gels, and prolong the residence time *in vivo* (192). For example, Poloxamer hydrogels were reinforced with CS and glutaraldehyde, resulting in a significantly prolonged release profile of insulin (193). Additionally, it is possible to chemically modify the Poloxamer structure to retard disintegration rates (194).

The sol-gel transition temperature of P407 thermoresponsive hydrogels can also be modified by the addition of other excipients. Excipients in the final formulation have been found to dramatically alter the thermoreversible properties of P407 due to the effect on micelle formation and packing. In particular, salts significantly affect the sol-gel transition temperature of P407 formulations, with the addition of sodium chloride seen to decrease the critical micelle concentration and the critical micelle temperature (195). The release rates of drugs from P407 thermoresponsive hydrogels can also undergo changes following addition of salts to the final formulation (196). Therefore, careful consideration must be given to choice and concentration of excipients in P407 formulations, in order to ensure that the thermoresponsive nature is maintained.

Due to its pseudoplastic behaviour, the viscosity of P407 formulation decreases with increasing shear rates, which facilitates the use of P407 as an injectable liquid formulation at room temperature. Injected P407 can then undergo *in situ* gelation in response to the increased temperature, to form a gel bolus in the body, and increase retention of loaded drugs at the site of administration. (30).

2.1.1.2 Biological properties

P407 has commonly been suggested for use in chemotherapeutic-loaded drug delivery platforms, as it demonstrates chemosensitisation properties in multidrug resistant cancer cells. The mechanism of action of the chemosensitisation has been suggested to involve ATP depletion in the cancer cell, disruption of the microviscosity of the cancer cell membrane, interference in the drug efflux process via P-glycoprotein inhibition to increase intracellular concentration of chemotherapeutics, and the glutathione/glutathione S-transferase detoxification activity (197, 198). Doxorubicin and daunorubicin cytotoxicity was demonstrated to be increased two to three fold following administration with P407 in animal models (32). P407 was also seen to act as a chemoprevention agent, as it reduced the number of aberrant crypt foci developed in a rat model of carcinogen-induced colon cancer (199).

Intraperitoneal (IP) administered P407 in a rat model was found to be almost entirely excreted from the body in urine over a 24 h period, with accumulation of P407 observed in kidney and liver homogenates (200). The FDA summary of safety and effectiveness document for LeGoo®, a 20% w/w P407 product for endovascular occlusion, also indicates that P407 is excreted in the urine (201).

2.1.2 2-Hydroxypropyl- β -Cyclodextrin

2.1.2.1 Physicochemical properties

Cyclodextrins (CDs) are commercially available amphiphilic pharmaceutical excipients, commonly used to improve solubility of drugs with poor aqueous solubility. CDs are large molecules, with a MW range of 1,000 – 2,000 Da or greater. It has been suggested that they can self-aggregate into super-complexes, further increasing their size. They consist of cyclic oligosaccharides made up of 6 or more (α -1,4)-linked D-glucopyranoside units, produced by bacterial digestion of starch (202). Parent CDs can consist of six (α), seven (β), eight (γ), nine (δ), ten (ϵ) or more of these units. The chair conformation of the glucopyranoside units produces a truncated cone shape, characteristic of CDs. The outside of this truncated cone contains one primary and two secondary hydroxyl groups (on the wider and narrower edge respectively) which impart the hydrophilic nature to the CD molecule. The inner cavity has higher hydrophobicity and this facilitates complexation of hydrophobic molecules to the CD (Fig. 2.2 A). (203, 204). According to the Biopharmaceutical Classification System (BCS), Class II or IV drug molecules are drugs with poor aqueous solubility, accompanied by high or low permeability respectively. The use of CDs to improve aqueous solubility facilitates these drugs to act more like Class I molecules (high solubility, high permeability) (203).

Parent CDs have relatively poor aqueous solubility and contain large amounts of hydrogen bond donors and acceptors, which imparts poor bioavailability characteristics. CD parent molecules are chemically modified for use as pharmaceutical excipients by substituting the hydroxyl groups on the parent molecule with an alternative group, such as an alkyl or hydroxyalkyl groups. HP- β -CD is a commercially available chemically modified CD, which involves the substitution of one to three of the available hydroxyl groups on the parent β -CD with hydroxypropyl groups (Fig. 2.2 B) (205).

The incorporation of HP- β -CD in P407 formulations has been shown to increase the sol-gel transition temperature in a concentration dependent manner (206). The increased gelation is proposed to be as a result of steric hindrance caused by the large size of the HP- β -CD molecule interfering with the P407 micelle network formation, as well as increased competition for hydrogen bond formation with water molecules. The ability of HP- β -CD to solubilise hydrophobic drugs, and to

manipulate the thermoresponse of the hydrogel, makes it an attractive candidate for inclusion in P407 formulations.

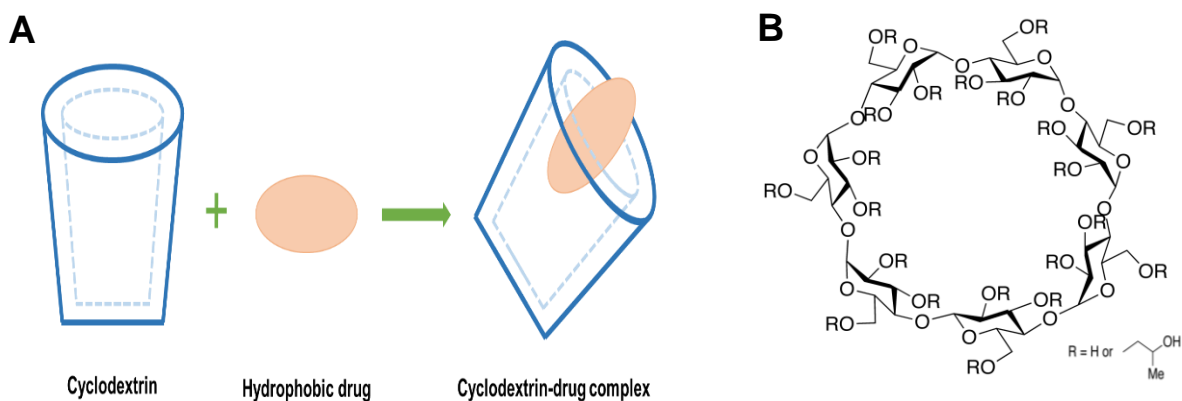


Figure 2.2 (A) Truncated cone shape of cyclodextrins, which can complex with hydrophobic drug molecules. **(B)** Chemical structure of 2-Hydroxypropyl-β-cyclodextrin.

2.1.2.2 Biological properties

It has been demonstrated that HP-β-CD can act as an anti-cancer agent in its own right (207). Yokoo *et al.* (2015) hypothesised that the mechanism of action may involve HP-β-CD mediated interference with cholesterol homeostasis. They propose that the increased cholesterol demands of a rapidly proliferating cancer cell make this cell type more vulnerable to HP-β-CD directed cytotoxicity, although they acknowledge more work is required to elucidate the exact mechanism (208).

HP-β-CD is almost exclusively eliminated unchanged by the kidneys following oral administration, and is considered non-toxic at low to moderate oral and IV doses (203). 1 g of HP-β-CD administered orally for one week has been shown to demonstrate no adverse effects in humans (209). This low toxicity profile situates CDs as a preferred solubilisers to organic solvents, which are commonly associated with significant off-site toxicity profiles (210).

2.1.3 Chitosan

2.1.3.1 Physicochemical properties

CS is a polycationic polysaccharide derived from chitin, which is found in the exoskeleton of many crustaceans, insects and fungi. Deacetylation of the chitin units produces repeating units of glucosamine (β(1-4)-linked 2-amino-2-deoxy-D-glucose) and N-acetylglucosamine (2-acetamido-2-deoxy-D-glucose) (Fig. 2.3). The quality of CS is defined by pharmacopoeial standards. The degree of

deacetylation (DD) is defined as the ratio of glucosamine units to N-acetylglucosamine units. The broadly accepted definition of CS is a DD of 70% or more, with chitin being defined as a DD of 20% or less (211, 212).

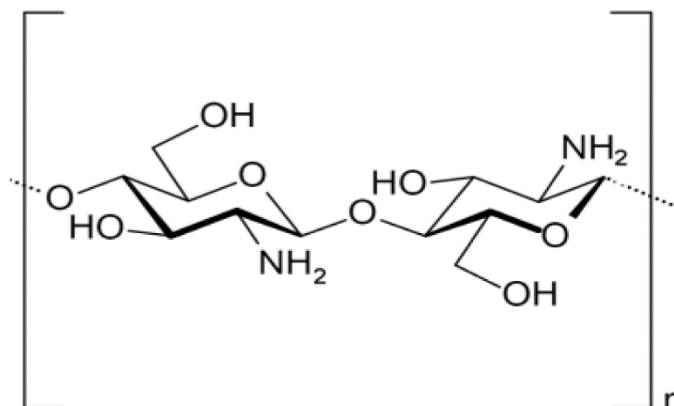


Figure 2.3 Chemical structure of Chitosan (213).

The physicochemical properties of CS are highly dependent on the DD and MW of the CS produced. The hydrophilicity, hygroscopicity and viscosity are all mediated by the DD and MW (211). It is of critical importance that these parameters are well defined during production to ensure uniformity of products. The rate of degradation of CS is also controlled by these parameters. The *in vitro* degradation of CS, using a β -glucosidase enzyme, demonstrated that CS products with higher DD and MW demonstrated a slower rate of enzymatic degradation (214). Increasing DD and MW produces a more tightly packed structure, which reduces the capacity of CS to imbibe water, thus reducing the rate of degradation in acidic, aqueous environments (211). CS can undergo crosslinking via a number of different methods; chemical, radiation or physical, depending on the molecule used. (215). The disintegration time of P407 hydrogels has been shown to be increased by the addition of CS and an additional crosslinking molecule (216).

2.1.3.2 Biological properties

CS is widely considered to be biocompatible, with a wide variety of applications in tissue engineering, wound healing and as an antimicrobial (217). The apparent pK_a of the amino group is 6.5, and therefore, in acidic environments, the amino group is positively charged ($-\text{NH}_3^+$). This facilitates the binding of CS to the negatively charged sialic acid, present in mucin, and prolongs retention time (218, 219). Localised delivery of CS-based drug delivery systems benefits from this property, as the retention time will be increased at site of action. CS has been shown to

improve absorption through tight junctions in the epithelial layer, and therefore may improve uptake of drugs delivered (211, 212).

CS has also been shown to have cancer cell-directed cytotoxicity. One study demonstrated that treatment with CS induced cell death *in vitro* in an oral cancer cell line (Ca9-22), but not in a non-cancerous human keratinocyte cell line (HaCaT). Authors of this study propose that the cancer cell-directed cytotoxicity was as a result of apoptosis and cell-cycle arrest in the CS treated cancer cells (220). Gastric cancer cells (MGC803) treated *in vitro* with CS nanoparticles also demonstrated apoptotic cell death (221). CS treatment of *in vitro* melanoma cell lines determined that upregulation of pro-apoptotic mediator Bax, and down regulation of anti-apoptotic mediators Bcl-2 and Bcl-XL, could be responsible for the cytotoxic effects, with varying degrees of efficacy seen across the three cell lines evaluated (222). Efficacy of CS nanoparticle treatment was also established in *in vivo* murine models of sarcoma and liver cancer (223).

2.1.4 Genipin

2.1.4.1 Physicochemical properties

GP is a metabolite of geniposide, which is found in dried fruit of the Gardenia plant. This plant has been used in traditional Chinese medicine as a treatment for a myriad of ailments, including headache, fever, jaundice, hepatic disorders and diabetes (224, 225). In recent years, attention has been brought to the metabolite, GP, as a “non-toxic” and “natural” alternative crosslinker in pharmaceutical formulations.

GP can be employed as a chemical crosslinker, to impart improved mechanical properties and disintegration profiles to pharmaceutical formulations. Chemical links are formed by irreversible covalent linkages between GP and the biomaterial to be crosslinked (192). GP is thought to react with amino groups on CS through nucleophilic attack in order to establish these crosslinks (Fig. 2.4) (226). It is commonly investigated as a crosslinking agent for CS and gelatin formulations, fixing agents used in tissue grafts and scaffolds for tissue regeneration (227-229).

2.1.4.2 Biological properties

GP has been found to induce apoptosis in cancer cells and sensitise cancer cells to chemotherapeutics (230). The cytotoxic capacity of GP is thought to arise from its interaction with Uncoupling Protein 2 (UCP2) in tumour cells. Under normal homeostatic conditions Reactive Oxygen Species (ROS) is produced in response

to hypoxia. Cancer cells attempt to decrease ROS production, which threatens their survival, by activating UCP2 found on the surface of mitochondria (230). The UCP2-mediated reduction in ROS production facilitates maintenance of the hypoxic TME, and thus potentiates tumourigenesis and treatment failure (231). Increased levels of UCP2 have been identified in LC cells, as well as in ovarian, breast, bladder, oesophagus, testicular, colorectal, kidney, pancreatic and prostate tumours and leukaemia (232). The cytotoxicity appears to be tumour cell selective as L929 fibroblast cells treated with GP crosslinked CS have demonstrated ability to undergo normal functions of attachment and growth (233). The *in vitro* expression of UCP2 in an A549 NSCLC cell line was found to have a dose-dependent increase in response to the levels of hypoxia induced in the model. UCP2 knockdown in this *in vitro* A549 model was also found to result in increased apoptosis (231). As mentioned in Chapter 1, various tumourigenesis mediators, such as HIF1 α and VEGF are increased in the hypoxic TME, and GP was shown to reduce the accumulation and expression of these mediators *in vitro*, which subsequently reduced the invasive capacity of the cancer cells (234). *In vivo* studies have also demonstrated the inhibitory effect of oral GP treatment on tumour burden, which is proposed to have been as a result of interference with cytokine production and recruitment of tumour associated macrophages (235).

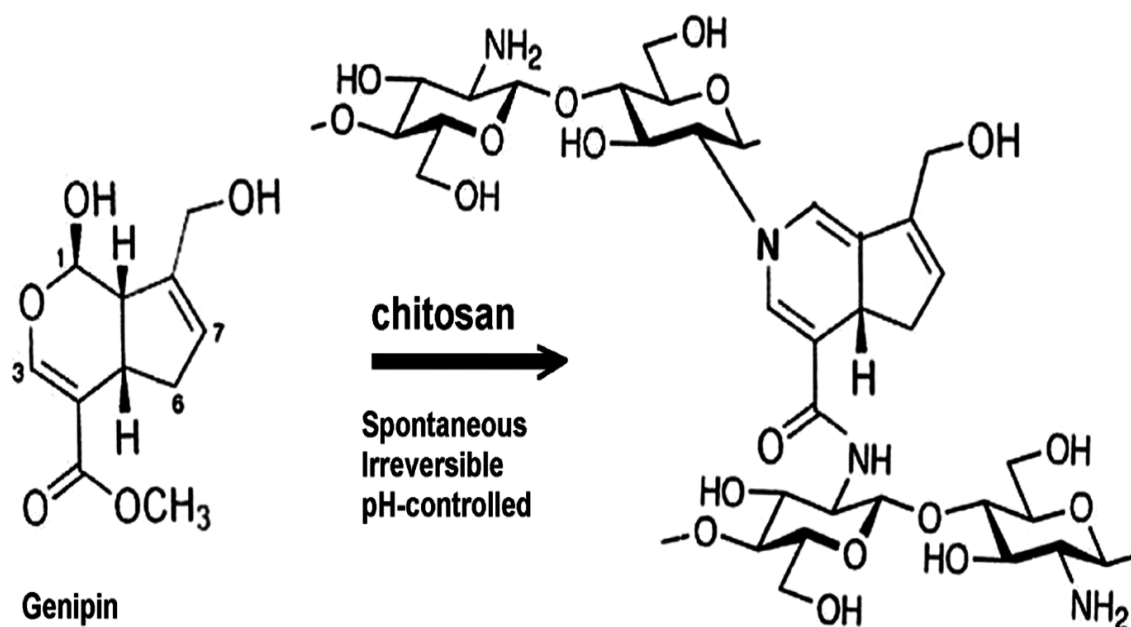


Figure 2.4 Chemical structure of Genipin (left) and Genipin crosslinked Chitosan chains (right). Adapted from (236).

2.1.5 ChemoGel formulation

As outlined above, each of the excipients included in the ChemoGel formulation has a multifunctional purpose, with physicochemical and biological effects relevant to the treatment of solid tumours using drug-loaded thermoresponsive hydrogels.

P407 functions as the main thermoresponsive constituent of the formulation. The solubilisation properties of P407 will be used to increase the solubilisation of the cisplatin and paclitaxel drugs loaded into the final formulation. The promotion of the cytotoxic mechanism of these drugs may also increase the effectiveness of the drug delivery platform. The pseudoplastic nature of P407 will facilitate IT injection.

HP- β -CD will be used to aid the solubilisation of the paclitaxel. The aqueous solubility of paclitaxel has been documented as 0.4 μ M or 0.34 μ g/ml, and complexation with CDs has been shown to increase this (237). HP- β -CD will be used to manipulate the sol-gel transition temperature of the formulation, to ensure it remains within a clinically relevant range. HP- β -CD may also hold potential to act as an anti-cancer agent.

CS will be used as the interpenetrating net of the formulation, in order to improve the disintegration profile of P407. The mucoadhesive properties may also act to aid the retention of the drug delivery platform following gelation in the tumour, with a possible anti-cancer effect also being exerted by CS.

GP will act as a crosslinker to improve the robustness and disintegration profile of the hydrogel. It may also act to increase the cytotoxic capacity of the drug delivery system in cancer cells.

Cisplatin and paclitaxel will be loaded as hydrophilic and hydrophobic chemotherapeutics, respectively, into the ChemoGel formulation, to provide preliminary evidence to support the use of ChemoGel as a dual drug delivery platform.

This Chapter will assess the physicochemical attributes of the ChemoGel formulation, with future chapters exploring the *in vitro* (Chapter 3) and *in vivo* (Chapter 5) efficacy of treatment in LC.

2.1.6 Aim and objectives

The overall aim of this chapter was to develop and characterise a clinically relevant lead blank and dual drug-loaded thermoresponsive hydrogel for LC applications.

The specific objectives of this chapter were to:

- ◁ Optimise the rheological profile of the blank thermoresponsive drug delivery platform previously developed in the Kelly lab by modifying concentrations of excipients used, and determining the impact of excipients on the sol-gel transition behaviour of the overall formulation
- ◁ Formulate a dual drug-loaded thermoresponsive hydrogel containing “gold-standard” chemotherapeutics for LC, cisplatin and paclitaxel, which maintains a clinically relevant sol-gel transition temperature above room temperature (21°C) and below body temperature (37°C)
- ◁ Carry out physicochemical characterisation of the lead formulations, including a disintegration and release profile for the blank and dual drug-loaded hydrogel

2.2 Materials and Methods

P407 was obtained from BASF Corp. (Ludwigshafen, Germany). HP- β -CD (Molecular weight ~1396 Da), GP, Sodium Tripolyphosphate (TPP), Cisplatin, Paclitaxel, Dulbecco's Phosphate Buffered Saline (PBS) and Platinum (Pt) standard for inductively coupled plasma (ICP) were all purchased from Sigma-Aldrich (St. Louis, MO, USA). CS chloride salt (Protasan UP CL214) was purchased from FMC BioPolymer (Sandvika, Norway). Acetonitrile (HPLC grade) and Water (HPLC grade) were purchased from Fisher Scientific Ireland (Dublin, Ireland).

2.2.1 Formulation optimisation

Formulation composition and excipient concentration was modified to produce a lead blank and dual drug-loaded thermoresponsive hydrogel in a stepwise manner as outlined in Figure 2.5.

2.2.1.1 Preparation of the blank thermoresponsive hydrogel

A general formulation method was developed, and concentrations of excipients were varied as required (Table 2.1, Fig. 2.6). HP- β -CD was dissolved in deionised water (dH₂O) at pH < 6 and stirred at room temperature, for 30 min. The solution was then chilled on ice at 4°C. CS was incorporated in a few drops of dH₂O and added to the solution on the stirring plate, which was maintained at 4°C. P407 was then sprinkled into the solution while on the stirring plate, based on the "cold method" developed by Schmolka (1972) (33). This was allowed to stir for 1 h until all components were in solution. The solution was stored at 4°C overnight to allow it to hydrate. GP was added to the solution the following day, and stirred for a minimum of 4 h on ice to ensure complete dissolution. If TPP was required, this was added at the same time as GP. The solution was then weighed and made up to final weight with dH₂O. If curing was required, the solution cured for 24 h in a water bath at 37°C

2.2.1.2 Preparation of a paclitaxel-Cyclodextrin complex

Paclitaxel was incorporated into a HP- β -CD inclusion complex based on methods developed by Choi *et al.* (2014) (238). HP- β -CD was dissolved in the required amount of dH₂O on a stirring plate for 5 min at room temperature. Paclitaxel was then added to this solution and stirred at high speed for 30 min. The speed was reduced stirred for 72 h to allow for complexation to occur. The contents were frozen in a -80°C freezer for 2 h, and freeze-dried overnight using a freeze dryer and

vacuum pump at -55°C and 0.018 mbar (Labcono, MO, USA) to produce a lyophilised powder consisting of paclitaxel/HP- β -CD inclusion complexes. Depending on the hydrogel formulation the paclitaxel/HP- β -CD inclusion complexes were formulated in 100% of the final HP- β -CD content (10% w/w of final formulation) or in a ratio of 2:1 (freeze dried complex:free HP- β -CD) of the final HP- β -CD content.

2.2.1.3 Preparation of a dual drug-loaded thermoresponsive hydrogel

Cisplatin and paclitaxel were incorporated into the blank thermoresponsive hydrogel at separate points in the formulation process (Fig 2.6). Cisplatin was dissolved in the required amount of dH₂O, and the freeze-dried paclitaxel/HP- β -CD powder was added to this solution. If additional uncomplexed HP- β -CD was required, this was added to the stirring solution, and the rest of the thermoresponsive hydrogel was formulated as in Section 2.2.1.1. The final formulation of the blank and dual drug-loaded hydrogel will hereafter be referred to as blank ChemoGel and drug ChemoGel respectively.

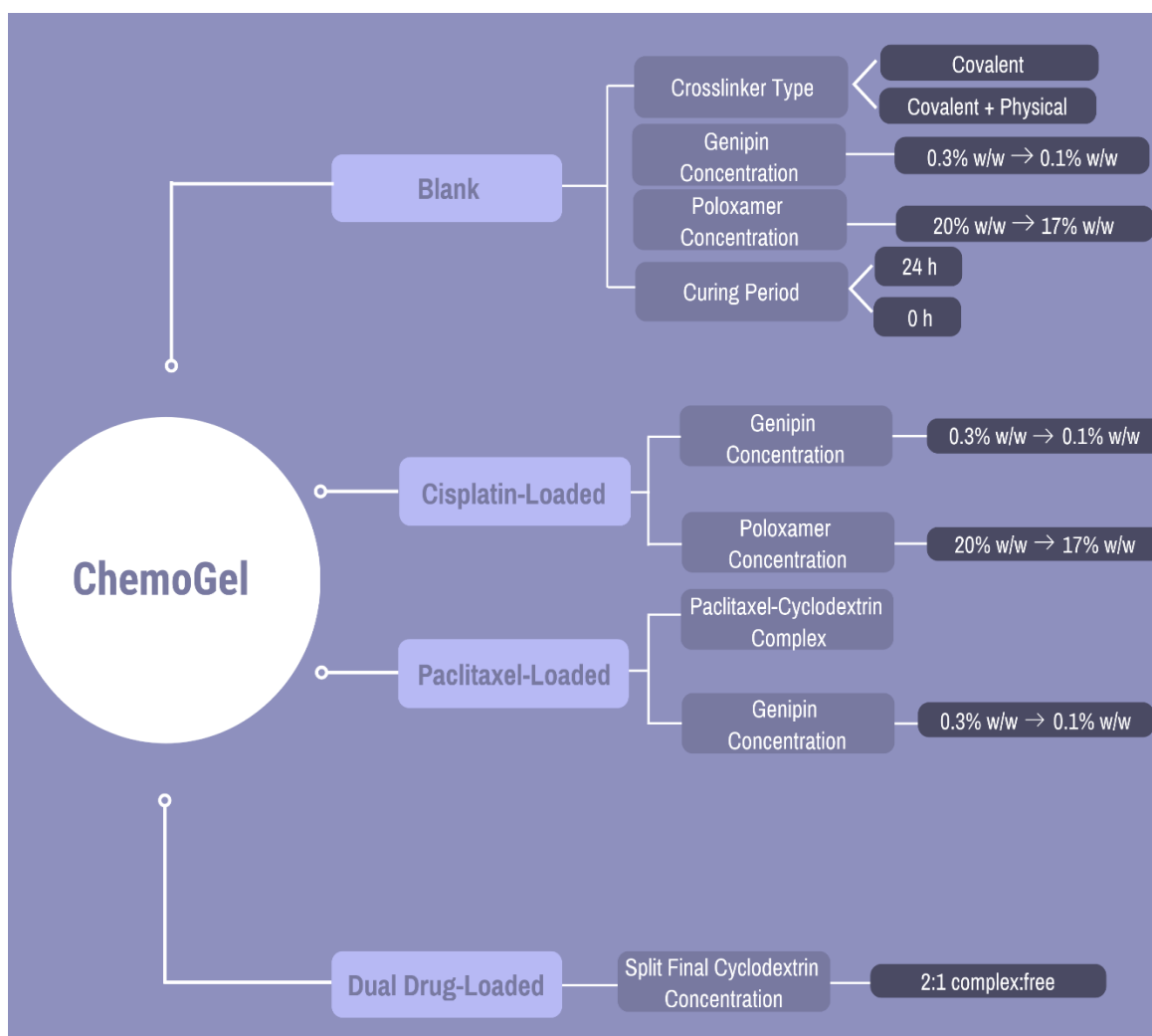


Figure 2.5 Overview of optimisation process of blank and drug-loaded thermoresponsive hydrogel.

Table 2.1 Formulation composition of preparations evaluated for thermoresponsivity. P407, Poloxamer 407; HP- β -CD, 2-Hydroxypropyl- β -Cyclodextrin; CS, Chitosan; GP, Genipin; TPP, Sodium Tripolyphosphate.

Gel formulation (GF)	% w/w					Curing period	% w/w	
	P407	HP- β -CD	CS	GP	TPP		Cisplatin	Paclitaxel
1	20	10	0.5	0.3	-	J	-	-
2	20	10	0.5	0.3	0.2	J	-	-
3	20	10	0.5	0.1	-	J	-	-
4	20	10	0.5	0.1	-	-	-	-
5	17	10	0.5	0.3	-	-	-	-
6	17	10	0.5	0.1	-	-	-	-
7	20	10	0.5	0.3	-	-	0.02	-
8	20	-	-	-	-	-	-	-
9	20	-	-	-	-	-	0.02	-
10	20	-	0.5	-	-	-	-	-
11	20	-	0.5	-	-	-	0.02	-

Gel formulation (GF)	% w/w					Curing period	% w/w	
	P407	HP- β -CD	CS	GP	TPP		Cisplatin	Paclitaxel
12	20	-	0.5	0.3	-	-	-	-
13	20	-	0.5	0.3	-	-	0.02	-
14	20	-	0.5	0.1	-	-	-	-
15	20	-	0.5	0.1	-	-	0.02	-
16	17	-	0.5	0.1	-	-	-	-
17	17	-	0.5	0.1	-	-	0.02	-
18	17	10	0.5	0.1	-	-	0.02	-
19	17	10	0.5	0.3	-	-	-	0.01
20	17	10	0.5	0.1	-	-	-	0.01
21	17	10	0.5	0.1	-	-	0.02	0.01
22	17	10 2:1 (complex:free)	0.5	0.1	-	-	0.02	0.01

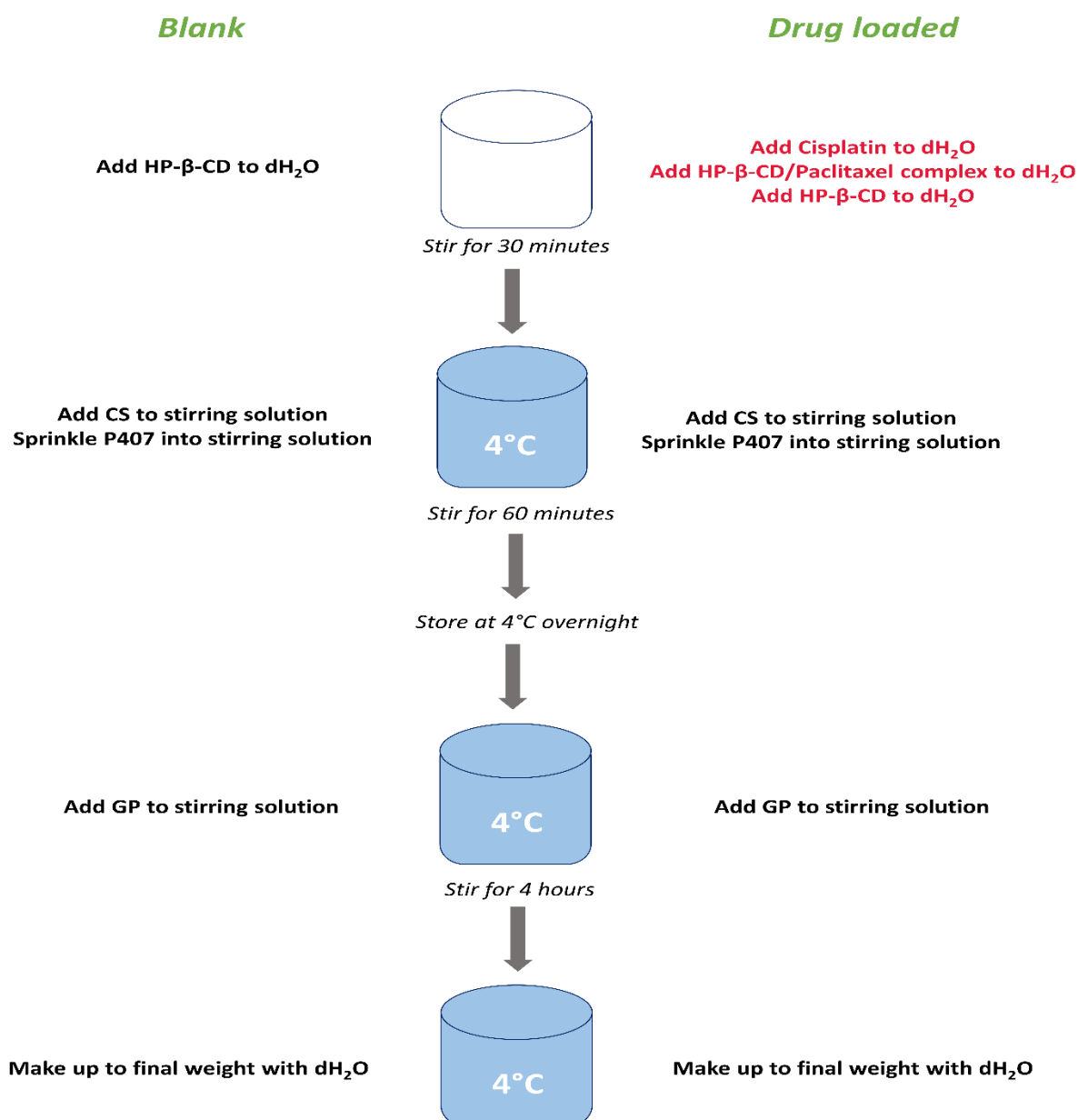


Figure 2.6 Formulation protocol for the blank and dual drug-loaded thermoresponsive hydrogel. Divergence in protocols highlighted in red.

2.2.2 Material characterisation

2.2.2.1 Rheological assessment

The rheological characteristics of the various hydrogel formulations were assessed using oscillatory measurements, performed on an AR-1000 constant stress rheometer (TA instruments, DE, USA) with built-in temperature and gap calibration. The rheometer was equipped with cone/plate geometry (40 mm diameter, 4° cone angle). Degassed samples were dispensed onto the temperature controlled

rheometer plate, pre-equilibrated to 20°C. A solvent trap, containing water, was used to cover the sample to prevent evaporation from the sample during the rheological testing. A LAUDA Ecoline 003 E100 water-bath (Lauda-Königshofen, Germany) was employed as a heat-sink for the peltier plate, which controlled temperature during testing. The temperature of the sample plate was controlled within $\pm 0.1^\circ\text{C}$ of the desired value at all times during testing. Prior to testing, the geometry gap was calibrated and rotational mapping of the geometry was performed. Following loading of excess sample, the geometry was lowered to this pre-determined gap. Excess sample was carefully removed from the peltier plate and discarded to ensure correct filling was achieved. Samples were allowed to equilibrate for 2 min before commencing testing. Data was processed using TA Data Analysis software (TA instruments, DE, USA).

Temperature sweeps from 20°C – 40°C were carried out on all formulations to screen for an appropriate sol-gel transition temperature, which was deemed to be a temperature above average room temperature (21°C – 23°C), and ideally close to body temperature (37°C). The temperature was increased at a rate of 1°C/min, with oscillatory shear stress (5 Pa) and angular frequency (1 Hz) remaining constant. All samples were analysed in triplicate. Data shown is representative of the norm.

Lead formulations were subjected to additional oscillatory rheological assessment as outlined in Table 2.2. Oscillatory stress sweeps were carried out across a range of shear stresses to determine the linear viscoelastic region (LVR) of the lead formulations in liquid and gel states, and whether deformation occurs across a range of shear stresses. The LVR is defined as the area within which the storage and loss moduli are independent of shear stress applied. All experiments were conducted on a minimum of three independent samples. Data shown is representative of the norm.

Table 2.2 Oscillatory experimental parameters for rheological characterisation of lead formulations, blank ChemoGel and drug ChemoGel.

Oscillatory Procedure	Shear stress (Pa)	Angular frequency (Hz)	Temperature (°C)	Time (min)
Stress sweep	1 - 60	1	20	N/a
Stress sweep	1 - 60	1	37	N/a
Temperature sweep	5	1	20 – 40	N/a
Time sweep	5	1	20	60
Time sweep	5	1	37	60
Time sweep	5	1	20 & 37 (Alternate every 10 min)	70

2.2.2.2 Scanning Electron Microscopy

Scanning Electron Microscopy (SEM) was performed using Supra 35VP Scanning Electron Microscope (Zeiss, Jena, Germany). Dry samples were mounted on aluminium stubs and sputter coated with a thin layer of gold prior to SEM examination. The morphology of the freeze-dried paclitaxel/HP- β -CD inclusion complex was compared to the morphology of HP- β -CD powder alone, paclitaxel powder alone and a physical mixture of HP- β -CD and paclitaxel powders. A magnification of 4.72 KX and an accelerating voltage of 5 kV was used.

2.2.2.3 Differential Scanning Calorimetry

Differential Scanning Calorimetry (DSC) was performed on a Q100 DSC (TA instruments, DE, USA). DSC was used to confirm complexation of paclitaxel and HP- β -CD. Samples were loaded into standard aluminium sample pans and the weight of each sample was recorded (< 5 mg). Pans were sealed with a sample pan press to prevent sample loss during the experiment. An empty pan was prepared in the same manner to act as a reference. A heat ramp was conducted at a rate of 10°C/min from 0°C to 300°C. Data was analysed using TA Universal

Analysis software (TA instruments, DE, USA). All samples were analysed in duplicate. Data shown is representative of the norm.

2.2.2.4 Macroscopic inspection of thermogelation

Blank ChemoGel and drug ChemoGel were observed at room temperature and following incubation in a waterbath at 37°C for 5 min to visually confirm thermogelation. Thermoresponsivity of the formulation was assessed based on the ability to transition from solution to gel, and back to solution, at appropriate temperatures. Gelation was determined to have occurred if no flow of the material was observed following inversion for 15 sec. Blue food colouring was added to the hydrogel solution to aid visual inspection.

2.2.2.5 Disintegration studies

1 g of blank ChemoGel or drug ChemoGel was added to a glass vial and submerged in a shaking water bath at 75 rpm, maintained at 37°C, for 30 min to ensure complete gelation had taken place. 1 ml of pre-warmed PBS (pH 7.4) was added to the gelled hydrogel. At pre-determined timepoints (4h, 24h, 48h, 72h, Day 5, Day 7, Day 10, Day 14, Day 21 and Day 28), PBS was completely removed from the glass vial, and the weight of the hydrogel and glass vial was recorded. The hydrogel was quickly returned to the waterbath to ensure that liquefaction did not occur, and 1 ml of fresh pre-warmed PBS was added to the glass vial. All experiments were carried out in triplicate, for three independent batches. Results are represented as the mean of the three independent experiments \pm SEM (n=3).

2.2.3 Analytical determination of chemotherapeutics

2.2.3.1 High-performance liquid chromatography determination of paclitaxel

High-performance liquid chromatography (HPLC) was conducted on an Agilent Technologies 1120 Compact LC with a UV detector (CA, USA). A chromatographic method was developed to analytically identify paclitaxel, based on a method by Kraitzer *et al.* (2008) (239). Calibration curves were produced using known concentrations of paclitaxel dissolved in the mobile phase (Appendix 1, Fig. A.1). The analytical parameters are set out in Table 2.3.

Table 2.3 Analytical parameters employed in detection of paclitaxel using high performance liquid chromatography.

Column	Synergi 4u Hydro-RP 80A (150 x 4.6 mm) (Phenomenex, Cheshire, UK)
Column temperature	Uncontrolled
Mobile phase	Acetonitrile : Water (55 : 45)
Flow rate	1 ml/min
Run time	10 min
Detection wavelength	227 nm

2.2.3.2 Inductively coupled plasma mass spectrometry determination of platinum

Inductively coupled plasma mass spectrometry (ICP-MS) was conducted on a Liberty 150 ICP-MS (Varian Inc., CA, USA) for the detection of Pt as a surrogate marker of cisplatin. Calibration curves were produced using Pt standards (1000 mg/L Pt in hydrochloric acid), diluted to appropriate parts per million (ppm) using PBS (Appendix 2, Fig. A.2). Samples were manually introduced into the ICP-MS. The analytical parameters are set out in Table 2.4.

Table 2.4 Analytical parameters employed in detection of platinum using inductively coupled plasma mass spectrometry.

Power	1.2 kW
Plasma flow	15 L/min
Auxiliary flow	1.5 L/min
Nebuliser pressure	200 kPa
Pt detection wavelength	214.423 nm

2.2.3.3 Analysis of paclitaxel content in paclitaxel/HP-β-CD complex

Whole freeze-dried paclitaxel/HP-β-CD complexes were solubilised in a known volume of the paclitaxel HPLC mobile phase and 150 μL of this was transferred into a brown HPLC vial. HPLC analysis of the paclitaxel content was performed as per Section 2.2.3.1. The percentage of the expected paclitaxel content in the freeze-dried complex was calculated as per Equation 4.

$$\text{Percentage of paclitaxel content} = \frac{\text{Paclitaxel content in sample}}{\text{Expected paclitaxel content}} \times 100 \quad (\text{Equation 4})$$

Three samples were analysed per complex from three independent batches. Each sample was analysed in duplicate. Results are represented as the mean of the three independent batches ± SEM (n=3).

2.2.3.4 Chemotherapeutic release studies

1 g of drug ChemoGel was added to a glass vial and submerged in a shaking water bath at 75 rpm, maintained at 37°C, for 30 min to ensure complete gelation had taken place. 1 ml of pre-warmed PBS (pH 7.4) was added to the gelled hydrogel, based on methods previously described (240, 241). At pre-determined timepoints (4h, 24h, 48h, 72h, Day 5, Day 7, Day 10, Day 14, Day 21 and Day 28), PBS was completely removed from the glass vial and each sample was transferred to an individual falcon tube. The hydrogel was quickly returned to the waterbath to ensure that liquefaction did not occur, and 1 ml of fresh pre-warmed PBS was added to the glass vial. Samples were stored at -20°C until analysis. Analysis of released paclitaxel was performed using HPLC as outlined in Section 2.2.3.1. Analysis of released cisplatin was performed using ICP-MS as outlined in Section 2.2.3.2 to determine quantity of Pt in the release medium. Cisplatin is composed of 65.03% Pt by weight, and therefore initial quantity of Pt was calculated by Equation 5.

$$\text{Quantity of Pt loaded} = \frac{\text{Quantity of Pt in release medium}}{\text{Initial quantity of Pt}} \times 100 \quad (\text{Equation 5})$$

All experiments were carried out in triplicate, for three independent batches. Each sample was analysed in duplicate. Results are represented as the mean of the three independent experiments ± SEM (n=3).

2.3 Results

2.3.1 Assessment of rheological properties of the blank thermoresponsive hydrogel

Initial formulation work previously carried out in the Kelly Lab produced a thermoresponsive hydrogel that underwent a sol-gel transition at 25°C (GF1, Table 2.5). GF1 – 3 underwent a curing process as part of the formulation protocol, to accelerate the crosslinking mechanism between CS and GP, and a light blue/green hydrogel was produced in these formulations after the 24 h exposure to 37°C. TPP was added to GF1 to determine if an additional crosslinking molecule would improve the strength of the hydrogel (GF2, Table 2.5). The addition of TPP resulted in an increase of the storage modulus to 21,580 Pa, with a 1°C decrease in sol-gel transition temperature to 24°C. However, an inhomogeneous appearance was observed after curing for 24 h, and so, despite the increased G', the addition of TPP was disregarded. A reduction in GP concentration to 0.1% w/w was assessed to determine the impact of GP concentration on the storage modulus (GF3, Table 2.5). The decreased GP concentration was accompanied with a corresponding decrease in storage modulus to 8,957 Pa. However, the reduced GP concentration produced a thermoresponsive hydrogel with a sol-gel transition temperature of 30°C. In an effort to reduce the length of time required for formulation, the 24 h curing period was removed from the formulation process to investigate if a suitable hydrogel could be produced at the reduced GP concentration, with no curing period (GF4, Table 2.5). The blue/green colour was not observed for the thermoresponsive solutions that did not undergo a curing period. Removal of the curing period from the formulation process produced a thermoresponsive hydrogel with a lower storage modulus at 37°C (7,428 Pa), with no change to the sol-gel transition temperature, compared to GF3. P407 concentration was then reduced to 17% w/w to investigate whether the sol-gel transition temperature could be increased further, at both GP concentrations (0.1% w/w and 0.3% w/w). GF5 demonstrated the highest sol-gel transition temperature of all blank thermoresponsive hydrogels at 33°C, but GF6 underwent a slight decrease in sol-gel temperature to 29°C, compared to GF4, which contained P407 20% w/w.

Table 2.5 Sol-gel transition temperatures and storage modulus of hydrogels prepared by varying crosslinking procedures. Data shown is representative of the norm.

	Gel Formulation (GF)					
	1	2	3	4	5	6
P407 (%w/w)	20	20	20	20	17	17
HP-β-CD (%w/w)	10	10	10	10	10	10
CS (%w/w)	0.5	0.5	0.5	0.5	0.5	0.5
GP (%w/w)	0.3	0.3	0.1	0.1	0.3	0.1
TPP (%w/w)	-	0.2	-	-	-	-
24 h curing period	J	J	J	-	-	-
Thermoresponse (°C)	25	24	30	30	33	29
G' @ 37°C (Pa)	13,210	21,580	8,957	7,428	7,679	11,380

2.3.2 Assessment of the effect of cisplatin-loading on the thermoresponsive hydrogel

Addition of cisplatin at a concentration of 0.02% w/w to GF1 produced a formulation that was in the gel-state at 20°C, GF7 (Fig. 2.7), which necessitated an assessment of the formulation to determine the reason for the loss of thermoresponsivity (Appendix 3, Table A.1).

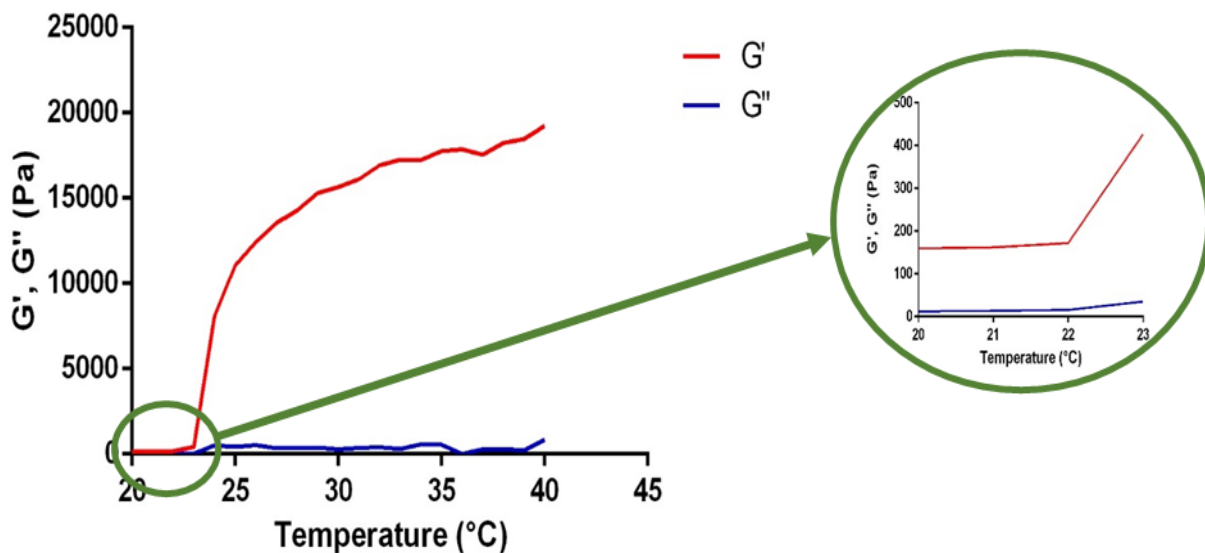


Figure 2.7 Addition of cisplatin (0.02% w/w) to GF1 resulted in loss of the thermoresponsive nature of GF7 at clinically relevant temperatures. Rheogram of temperature sweep of GF7 from 20°C-40°C $\dot{\gamma} = 100 \text{ s}^{-1}$, depicted in the magnified segment of graph (green circle). Data shown is representative of the norm.

Following this investigation, a reduction in the concentration of P407 to 17% w/w and GP to 0.1% w/w was determined to produce a cisplatin loaded thermoresponsive formulation (GF18, Fig. 2.8).

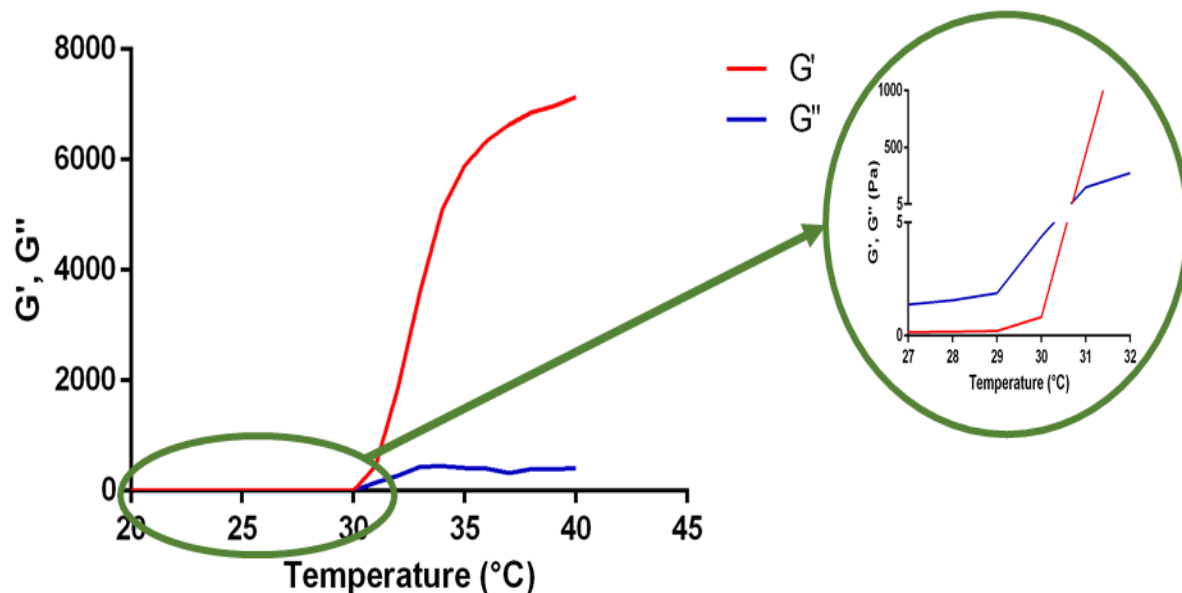


Figure 2.8 Addition of cisplatin (0.02% w/w) to GF6 produced a thermoresponsive hydrogel, GF18, at clinically relevant temperatures. Rheogram of temperature sweep of GF18 from 20°C-40°C $\dot{\gamma} = 100 \text{ s}^{-1}$, depicted in magnified segment of graph (green circle). Data shown is representative of the norm.

2.3.3 Formulation and characterisation of a paclitaxel-Cyclodextrin complex

2.3.3.1 Material characterisation of the paclitaxel-Cyclodextrin complex

The freeze-dried paclitaxel/HP- β -CD complex was produced as a white, lyophilised powder, and the morphology was investigated using SEM (Fig. 2.9). The individual morphological characteristics of the HP- β -CD and paclitaxel powders are retained following physical mixture, as the stick-like shape of paclitaxel and the spherical appearance of HP- β -CD are still clearly evident. The freeze-drying process produced a powder that was porous, and retained no similar morphological characteristics of the individual powders, indicating that successful complexation had occurred.

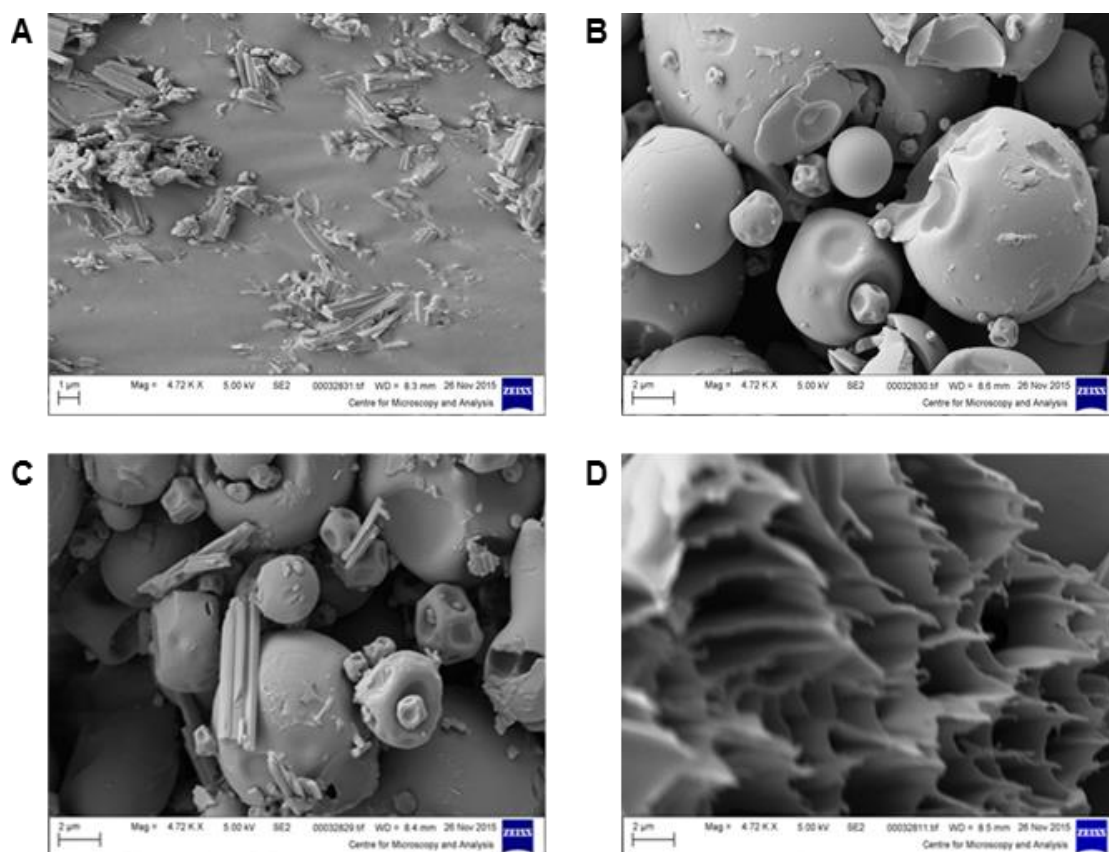


Figure 2.9 Scanning electron microscopy (SEM) qualitatively demonstrated the formation of a paclitaxel/HP- β -CD inclusion complex. Representative SEM images of (A) paclitaxel alone (B) HP- β -CD alone (C) Physical mixture of paclitaxel and HP- β -CD (D) Freeze dried paclitaxel/HP- β -CD inclusion complex.

DSC thermograms were used to determine differences between the paclitaxel/HP- β -CD complex and the raw materials. A characteristic endothermic peak maximum at 224°C and exothermic peak at 245°C were seen in the paclitaxel powder. HP- β -CD powder was seen to have a broad endothermic peak with a peak maximum at 61°C. The paclitaxel peaks were not seen in the freeze-dried complex, but were still evident in the physical mix of powders. The endothermic peak of HP- β -CD was maintained in the following complexation with paclitaxel, with a shift in the peak maximum to 70°C (Fig. 2.10).

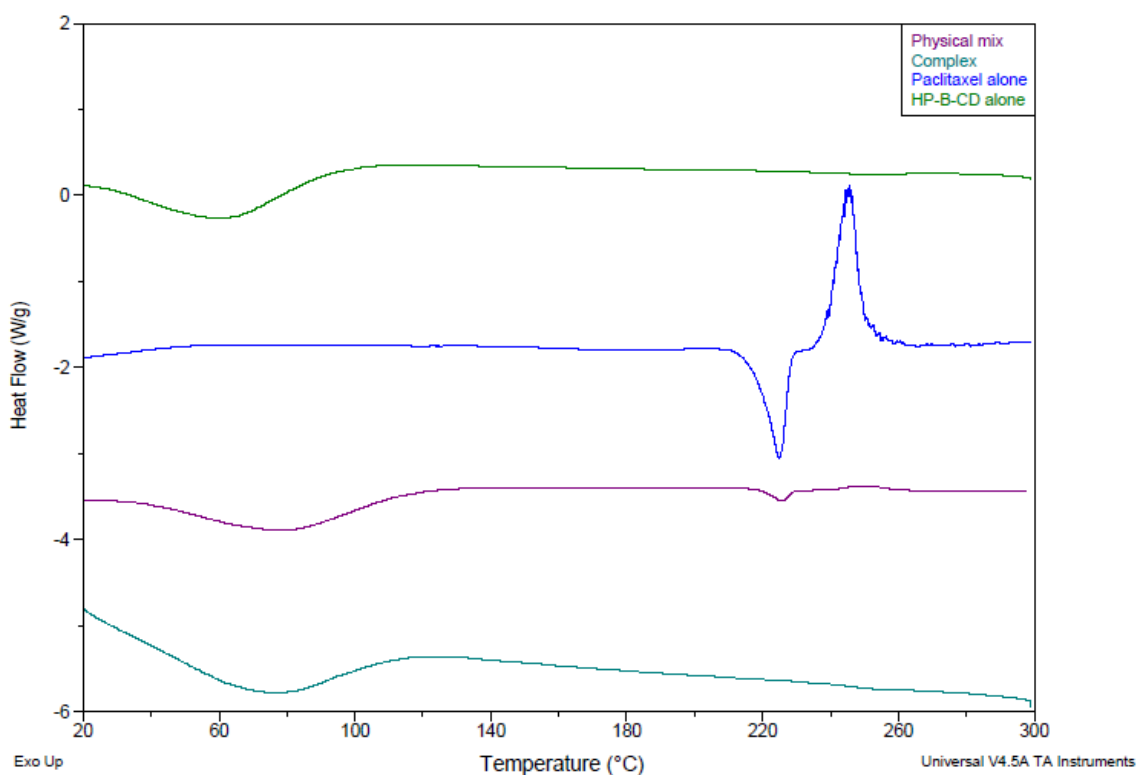


Figure 2.10 Differential Scanning Calorimetry (DSC) demonstrated complexation of paclitaxel occurs following freeze-drying with HP- β -CD. Overlay of representative DSC thermograms of HP- β -CD, paclitaxel and paclitaxel/HP- β -CD complex. Data shown is representative of the norm. Thermograms are displaced along y-axis for better visualisation.

2.3.3.2 Quantification of paclitaxel in paclitaxel/HP- β -CD complex

An investigation into the quantity of paclitaxel contained in the paclitaxel/HP- β -CD complex revealed that $95.3\% \pm 2.05\%$ of the original quantity of paclitaxel loaded was recovered after the freeze-drying process, indicating that the complexation process does not have a detrimental effect on the paclitaxel content (Table 2.6).

Table 2.6 Analytical quantification of paclitaxel in paclitaxel/HP- β -CD complex using high-performance liquid chromatography revealed almost complete recovery of paclitaxel. Data shown is represented as the mean \pm SEM of three independent batches (n=3).

Amount of paclitaxel loaded (μ g)	Paclitaxel Recovered (Mean % of initial quantity \pm SEM)
600	95.3% \pm 2.05%

2.3.4 Assessment of the effect of paclitaxel-loading on thermoresponsive hydrogel

The paclitaxel/HP- β -CD complex was added to GF5, and produced a paclitaxel-loaded hydrogel, which was not thermoresponsive at clinically relevant temperatures (GF19, Table 2.7). In a similar fashion to the optimisation process for the cisplatin-loaded hydrogel, the GP concentration was reduced to 0.1% w/w in order to determine if the thermoresponsive nature could be restored to a clinically relevant range. The resulting hydrogel, GF20, was determined to undergo a sol-gel transition at 31°C, with a G' at 37°C of 10,935 Pa. The incorporation of cisplatin into this paclitaxel-loaded thermoresponsive hydrogel produced a dual drug-loaded thermoresponsive hydrogel, which underwent a sol-gel phase transition at 23°C, with a G' at 37°C of 17,410 Pa (GF21, Table 2.7).

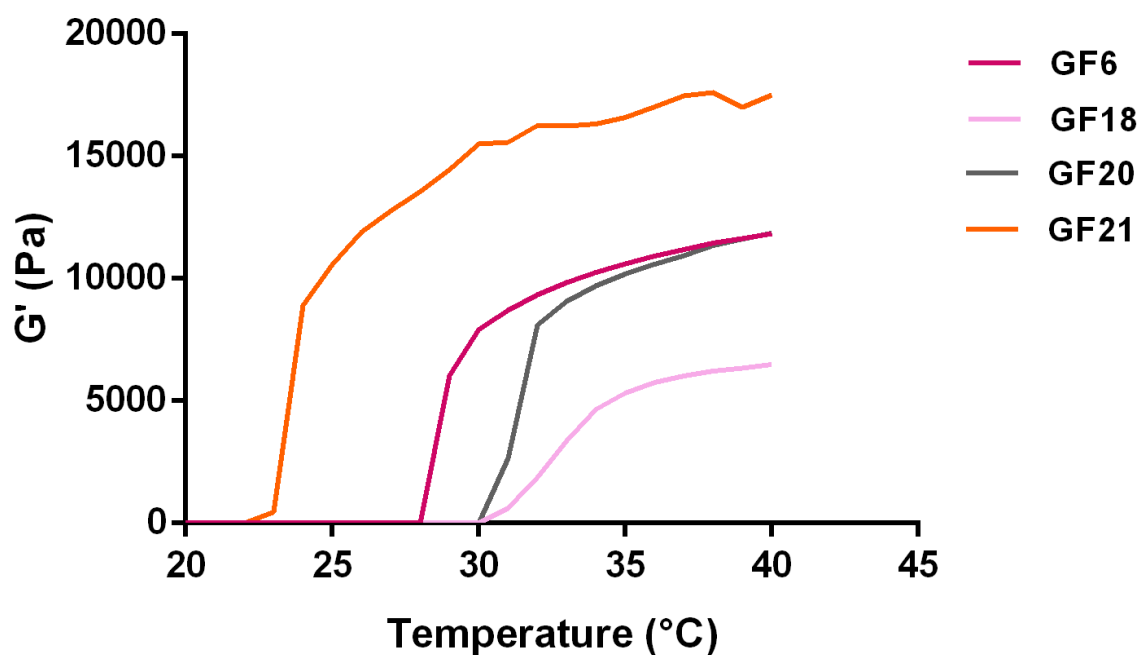


Figure 2.11 Loading of chemotherapeutics into the thermoresponsive hydrogel GF6 causes variable effects on the sol-gel transition temperature and the storage modulus G' of the blank hydrogel. Rheogram of temperature sweep of formulations to determine impact of addition of cisplatin (GF18), paclitaxel (GF20) and cisplatin and paclitaxel (GF21) to the blank hydrogel formulation (GF6). Data shown is representative of the norm.

While the dual drug-loaded GF21 was thermoresponsive, further optimisation of this formulation was required to increase the sol-gel transition temperature higher than 23°C. The impact of dividing the total HP- β -CD content between HP- β -CD complexed with paclitaxel and free HP- β -CD at a ratio of 2:1 was assessed. For the purpose of this study, free HP- β -CD powder refers to non-complexed HP- β -CD powder. The addition of the free HP- β -CD powder increased the sol-gel transition temperature to 32°C, and the G' at 37°C was determined to be 7,663 Pa (GF22, Fig. 2.12), and this was determined to be the lead dual drug-loaded formulation.

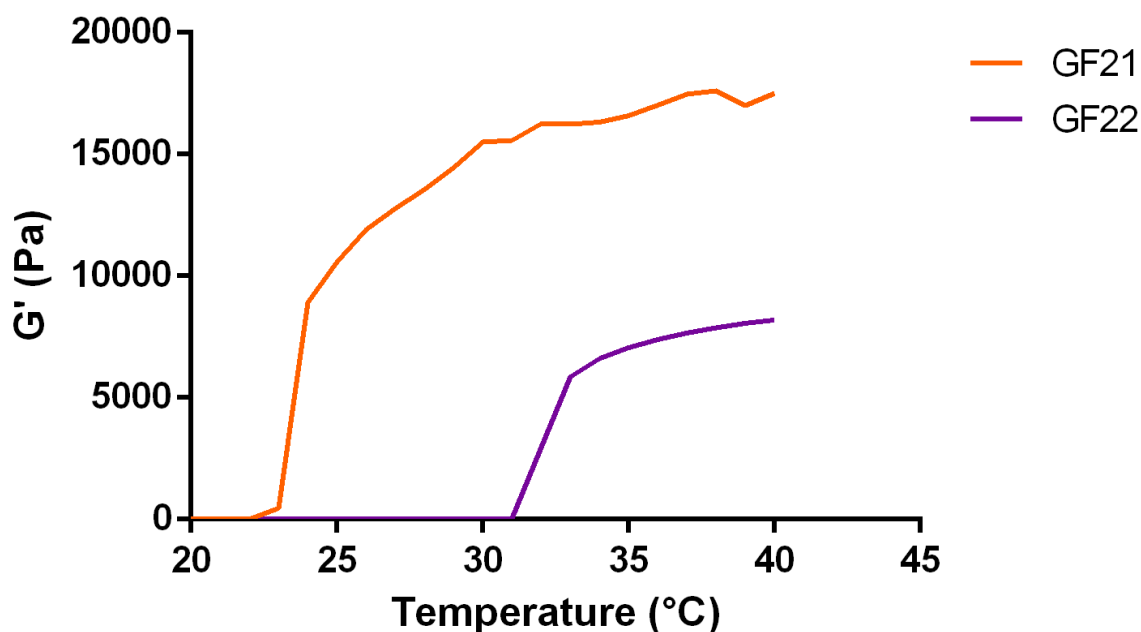


Figure 2.12 Division of the final HP- β -CD concentration (10% w/w) between HP- β -CD complexed with paclitaxel and free HP- β -CD caused an increase in thermoresponse temperature to 31°C. The data shown is representative of the norm.

2.3.5 Characterisation of blank ChemoGel and drug ChemoGel formulations

2.3.5.1 Rheological characterisation

GF6 and GF22, hereafter referred to as blank ChemoGel and drug ChemoGel, were selected as the lead blank and drug-loaded hydrogels respectively. Their compositions, and thermoresponsive profiles are compared in Table 2.8 and Figure 2.13.

Following a short incubation time at 37°C, both hydrogels underwent a characteristic sol-gel thermoresponse and gelled completely (Fig. 2.13 A & B). This gelation was reversible, and the hydrogels returned to liquid state following termination of incubation. This thermoreversibility occurred more rapidly upon chilling on ice at 4°C. Blank ChemoGel and drug ChemoGel were then subjected to further rheological testing to establish their rheological profile under various parameters (LVR contained in Appendix 4, Fig. A.3). The lead thermoresponsive hydrogel formulations were found to maintain a constant G' and G'' at both 20°C

and 37°C over a period of 60 min, with the liquid and gel states being maintained respectively (Fig. 2.13 C). Varying temperatures from 20°C to 37°C every 5 min showed that both blank and drug ChemoGel were thermoreversible, as the formulations successfully underwent phase transition between liquid and gel states across a minimum of six temperature changes (Fig. 2.13 D). The phase transitions were observed to occur rapidly, as represented by rapid change in storage modulus from low (liquid) to high (gel) as temperature cycled repeatedly from room to body temperature respectively.

Table 2.8 Blank and drug ChemoGel (GF6 and GF22 respectively) were selected as the lead formulations for further analysis. Sol-^{*} and drug ChemoGel. Data shown is representative of the norm.

	Gel formulation (GF)	
	6 Blank ChemoGel	22 Drug ChemoGel
P407 (% w/w)	17	17
HP-β-CD (% w/w)	10	10
CS (% w/w)	0.5	0.5
GP (% w/w)	0.1	0.1
Cisplatin (% w/w)	-	0.02
Paclitaxel (% w/w)	-	0.01
Thermoresponse (°C)	29	32
G' @ 37°C (Pa)	11,380	7,663

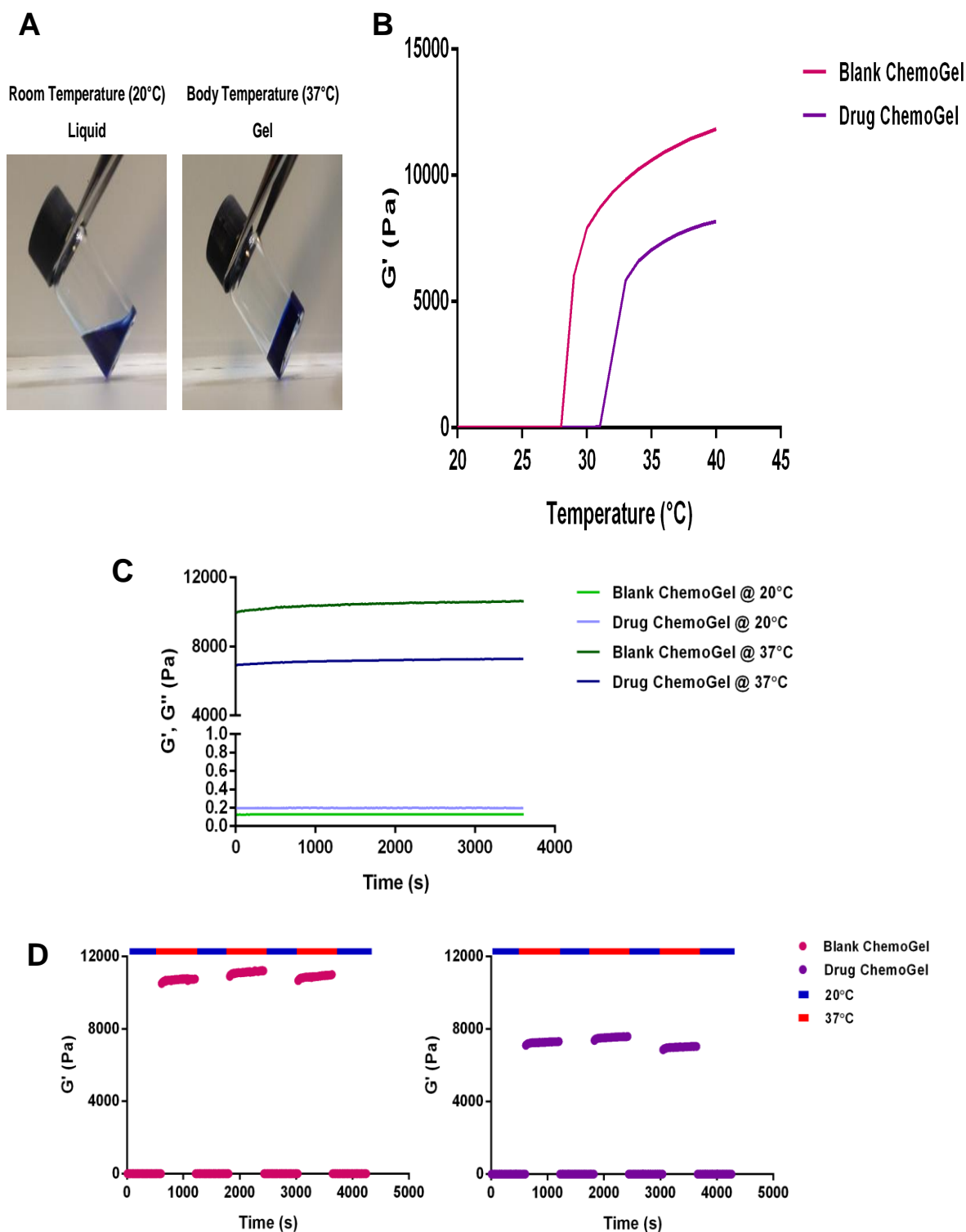


Figure 2.13 Rheological characterisation of blank and drug ChemoGel. **(A)** Representative image of ChemoGel, at room temperature, in liquid state (left) and following incubation at 37°C, in gelled state (right). ChemoGel coloured blue for clarity. **(B)** Rheogram of oscillatory temperature sweeps. **(C)** Rheograms of oscillatory time sweeps of blank and drug ChemoGel at 20°C and 37°C over a 60 min period. **(D)** Rheograms of oscillatory time sweeps of blank and drug ChemoGel with varying temperatures of 20°C and 37°C. Data shown is representative of the norm.

2.3.5.2 Disintegration studies

Similar disintegration profiles for both blank and drug ChemoGel were observed *in vitro* over 28 days (Fig. 2.14 A). Both blank and drug ChemoGel demonstrated extended disintegration profiles, compared to P407 17% w/w and blank ChemoGel without Genipin, which were completely disintegrated by 72 h (Fig. 2.14 A). An initial decrease in mass was observed for both blank and drug ChemoGel after 4 h of exposure. This mass loss was largely recovered after 24 h, with a steady decrease in mass observed thereafter until Day 7. Mass loss of blank ChemoGel and drug ChemoGel levelled off from Day 7 to 28, with $20.59\% \pm 1.34\%$ and $17.76\% \pm 1.47\%$ remaining respectively after 28 days of exposure to PBS at 37°C.

Images of the disintegration of blank and drug ChemoGel revealed that the *in situ* curing process of the hydrogels occurred over the initial 48 h of exposure to PBS at 37°C, as evidenced by the colouration of the hydrogel mass (representative images of blank ChemoGel shown, Fig. 2.14 B). Crosslinking was not visually evident at 4 h post exposure to PBS at 37°C. By 24 h, the blue-green pigment had developed throughout the mass of the hydrogel, with complete colouration having occurred by 48 h. Uniform disintegration of the hydrogel mass is also visually observed to occur across the 28 day exposure, with a crosslinked gel bolus remaining at Day 28.

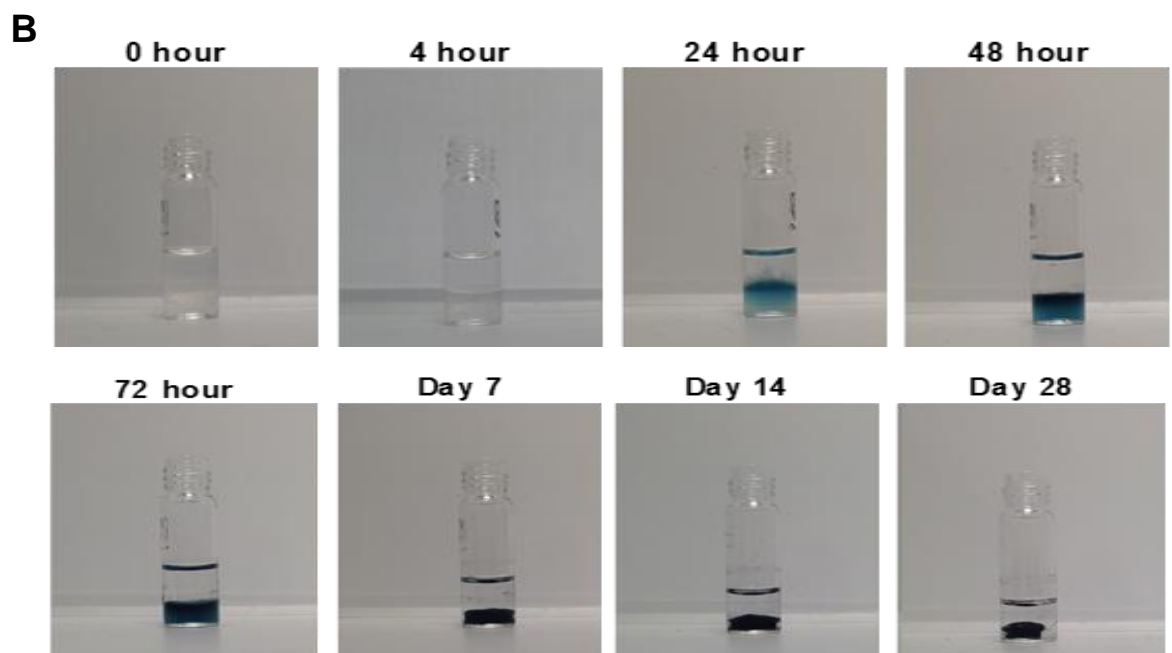
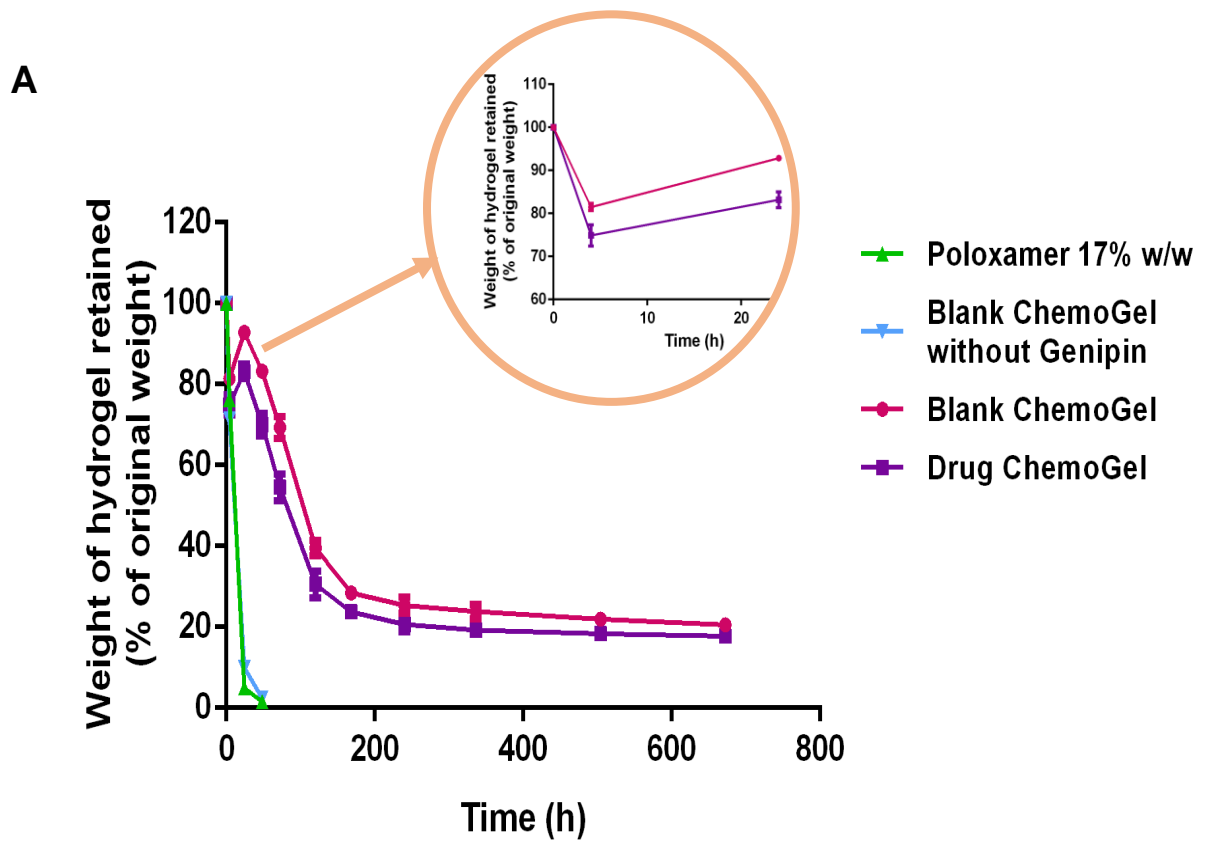


Figure 2.14 Disintegration of blank and drug ChemoGel was slower than Poloxamer 407 17% w/w or non-crosslinked blank ChemoGel over 28 days (A) Disintegration profile of Poloxamer 407 17% w/w, blank ChemoGel without Genipin, blank ChemoGel or drug ChemoGel over 28 days. Disintegration of blank and drug ChemoGel over initial 24 h depicted in magnified section (orange circle). Data shown is representative of the mean of three independent experiments \pm SEM ($n=3$). (B) Representative images of blank ChemoGel exposed to PBS for predetermined timepoints.

2.3.5.3 Release of chemotherapeutics from dual drug-loaded formulations

The *in vitro* release of Pt and paclitaxel from drug ChemoGel over 10 days was assessed to determine whether the loaded chemotherapeutics could be successfully released following gelation of the thermoresponsive hydrogel (Fig. 2.15 A & B). Pt was detected as a surrogate marker of cisplatin release. 44.36% \pm 9.43% of loaded Pt and 63.34% \pm 3.11% of loaded paclitaxel was cumulatively released *in vitro* over 10 days (Fig. 2.15 A). More rapid release of both drugs was observed over the initial 48 h, with Pt release ceasing after 120 h (Fig. 2.15 B, left). Paclitaxel was released over a longer timeframe than Pt, with release still being observed at Day 10 (Fig. 2.15 B, left). By the end of the 10 day release study, the same quantity of both Pt and paclitaxel was detected in release buffer (Fig. 2.15 B, right).

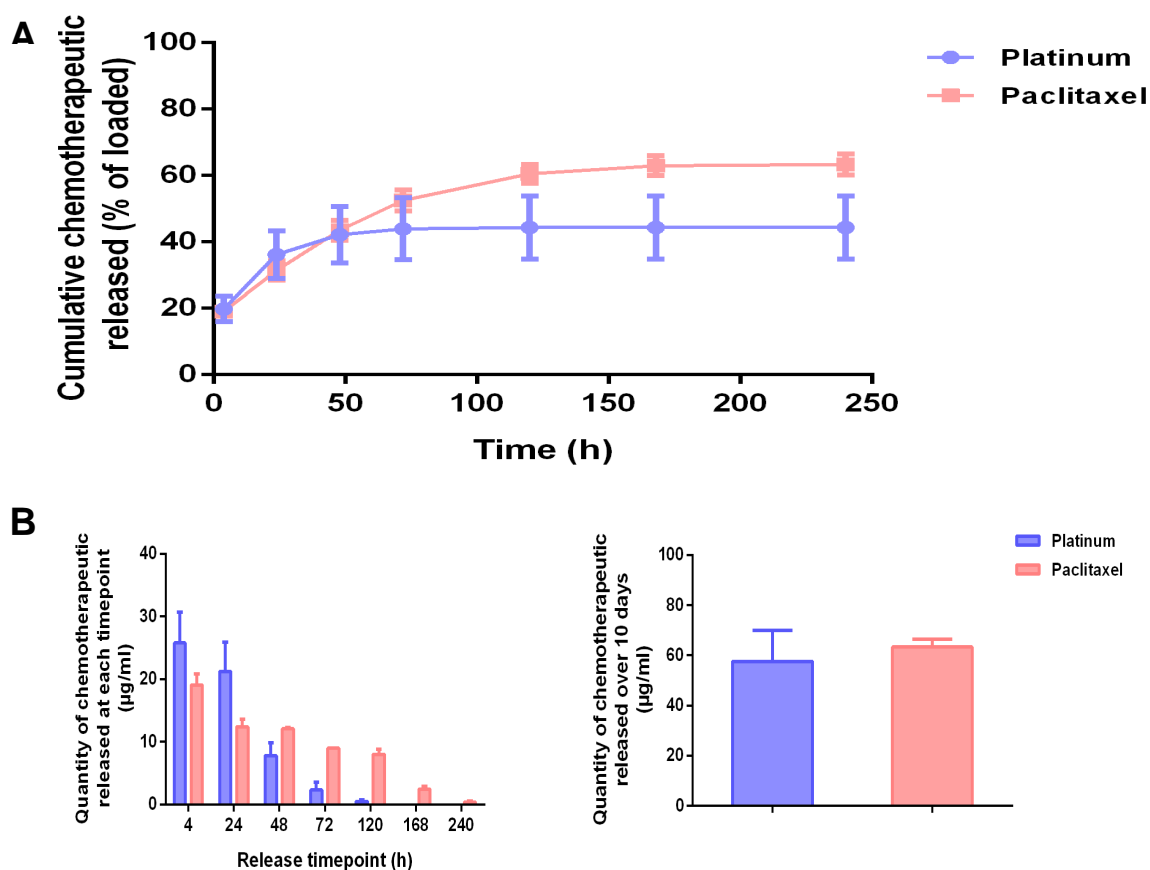


Figure 2.15 Platinum and paclitaxel were released in a sustained manner from drug ChemoGel over a 10 day period. **(A)** Cumulative percentage of loaded platinum and paclitaxel released over a 10 day period (240 h). **(B)** Quantity of platinum and paclitaxel released ($\mu\text{g/ml}$) measured at each timepoint over a 10 day period (left). Total quantity of platinum and paclitaxel released over a 10 day period (right). Data shown is representative of the mean of three independent experiments \pm SEM ($n=3$).

2.4 Discussion

The objective of the formulation process presented in this Chapter was to produce a thermoresponsive hydrogel, which could be dual drug-loaded with cisplatin and paclitaxel, while maintaining a clinically relevant sol-gel transition temperature. One of the major challenges associated with drug delivery is the vast quantity of molecules that are poorly soluble in aqueous medium. In the region of 40% of currently marketed drugs, and 90% of drugs under development, face this problem (242). The difficulty associated with delivering a poorly soluble drug, such as paclitaxel, becomes even greater when attempting to formulate a dual drug-loaded delivery platform (243). This objective is further complicated when dealing with thermoresponsive hydrogels, in which the delicate balance of thermoresponsivity must be maintained.

For the purposes of the optimisation process, an appropriate sol-gel transition temperature was defined as a temperature above 23°C, but below 37°C, to ensure that the formulation would remain in a solution state at room temperature (21°C), and undergo gelation upon injection into the body. The storage modulus (G') at 37°C was also reported to give an indication of how the elasticity of the formulations was impacted with modification of excipients and/or chemotherapeutics. The G' of all formulations at 37°C was observed to be above 6,000 Pa. While it has been noted that a high elastic component of hydrogel formulations favours their use as drug delivery platforms (244), it does not represent the robustness of the hydrogel, which must be assessed using disintegration testing.

Initial optimisation work was directed at tailoring the degree of crosslinking in the blank hydrogel (Table 2.5). GP, which acts as the crosslinking agent, was in the initial formulation at a concentration of 0.3% w/w, in conjunction with a curing period of 24 h. The curing period was introduced as a method to accelerate the crosslinking mechanism between CS and GP. Amine groups on CS are crosslinked by GP through nucleophilic attack in order to establish covalent crosslinks (226), which results in the development of a blue colour as the crosslinks develop (245).

It was hypothesised that the addition of an ionic crosslinker in combination with GP might improve the rheological properties of the formulation (246). TPP, a “Generally Recognised as Safe” (GRAS) listed small molecule crosslinker (192), is a polyanion which undergoes physical crosslinking with CS via ionic interactions (246). 0.2 – 0.5% w/w TPP was cited as being within optimal concentrations to maintain

syringeability. Therefore, a concentration of 0.2% w/w was selected for evaluation (GF2, Table 2.5). The increased G' at 37°C of GF2 following the addition of TPP, has also been reported in other studies utilising a GP/TPP co-crosslinked CS formulation (246). However, the inhomogeneous appearance of the hydrogel following the addition of TPP resulted in the removal of TPP from the formulation protocol.

The decreased concentration of GP in GF3 resulted in a reduction in the occurrence of crosslinking, which decreased the 3D structure of the hydrogel, culminating in a reduced G' . This is in agreement with previous work, which demonstrated that increasing crosslinker concentration increases the elastic modulus of CS hydrogels (247). The altered structural formation of the hydrogel, and the change in polymer-polymer interactions, resulted in a higher sol-gel transition temperature of GF3. The removal of the curing period from this formulation protocol was found to have no effect on the sol-gel transition temperature, but reduced the G' at 37°C by approximately 1,500 Pa (GF4). It is also of note that the curing period will still occur as the hydrogel will undergo *in situ* crosslinking following *in vivo* administration, at which point the elastic modulus of the uncured formulation would increase. GF5 assessed the impact of reducing P407 concentration to 17% w/w, which has been previously shown to increase sol-gel transition temperature, due to the reduction in the amount of the hydrophobic PPO constituent (24, 248). This change in P407 concentration resulted in a formulation (GF5) with the highest sol-gel transition temperature, 33°C, with a G' at 37°C of 7,679 Pa. The reduction in storage modulus between GF1 and GF5 is due to a combination of reducing the P407 content, and also the removal of the curing period (Table 2.5). GF6 consisted of a reduced P407 concentration (17% w/w) and GP concentration (0.1% w/w). Compared to the GF3 (P407 20% w/w, GP 0.1% w/w), the reduced P407 concentration of GF6 did not induce a higher sol-gel transition temperature. Rather, the sol-gel transition temperature decreased by 1°C, with an increased G' at 37°C. This further demonstrates the complex balance required to tailor the thermoresponsive nature of such hydrogels, as altering each excipient can have an unanticipated effect on overall formulation behaviour. It is hypothesised that the reduction of polymer entanglement associated with P407, may have facilitated increased interaction between CS and GP which resulted in an increased storage modulus (249).

The next stage of the development process involved the loading of the thermoresponsive hydrogel with first line chemotherapeutics for NSCLC, cisplatin

and paclitaxel (125). GF1 was selected as the initial formulation to be loaded with the hydrophilic chemotherapeutic, cisplatin. The inclusion of cisplatin into the formulation produced a hydrogel that existed in the gel state at 20°C (Fig 2.7). Addition of cisplatin to CS hydrogel solutions has been noted to result in complexation and subsequent gelation. The mechanism of this interaction has been attributed to the bond formation between cisplatin and CS. In acidic conditions the amine group on CS is protonated. This protonated species is available for bonding with the Pt group in cisplatin to form a Pt-N bond (250). Other suggested mechanisms include hydrogen bonding and decreased electrostatic repulsion following addition of cisplatin. It is important to be cognisant of the fact that in the overall hydrogel formulation, interactions between excipients and drug molecules do not occur in isolation. Rather, it is a combination of different interactions between all of the excipients that produce the material characteristics of the final formulation. Therefore, it was hypothesised that the potential crosslinking of CS with cisplatin, in combination with the covalent GP-CS crosslinking, resulted in the elimination of a clinically relevant sol-gel transition temperature.

To identify if the loss of thermoresponsivity was associated with a specific excipient, or the whole formulation, stepwise addition of the formulation excipients without and with cisplatin was undertaken (Appendix 3, Table A.1). GF6, which had a reduced P407 (17% w/w) and GP (0.1% w/w) concentration, was determined to be the optimal blank formulation to incorporate cisplatin to produce GF18 (Fig. 2.8). GF18 was determined to be a thermoresponsive hydrogel with a sol-gel transition temperature of 31°C. The G' of this formulation at 37°C was reduced compared to GF6 (6,030 Pa vs 11,380 Pa respectively), which may be due to reduction of CS-GP crosslinking in favour of Pt-N bonding between the CS and cisplatin molecules (250).

Paclitaxel is a poorly soluble chemotherapeutic drug, which presents significant formulation challenges (251, 252). In an effort to improve the aqueous solubility of paclitaxel, it was complexed with HP- β -CD. Distinct morphological difference could be observed between the freeze-dried complex (Fig. 2.9 D) and the powders alone (Fig. 2.9 A & B) or physically mixed (Fig. 2.9 C) using SEM. The inclusion complex protocol was based on a protocol published by Choi *et al.* (2014) (238). This protocol used a dimethyl- β -cyclodextrin as the inclusion complex for paclitaxel. The morphological differences observed in this paper support those seen in Figure 2.9. The use of dimethyl- β -cyclodextrin produced different specific morphological

characteristics in the Choi study, however the pattern of change is similar. DSC thermograms demonstrated that following the freeze-drying procedure the characteristic endo- and exo- thermic peak of paclitaxel was no longer evident, indicating that complexation had taken place (Fig. 2.10). This endothermic peak observed in the single paclitaxel powder is representative of the melting point of the drug powder. The exothermic peak indicates degradation of the drug has occurred (253). Similar results have been observed in which this endothermic peak disappears following complexation with paclitaxel (254). The broad endothermic peak of HP- β -CD has also previously been demonstrated, and is said to be as a results of water loss from the inclusion cavity (255). This peak is seen to still remain in the freeze-dried complex although its maximum is shifted to a higher temperature, further indicating complexation with paclitaxel had occurred (Fig. 2.10). Close to 100% of the loaded paclitaxel was recovered following the freeze-drying process ($95.3\% \pm 2.05\%$, Table 2.6), indicating that the complexation was not detrimental to the quantity of paclitaxel loaded.

GF19 demonstrated that the addition of the inclusion complex to the GF5 blank thermoresponsive hydrogel formulation produced a hydrogel that existed in the gel-state at 20°C (Table 2.7). Based on this, and previous results with cisplatin, the 0.3% w/w concentration of GP was confirmed to be a non-feasible choice for continued evaluation. The reduced P407 and GP concentration (17% w/w and 0.1% w/w respectively) of GF20 restored a clinically relevant sol-gel transition temperature for paclitaxel-loaded formulation (Table 2.7). However, upon dual drug-loading, this formulation demonstrated a reduced sol-gel transition temperature of 23°C (GF21), further highlighting the complexity associated with the formulation of multi-drug-loaded thermoresponsive hydrogels (256).

In order to address the reduced sol-gel transition temperature of GF21, it was hypothesised that reintroduction of uncomplexed HP- β -CD powder, referred to as free HP- β -CD, would increase the sol-gel transition temperature of the formulation as HP- β -CD is known to increase the sol-gel transition temperature of P407-based thermoresponsive hydrogels (206). The overall concentration of HP- β -CD remained constant (10% w/w), but the amount of HP- β -CD freeze-dried with paclitaxel was reduced in order to allow for the addition of free powder. A ratio of 2:1 (freeze-dried complex:free HP- β -CD powder) was assessed (GF22, Table 2.8). The inclusion of free HP- β -CD powder increased the sol-gel transition temperature to 32°C and reduced the G' of the formulation to 7,663 Pa at 37°C (Fig. 2.12). This formulation

was determined to be the optimal formulation as the dual drug-loaded hydrogel maintained a sol-gel transition temperature above room temperature. GF6 and GF22 were then selected as lead blank and drug-loaded thermoresponsive hydrogels and identified as blank ChemoGel and drug ChemoGel respectively.

Blank and drug ChemoGel were subjected to further rheological analysis to determine their behaviour, in response to time, or to cycling of temperature between room and body temperature (Fig. 2.13 B – D). The time sweeps indicated that in both liquid and gelled states, blank and drug ChemoGel maintained a constant rheological profile (Fig. 2.13 C). This demonstrates the formulation stability at room and body temperature. It is of note that, although 60 min is a relatively short time frame, it provides evidence that the short term storage of blank and drug ChemoGel at room temperature does not adversely affect the structure of the hydrogels. This is of clinical relevance as it demonstrates that the formulations maybe kept at room temperature for at least 60 min prior to administration. Both blank ChemoGel and drug ChemoGel demonstrated satisfactory thermoreversibility, when exposed to repeated cycles of room temperature (20°C) and body temperature (37°C) (Fig. 2.13 D). The transitions between solution (low G') and gel (high G') and between gel and solution were sharp over the time sweep, indicating that the gelation and liquefaction were rapid process. Thermoreversibility is an important feature, as this means that should accidental gelation occur during transport or storage of the final product, the product can be returned to liquid state upon cooling. Rapid gelation is also important to ensure that the hydrogel will form rapidly *in vivo*, preventing uncontrolled spread of ChemoGel.

Rapid disintegration of Poloxamer hydrogels limits their use in a clinical setting (25). Sun *et al.* (2006) demonstrated that a Poloxamer hydrogel (P85) alone disintegrated within 6 h following exposure to PBS (pH 7.4) at 37°C, which is characteristic of Poloxamer hydrogels (257). The *in situ* crosslinking of both the blank and drug ChemoGel resulted in the retardation of this rapid disintegration process (Fig. 2.14 A). Both hydrogels were not fully disintegrated at the end of the 28 day evaluation. This was in stark contrast to P407 alone, and the blank ChemoGel formulation without GP, which had completely disintegrated within 72 h. The rate of disintegration slowed after 5 days exposure to PBS for both hydrogels. Representative images of the disintegration study of ChemoGel demonstrated that crosslinking of the CS-GP occurred *in situ* over 72 h, as depicted by the deepening of the colouration of the hydrogel of this timeframe. Thereafter, ChemoGel had a

dark blue pigmented appearance for the remainder of the study. This colouration was not seen in blank ChemoGel without GP (data not shown), indicating that crosslinking is as a result of GP. Pigmentation of CS-GP hydrogels following exposure to 37°C has previously been shown to deepen over time due to increased crosslinking between CS and GP, with the rate of crosslinking affected by concentration of both CS and GP used, and by the pH of the CS solution (258).

The rate of drug release from hydrogels has been attributed to chemical, physical and biological interactions between the hydrogel matrix, the drugs loaded and surrounding release medium (259). With reference to the hydrogel matrix, the 3D arrangement of polymers, with the swelling or disintegration of the polymeric network, influences the rate of release. Release of chemotherapeutics from drug ChemoGel appears to be mediated by rate of disintegration of the hydrogel. Drug release had ceased by 240 h (Fig. 2.15), coinciding with the end of the bulk disintegration seen in Figure 2.15. Disintegration or dissolution mediated release is commonly reported for hydrophobic drug molecules released from hydrogel matrices (260, 261). As crosslinking progresses in the ChemoGel structure (Fig. 2.145 B), the rate of release is also seen to slow (Fig. 2.15). This may be due to tightening of the polymeric network, making drug release more difficult. Over the course of the release study, an equal quantity of chemotherapeutics was released, despite a higher concentration of cisplatin being initially loaded into the hydrogel than paclitaxel (Fig. 2.15 B).

2.5 Conclusion

Results presented in this Chapter detail the formulation of a dual drug-loaded thermoresponsive hydrogel. The final ChemoGel formulation could be loaded with a hydrophilic and hydrophobic chemotherapeutic separately and simultaneously, indicating its flexibility for drug delivery. The evaluation of excipients in the formulation confirmed their unique and critical effect on the overall material behaviour, and underlined the fine balance called for in thermoresponsive hydrogel formulation. In conclusion, this Chapter defined the rheological and physicochemical properties of the ChemoGel formulation, specifically:

- ◁ The impact of the ChemoGel excipients on the rheological properties were determined:
 - P407 acts as the thermoresponsive base of the hydrogel, which influences sol-gel transition temperature and storage modulus, but undergoes rapid disintegration in the presence of PBS
 - HP- β -CD influences sol-gel transition temperature, and is required for complexation of paclitaxel in the drug-loaded formulation
 - CS alone is not sufficient to retard the rapid disintegration of P407, but provides the interpenetrating net for GP crosslinking
 - GP concentration influences the thermoresponsivity of the drug-loaded formulations, and crosslinks CS to slow the rate of disintegration of both blank and drug ChemoGel
- ◁ Blank and drug ChemoGel were determined to demonstrate a clinically relevant sol-gel transition temperatures, rheological stability at room and body temperature over 60 min, and thermoreversible properties
- ◁ Dual drug-loading of ChemoGel facilitated sustained release of the chemotherapeutics *in vitro* for up to ten days

Chapter 3 will assess the *in vitro* cytotoxicity of the ChemoGel formulations to determine whether the drug delivery platform demonstrates efficacy against LC cell lines, and to assess if the inherent cancer cell directed cytotoxicity of the excipients has been maintained.

„Šň°j ®

L^a '2Ÿ® ; 2Š°±Š°Ÿ^a '«Ÿ, Ÿj ©«fi;'''
Ÿ® ±Š°Ÿ^a -

3.1 Introduction	107
3.1.1 Cancer biology.....	107
3.1.2 <i>In vitro</i> lung cancer cell culture.....	108
3.1.3 <i>In vitro</i> fibroblast cell culture	108
3.1.4 2D and 3D <i>in vitro</i> cell culture models.....	108
3.1.4.1 3D <i>in vitro</i> models of lung cancer	110
3.1.5 <i>In vitro</i> cytotoxicity assessment of thermoresponsive hydrogels in 2D and 3D models ...	111
3.1.6 Aim and objectives	112
3.2 Materials and Methods	113
3.2.1 Cell culture and subculturing of cell lines	113
3.2.2 2D <i>in vitro</i> cell viability assays.....	114
3.2.2.1. Cell Counting Kit-8 assay	114
3.2.2.2 LIVE/DEAD Viability/Cytotoxicity assay	115
3.2.3 Assessment of cytotoxicity of blank and drug ChemoGel	115
3.2.4 Apoptosis analysis	116
3.2.5 Assessment of cytotoxicity of degradation products from blank ChemoGel	117
3.2.6 Assessment of cytotoxicity of the individual excipients of ChemoGel formulation	117
3.2.7 Development of 3D <i>in vitro</i> model of lung cancer.....	118
3.2.7.1 Scaffold fabrication	118
3.2.7.2 <i>In vitro</i> cell culture of A549 cells in 2D and 3D	119
3.2.8 Comparison of A549 cell proliferation in 2D and 3D cell culture	119
3.2.9 Assessment of viability/cytotoxicity of A459 cells in 2D and 3D culture	120
3.2.10 Assessment of migration of A549 cells in a collagen scaffold	120
3.2.11 Assessment of cytotoxicity of blank and drug ChemoGel in a 3D <i>in vitro</i> model of lung cancer	121
3.2.12 Statistical analysis.....	122
3.3 Results	123
3.3.1 Assessment of cytotoxicity of blank and drug ChemoGel in a human lung cancer cell line.....	123
3.3.1.1 Impact of seeding density on cytotoxicity of blank ChemoGel.....	123
3.3.1.2 Dose-dependent cytotoxicity of blank ChemoGel	124
3.3.1.3 Dose-dependent cytotoxicity of drug ChemoGel.....	125
3.3.1.4 Cytotoxicity of lead ChemoGel formulations.....	126
3.3.2 Apoptosis analysis	128
3.3.3 Assessment of cytotoxicity of ChemoGel in a non-cancerous murine cell line.....	130
3.3.4 Assessment of cytotoxicity of the individual excipients of ChemoGel formulation	131
3.3.5 Development of an <i>in vitro</i> 3D lung cancer model.....	132
3.3.5.1 Proliferation of A549 cells in 2D and 3D over 21 days.....	132
3.3.5.2 Viability of A459 cells in 2D and 3D over 21 days.....	134
3.3.5.3 Migration of A549 cells through 3D environment	135
3.3.5.4 Assessment of blank and drug ChemoGel cytotoxicity in 3D model of lung cancer.....	136
3.4 Discussion.....	138
3.5 Conclusion	145

3.1 Introduction

As discussed in Chapter 2, the ChemoGel excipients were selected due to their multipurpose nature, in that each excipient contributed to the formulations final rheological and material properties, as well as being associated with cancer cell-directed inherent cytotoxicity. In this Chapter, blank and drug ChemoGel were evaluated to determine their *in vitro* cytotoxicity profiles in 2D and 3D cell culture models of NSCLC. To this end, a 3D model of NSCLC was developed to create a more physiologically relevant *in vitro* environment for the assessment of the lead ChemoGel formulations. Determination of *in vitro* cytotoxicity in a non-cancerous cell line was also undertaken to facilitate assessment of off-site toxicity in non-target cells.

3.1.1 Cancer biology

Hanahan and Weinberg (2000) listed six “hallmarks of cancer” in their seminal paper, which has been cited over 15,800 times according to Web of Science (262). Their update in 2011, added two additional hallmarks which have emerged due to the “remarkable progress in cancer research” (263). The hallmarks cited by Hanahan and Weinberg are:

1. Sustaining proliferative signalling
2. Evading growth suppressors
3. Activating invasion and metastasis
4. Enabling replicative immortality
5. Inducing angiogenesis
6. Resisting cell death
7. Avoiding immune destruction
8. Deregulating cellular energetics

In addition, two “enabling characteristics” of cancer were referenced; tumour promoting inflammation, and genome instability and mutation. These hallmarks and characteristics are proposed as the key targets for therapeutic agents, both currently available, and in development. The authors note that by inhibiting one or more of the hallmarks of cancer, therapeutic agents can limit or prevent tumourigenesis and, therefore, these mechanisms are commonly targeted in early stage *in vitro* research (263).

3.1.2 *In vitro* lung cancer cell culture

The American Tissue Type Culture Collection (ATCC) catalogue has 167 human LC cell lines, which can be sub-classified by cell type, stage of cancer progression and site of origin, i.e. primary tumour or metastatic site (264). The A549 cell line, a human lung adenocarcinoma cell line, was derived from a primary epithelial lung carcinoma of a 58-year old Caucasian male in 1972 (265). This cell line was selected as an *in vitro* model of NSCLC as adenocarcinoma accounts for approximately 40% of all LC cases (87), and therefore the most common subtype of LC would be assessed. The A549 cell line is included in the National Cancer Institute's NCI-60 Human Cancer Cell Line Screen, which consists of 60 cell lines commonly used in the screening of new therapeutic compounds (266). Additionally, the A549 cell line is commonly cited as an *in vitro* model of NSCLC in the literature, with a PubMed search indicating that over 21,000 articles contain this term since 1976.

3.1.3 *In vitro* fibroblast cell culture

Balb/c 3T3 clone A31 cells are a murine fibroblast cell line, which can be used to evaluate the effects of cancer treatments on non-cancerous cells in off-target sites (267). Another murine fibroblast cell line commonly used is the L929 cell line, with human fibroblast cell lines also available, including Wi38 a human lung fibroblast cell line. While it must be acknowledged that murine cell lines are not wholly representative of human tissue, they are the most widely used cell line to evaluate cytotoxicity. One of the benefits of using such a cell line is that, due to its common application in cytotoxicity evaluation, a large bank of data is available for reference and comparison (268). In addition, the International Organization for Standardization (ISO) recommends the use of Balb/c 3T3 clone A31 in cytotoxicity testing in their published standards for the "Biological Evaluation of Medical Devices" (269).

3.1.4 2D and 3D *in vitro* cell culture models

2D cancer cell culture is the most common method of *in vitro* cytotoxicity assessment, and utilises monolayers of cells to model tumourigenesis *in vitro* (270). This model of cancer has little relevance to the *in vivo* environment, and inadequate biorelevance of *in vitro* testing has been cited as one of the reasons associated with the poor clinical translation rate of therapies (271). 2D cell culture is often carried

out with cancer cells that adhere to the plastic structure on which they are cultured, which forces the growth in 2D against the natural development of 3D structures *in vivo* (272). As discussed in Chapter 1, the composition of the TME is unique and has a critical impact on tumourigenesis (273). Without cellular crosstalk many of the tumours “self-preservation” pathways are unable to function, and efficacy of treatment may be overestimated. Additionally, cells grown in a 2D monolayer receive an equal amount of oxygen and nutrients. However, a key feature of tumours *in vivo* is the formation of a necrotic core, with leaky vasculature produced unevenly throughout the tumour leading to areas of hypoxia. This disorganised structure of an *in vivo* tumour is lost in monolayer culture (69, 274).

Despite the limited biorelevance outlined above, 2D cell culture still has value in the experimental process as it facilitates rapid and inexpensive screening of the drug molecules and drug delivery formulations. It allows for initial evaluation to be carried out before investing in the more expensive 3D models or *in vivo* studies. Therefore, 2D cell culture is a simple and cost-effective screening system for initial cytotoxicity analysis, but results should be interpreted with caution, and with the view to progressing to 3D *in vitro* models and *in vivo* testing (274).

In an effort to address some of the limitations of monolayer cancer cell culture highlighted above, a significant amount of research has been directed towards the development of more physiologically relevant *in vitro* models of cancer by culturing the cells in a 3D environment. The 3D environment provides for the critical cell-cell, and cell-ECM interactions, that induce the biological and physical cues for tumourigenesis in the TME, as discussed in Chapter 1 (275). Different methods have been proposed to achieve this, including spheroid formation, scaffolds and matrices, or microfluidics (276).

Spheroid formation can be achieved relatively easily, for low cost, and with high throughput using methods like forced floating, hanging drop and agitation induced formation (277). This method relies on the cells forming aggregates and creating their own 3D structure by secreting their own ECM. Larger spheroids (>500 µm) are capable of forming different zones of proliferation moving towards a necrotic core, similar to the *in vivo* reality (278). Depending on cell type used, spheroid formation has varying degrees of success, and so validated culture methods are called for (277).

Scaffolds and matrices provide 3D structural support, acting as a surrogate ECM to allow the cancer cells to adhere, proliferate, migrate and deposit their own ECM to produce a more representative tumour model. They can consist of natural or synthetic polymers, decellularised tissue or cell derived matrices, and can be treated with growth factors to further induce a biomimetic environment (276). This type of 3D model is more expensive and technically challenging than spheroid culture (279).

Microfluidics or organ-on-a-chip cell culture uses controlled dynamic fluid flow through the culture cells to mimic the *in vivo* environment, and transport of nutrients and waste to and from the tumour. Microfluidic cell culture can be carried out using 2D or 3D models of cancer, and holds the potential to effectively mimic the complex *in vivo* TME on a micro-scale. However, universal application of microfluidic cell culture is currently limited by the high-cost and technical complexities associated with the system (280).

3.1.4.1 3D *in vitro* models of lung cancer

The aforementioned methods of 3D *in vitro* culture have all been applied to *in vitro* LC research. The development of high throughput screening (HTS) using these 3D models would facilitate large scale assessment of LC treatments in a more biorelevant setting. Algimatrix™ is a porous sponge which has been used in the development of a 96-well plate-based HTS system using a panel of three LC cell lines. This study demonstrated the application of 3D culture systems in the assessment of nanoparticle-based advanced drug delivery platforms. It was determined that uptake of the nanoparticles was lower in the 3D model, compared to 2D, which the authors concluded to be more representative of the process *in vivo* (281). An *in vitro* 3D HTS model of LC was also developed to assess the invasive behaviour of two LC cell lines, in which a 3D LC cell cluster was encapsulated in a collagen-based ECM. The invasive behaviour of the two LC cell lines studied, H1229 and A549 cells, was determined to be different, with only the H1229 cells demonstrating multidirectional invasive pattern (282). In general, it has been found that different LC cell types behave differently in response to the same matrix, and that different matrices induce different responses in the same cell type, indicating that validation of 3D models is required for each histological subtype and matrix used (283). Decellularised lung matrices from rats have also been used to culture A549s in an *ex vivo* 3D model of LC, and were found to form tumour nodules similar to those observed *in vivo* (284). More advanced *in vitro* 3D models of LC have also

been developed using primary LC cells to further increase the biorelevance of these systems (285). *In vitro* 3D co-culture models of LC have also been developed, with improved biorelevance demonstrated upon inclusion of non-cancerous cell lines in the culture system, compared to monoculture (285). Tri-culture 3D models using cancer cells, fibroblasts and endothelial cells have been established using the hanging drop method (286). OncoCilAir™ is a commercially available tri-culture *in vitro* 3D model of LC, which uses bronchial cells, lung fibroblasts and A549 LC cells. Authors suggest that different molecular subtypes could be cultured using the OncoCilAir™ technology and this model is suggested as a tool for predictive anti-cancer drug screening (287).

3.1.5 *In vitro* cytotoxicity assessment of thermoresponsive hydrogels in 2D and 3D models

2D *in vitro* evaluation of cytotoxicity of thermoresponsive hydrogels as drug delivery platforms presents a number of challenges. The function of many advanced drug delivery platforms is to deliver a chemotherapeutic payload over an extended period of time. Due to the disparity between therapeutic dosing and number of cells seeded in 2D monolayer studies, total cell death is often seen at early time points *in vitro*, negating the use of later timepoints. In considering thermoresponsive hydrogels specifically, 2D *in vitro* evaluation of cytotoxicity fails to take account of the other potential mechanisms of cell death, including embolisation of tumour supplying arteries, and distribution of hydrogel throughout the tumour, which will affect how cells are exposed to the hydrogel. 2D *in vitro* toxicity evaluation does hold value in assessing comparatively between excipients used, delivery methods and dosing, but results should not be interpreted in isolation as absolute measures. 3D *in vitro* studies provide an opportunity to gain additional insights into the cytotoxicity of cancer treatment delivered via thermoresponsive hydrogels, as they represent cellular behaviour more representative of that *in vivo* as discussed above in Section 3.1.4 (69, 274, 276). In terms of IT administration of thermoresponsive hydrogels, the use of a 3D model provides an opportunity to mimic the clinical procedure in an *in vitro* setting, thereby more accurately assessing function of the drug delivery platform. Finally, with regard to the drug delivery functionality of thermoresponsive hydrogels, the extended culture timeframe associated with 3D *in vitro* models facilitates the evaluation of the impact of sustained release of chemotherapeutics over time.

3.1.6 Aim and objectives

The overall aim of this chapter was to determine the *in vitro* cytotoxicity profile of blank and drug ChemoGel in a 2D and 3D model of NSCLC.

The specific objectives of this chapter were to:

- ◁ Assess cytotoxicity of blank and drug ChemoGel using a human NSCLC cell line (A549)
- ◁ Determine the apoptotic/necrotic contributions to cytotoxicity
- ◁ Assess cytotoxicity of blank ChemoGel in non-cancerous cell line (Balb/c 3T3 A31)
- ◁ Assess cytotoxicity of individual excipients of ChemoGel
- ◁ Establish a 3D model of lung cancer
- ◁ Evaluate the cytotoxicity of blank and drug ChemoGel in the 3D model of lung cancer

3.2 Materials and Methods

A human epithelial carcinoma cell line, A549, and a murine fibroblast cell line, Balb/c 3T3 clone A31, were purchased from LGC Standards (Middlesex, UK). Dulbecco's Modified Eagles Medium /Hams' Nutrient Mixture F12 (DMEM:F12) (D8062), DMEM – high glucose (D6429), Penicillin 10,000 units/ml – Streptomycin 10mg/ml solution (Pen/Strep), Trypsin, Dimethyl sulfoxide (DMSO), N-(3-Dimethylaminopropyl)-N'-ethylcarbodiimide hydrochloride (EDAC), N-Hydroxysuccinimide (NHS), Hyaluronic acid (HyA) sodium salt derived from *Streptococcus equi* and neutral buffered formalin (NBF) 10% v/v were all purchased from Sigma Aldrich (MO, USA). Collagen type I derived from bovine Achilles tendon (Collagen Matrix, USA). Fetal bovine serum (FBS) and newborn calf serum (NBCS) were purchased from BioSera (Nuaille, France). Cell Counting Kit-8 (CCK-8) was purchased from NBS Biologicals Ltd. (Cambridgeshire, UK). LIVE/DEAD® Viability/Cytotoxicity Kit for Mammalian Cells was purchased from Invitrogen Ireland. APC Annexin V Apoptosis Detection Kit with Propidium Iodide (PI) was purchased from BioLegend (CA, USA).

3.2.1 Cell culture and sub-culturing of cell lines

All cell culture was carried out in a class II laminar airflow cabinet, which was cleaned down with 70% ethanol prior to, and following, use. All items entering the airflow cabinet were also sterilised with 70% ethanol. UV sterilisation was used for at least 15 min prior to use of different cell lines to avoid cross contamination. Cell lines were resurrected from storage in liquid nitrogen prior to use. The vial containing the cell line was defrosted quickly in a waterbath at 37°C, turning it often to minimise temperature gradients. Cell culture medium was added dropwise to the defrosted cells, and this was centrifuged at 1,200 rpm for 5 min at room temperature. The supernatant was aspirated off the pellet to remove any DMSO from the freezing medium, and the cells were resuspended in supplemented cell culture medium and transferred to a T175 cm² flask (Starstedt, Ireland).

Supplemented medium was replaced every three days, and cells were passaged when they had reached 80-90% confluency (A549 cells) or 60% confluency (Balb/c 3T3 clone A31 cells). Passaging of cells was carried out by removing all medium from the flask. Cells were detached from the flask by adding 5 ml of trypsin to the flask and incubating at 37°C for 5 min in a 5% CO₂, 90% humidity environment. The flask was physically agitated to ensure complete detachment. 10 ml of

supplemented medium was then added to the flask to stop the trypsinisation process, and prevent cell death. This mixture was removed from the flask and added to a 50 ml Falcon Tube. The mixture was centrifuged at 1,200 rpm for 5 min at room temperature. The trypsin/medium supernatant was carefully discarded, and the pellet of cells formed was then resuspended in fresh medium, and reseeded in a T175 cm² flask at an appropriate seeding density. Cell culture specifics are outlined in Table 3.1 for the two cell lines used.

Table 3.1 Modified Eagles Medium; FBS, Fetal bovine serum; NBCS, Newborn calf serum; Pen/Strep, Penicillin-Streptomycin.

Cell line	A549	Balb/c 3T3 clone A31
Cell culture medium	DMEM:F12 supplemented with 10% v/v FBS, 1% v/v Pen/Strep	DMEM – high glucose supplemented with 10% v/v NBCS, 1% v/v Pen/Strep
Doubling Time	22 h	18 h
Sub-culturing ratio	1:3 – 1:8	For 60 mm plates, use an inoculum of 300,000 cells per plate and subculture every 3 days. Highly sensitive to contact inhibition.

3.2.2 2D *in vitro* cell viability assays

3.2.2.1. Cell Counting Kit-8 assay

For cytotoxicity assessment, viability was determined using the CCK-8 assay according to manufacturer’s instructions. The CCK-8 assay is a colorimetric assay, which quantifies the reduction of a water-soluble tetrazolium salt, WST-8, to soluble formazan dyes. The production of the formazan dyes is dependent on the ability of the cell to produce dehydrogenase, and therefore linked to cellular viability. CCK-8 is said to be most sensitive of the tetrazolium assays, as it is reduced by the majority of the cellular dehydrogenase (288). At the pre-determined timepoint, the appropriate treatment was discarded from the well, and the well was washed once with PBS. 200 µL fresh supplemented medium was added to each well. 20 µL of CCK-8 reagent was added to each well, and the plates were returned to the incubator for 90 min or 3 h for A549 cells or Balb/c 3T3 clone A31 cells, respectively. The same volume of CCK-8 in medium was also added to wells with no cells seeded

to act as a control for absorbance detected from cell free medium (blank). 100 μ L of the CCK-8 incubated medium from each well was then transferred to a 96-well plate and absorbance was read at 450 nm on a Varioskan Flash Plate Reader (Thermo Fisher Scientific, MA, USA). Medium treated cells were taken as 100% viability, and the viability of each treatment group was expressed as a percentage of this (Equation 6).

(Equation 6)

3.2.2.2 LIVE/DEAD Viability/Cytotoxicity assay

Live/Dead staining was performed as a qualitative indicator of viability and cytotoxicity of treatment; Live cells were stained green using Calcein AM and dead cells were stained red using Ethidium homodimer-1. Cell staining was carried out according to the manufacturers protocol (Invitrogen, Ireland) (289). 2.5 μ L Calcein AM and 10 μ L Ethidium homodimer-1 was added to 5 ml PBS. At the pre-determined timepoint, the appropriate treatment was discarded from the well and washed once with PBS. 300 μ L of this Calcein AM/Ethidium homodimer-1 solution was added to each treatment well and allowed to develop for 30 min. The stains were then removed, and 300 μ L of PBS was added to the wells. Live and dead cells were fluorescently imaged individually using blue (FITC/GFP) and green (TRITC) filters respectively on the same field of view with a Leica DMIL microscope (Leica Microsystems, Switzerland). Image J was used to generate composite images of cell viability/cytotoxicity.

3.2.3 Assessment of cytotoxicity of blank and drug ChemoGel

Initial seeding density selection experiments were conducted to select optimal seeding density of A549 cells for 2D cell culture. 5,000 or 10,000 cells were seeded in a 96-well plate (Corning™ Costar™, NY, USA). 20,000 cells were seeded in a 24-well plate (Corning™ Costar™, NY, USA). Cells were allowed to adhere for 24 h at 37°C in a 5% CO₂, 90% humidity environment. After 24 h, medium was removed from wells, and replaced with fresh supplemented medium, containing 20 μ L of blank ChemoGel. Plates were returned to the incubator at 37°C in a 5% CO₂, 90% humidity environment for 24 or 48 h. The 48 h timepoint was included as it is used by the NCI in the aforementioned NCI-60 Human Cancer Cell Line Screen protocol (290). The inclusion of this later timepoint is said to ensure that the treatment has sufficient time to carry out the cytotoxic function. Following the pre-determined incubation period, the plates were removed from the incubator, and the

supernatant was discarded. The wells were washed once with PBS, and the appropriate viability assay was carried out as outlined above (Section 3.2.2.1 and 3.2.2.2). Data shown is representative of the mean of three triplicate wells + SEM.

Based on initial seeding density experiments, a seeding density of 20,000 cells per well was chosen for further experiments. A549 cells were seeded at a density of 20,000 cells per well in a 24-well plate with 500 μ L of supplemented medium. Cells were allowed to adhere for 24 h at 37°C in a 5% CO₂, 90% humidity environment. After 24 h, medium was removed from wells, and replaced with fresh supplemented medium. Appropriate volumes of blank or drug ChemoGel or cisplatin/paclitaxel solution (0, 10, 20 or 30 μ L) were added to the fresh supplemented medium to bring the final volume of each well to 500 μ L, based on methods by Ma *et al.* (2014) (58). Plates were returned to the incubator at 37°C in a 5% CO₂, 90% humidity environment for 24 or 48 h. Following the pre-determined incubation period, the plates were removed from the incubator, and the supernatant was discarded. The wells were washed once with PBS, and the appropriate viability assay was carried out as outlined above (Section 3.2.2.1 and 3.2.2.2). All experiments were conducted in quadruplicate, and data shown is representative of the mean of three independent experiments + SEM.

This protocol was repeated using Balb/c 3T3 clone A31 cells under identical experimental conditions to determine the cytotoxicity of 10, 20 and 30 μ L of blank ChemoGel in a non-cancerous cell line. All experiments were conducted in quadruplicate, and data shown is representative of the mean of three independent experiments + SEM.

3.2.4 Apoptosis analysis

Apoptosis of A549 cells induced by treatment with 30 μ L of Medium, cisplatin/paclitaxel solution, blank ChemoGel or drug ChemoGel was evaluated using APC Annexin V Apoptosis Detection Kit with PI (BioLegend, CA, USA) according to manufacturer's instructions, and detected via flow cytometry (291). Cells were seeded at 200,000 cells per well in 2 ml supplemented medium in 6-well plates (Corning™ Costar™, NY, USA), and allowed to adhere for 24 h. Medium was removed, and 30 μ L of treatment was added to each well with 1970 μ L of fresh supplemented medium. Plates were returned to the incubator for 24 h. Treatment and medium were removed after 24 h treatment, and plates were washed once with PBS. Cells were detached from the wells via trypsinisation, and centrifuged at 1,200

rpm for 5 min to produce a cell pellet. Supernatant was removed from the cell pellet, and the cells were washed twice with FACS buffer. Cells were resuspended in 100 μ L Annexin V binding buffer (BioLegend, CA, USA) in a 5 ml tube. 5 μ l of APC Annexin V and 10 μ l of Propidium Iodide Solution were added to each tube. Tubes were gently vortexed and incubated for 15 min at room temperature ($< 25^{\circ}\text{C}$) in the dark. 400 μ l of Annexin V Binding Buffer was added to each tube, and cells were analysed by flow cytometry. All experiments were carried out in triplicate, and data shown is representative of the mean of two independent experiments + SEM.

3.2.5 Assessment of cytotoxicity of disintegration products from blank ChemoGel

Disintegration products of ChemoGel were prepared by incubating blank Chemogel in supplemented Balb/c 3T3 clone A31 medium. 0.5 g of blank ChemoGel was added to a 15 ml falcon tube and incubated at 37°C for 30 min to allow for complete gelation. 1 ml of pre-warmed supplemented Balb/c 3T3 clone A31 medium was added to the falcon tube. After 24 h, the medium was removed and stored at -20°C until required.

Cells were seeded at a density of 10,000 cells per well in a 96-well plate with 200 μ L of supplemented medium. Cells were allowed to adhere for 24 h at 37°C in a 5% CO_2 , 90% humidity environment. The disintegration products were then removed from storage at -20°C , defrosted and warmed to 37°C . The disintegration products were added to each well in fresh supplemented Balb/c 3T3 clone A31, to bring the final volume in each well to 200 μ L. Plates were returned to the incubator at 37°C in a 5% CO_2 , 90% humidity environment for 24 h. Following the pre-determined incubation period, the plates were removed from the incubator, and the supernatant was discarded. The wells were washed once with PBS, and the CCK-8 viability assay was carried out as outlined in Section 3.2.2.1. Data shown is represented as the mean of four technical replicates + SEM.

3.2.6 Assessment of cytotoxicity of the individual excipients of ChemoGel formulation

The cytotoxicity of each excipient in the ChemoGel formulation was assessed to determine its contribution to the overall cytotoxicity of the final formulation. Each individual component was dissolved in the appropriate supplemented cell culture medium for the cell line used, as outlined in Table 3.2.

Table 3.2 Concentrations of individual excipients evaluated for cytotoxicity.

Excipient	% w/w	Diluent
Poloxamer 407	17	Supplemented A549 or Balb/c 3T3 clone A31 medium
Chitosan	0.5	
2-Hydroxypropyl- β -Cyclodextrin	10	
Genipin	0.1	

Cells were seeded at a density of 20,000 cells per well in a 24-well plate with 500 μ L of supplemented medium. Cells were allowed to adhere for 24 h at 37°C in a 5% CO₂, 90% humidity environment. After 24 h, medium was removed from wells, and replaced with 470 μ L of fresh supplemented medium. 30 μ L of the appropriate excipient was added to the fresh supplemented medium to bring the final volume each well to 500 μ L. 30 μ L was chosen as this was the highest volume of ChemoGel used in Section 3.2.3. Plates were returned to the incubator at 37°C in a 5% CO₂, 90% humidity environment for 24 or 48 h. Following the pre-determined incubation period, the plates were removed from the incubator, and the supernatant was discarded. The wells were washed once with PBS, and the CCK-8 viability assay was carried out as outlined in Section 3.2.2.1. All experiments were conducted in quadruplicate, and data shown is representative of the mean of three independent experiments + SEM.

3.2.7 Development of 3D *in vitro* model of lung cancer

3.2.7.1 Scaffold fabrication

Collagen-hyaluronic acid (CHyA) scaffolds were manufactured by Dr Caroline Curtin as previously described, using collagen type I derived from bovine Achilles tendon and HyA sodium salt derived from *Streptococcus equi* (292). CHyA suspensions were made by dissolving collagen and HyA in 0.5 M (pH 2.8) glacial acetic acid separately, and blended at 15,000 rpm (IKAT18, IKA Works Inc, NC, USA) for 3.5 h in a cooling system (WKL230, Lauda Brinkman, Westbury, CT, USA) at 4°C in order to prevent denaturation. The final concentrations of the suspensions were composed of collagen 0.5% w/v and HyA 0.05% w/v.

Slurries were degassed and freeze-dried (Virtis Genesis 25EL, Biopharma, Winchester, UK) at a constant cooling rate of 1°C/min to a final temperature of

-40°C. All scaffolds were cross-linked and sterilized using a dehydrothermal (DHT) treatment under vacuum of 50 mTorr at 105°C in a vacuum oven (VacuCell, MMM, Germany) for 24 h. Cylindrical scaffold samples (8 mm diameter, 4 mm height) cut by a biopsy punch were further cross-linked with 6 mM EDAC and 2.4 mM NHS in dH₂O to improve the mechanical properties of the constructs prior to experimentation.

3.2.7.2 In vitro cell culture of A549 cells in 2D and 3D

A549 cells were seeded at a density of 100,000 or 200,000 cells per well in 6-well adherent tissue culture plates to evaluate their proliferation kinetics in 2D cell culture over 21 days. The same densities of A549 cells were seeded onto CHyA scaffolds fabricated as per Section 3.2.7.1 to determine if culturing in 3D impacted on proliferation. Cells were seeded onto the CHyA scaffolds in two portions in 24-well non-adherent tissue culture plates (Grenier Cellstar, Sigma-Aldrich, MO, USA). For 100,000 cells per scaffold, 50,000 cells in 20 µL of supplemented cell culture medium were seeded onto one side of the scaffold, and allowed to adhere for 15 min at room temperature. Scaffolds were then turned over, and the process was repeated on the unseeded side of the scaffold. 2 ml of supplemented cell culture medium was then added to each well, and plates were maintained in an incubator at 37°C in a 5% CO₂, 90% humidity environment. This process was repeated for the 200,000 cell density, by seeding 100,000 cells in 20 µL of supplemented cell culture medium onto both sides of the scaffold, as outlined above. Culture medium was changed every 2 to 3 days for 2D and 3D experiments.

3.2.8 Comparison of A549 cell proliferation in 2D and 3D cell culture

The quantification of dsDNA of A549 cells seeded in 2D and 3D, as outlined in Section 3.2.7.2, was undertaken to determine if differences in proliferation kinetics occurred under these conditions. Cells were lysed with 1% v/v Triton-X in 0.1 M carbonate buffer at Day 1, 5, 7, 14 and 21 post seeding to enable quantification of dsDNA. 1 ml of lysis buffer was added to the 2D cell culture wells for 30 min under agitation, and subsequently stored at -80°C until analysis. 3D scaffolds were submerged in 1 ml of lysis buffer and stored at -80°C until analysis. 3 freeze-thaw cycles at -80°C were conducted to ensure total cell lysis had occurred to free the cellular dsDNA for quantification using the Quant-iT™ Picogreen® dsDNA assay kit (Invitrogen, Dublin, Ireland) as per manufacturer's instructions (293, 294). Fluorescence intensity was measured using a Perkin Elmer Victor² 1420 multilabel

counter plate reader (MA, USA) (excitation 485 nm, emission 538 nm), and total dsDNA content ($\mu\text{g/ml}$) was quantified within the linear range of a dsDNA calibration curve from dilutions of DNA standards provided with the Picogreen® kit. All experiments were performed in triplicate and fluorescent measurements were made in duplicate. Data shown is representative of the mean of three independent experiments \pm SEM.

3.2.9 Assessment of viability/cytotoxicity of A459 cells in 2D and 3D culture

Viability of A549 cells cultured in 2D and 3D as per Section 3.2.7.2 was qualitatively confirmed using LIVE/DEAD™ Viability/Cytotoxicity kit (Life Technologies, CA, USA) according to the manufacturer's protocol. Briefly, at each timepoint (Day 1, 5, 7, 14 and 21) culture medium was removed from the 2D culture wells, and 3D scaffolds were transferred to fresh wells with no medium. 2D and 3D samples were rinsed with PBS, and staining was carried out as per Section 3.2.2.2 using 1 ml of the Calcein AM/Ethidium homodimer-1 solution per sample. Fluorescent images of the 2D samples were captured on a Leica DMIL microscope (Leica Microsystems, Switzerland) as outlined in Section 3.2.2.2. 3D samples were fluorescently imaged using confocal microscopy (LSM 710 confocal microscope with Zen® 2008 software, Carl Zeiss AG, Oberkochen, Germany) to create a Z-stack of 12 images, at a depth of 100 μm to 30 μm below the surface of the scaffold. Image J was used to generate composite images of cell viability/cytotoxicity.

3.2.10 Assessment of migration of A549 cells in a collagen scaffold

Samples were fixed in 10% v/v NBF for 2 h, washed in PBS, and dehydrated with increasing grades of ethanol, before being infiltrated in paraffin and embedded in paraffin blocks. Paraffin blocks were then sectioned at 5 μm using a microtome and mounted onto glass slides. Haematoxylin and Eosin (H & E) staining was performed by Mr. David Monahan in National University Ireland, Galway in order to assess general morphology of the system. Briefly, samples were dewaxed and rehydrated through decreasing grades of alcohol stained using hematoxylin, differentiated in acid alcohol and counter stained using eosin. Samples were then dehydrated and cleared before being coverslipped using DPX Mountant, and imaged using a Leica DM 1000 microscope (Leica Microsystems, Switzerland) at a magnification of 20X.

3.2.11 Assessment of cytotoxicity of blank and drug ChemoGel in a 3D *in vitro* model of lung cancer

100,000 cells were seeded onto CHyA scaffolds as outlined in Section 3.2.7.2. Cells were allowed to proliferate over 7 days before treatment to facilitate establishment of the 3D model. At Day 0 (Day 7 post seeding), 50 μ L of the appropriate treatment (Medium, cisplatin/paclitaxel solution, blank ChemoGel or drug ChemoGel) was injected into the centre of the scaffold using a 1 ml luer-lock syringe and 25G needle. Scaffolds were returned to 37°C for 30 min to allow for gelation to occur, before adding 2 ml of fresh medium to each well. Plates were returned to the incubator at 37°C in a 5% CO₂, 90% humidity environment for 2, 5, 7 or 14 days post-intra-scaffold injection. Following the pre-determined incubation period, the plates were removed from the incubator, and the supernatant was discarded. The wells were washed once with PBS, and the appropriate viability assay was carried out as outlined above (Section 3.2.2.1 and 3.2.2.2) (Fig. 3.1). All experiments were conducted in quadruplicate, and data shown is representative of the mean of three independent experiments + SEM.

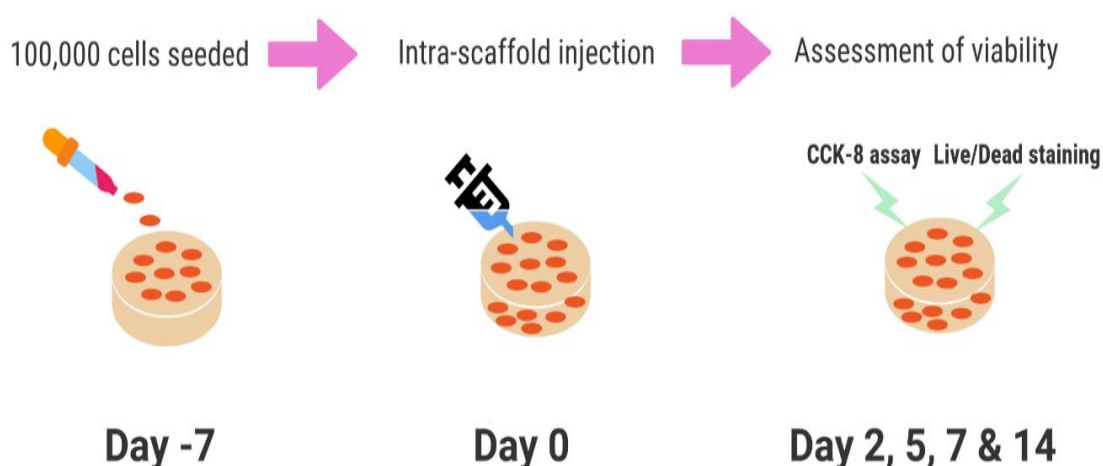


Figure 3.1 Schematic of experimental set up for 3D *in vitro* cytotoxicity evaluation of blank and drug ChemoGel.

3.2.12 Statistical analysis

Two-way analysis of variance (ANOVA) followed by Tukey's multiple comparisons test was performed in cytotoxicity studies described in Sections 3.2.3, 3.2.5, 3.2.6 and 3.2.11 to determine statistical differences between viability post-treatment *in vitro*. One-way ANOVA followed by Tukey's multiple comparisons test was used to compare results for statistical significance from apoptosis analysis in Section 3.2.4. All statistical tests were performed using GraphPad Prism v6 (GraphPad Software Inc., CA, USA). Error is reported as SEM of three independent repeats, unless otherwise stated, and significance was determined using a probability value of $p \leq 0.05$.

3.3 Results

3.3.1 Assessment of cytotoxicity of blank and drug ChemoGel in a human lung cancer cell line

3.3.1.1 Impact of seeding density on cytotoxicity of blank ChemoGel

Increasing the initial seeding density of A549 cells had a significant effect on the cytotoxicity of blank ChemoGel (Fig. 3.2 A). The cytotoxic capacity of the same volume of blank ChemoGel decreased as cell seeding density increased, and was significantly reduced at 20,000 cells per well compared to 5,000 cells per well following 24 h of treatment ($50.64\% \pm 3.1\%$ vs $7.84\% \pm 3.52\%$ respectively, $p = 0.0229$). The quantitative viability results were confirmed by qualitative Live/Dead cell imaging, as increasing seeding density was observed to have an increasing proportion of live cells (green) compared to dead cells (red) following blank ChemoGel treatment (Fig. 3.2 B).

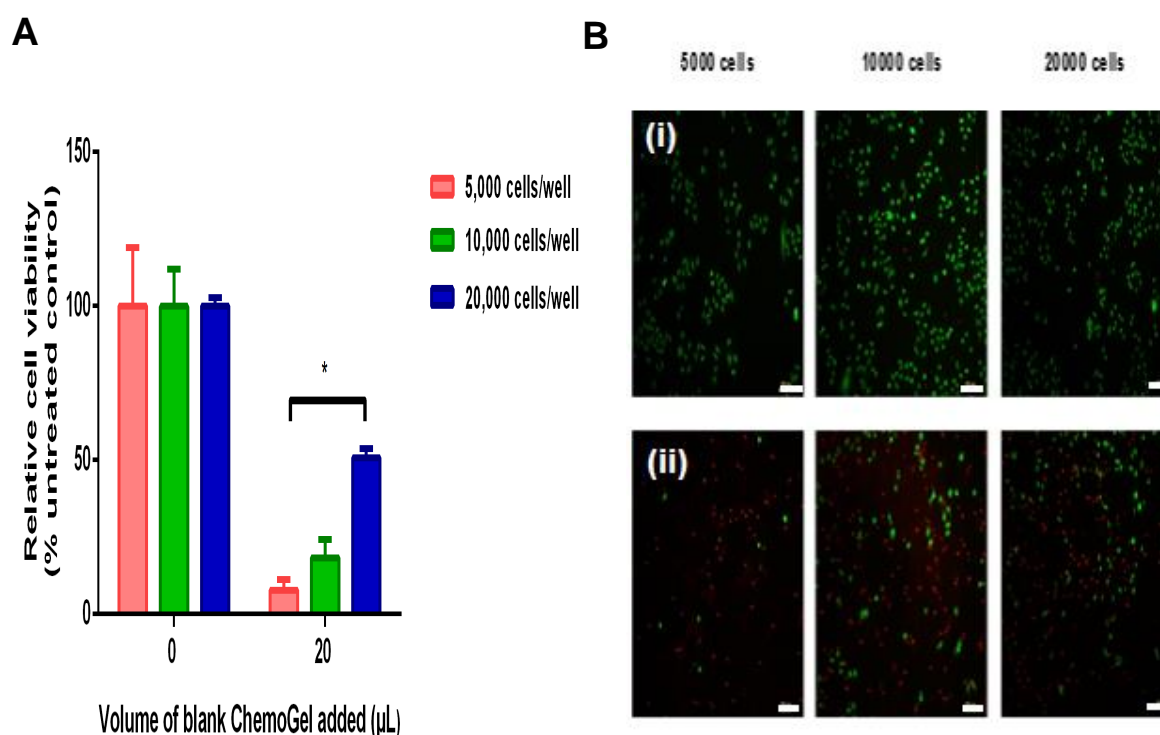


Figure 3.2 Seeding density of A549 cells had a significant effect on viability following treatment with 20 μL of blank ChemoGel for 24 h. **(A)** Relative viability of A549 cells at different seeding densities after exposure to 0 or 20 μL of blank ChemoGel for 24 h. Data shown is represented as the mean + SEM ($n=3$ replicates). Significance was determined using a two-way ANOVA, with Tukey's multiple comparisons test. $* = p < 0.05$ **(B)** Representative images of Live/Dead staining of increasing A549 cell densities treated with (i) 0 μL or (ii) 20 μL of blank ChemoGel for 24 h. Live cells are stained green, dead cells are stained red. Magnification, 10X. Scale bar, 200 μm .

3.3.1.2 Dose-dependent cytotoxicity of blank ChemoGel

A seeding density of 20,000 cells per well was subsequently chosen to investigate if ChemoGel treatment demonstrated a dose-dependent toxicity. Blank ChemoGel treatment at all doses evaluated demonstrated a significant decrease in viability of A549 cells (Fig. 3.3 A), with viability data confirmed qualitatively with Live/Dead staining (Fig. 3.3 B). Although not statistically significant, increasing blank ChemoGel doses resulted in increasing toxicity in A549 cells as viability decreased by approximately 30% after 24 h between treatment with 10 μ L and 30 μ L (46.97% \pm 10.32% vs. 16.38% \pm 3.6% respectively, $p = 0.109$).

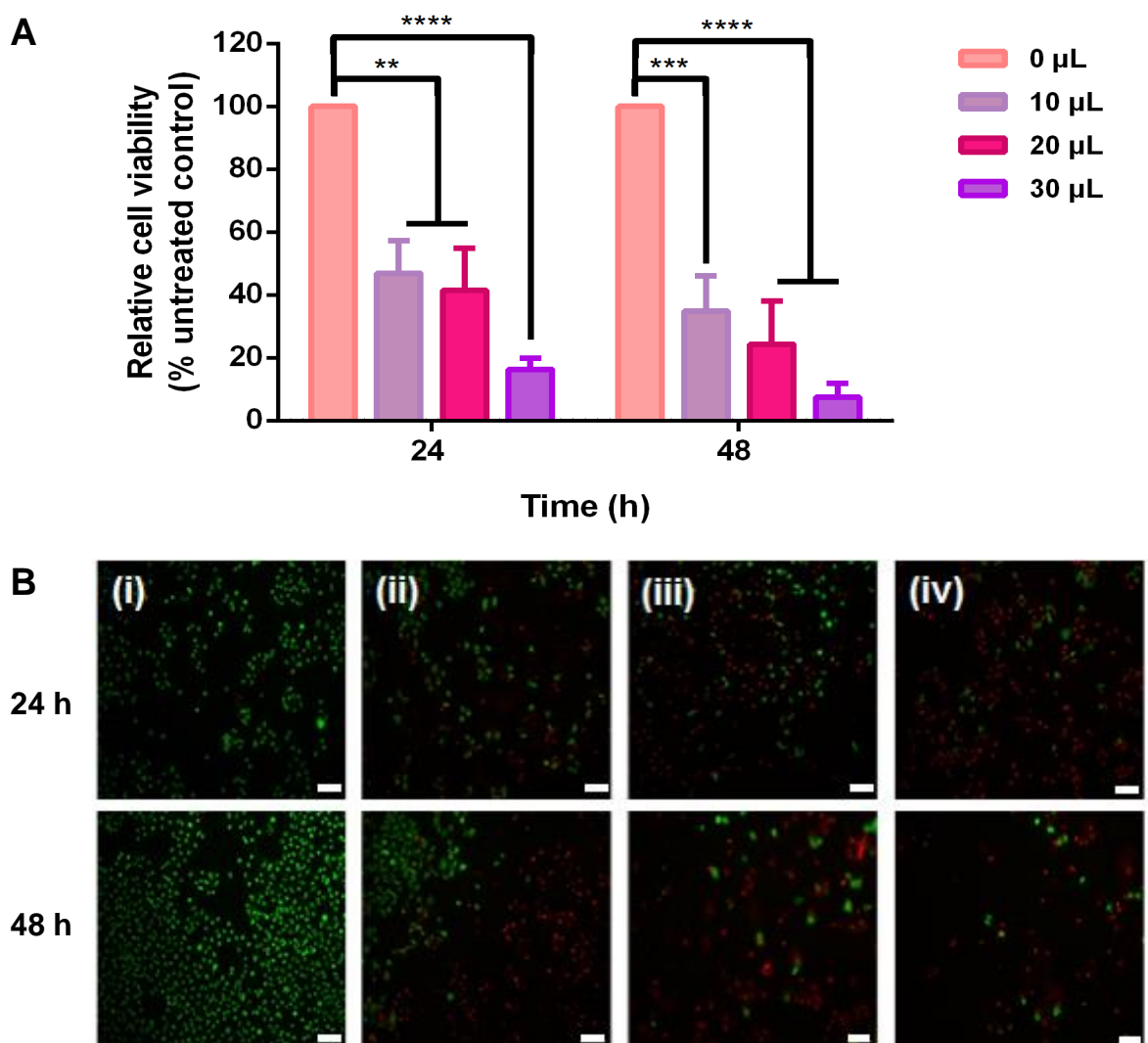


Figure 3.3 Blank ChemoGel treatment significantly reduced viability of A549 cells. **(A)** Relative viability of A549 cells treated with 0 . 30 μ L of blank ChemoGel for 24 and 48 h. Data shown is represented as the mean + SEM of three independent experiments ($n=3$). Significance was determined using a two-way ANOVA, with Tukey's multiple comparisons test. ** = $p < 0.01$, *** = $p < 0.001$, **** = $p < 0.0001$ **(B)** Representative images of Live/Dead staining of A549 cells treated with (i) 0 μ L, (ii) 10 μ L, (iii) 20 μ L or (iv) 30 μ L of ChemoGel for 24 and 48 h. Live cells stained green, dead cells stained red. Magnification, 10X. Scale bar, 200 μ m.

3.3.1.3 Dose-dependent cytotoxicity of drug ChemoGel

All doses of drug ChemoGel evaluated (0 – 30 μ L) caused a statistically significant decrease in viability of A549 cells, compared to untreated control at the same timepoints ($p < 0.0001$) (Fig. 3.4 A). Treatment with 30 μ L of ChemoGel caused a statistically significantly greater reduction in viability than 10 μ L of ChemoGel at 24 h ($6.25\% \pm 2.41\%$ vs. $31.74\% \pm 11.7\%$ respectively, $p = 0.0205$). Qualitative Live/Dead staining confirmed viability results, with increasing number of dead cells (red) and decreasing number of live cells (green) observed with increasing dose (Fig. 3.4 B).

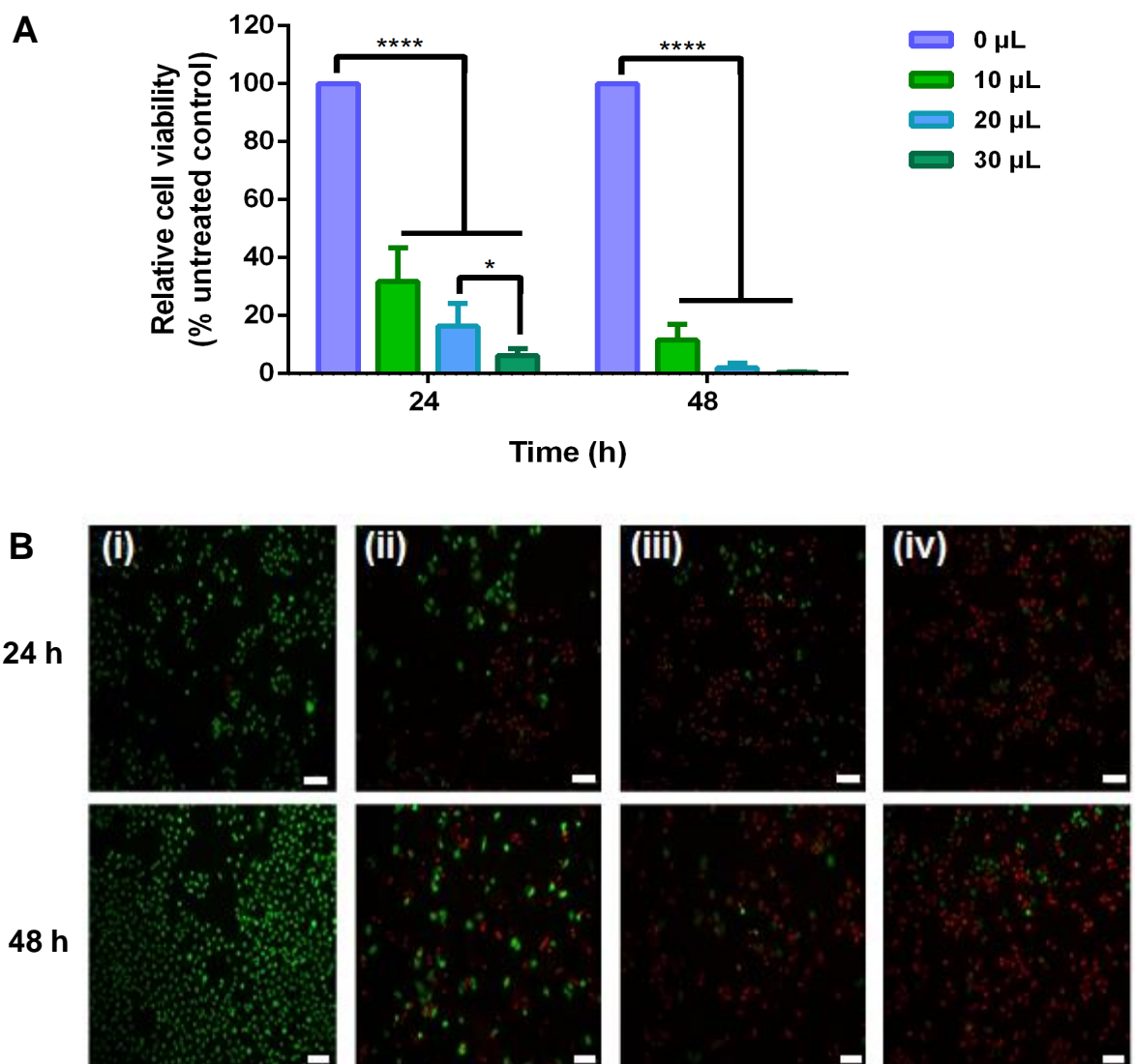


Figure 3.4 Drug ChemoGel treatment significantly reduced viability of A549 cells. **(A)** Relative viability of A549 cells treated with 0 . 30 μ L of drug ChemoGel for 24 and 48 h. Data shown is represented as the mean + SEM of three independent experiments ($n=3$). Significance was determined using a two-way ANOVA, with Tukey's multiple comparisons test. * = $p < 0.05$, **** = $p < 0.0001$ **(B)** Representative images of Live/Dead staining of A549 cells exposed to (i) 0 μ L, (ii) 10 μ L, (iii) 20 μ L or (iv) 30 μ L of drug ChemoGel for 24 (top) and 48 (bottom) h. Live cells are stained green, dead cells are stained red. Magnification, 10X. Scale bar, 200 μ m.

3.3.1.4 Cytotoxicity of lead ChemoGel formulations

Comparison of the same volume of blank ChemoGel, drug ChemoGel and cisplatin/paclitaxel solution revealed that all treatments caused a statistically significant decrease in viability compared to untreated controls (Fig. 3.5 A). At 24 h, a statistically significant greater reduction in viability was observed following treatment with drug ChemoGel ($6.25\% \pm 2.41\%$) compared to both blank ChemoGel ($16.38\% \pm 3.6\%$, $p = 0.0436$) and cisplatin/paclitaxel solution ($17.05\% \pm 2.41\%$, $p = 0.03$) (Fig. 3.5 A). Live/Dead imaging qualitatively confirmed these results (Fig. 3.5 B).

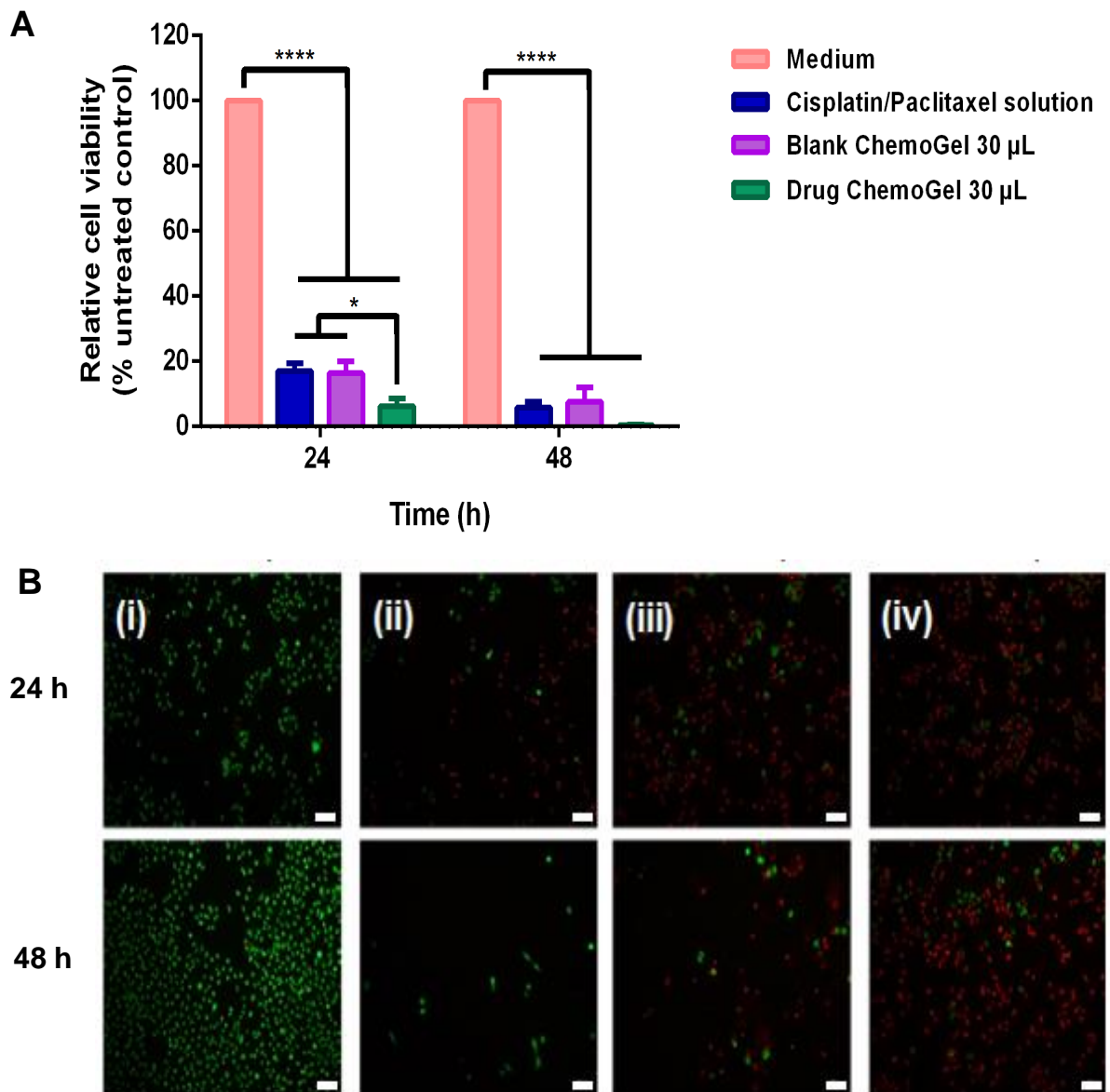


Figure 3.5 Treatment with cisplatin/paclitaxel solution, blank ChemoGel or drug ChemoGel significantly reduced viability of A549 cells. **(A)** Relative viability of A549 cells treated with 30 μ L of cisplatin/paclitaxel 0.01% w/w solution, blank ChemoGel or drug ChemoGel for 24 and 48 h. Data shown is represented as the mean + SEM of three independent experiments ($n=3$). Significance was determined using a two-way ANOVA, with Tukey's multiple comparisons test. $*$ = $p < 0.05$, $****$ = $p < 0.0001$. **(B)** Representative images of Live/Dead staining of A549 cells exposed to (i) Medium, (ii) cisplatin/aclitaxel solution, (iii) blank ChemoGel or (iv) drug ChemoGel for 24 (top) and 48 (bottom) h. Live cells are stained green, dead cells are stained red. Magnification, 10X. Scale bar, 200 μ m.

3.3.2 Apoptosis analysis

Apoptosis analysis of blank ChemoGel, drug ChemoGel and cisplatin/paclitaxel solution treatment of A549 cells *in vitro* revealed that all treatments statistically significantly reduced viability of A549 cells compared to Medium alone (Fig. 3.6). Blank ChemoGel reduced the percentage of live cells to $64.1\% \pm 4.2\%$ ($p = 0.0025$), with the greatest amount of dead cells in the early apoptotic stages ($14.7\% \pm 0.4\%$) (Fig. 3.6 B). Drug ChemoGel showed the greatest reduction in viability, as only $50.75\% \pm 0.85\%$ of cells were determined to be live ($p = 0.0006$) (Fig. 3.6 C). A similar proportion of drug ChemoGel treated cells were found to be in early apoptotic stages compared to blank ChemoGel, with an increase in the proportion of late apoptotic and necrotic cells, accounting for the decrease in viability.

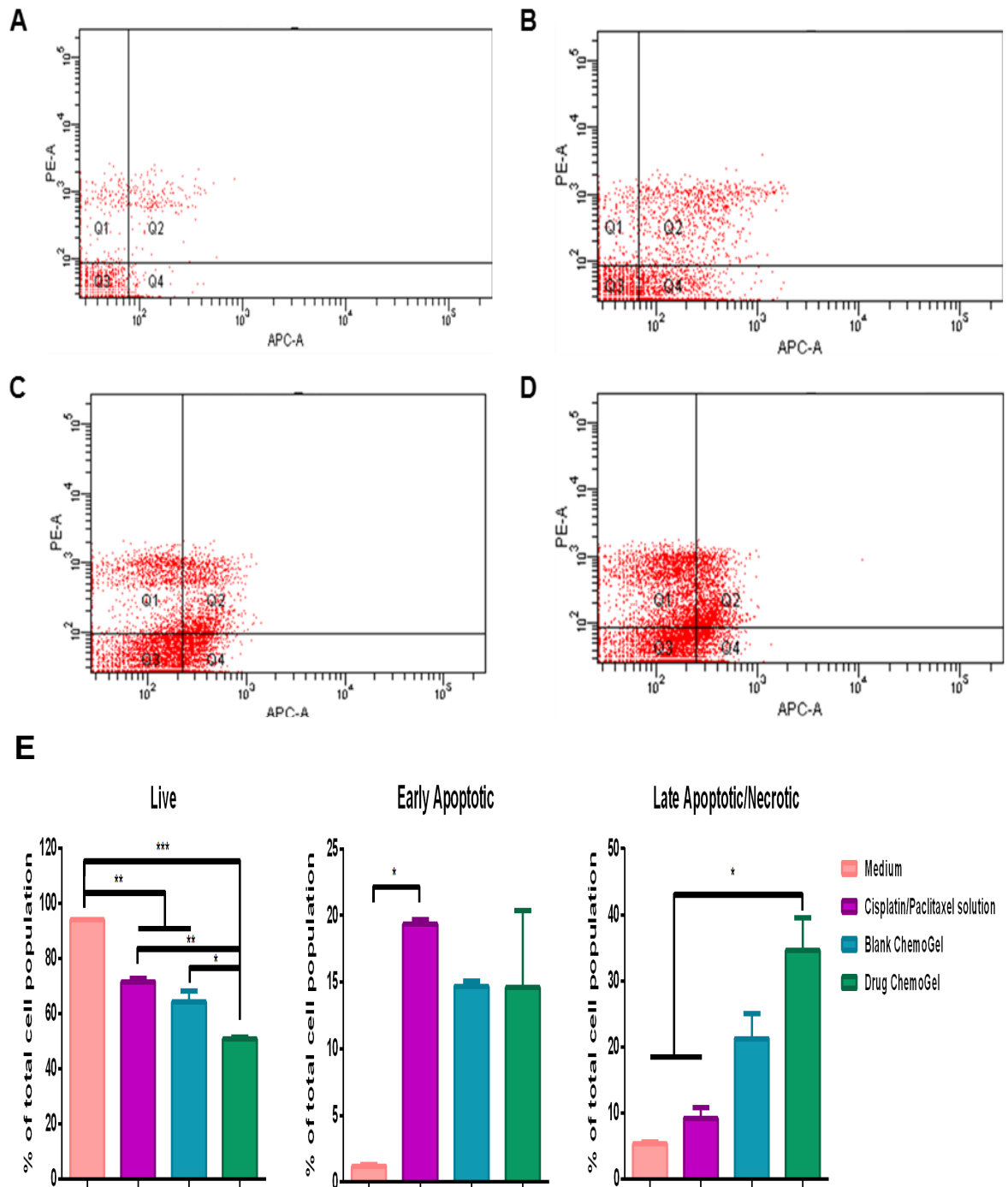


Figure 3.6 Flow cytometric analysis of apoptosis using APC Annexin V and PI staining of (A) Medium, (B) cisplatin/paclitaxel solution, (C) blank ChemoGel and (D) drug ChemoGel treated A549 cells for 24 h *in vitro*. (E) Proportion of live, early apoptotic, late apoptotic/necrotic cells treated with Medium, blank ChemoGel, drug ChemoGel and cisplatin/paclitaxel. Q 1 & Q 2= late apoptotic/necrotic cells, Q 3 = live cells Q 4 = early apoptotic cells, Data shown is represented as the mean + SEM of two independent repeats (n=2). Significance was determined using a one-way ANOVA, with Tukey's multiple comparisons test. * = $p < 0.05$, ** = $p < 0.01$, *** = $p < 0.001$.

3.3.3 Assessment of cytotoxicity of ChemoGel in a non-cancerous murine cell line

Treatment of a non-cancerous cell line, Balb/c 3T3 clone A31 with 0 – 30 μ L of blank ChemoGel was then used to assess the cytotoxicity in off-target cells (Fig 3.7 A). Treatment with 10 μ L of ChemoGel resulted in an increase in viability of the Balb/c 3T3 clone A31 cells at 24 and 48 h (106.44% \pm 19.89% and 115.89% \pm 17.22% respectively). Increasing ChemoGel dose to 20 μ L and 30 μ L resulted in a statistically significant decrease in viability compared to untreated cells (20 μ L: 50.61% \pm 2.36% [p = 0.0178] and 30 μ L: 11.77% \pm 3.45% [p = 0.002] at 48 h).

The cytotoxicity of the blank ChemoGel disintegration products was also assessed in the fibroblast cell line to determine the effect of disintegration products on healthy cells (Fig. 3.7 B). The disintegration products were seen to reduce the viability of A549 cells to 67.59% \pm 8.62%. It is of note that these results are difficult to compare to other toxicity data, due to the large mass of hydrogel used in the disintegration product test (0.5 g of blank ChemoGel), compared to quantities of blank ChemoGel used in previous Balb/c 3T3 clone A31 cytotoxicity studies of 10 - 30 μ L (Fig. 3.7 A).

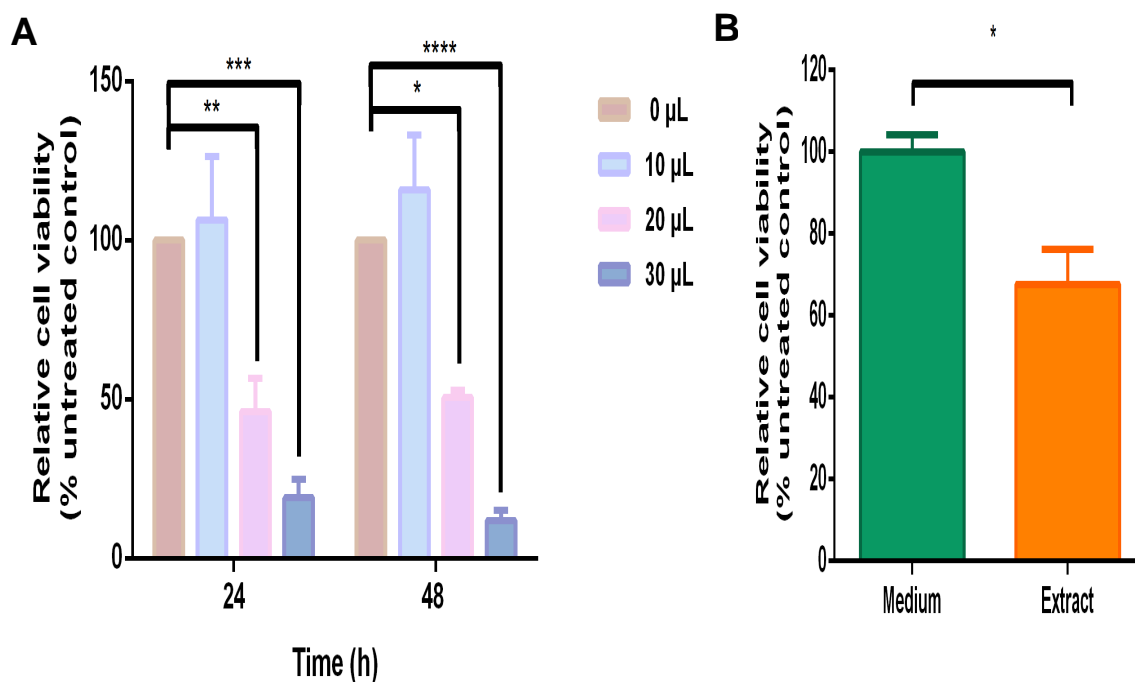


Figure 3.7 Blank ChemoGel treatment did not negatively affect viability of Balb/c 3T3 clone A31 cells at low doses. **(A)** Relative viability of Balb/c 3T3 clone A31 cells treated with 0 . 30 µL of ChemoGel for 24 and 48 h. Data shown is represented as the mean + SEM of three independent experiments (n=3). Significance was determined using a two-way ANOVA, with Tukey's multiple comparisons test. **(B)** Relative viability of Balb/c 3T3 clone A31 cells treated with degradation products of ChemoGel (extract) for 24 h. Data shown is represented as the mean + SEM (n=4 replicates). Significance was determined using an unpaired t test. * = $p < 0.05$, ** = $p < 0.01$, *** = $p < 0.001$, **** = $p < 0.0001$.

3.3.4 Assessment of cytotoxicity of the individual excipients of ChemoGel formulation

Assessment of the cytotoxicity of individual excipients of the ChemoGel formulation, used at the same concentration as that in 30 µL of blank ChemoGel (Table 3.2), in A549 cells and Balb/c 3T3 clone A31 cells revealed that the excipients tended to exert greater cytotoxicity in the cancerous cell line (Fig 3.8 A & B). P407 was the only excipient to induce a statistically significant reduction in viability in A549 cells, with no significant reduction observed for any excipients in Balb/c 3T3 clone A31 cells.

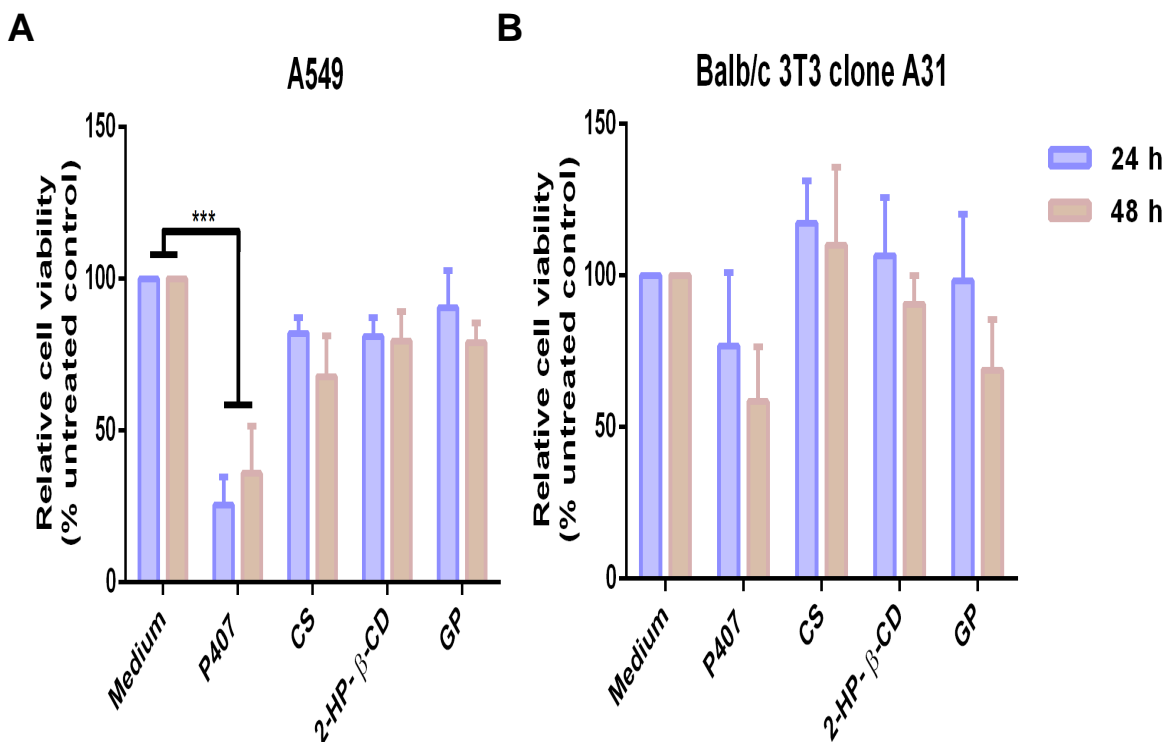


Figure 3.8 Cytotoxic capacity of individual excipients of the ChemoGel formulation varied between A549 and Balb/c 3T3 clone A31 cells. Relative viability of **(A)** A549 cells and **(B)** Balb/c 3T3 A31 cells following treatment with Poloxamer 407 (P407), Chitosan (CS), 2-Hydroxypropyl-β-Cyclodextrin (2-HP-β-CD) or Genipin (GP) for 24 and 48 h. Data shown is represented as the mean + SEM of three independent repeats (n=3). Significance was determined using a two-way ANOVA, with Tukey's multiple comparisons test. *** = $p < 0.001$.

3.3.5 Development of an *in vitro* 3D lung cancer model

3.3.5.1 Proliferation of A549 cells in 2D and 3D over 21 days

Evaluation of proliferation of A549 cells cultured in 2D at two different seeding densities demonstrated that both seeding densities proliferated rapidly over 14 days, as evidenced by increasing dsDNA. Between Day 14 and Day 21, a decrease in dsDNA content was observed in the higher seeding density from $26.05 \mu\text{g/ml} \pm 3.125 \mu\text{g/ml}$ to $18.69 \mu\text{g/ml} \pm 2.58 \mu\text{g/ml}$ (Fig. 3.9 A). The same pattern was not observed in the lower seeding density in 2D between Day 14 and Day 21, but the rate of proliferation slowed compared to earlier timepoints. Culture of A549 cells in 3D CHyA scaffolds revealed that both seeding densities proliferated over 21 days, although they did not undergo the same pattern of rapid proliferation. At Day 21 similar levels of dsDNA were observed for both seeding densities in 3D, with $3.01 \pm 0.31 \mu\text{g/ml}$ and $3.06 \pm 0.19 \mu\text{g/ml}$ of dsDNA quantified for the 100,000 cell and 200,000 cell seeding density respectively (Fig. 3.9 B). Comparing fold change of

dsDNA over the 21 day period revealed that 100,000 cells per well or scaffold in 2D or 3D respectively underwent the higher rates of fold change of proliferation than 200,000 cells under the same conditions (Fig. 3.9 C). Increased numbers of dead cells (red) were qualitatively observed in 2D culture than 3D culture following Live/Dead staining from Day 7 onwards, although it is of note that cells imaged in the 3D were from an X depth Z-stack, so are not representative of the entire culture system (Fig. 3.10).

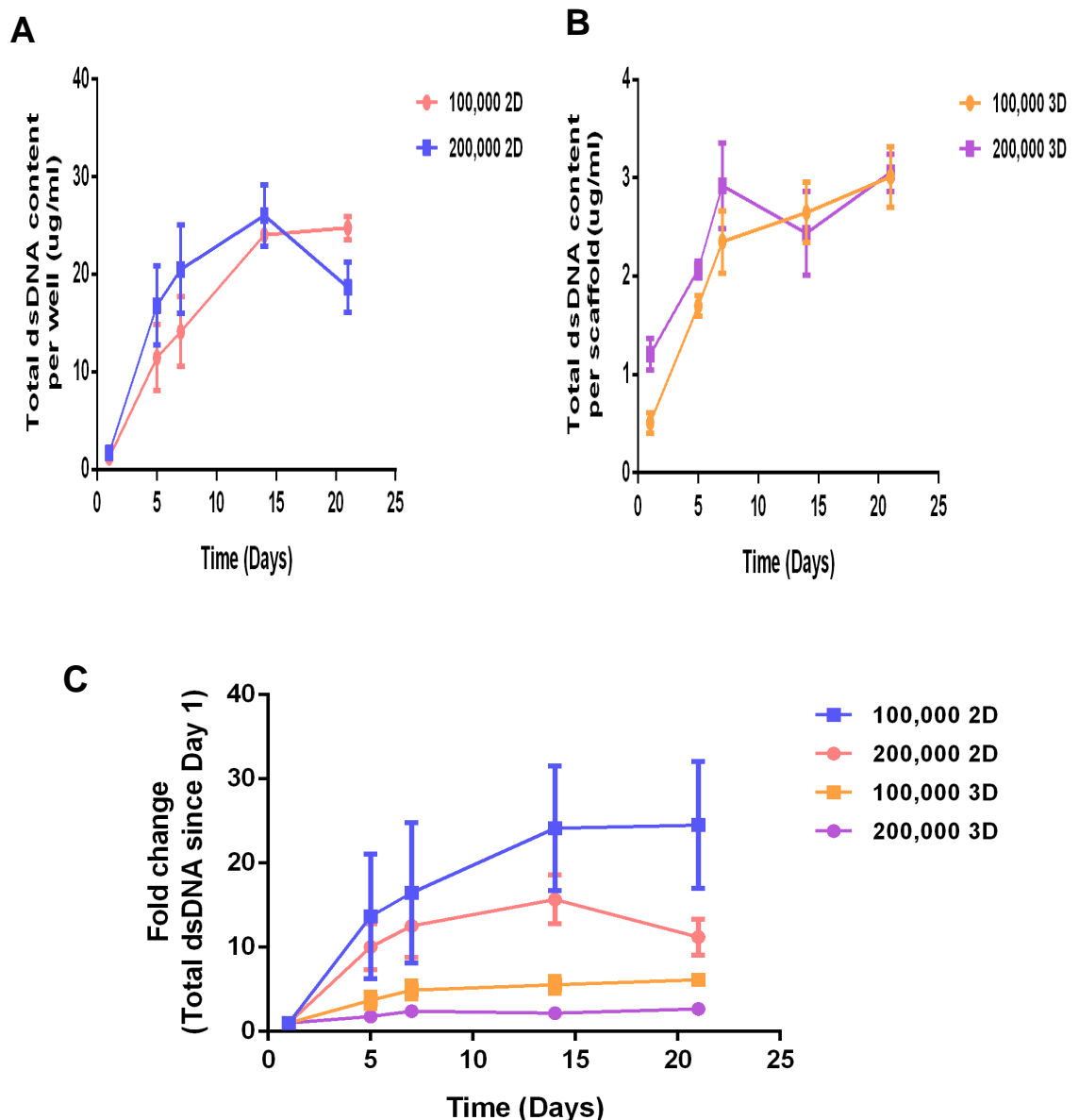


Figure 3.9 Proliferation pattern of A549 cells was dependent on initial cell number seeded and matrix upon which they are cultured. dsDNA content of A549 cells seeded at 100,000 or 200,000 cells per well and cultured in (A) 2D monolayers and (B) 3D Collagen-Hyaluronic acid scaffolds over 21 days. (C) Fold change in dsDNA of A549 cells at two seeding densities seeded in 2D or 3D over 21 days. Data shown is represented as the mean \pm SEM of three independent repeats ($n=3$).

3.3.5.2 Viability of A459 cells in 2D and 3D over 21 days

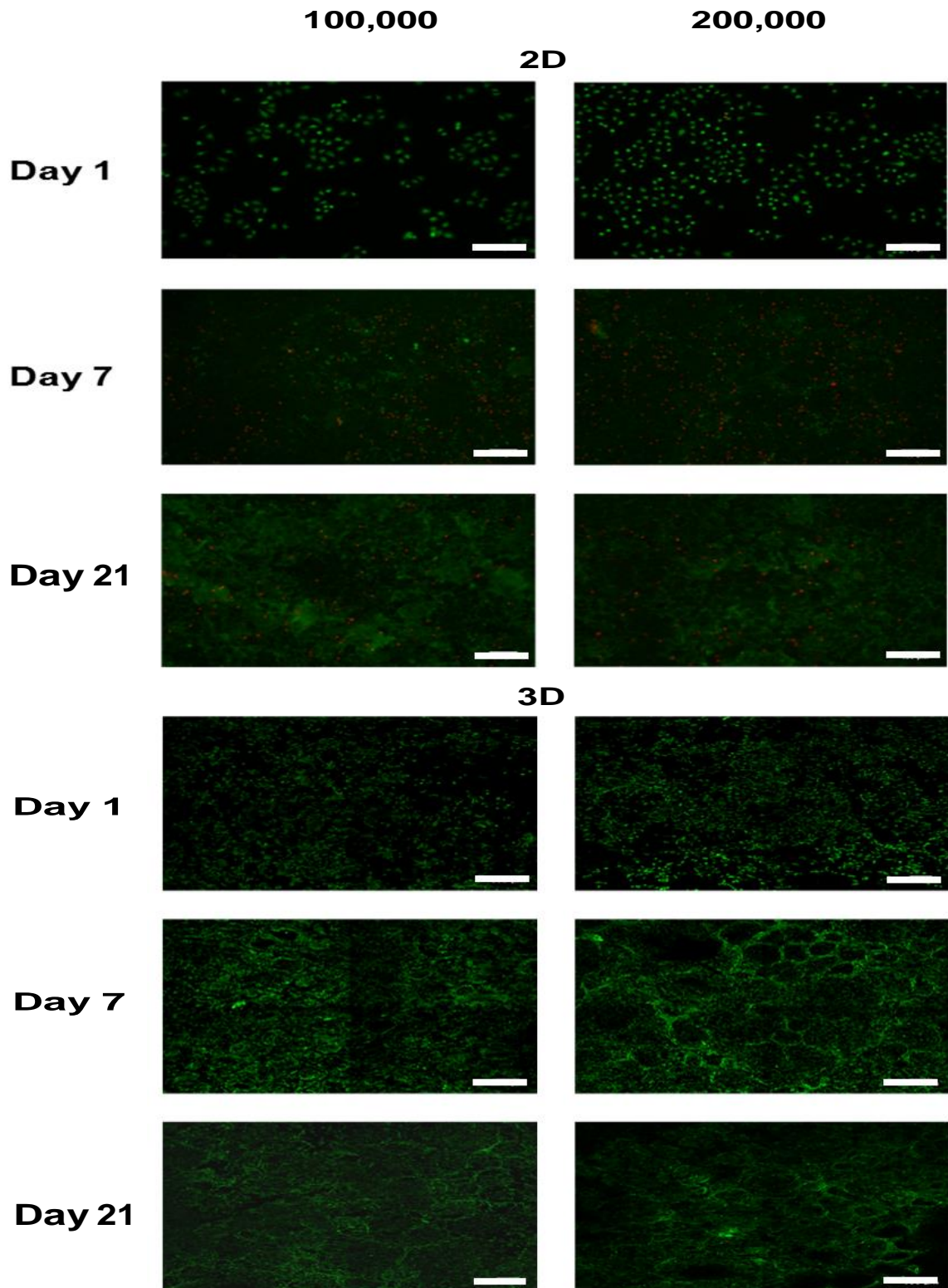


Figure 3.10 More dead cells (red) are qualitatively observed in 2D culture, compared to the same timepoint in 3D. Representative images of Live/Dead staining of A549 cells cultured in 2D and 3D at two seeding densities (100,000 or 200,000 cells per well or scaffold) over 21 days. Live cells are stained green, dead cells are stained red. Magnification, 10X. Scale bar, 200 μm .

3.3.5.3 Migration of A549 cells through 3D environment

Qualitative assessment of migration of A549 cells through the CHyA scaffold was conducted to evaluate the establishment of a 3D system. At both cell densities A549 cells were observed to have migrated through the scaffold at Day 7 and 14. A denser cell population was observed at the surface of the scaffold at all timepoints at both seeding densities (Fig. 3.11)

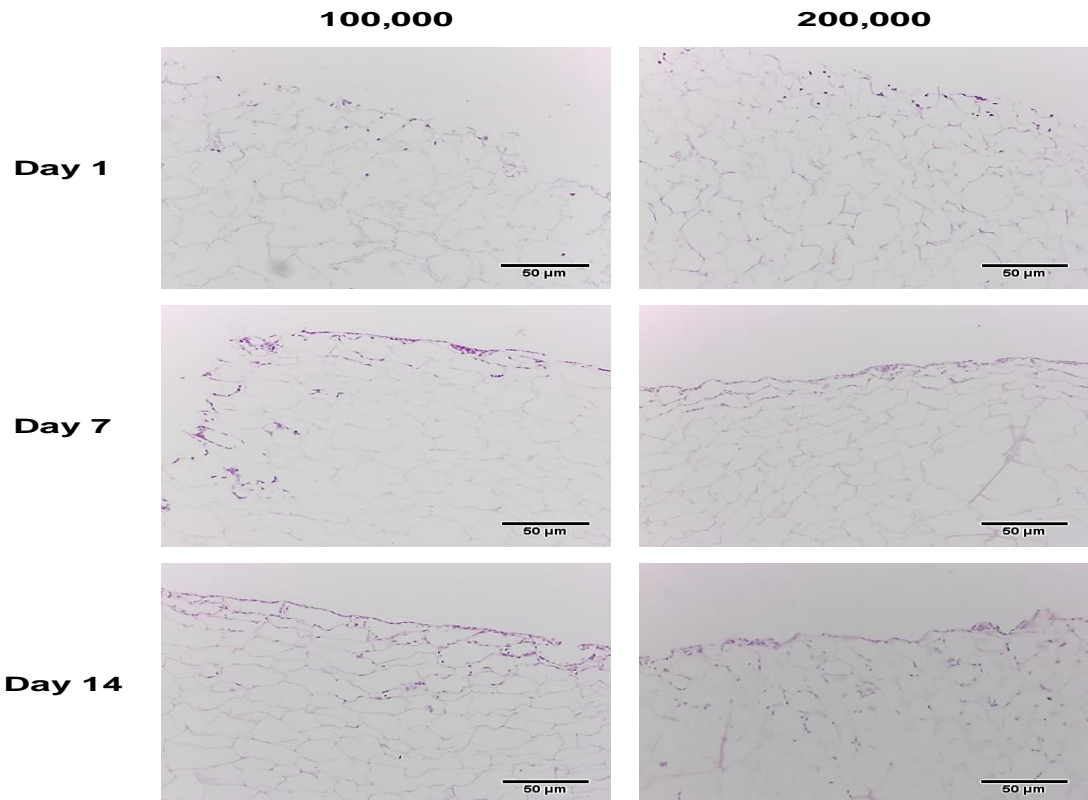


Figure 3.11 Migration of A549 cells seeded on Collagen-Hyaluronic acid scaffolds at different seeding densities was observed at Day 7 and 14. Representative images of H&E staining of A549 cells seeded at 100,000 (left) or 200,000 (right) cells per scaffold at Day 1, 7 and 14. Magnification, 20X. Scale bar, 50 µm.

3.3.5.4 Assessment of blank and drug ChemoGel cytotoxicity in 3D model of lung cancer

The 3D *in vitro* model of NSCLC facilitated the cytotoxicity evaluation of blank and drug ChemoGel over 14 days in an environment that was more biomimetic than 2D monolayer culture. Following intra-scaffold injection, designed to mimic IT administration, blank and drug ChemoGel underwent gelation to form a bolus within the scaffold, which remained *in situ* for the duration of the study (Fig. 3.12 A). Viability of the blank ChemoGel treated A549s was significantly reduced at all timepoints analysed post administration compared to Medium treated control, with viability reduced to 39.04% \pm 3.43% at Day 14 ($p < 0.0001$) (Fig. 3.12 B). Drug ChemoGel reduced viability of the A549 cells to 19.1% \pm 0.42% compared to Medium treated control at Day 2 ($p < 0.0001$), and maintained this reduced viability until Day 14 (11.44% \pm 2.51%, $p < 0.0001$). There was a statistically significant difference between viability of blank and drug ChemoGel at Day 2, 5 and 7, with drug ChemoGel being more effective at reducing viability than blank ChemoGel. At Day 14, drug ChemoGel reduced viability to a greater extent than blank ChemoGel, with a trend towards statistical significance ($p = 0.0719$). Blank ChemoGel reduced viability to a statistically significantly greater extent than the cisplatin/paclitaxel solution at Day 2 (52.83% \pm 3.76% vs 94.92% \pm 13.14% respectively, $p = 0.0026$), with no statistical difference between these two groups observed thereafter. Drug ChemoGel reduced viability to a statistically significantly higher degree than cisplatin/paclitaxel solution at all timepoints (Day 14: 11.44% \pm 2.51% vs 66.07% \pm 12.59%, $p < 0.0001$).

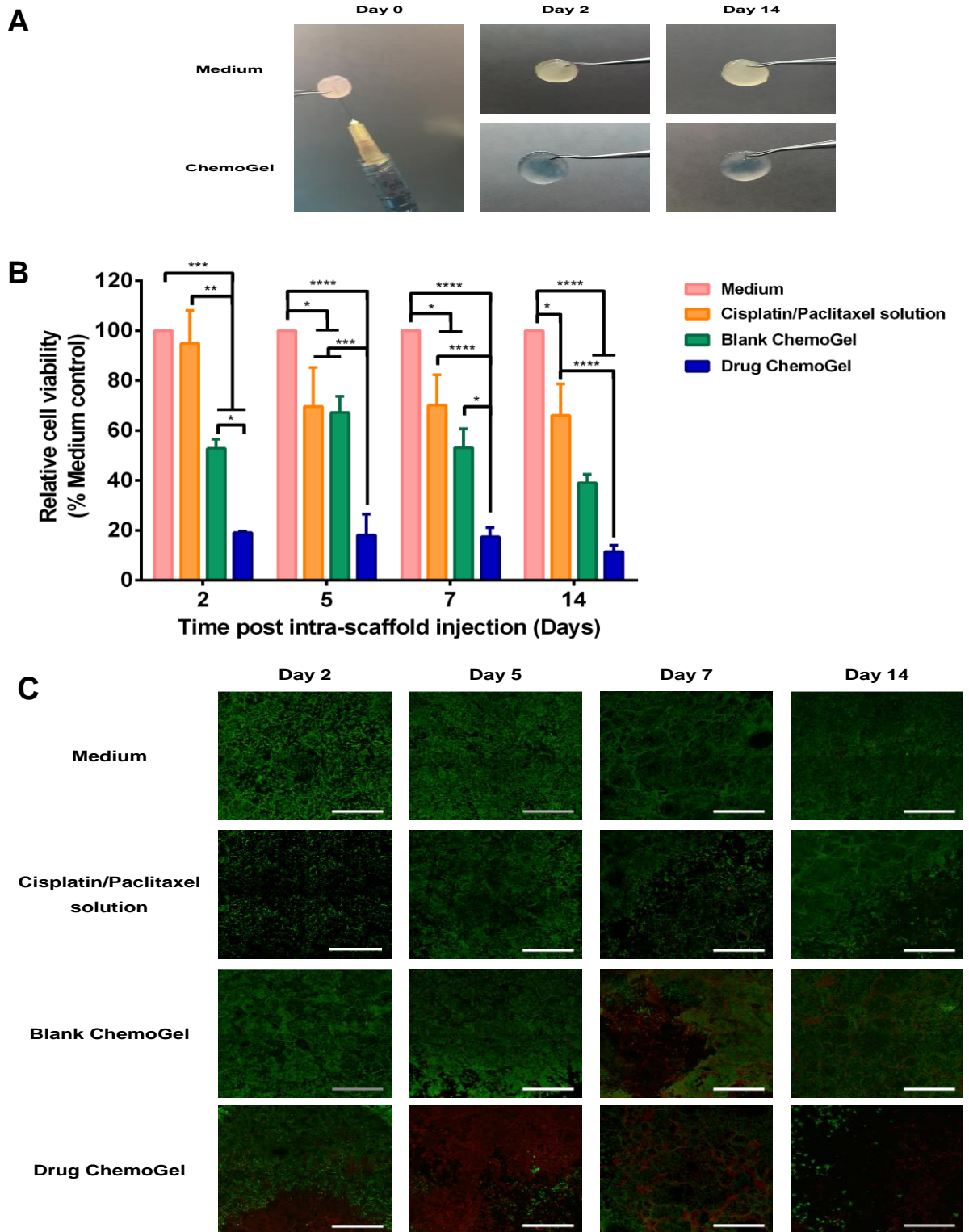


Figure 3.12 3D cell culture of A549 cells on Collagen-Hyaluronic acid scaffolds facilitated cytotoxicity evaluation of blank and drug ChemoGel over 14 days. **(A)** Representative images of intra-scaffold injection of Medium or ChemoGel over time. **(B)** Relative viability of A549 cells cultured on a 3D scaffold following intra-scaffold injection of Medium, cisplatin/paclitaxel solution, blank ChemoGel or drug ChemoGel. Data shown is represented as the mean + SEM of three independent repeats ($n=3$). Significance was determined using a two-, æÁ CEUXCEÁ, æ@ V \ ^ ^ q Á{ ~ |ç | ^ Á comparisons test. * = $p < 0.05$, ** = $p < 0.01$, *** = $p < 0.001$, **** = $p < 0.0001$. **(C)** Representative images of Live/Dead staining of A549-seeded scaffolds treated with Medium, cisplatin/paclitaxel solution, blank ChemoGel or drug ChemoGel over time. Live cells stained green and dead cells stained red. Magnification, 10X. Scale bar, 500µm.

3.4 Discussion

The challenge associated with biorelevant cytotoxicity evaluation is well documented, and in the case of thermoresponsive hydrogels an additional layer of complexity is presented due to the multifaceted behaviour of the composite materials (295). This chapter sought to assess the *in vitro* cytotoxicity of blank and drug ChemoGel treatment in a 2D model of NSCLC, in order to establish preliminary cytotoxicity data. A non-cancerous cell line was also treated with blank ChemoGel to compare *in vitro* cytotoxicity between target and non-target cells types. Finally, a 3D model of NSCLC was developed to create a more biomimetic environment for *in vitro* cytotoxicity evaluation over longer timeframes, to gain further insight into the biological actions of the ChemoGel technology.

As the quantity of thermoresponsive hydrogels used in *in vitro* cytotoxicity studies varies widely, this makes prediction of *in vivo* cytotoxicity difficult, as very low doses evaluated *in vitro* may shield potential inherent cytotoxicity. Elias *et al.* (2015) highlighted the discrepancies in cytotoxicity evaluation of a polymeric hydrogel, which they found to be cytotoxic at the concentrations assessed (296). The authors note that this polymeric hydrogel is generally reported as non-toxic, but these assessments have been carried out at doses at which gelation was not feasible. This study also demonstrates the divergences which can arise from direct and indirect contact assays. Cells encapsulated in the hydrogel (direct contact) resulted in a 90% reduction in cell viability after 24 h, but the same quantity of polymer separated from cells by a Transwell (indirect contact) only reduced viability by less than 10% after 48 h, which may lead to an underestimation of the true cytotoxicity of the intact hydrogel (296). The studies contained in this Chapter were designed to utilise blank ChemoGel and drug ChemoGel at doses at which gelation was feasible, in combination with a direct contact assay to ascertain the true cytotoxicity of the blank and drug-loaded delivery platforms.

An *in vitro* cytotoxicity profile of the ChemoGel formulation was first established in a 2D model of NSCLC. 20,000 cells seeded in 24-well plates was chosen for cytotoxicity assessments as this falls within the recommended seeding density per surface area for A549 cells (265), and enables dose-dependency of ChemoGel treatment to be elucidated (Fig. 3.2). Previous studies have also employed a similar study design with 24-well plates, which offers a larger surface area than the 96-well

plate format commonly used, to investigate the cytotoxicity of drug-loaded thermoresponsive hydrogels (58, 297).

A range of ChemoGel doses were evaluated to investigate if the previously observed cytotoxicity was dose-dependent. Treatment with blank ChemoGel demonstrated that this drug delivery platform may exert pharmacological effects in its own right, with increasing doses resulting in increasing toxicity to A549 cells *in vitro* (Fig. 3.2 & 3.3). While it is recognised that many studies employing thermoresponsive hydrogels as drug carriers promote their *in vitro* biocompatibility as a positive attribute of their formulation design (24), the concept supporting the use of a cytotoxic drug delivery platform is to create a multipurpose treatment modality; one which is capable of releasing chemotherapeutics over a defined period, and augmenting the cytotoxicity of the released drug molecules.

Analysis of the cytotoxicity of drug ChemoGel, and comparison of blank and drug ChemoGel with a cisplatin/paclitaxel solution, resulted in almost complete cell death after 48 h, preventing the long term analysis of cytotoxicity (Fig. 3.3 & 3.4). This highlighted the need for an *in vitro* cell culture system that would facilitate cytotoxicity evaluation over longer time frames, in order to determine if cytotoxicity was maintained after 48 h of treatment. It is also of note that often other studies do not report on the *in vitro* cytotoxicity of the hydrogel carrier, for example a nanoparticle-loaded thermoresponsive hydrogels for cancer therapy only included *in vitro* toxicity data on the blank and drug-loaded nanoparticles, but did not include blank and drug-loaded hydrogel toxicity (298).

Scale down from *in vivo* doses to *in vitro* quantities is particularly difficult for thermoresponsive hydrogels because a number of factors must be considered and extrapolated to a smaller scale; volume required for gelation, volume required for drug-loading, maximum volume capacity *in vivo*, and multiple dosing regimen considerations. In order to gain maximal value from *in vitro* cytotoxicity evaluations of thermoresponsive hydrogels, a standardised approach to methodology is required. In the case of blank and drug ChemoGel, gelation was feasible at volumes of 10 – 30 μL , however injection into the cell culture well plate did not facilitate the formation of an intact bolus following gelation. Rather, segments of gelled hydrogel formed in the medium. This further indicates limitations of 2D cytotoxicity testing of thermoresponsive hydrogels.

Apoptosis analysis revealed a similar trend to the cytotoxicity assessment, in that, drug ChemoGel exerted the greatest reduction in viability on the A459 cells (Fig. 3.6 D). The increased viability across all groups compared to the cytotoxicity assessments in Figure 3.3 – 3.5 may be attributed to the greater number of cells seeded. At this seeding density some differences between groups were seen, which could not be elucidated in the viability assays. Drug ChemoGel significantly reduced the proportion of live cells compared to blank ChemoGel and cisplatin/paclitaxel solution (Fig. 3.6 E). Live cells were quantified by determining the percentage of total cell population which did not stain for Annexin V or PI. In healthy cells, phosphatidylserine is found in an intracellular leaflet of the cell membrane. It undergoes translocation to an external leaflet during apoptosis, at which point Annexin V can interact with it in a calcium dependent manner, and thus cells which stain positively for Annexin V are said to be apoptotic. For the purposes of flow cytometry analysis of apoptosis, early apoptosis is defined as Annexin V +/ PI -, indicating that the phosphatidylserine has translocated to an external leaflet, but the cell membrane is still intact. PI is used to determine late stage apoptosis/necrosis as this requires a disrupted membrane to pass into the cell and interact with the DNA in the nucleus to produce fluorescence (291).

Balb/c 3T3 clone A31 cells are recommended for cytotoxicity testing by ISO standard 10993-5:2009 (269), and were employed in this Chapter to evaluate the effects of blank ChemoGel in off-target cell types (Fig. 3.7 A). 10 μ L of ChemoGel was seen to have proliferative effects on the non-cancerous cell line, at 24 and 48 h post treatment. This was not seen in the cancerous cell line, as the same dose administered resulted in a statistically significant decrease in viability at these time points (Fig. 3.3 A). 20 μ L and 30 μ L resulted in decreased viability in line with the results obtained in the cancer cell line. The ChemoGel components were chosen in part based on their suggested cancer cell directed cytotoxicity, as outlined in Chapter 2. The cytotoxic specificity is seen at 10 μ L, but is lost as the dose is increased. In the clinical setting, ChemoGel will be delivered only to tumour tissue, reducing the amount of direct contact with tumour tissue. Paracelsus said “the dose makes the poison” and this seems to be held true in relation to ChemoGel. Above a certain concentration the tumour cell directed cytotoxicity is lost; therefore it will be important to establish this level *in vivo* through maximum tolerated dose testing, and evaluation of off target organs for toxicity.

While it is expected that delivery of ChemoGel in the clinical setting will be restricted to cancerous tissue only, the breakdown products of ChemoGel will most likely be removed via systemic circulation and excreted. To assess the potential off-site toxicity arising from the removal of these breakdown products of ChemoGel, the cytotoxicity of the disintegration products (extracts) from blank ChemoGel was evaluated in non-target cells (Fig. 3.7 B). A statistically significant reduction in viability of the Balb/c 3T3 clone A31 cells was observed following 24 h exposure. However, it should be borne in mind that the disintegration products were from 0.5 g of ChemoGel, which is more than ten-fold than the volumes evaluated of whole ChemoGel. The ISO standard for the *in vitro* cytotoxicity evaluation of medical devices determines that viability of 70% or above following exposure to extracts indicates an acceptable level of biocompatibility (269). As the exposure of the degradation products of blank ChemoGel caused a reduction of viability to 67.59% \pm 8.62%, this indicates that the biocompatibility of ChemoGel extracts is nearing acceptable limits. Further studies are required to determine toxicity of ChemoGel disintegration products at later timepoints.

Assessment of the individual components of ChemoGel was undertaken in both the cancerous and non-cancerous cell lines (Fig. 3.8 A & B). P407 was seen to be the most cytotoxic component in both cell lines. P407 is an FDA approved inactive ingredient. Maximum potencies of P407 listed as inactive ingredients only reach as high as 15.1% w/w and 15.5% w/w for an intratympanic suspension and a periodontal gel respectively (299). P407 is used at a concentration of 20% w/v in LeGoo®, an endovascular occlusion gel. LeGoo® was found to be safe and non-cytotoxic according to the Summary of Safety and Effectiveness published by the FDA. However, this product is only licensed for short term use, and remains *in situ* for less than 24 h. An IC₅₀ at 48 h for P407 has been reported as 4.78 mg/ml in human corneal epithelial cells (300). The dose used in the studies in this report is 10.2 mg/ml. Despite differences in cell line used, this would suggest that these results are in line with reported toxicity. Authors of a study evaluating the intraocular use of P407 reported neuro-retinal toxicity at a concentration of 20% w/w, and they also note that conflicting toxicity results are published in the literature (301). The discrepancies in toxicity of P407 seen *in vitro* and *in vivo* reiterates the challenge associated with utilising clinically relevant doses of thermoresponsive hydrogels *in vitro*, and further highlights the need for caution in interpreting toxicity data *in vitro*. CS and HP- β -CD are commonly regarded as non-toxic excipients, and this is in agreement with results obtained following treatment of Balb/c 3T3 clone A31 cells

(Fig. 3.8 B) (203, 209, 302). Treatment with CS reduced the viability of A549 cells at 24 and 48 h. Although, this reduction was not statistically significant, the same volume of CS applied to the Balb/c 3T3 clone A31 cells resulted in an increase in viability compared to Medium control. It is of note that cancer cell-directed cytotoxicity has been reported for CS (217), with increasing DD associated with increasing cytotoxic capacity (303, 304). This has been suggested to be as a result of the greater availability of cationic groups on the 3D structure of CS with higher DD, which can interact with, and disrupt, cellular membranes (304). HP- β -CD reduced viability over at 24 and 48 h in A549 cells to $81\% \pm 6.25\%$ and $79.48\% \pm 9.74\%$ respectively. As previously mentioned in Chapter 2, it has been shown that HP- β -CD can act as an anti-cancer agent in its own right (208). GP was seen to reduce viability in both cell lines after 48 h. It was expected that GP would be more toxic to cancer cells due to the UCP-2 interaction, which is more prevalent in cancer cells (230), and reports of *in vitro* biocompatibility of GP treatment of non-cancerous cell lines.

The cytotoxic effect of the composite ChemoGel is greater than the individual components, indicating that a potential synergistic effect is occurring upon co-administration. It is hypothesised that the solubilisation capacity of the P407 may increase trafficking of the other excipients into the cell, thereby increasing the cancer cell directed toxicity of the other excipients as outlined above, although further *in vitro* assessment would be required to determine this.

The concept of “tumour engineering” in 3D has long been promoted as an intermediary between *in vitro* 2D cell culture and pre-clinical animal testing, and as a technique to embrace the “replacement” pillar of the three R’s associated with pre-clinical *in vivo* experimentation (305, 306). At both seeding densities used in this study, A549 cells seeded on CHyA scaffolds were capable of proliferating over a 21 day period (Fig. 3.9). It has been documented that cancer cells grown in 2D proliferate at a faster rate than those in 3D (272), and the cells cultured in this 3D environment demonstrated a lower fold change in DNA content over the 21 day period, compared to the same seeding density cultured in a 2D environment. This finding is further supported by other reports of increased proliferation rates of cancer cells seeded in 2D, compared to 3D culture (307-309). Interestingly in both 2D and 3D culture the lower seeding density of 100,000 cells had a more continuous pattern of proliferation, which was seen to continue over the 21 days. This was not seen at the 200,000 seeding density in 2D or 3D, with total dsDNA

undergoing a reduction in the second half of the study. Previous work carried out using similar scaffolds also demonstrated a similar decrease in total dsDNA at Day 21 when culturing 200,000 neuroblastoma cells (KellyLuc or KellyCis83Luc) on collagen scaffolds (307).

Increased numbers of dead cells were qualitatively observed in the Live/Dead staining of both seeding densities in 2D, compared to 3D culture. It has been suggested that the growth of cells in 2D culture is limited by the space of the flat well plate, and therefore when cells reach confluence they begin to die as they try to continue to proliferate over each other (284). A549 cells seeded in 2D in this study were observed to be confluent by Day 7, coinciding with the visualisation of the dead cells (Fig. 3.10). The CHyA scaffold offers a greater surface area for cell proliferation than the 2D well plate surface, thus facilitating continued proliferation, and reduced cell death. Taken together with the qualitative migration analysis, which determined that both seeding densities allowed migration through the 3D CHyA structure, the 100,000 seeding density was selected as the optimal model for 3D cytotoxicity assessment of ChemoGel.

In the 3D assessment of blank and drug ChemoGel cytotoxicity, cells were allowed to proliferate for 7 days before treatment, to create a more representative environment of the *in vivo* reality. In both murine models and clinical cases of NSCLC, the tumour would normally be well established before treatment (84). Intra-scaffold injection was utilised as a mimic to IT administration, and both blank and drug ChemoGel were observed to form a gel bolus within the scaffold, which remained for the duration of the 14 day study (Fig. 3.12 A). Scaffolds are more appropriate for the evaluation of thermoresponsive hydrogels in 3D than other forms of 3D *in vitro* tumour models as this injection process would not be possible using spheroids or microfluidic cultures, due to their small size. This cell seeded scaffold provides the 3D environment for the tumour cells to grow on, and also the 3D structural environment for ChemoGel to interact with. The quantitative evaluation of viability revealed stark differences between the 2D and 3D cytotoxicity evaluation, with viability of ChemoGel after 2 days determined to be $7.51\% \pm 4.47\%$ in 2D and $52.83\% \pm 3.76\%$ in 3D (Fig. 3.5 & 3.12). This reveals that the 2D environment, albeit with a lower seeding density, is more susceptible than the 3D culture system, which has previously been seen with other types of advanced drug delivery platforms (281). It was noted that the enhanced susceptibility of the 2D environment is less representative of the clinical reality. On the whole, the chemoablative nature of

ChemoGel has held true across both *in vitro* evaluations, indicating its potential to augment chemotherapeutic treatment in a clinical setting.

A similar pattern was observed following drug ChemoGel treatment with viability after 2 days of treatment in 2D determined to be $0.42\% \pm 0.11\%$, compared to $19.10\% \pm 0.42\%$ in 3D (Fig. 3.5 & 3.12). Perhaps the most striking difference is in the cisplatin/paclitaxel solution treated group, as treatment was determined to be non-toxic after 2 days in 3D ($94.92\% \pm 13.14\%$), compared to the high toxicity seen in 2D ($5.85\% \pm 1.8\%$) (Fig. 3.5 & 3.12). This dramatic difference may have led to incorrect conclusions drawn as to the comparative efficacy of blank and drug ChemoGel if only conducted in 2D. In particular, the 3D study confirmed the value of employing ChemoGel as a chemotherapeutic carrier, as drug ChemoGel induced a statistically significantly higher reduction in viability than the chemotherapeutic solution alone at all timepoints evaluated, which was not found in the 2D study. The improved efficacy of chemotherapeutics delivered via thermoresponsive hydrogels is commonly reported, often without citing the reason for improved treatment response (250). In the case of ChemoGel, this improved response can be attributed to the cytotoxicity of the carrier itself. The CHyA scaffold allowed for evaluation of all treatments over 14 days, which was not feasible in the 2D model. This provides a more realistic timeline to compare to *in vivo* studies. By the end of the 14 day study, it was determined that drug ChemoGel had the most consistently sustained effect on viability.

3.5 Conclusion

Presented in this Chapter is the *in vitro* evidence to support the use of ChemoGel as a chemoablative drug delivery platform for LC applications. A number of conclusions can be drawn based on the results of these *in vitro* studies:

- ◁ Both blank and drug ChemoGel have demonstrated *in vitro* efficacy in 2D and 3D models of NSCLC, and warrant further investigation
- ◁ Assessment of the *in vitro* toxicity revealed that individual administration of excipients did not induce the same level of cytotoxicity as that seen following administration of the composite thermoresponsive hydrogel, indicating that a potential synergism may be inducing the cytotoxicity of ChemoGel
- ◁ The cancer cell directed cytotoxicity of ChemoGel is evident at lower doses, but is lost as the dose increases in non-cancerous cell lines
- ◁ Development of the 3D *in vitro* model of LC using a CHyA scaffold was feasible and allowed for evaluation of blank and drug ChemoGel under more biorelevant conditions

As the therapeutic potential of the ChemoGel technology has been established *in vitro* in this Chapter, further consideration is called for concerning its translational potential. Assessment of the common pitfalls associated with bench to bedside translation of advanced drug delivery platforms may address some of the clinical and regulatory barriers at an early, product development stage, and this will be undertaken in Chapter 4.

4.1 Introduction	148
4.1.1 Imaging in Interventional Oncology	148
4.1.2 Injectability	150
4.1.3 Sterilisation.....	152
4.1.4 Aim and Objectives	155
4.2 Materials and Methods	156
4.2.1 Formulation of radiopaque ChemoGel	156
4.2.1.1 <i>Rheological assessment of thermoresponsivity of Visipaque® labelled ChemoGel formulation</i>	156
4.2.1.2 <i>Measurement of the radiopacity of a Visipaque® labelled ChemoGel formulation</i>	156
4.2.1.3 <i>Assessment of contrast release from Visipaque® labelled ChemoGel</i>	156
4.2.1.4 <i>Assessment of distribution of Visipaque® labelled ChemoGel in ex vivo animal tissue</i>	157
4.2.2 Injectability of ChemoGel.....	157
4.2.2.1 <i>Rheological assessment of shear thinning properties of lead thermoresponsive hydrogels</i>	157
4.2.2.2 <i>Injection force assessment</i>	158
4.2.3 <i>In vitro</i> cytotoxicity evaluation of blank and drug Visipaque® ChemoGel	159
4.2.4 Freeze-drying and rehydration of ChemoGel.....	160
4.2.5 Sterilisation of freeze-dried ChemoGel	160
4.2.5.1 <i>Dry heat sterilisation</i>	160
4.2.5.2 <i>Gamma-irradiation sterilisation</i>	160
4.2.5.3 <i>Ethylene Oxide sterilisation</i>	161
4.2.6 Disintegration studies	161
4.2.7 <i>In vitro</i> release studies of Visipaque® ChemoGel and sterilised ChemoGel formulations	161
4.2.8 Statistical analysis.....	162
4.3 Results	163
4.3.1 Assessment of the radiopacity of ChemoGel.....	163
4.3.1.1 <i>Rheological assessment of thermoresponsivity of Visipaque® labelled ChemoGel</i>	163
4.3.1.2 <i>Measurement of radiopacity of Visipaque® labelled ChemoGel</i>	164
4.3.2 Injectability of ChemoGel	166
4.3.3 Assessment of the cytotoxicity of blank and drug Visipaque® ChemoGel in a 3D model of lung cancer	169
4.3.4 Assessment of freeze-drying and sterilisation on the material properties of ChemoGel formulations	171
4.3.4.1 <i>Freeze-drying and rehydration of ChemoGel</i>	171
4.3.4.2 <i>Sterilisation of ChemoGel</i>	171
4.3.5 Disintegration studies	174
4.3.6 Release studies	175
4.4 Discussion	178
4.5 Conclusion	186

4.1 Introduction

The cost of bringing a new drug from “bench to bedside” is in the region of US \$1 billion (310). Approximately 8% of the new molecular entities (NME) that progress from the pre-clinical research stage will be granted regulatory approval for use in a clinical setting (311). Advanced drug delivery platforms have been proposed as a potential method of circumventing some of the most common reasons for failure of NMEs, including toxicity, efficacy and bioavailability issues (312). As discussed in Chapter 1, thermoresponsive hydrogels are theoretically ideally suited to overcoming the barriers for IT delivery of drug solutions to solid tumours, and improving efficacy and safety profiles. However, rational design and forward planning are called for during early stage formulation research, in order to pre-empt the various translational hurdles blocking entry to the clinic. Lee *et al.* (2013) noted that the current trend with hydrogel research is to develop novel hydrogel polymers with no clinical use in mind. They postulate that this approach further compounds the challenges associated with securing FDA approval for hydrogels as advanced drug delivery platforms. They suggest a better strategy would be to focus on using previously certified GRAS materials to design hydrogel formulations for predefined clinical indications (6). The focus of this thesis is to develop a thermoresponsive hydrogel for LC applications, with three out of the four excipients used designated as GRAS. GP is not currently listed as GRAS, however, a first in man clinical trial (n=5) of GP administered to the vertebral discs has demonstrated preliminary safety in humans (313). The incorporation of “gold-standard” chemotherapeutics, with established efficacy and toxicity profiles, further increases the potential for rapid clinical translation. However, there are still significant hurdles that any new delivery platform must address, in order to facilitate regulatory approval and clinical adoption. From a clinical perspective, imaging and delivery will be key considerations, while procedures for preparation and sterilisation of the final formulation will be a critical aspect of the regulatory approval process.

4.1.1 Imaging in Interventional Oncology

As discussed in Chapter 1, the principle of IO is to perform minimally invasive procedures under image guidance (154). A number of different modalities can be employed to facilitate the image guidance, including, but not limited to, CT, CT fluoroscopy, US and MRI (314). Choice of imaging modality depends on target organ, disease state, and medical devices available. Imaging should be utilised

throughout the four stages of the interventional procedure, as outlined in Table 4.1 (131, 314).

Table 4.1 Functions of image guidance in interventional oncology procedures (131, 314).

Imaging	Function
Comprehensive pre-procedural planning	Determines: <ul style="list-style-type: none"> - procedure appropriateness - feasibility - optimal approach - technical difficulties expected
Accurate targeting of intervention	<ul style="list-style-type: none"> - Usually facilitated by CT/ MRI combined with real time US - Ideally 3D real time imaging would be used - Enables targeting of catheter/needle to required site of action
Monitoring of procedure	<ul style="list-style-type: none"> - Real time monitoring can be used to indicate “procedure completeness” - US can monitor contrast agent labelled treatments and ablative procedures - Contrast agent labelled treatments and cryo-procedures can be detected by CT and MRI
Post-procedural assessment	<ul style="list-style-type: none"> - Success and complication assessment

Imaging before, during and after IO procedures allows for accurate evaluation of tumour burden, selective targeting of the cancerous tissue under real time image guidance, and generation of images post-treatment, which can be directly compared against pre-treatment tumour parameters to gauge treatment success. Some techniques, like cryoablation, do not require additional imaging agents for real time imaging, as the area of ablation is clearly delineated on CT during the procedure (315). Image guidance is usually provided using commercially available contrast agents. Visipaque® is a commercially available X-ray contrast medium licensed for use in Ireland for a number of diagnostic procedures specified in the Summary of Product Characteristics (SPC). The solution contains the active

ingredient, iodixanol, and a number of salts to make it isotonic. It is available in two strengths of iodixanol, 320 mg /ml or 270 mg /ml. Administration doses vary but are cited as between 4 ml – 150 ml per injection, depending on intended site of use. Investigational doses of up to 400 ml are also quoted in the SPC (316).

Pre-clinical research does not commonly deal with the importance of imaging thermoresponsive hydrogels during IT administration (317). Recently, some attention has been directed to the inclusion of contrast agents into thermoresponsive hydrogels to facilitate *in vivo* imaging of hydrogel administration and retention. Iodinated contrast agents have been incorporated into thermoresponsive hydrogels to assess the effect on radiopacity and thermoresponsivity of the delivery platforms (318, 319). An iodinated P407-based thermoresponsive hydrogel has previously been assessed for embolic applications in a VX2 rabbit model of liver cancer, with preliminary evidence established to support its use in image-guided procedures (320).

At a commercial level, the importance of intra-procedural imaging is beginning to be reflected in changes in the IO market, with a new radiopaque product being added to the DC Bead® portfolio. In March 2017, DC Bead LUMI™ received Class III CE mark certification, and became the first radiopaque DEB available in the EU. The radiopacity of DC Bead® is achieved by using a tri-iodobenzyl moiety, which allows for long term imaging of DC Bead LUMI™ following administration. The radiopacity of DC Bead LUMI™ allows for accurate visualisation and localisation of the chemoembolisation treatment, and represents a new milestone in commercially available IO technology (321). The investment in radiopaque technologies demonstrates the importance of imaging administration during the procedure.

4.1.2 Injectability

IO procedures require the integration of the treatment modality and appropriate medical device to ensure accurate delivery to the tumour site. Depending on the procedural requirements, needles, catheters, or thermal or electrical probes may be employed to achieve tumour ablation or embolisation. Instillation of chemically ablative treatment to the tumour can be achieved using a percutaneous, laparoscopic or endoscopic procedure. Locoregional access to lung tumours is currently employed in routine biopsy procedures to diagnose and stage LC. Adaption of these procedures could facilitate the translation of IT delivery of thermoresponsive hydrogels to the clinic.

Percutaneous trans-thoracic biopsy can be performed as a fine-needle-aspiration biopsy (FNAB) or core biopsy. These procedures are carried out under image guidance, with CT imaging being used most frequently. A wide range of needle gauges are used in these procedures, from 14 – 18G for core biopsy to 20 – 25G for FNAB. Increasing needle size is associated with increased complication rates throughout the procedure. Transthoracic lung biopsy is generally considered a safe and well tolerated technique, with pneumothorax cited as the most common complication (322-324). As tumour location can be a limiting factor in the feasibility of percutaneous access, bronchoscopic methods of biopsy are also employed. Bronchoscopy is cited as being safer, but less accurate in diagnosis. It offers a reduced risk of pneumothorax, but it is acknowledged that navigating through bronchial tubes below the fourth generation is technically difficult (325). Advances in image-guided bronchoscopy are improving success rates of bronchoscopic procedures, including autofluorescence bronchoscopy, near band imaging bronchoscopy and EBUS (326). A TBNA needle attached to an EBUS probe has been suggested as a feasible method for delivery of cisplatin to a tumour site (170). Oncogel™, a thermoresponsive hydrogel loaded with paclitaxel, has been delivered via endoscopic ultrasound to oesophageal tumours in a clinical trial setting, and this was determined to be a safe and feasible administration technique (55).

IT delivery of a thermoresponsive hydrogel is dependent on the ability of the hydrogel solution to be injected through a needle or catheter of suitable internal diameter and length. A number of factors impact the injectability of formulations, including formulation-based factors, such as viscosity and flow behaviour of the hydrogel, or device-based factors, such as needle length, internal diameter and inner coating on needle (327). The hydrogel-based factors can be assessed using rheological methods. Shear thinning materials will decrease viscosity in response to increasing shear rate, and therefore these materials are most suitable for injection purposes (328). Flow properties of a commercially available hydrogel are controlled by the formulation defined in the manufacturing license, but the characteristics of the medical device used in administration is often not specified. Medical device characteristics, such as barrel size, needle gauge, plunger dimensions should be tightly controlled to ensure that the correct dose is delivered each time (329). Another factor which may affect injectability is the composition of the tissue into which the hydrogel will be injected. Subcutaneous (SC), intramuscular (IM) and IT injections will all encounter different backpressures which may impact ease of injection (327). For thermoresponsive hydrogels, environmental

temperature conditions will also affect injectability due to a change in the viscosity of the formulation.

Currently, there are no pharmacopoeial standards defining acceptable levels of “injectability”, however, some efforts have been made to define a range of acceptable limits of injectability. Rungseevijitprapaa & Bodmeier (2009) correlated the *in vitro* injection force (N) required to expel an *in situ* forming microparticle system using a 500 N load cell, and the *in vivo* injectability of the system into SC tissue of male Sprague-Dawley rats. They determined that an injection force of 0 - 10 N was very easy to inject, 26 - 50 N was “injectable” by hand, and forces above 50 N were deemed “difficult to inject” by hand (330).

Assessment of injectability of formulations designed for delivery via needle or catheter early on in the development process is of critical importance when considering translation of a thermoresponsive hydrogel to the clinic. Use of previously approved or CE marked medical devices, such as those currently in use for transthoracic or bronchoscopic procedures, facilitates a smoother integration of drug delivery platform and device, and reduces the approval burden on the technology. In the early stages of research, formulation development can be tailored to facilitate currently approved devices, thus giving due consideration to this key aspect of translation.

4.1.3 Sterilisation

Sterility of a pharmaceutical product intended for human use is a regulatory requirement, and is defined by the Appendix XVIII of the British Pharmacopoeia (BP) as “the absence of viable micro-organisms” (331). Furthermore, this Appendix dictates that sterility cannot be defined by post-sterilisation evaluation, but rather sterility is assured by the application of validated procedures. Terminal sterilisation methods are methods in which the product is sterilised in its final container, by a validated sterilisation process. This is the preferred mode of sterilisation, and allows for batch release, based on the approved, validated processes, rather than sterility testing of the product. This is not only time- and cost- efficient for the manufacturer, but also for the product end user. Listed methods of terminal sterilisation include steam sterilisation, dry heat sterilisation, ionising radiation sterilisation and gas sterilisation (Table 4.2). Gas sterilisation should only be used if no other appropriate method can be applied (332).

Table 4.2 *Approved sterilisation methods. BP, British Pharmacopoeia; ISO, International Organisation for Standardization*

Sterilisation process	Method	Reference
Steam	<ul style="list-style-type: none"> - Autoclave at 121°C for 15 mins¹ - Saturated steam venting systems, Saturated steam active air removal systems - Air steam mixtures - Water spray - Water immersion² 	<ul style="list-style-type: none"> 1. BP 2017 Appendix XVIII (332) 2. ISO 17665-1:2006 (333)
Dry heat	<ul style="list-style-type: none"> - Minimum of 160 °C for at least 2 h^{1, 3} 	<ul style="list-style-type: none"> 1. BP 2017 Appendix XVIII 3. ISO 20857: 2010 (334)
Ionising radiation	<ul style="list-style-type: none"> - Exposure to gamma radiation from a suitable radioisotopic source/ of a beam of electrons energised by a suitable electron accelerator - Reference absorbed dose is 25 kGy - Lower dose, if process validated¹ 	<ul style="list-style-type: none"> 1. BP 2017 Appendix XVIII
Gas	<ul style="list-style-type: none"> - Ethylene oxide (batch samples must be evaluated for sterility) ¹ 	<ul style="list-style-type: none"> 1. BP 2017 Appendix XVIII

The European Medicines Agency (EMA) published decision trees for the selection of a sterilisation process (Fig. 4.1). The guidance states that sterility assurance is reduced as one moves down the decision tree. It is also highlighted that packaging and commercial concerns should not be defining factors when selecting a sterilisation process. Rather, the sterilisation method should be selected based on the properties of the final product, and the packaging of the final product should be selected based on appropriateness for the sterilisation method (335).

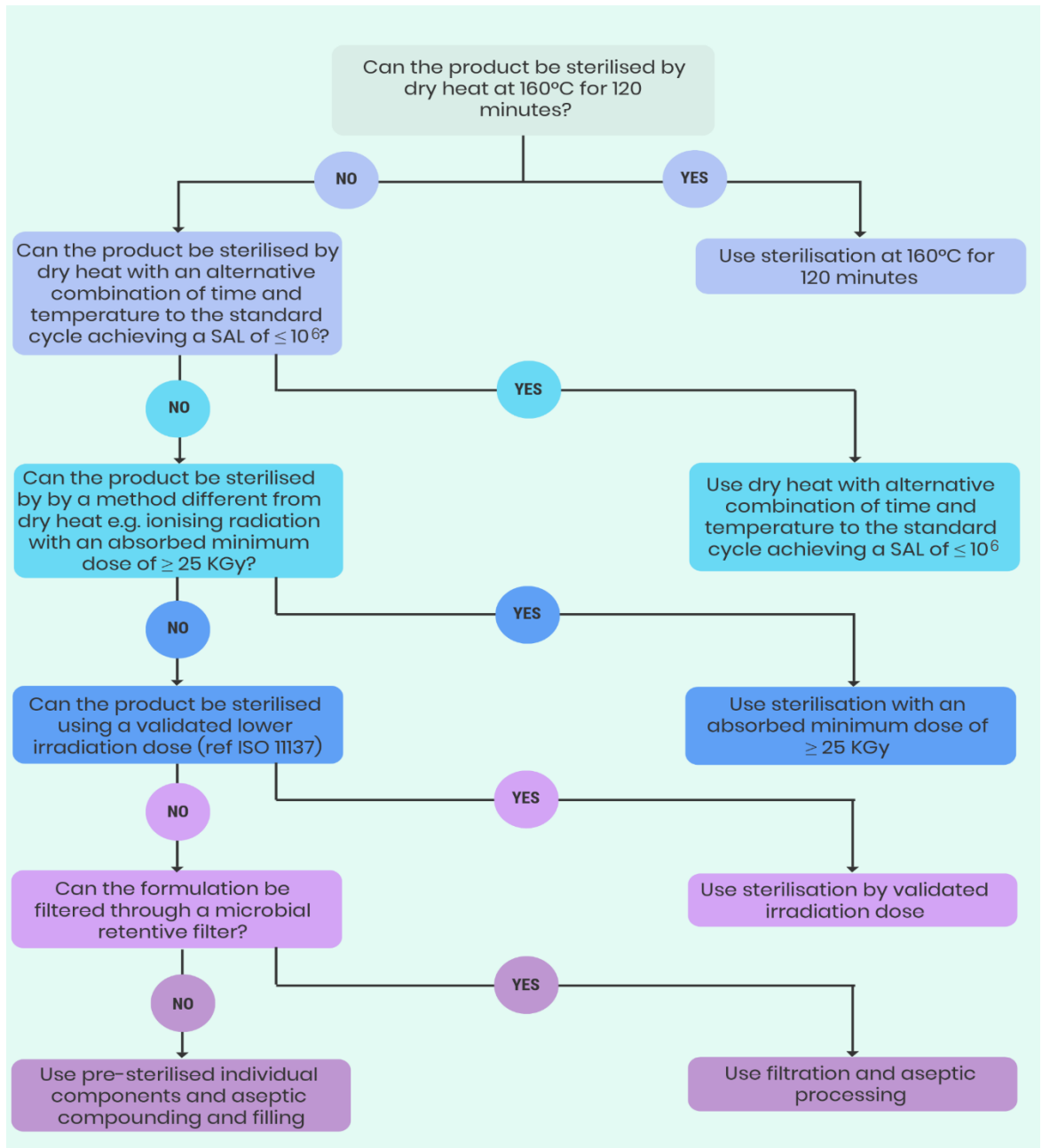


Figure 4.1 European Medicines Agency decision tree for selection of sterilisation methods for non-aqueous liquids, semi-solids or dry powder products. SAL, Sterility Assurance Level. Adapted from (335).

4.1.4 Aim and Objectives

The overall aim of this chapter was to increase the potential of the ChemoGel formulation for clinical translation in the IO space by addressing key clinical and regulatory considerations.

The specific objectives of this chapter were to:

- ◁ Formulate a radiopaque thermoresponsive hydrogel, which could be visualised using imaging modalities readily available to the interventional oncologist
- ◁ Ensure that lead thermoresponsive hydrogel formulations were compatible for injection across a range of suitable commercially available devices
- ◁ Identify a suitable storage and sterilisation method for the lead thermoresponsive hydrogels, which would not adversely affect the rheological properties
- ◁ Assess if the sterilisation process impacted on the disintegration of the lead thermoresponsive hydrogels and the release profile of the loaded chemotherapeutics

4.2 Materials and Methods

All needles, catheters and Visipaque® 320 mg /ml (GE Healthcare, Ireland) were kindly supplied by Dr Timothy Murray and Prof. Michael Lee, Beaumont Hospital, Dublin.

4.2.1 Formulation of radiopaque ChemoGel

Blank Chemogel was prepared as outlined in Section 2.2.1.1, with the required concentration of Visipaque® 320 mg /ml added to the initial dH₂O used to dissolve HP-β-CD in Step 1. Visipaque® was added at concentrations of 0% w/w, 10% w/w, 20% w/w or 30% w/w, based on previous work carried out by Fatimi *et al.* (2016) (319).

4.2.1.1 Rheological assessment of thermoresponsivity of Visipaque® labelled ChemoGel formulation

Oscillatory temperature sweeps from 20°C to 40°C were carried out on all formulations as outlined in Section 2.2.2.1 to determine the impact of the incorporation of Visipaque® on the thermoresponsive nature of resulting ChemoGel formulations. All measurements were carried out in triplicate. Data shown is representative of the norm.

4.2.1.2 Measurement of the radiopacity of a Visipaque® labelled ChemoGel formulation

2 ml of Visipaque® labelled (0 – 30% w/w) ChemoGel formulations was added per well in a 12-well plate. Radiopacity was determined using CT (Ingenuity Core 128, Philips) operated by Dr Timothy Murray and Mr José Bingay. Images were obtained using 0.8 mm slice thickness, 0.4 mm reconstruction interval, 168 mAs and 100 kV. A region of interest (100 mm diameter) within each well was selected and the average density was calculated (minimum, maximum and standard deviation also recorded). All measurements were carried out in triplicate. Data shown is represented as the mean ± SEM.

4.2.1.3 Assessment of contrast release from Visipaque® labelled ChemoGel

1 ml of 20% w/w Visipaque® labelled ChemoGel was incubated with 2 ml release buffer (PBS, pH 7.4) in a 12-well plate at 37°C for 24 h. Release buffer was removed at 4 h and 24 h and imaged using CT as outlined in Section 4.2.1.2 to determine radiopacity. The remaining ChemoGel with 20% w/w Visipaque® was also imaged

to determine residual radiopacity at each timepoint. All experiments were carried out in triplicate. Data shown is represented as the mean \pm SEM.

4.2.1.4 Assessment of distribution of Visipaque® labelled ChemoGel in ex vivo animal tissue

Ex vivo tissue (calves livers) was used to assess the distribution of injected radiopaque ChemoGel. Prior to injection, the *ex vivo* tissue was heated to 37°C in a water bath. Internal tissue temperature was recorded using a meat thermometer. 5 ml of ChemoGel with 20% w/w Visipaque® was injected into the *ex vivo* tissue model using an 18G needle of 5 cm length (Cook Medical, IN, USA) at a constant rate to assess distribution of injected ChemoGel in tissue. Three injections were made. Administration was monitored by Dr Timothy Murray using US (Xario, Toshiba) using a 12 MHz linear probe in Grayscale B-mode. *Ex vivo* distribution post-injection was imaged using CT as outlined in Section 4.2.1.2.

4.2.2 Injectability of ChemoGel

4.2.2.1 Rheological assessment of shear thinning properties of lead thermoresponsive hydrogels

Steady state flow experiments were performed on an AR-1000 constant stress rheometer (TA instruments, DE, USA) with built-in temperature and gap calibration. The rheometer was equipped with cone geometry (40 mm diameter, 4° cone angle). Degassed samples were dispensed onto the temperature controlled rheometer plate, pre-equilibrated to 20°C. A solvent trap, containing water, was used to cover the sample to prevent evaporation from the sample during the rheological testing. A LAUDA Ecoline 003 E100 water-bath (Lauda-Königshofen, Germany) was employed as a heat-sink for the peltier plate, which controlled temperature during testing. The temperature of the sample plate was controlled within $\pm 0.1^\circ\text{C}$ of the desired value at all times during testing. Prior to testing, the geometry gap was calibrated, and rotational mapping of the geometry was performed. Following loading of excess sample, the geometry was lowered to this pre-determined gap. Excess sample was carefully removed from the peltier plate, and discarded to ensure correct filling was achieved. Samples were allowed to equilibrate for 2 min before commencing testing. Data was processed using TA Data Analysis software (TA instruments, DE, USA). All samples were analysed in triplicate. Data shown is representative of the norm.

The viscosity of blank ChemoGel, drug ChemoGel and Visipaque® labelled ChemoGel (0 – 30% w/w) at 20°C was measured to determine the behaviour of the thermoresponsive hydrogel under increasing shear stress from 1 Pa to 100 Pa.

4.2.2.2 Injection force assessment

Uniaxial tensile testing was carried out to determine the force required to expel the thermoresponsive hydrogel solution from a syringe fitted with a needle or catheter, as specified in Table 4.3, using a mechanical testing machine (Z050, Zwick/Roell, Germany), fitted with a 5 kN load cell (Fig. 4.2).

Table 4.3 Summary of medical devices used in injectability testing of various ChemoGel formulations

Medical Device	Needle Gauge (G) / Catheter diameter (Fr)	Length (cm)	Formulation tested
Cook Medical Needle	18G	7 cm	ChemoGel Visipaque® labelled ChemoGel
Terumo Catheter	2.9Fr	130 cm	ChemoGel
Cook Medical Needle	18G	20 cm	Visipaque® labelled ChemoGel
Chiba Biopsy Needle	20G	10 cm	Visipaque® labelled ChemoGel
Terumo Spinal Needle	23G	9 cm	Visipaque® labelled ChemoGel
Cordis Catheter	5Fr	65 cm	Visipaque® labelled ChemoGel

Hydrogel samples were loaded into 2 ml leur-lock syringes (BD, Dublin, Ireland), and kept chilled on ice before tensile testing to ensure that the samples remained in a liquid state. The appropriate medical device was attached to the syringe via luer-lock to determine the maximum force required to expel 500 µL of thermoresponsive hydrogel solution.

Fixed grips were mounted onto the tensile testing machine for all tests, and the syringe was clamped into position attached to the load cell. A pre-load (preliminary force) of 1 N was applied and the end of test was determined to be the maximum extension (8.5 mm); the distance equivalent to 0.5 ml of gel (measured using a Vernier's callipers). The speed of injection was defined as 2 ml/min or 1 ml/min. The hydrogel solution samples were then loaded to failure and the solution expelled from the catheter was collected in a vial. All measurements were carried out in a minimum of triplicate. Results are represented as the mean \pm SEM.

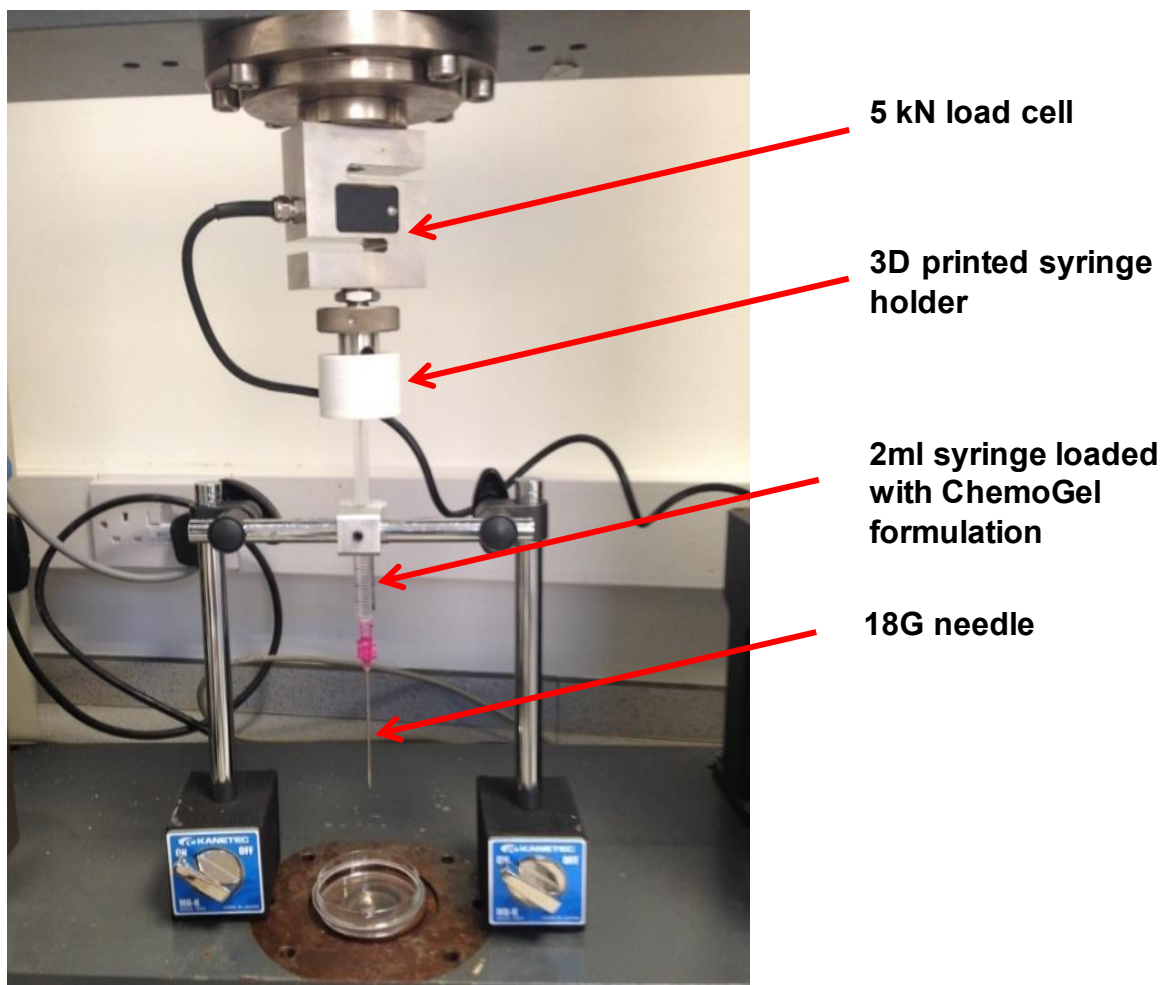


Figure 4.2 Representative image of injectability set up using a Zwick mechanical testing machine.

4.2.3 *In vitro* cytotoxicity evaluation of blank and drug Visipaque® ChemoGel

Cytotoxicity testing of 50 μ L of blank and drug Visipaque® ChemoGel over 14 days was carried out in a 3D model of NSCLC using A549 cells as per Section 3.2.11 to determine if addition of Visipaque® to the formulation had any impact on cytotoxicity

4.2.4 Freeze-drying and rehydration of ChemoGel

The effect of a freeze drying/rehydrating process on the thermoresponsive nature of ChemoGel was investigated. Blank ChemoGel was prepared as outlined in Section 2.2.1.1. A known weight of the hydrogel was transferred to a beaker with a screw top lid. The hydrogel solution was then flash frozen in liquid nitrogen and freeze dried for 48 h using a freeze dryer and vacuum pump at -55°C and 0.018 mbar (Labcono, MO, USA) to produce a lyophilised powder. The powder was rehydrated with dH₂O to bring the formulation up to the final weight, stirred on ice for a minimum of 6 h, and refrigerated overnight until fully rehydrated. Oscillatory temperature sweeps from 20°C – 40°C were carried out on the rehydrated formulations as outlined in Section 2.2.2.1.

4.2.5 Sterilisation of freeze-dried ChemoGel

Freeze-dried wafers of ChemoGel were prepared as per Section 4.2.4. Methods for sterilisation of freeze-dried ChemoGel were evaluated in a stepwise manner as recommended by the EMA decision tree for non-aqueous liquid, semi-solids or dry powder products (Fig. 4.1). As freeze-dried ChemoGel was in dry powder form it could not be filtered through a microbial retentive filter, and therefore this step was omitted from the evaluation process. Following each sterilisation method outlined below, the freeze-dried wafer was rehydrated by adding the required volume of dH₂O to the beaker under aseptic conditions. Samples were rheologically assessed using oscillatory temperature sweeps as outlined in Section 2.2.2.1, to determine if the thermoresponsivity of ChemoGel was affected by the sterilisation process.

4.2.5.1 Dry heat sterilisation

Freeze-dried samples were placed in aluminium foil bags in at 160°C for 2 h in an oven (Vacucell 22; MMM, Germany) as per pharmacopoeial and ISO specifications for sterilisation (332, 334). Samples were analysed in triplicate.

4.2.5.2 Gamma-irradiation sterilisation

Freeze-dried samples were sterilised using gamma-irradiation by Synergy Health, an EN ISO and FDA approved international provider of sterilisation services to the health care industry (Westport, Co. Mayo). Radioisotope Cobalt 60 is used by Synergy Health to deliver a minimum absorbed dose of 25 kGy, as recommended by the EMA guidance (335). Samples were analysed in triplicate.

4.2.5.3 Ethylene Oxide sterilisation

Ethylene oxide (EtO) sterilisation was carried out at the EtO facility in Trinity College Dublin with the assistance of Dr Simon Carroll. Freeze-dried samples were placed in plastic beakers, with the lid removed. The beakers were covered in tinfoil which was pierced several times and placed in a sterilisation pouch. The autoclave bag was then placed into a sterilisation liner bag in the sterilisation cabinet (Anprolene AN 74i, Andersen Products, Inc. Haw River, NC, USA). The sterilisation liner bag was purged of air, and an Anprolene ampule was broken to start the sterilisation cycle. The cycle was run for 18 h including a 2 h aeration period. Sterilisation was confirmed by the EtO sterilisation chemical indicator on the sterilisation pouch.

EtO sterilisation of drug ChemoGel was carried out on the paclitaxel-loaded ChemoGel, which was prepared as outlined in Section 2.2.1.3. Following sterilisation, an aqueous solution of cisplatin was used to rehydrate the wafer to final weight under aseptic conditions. For EtO sterilisation of blank and drug Visipaque® ChemoGel the same procedures were carried out as for non-radiopaque ChemoGel, with the Visipaque® solution included in formulation as per Section 4.2.1. Rheological assessment of impact of sterilisation on the viscosity of all EtO sterilised groups was also carried out as per Section 4.2.2.1. A minimum of three independent samples were used for rheological characterisation. Data shown is representative of the norm.

4.2.6 Disintegration studies

Disintegration studies were conducted as outlined in Section 2.2.2.5 on blank and drug ChemoGel post-sterilisation and blank and drug Visipaque® ChemoGel pre- and post- sterilisation. All experiments were carried out in triplicate, for three independent batches. Results are represented as the mean of the three independent experiments \pm SEM.

4.2.7 *In vitro* release studies of Visipaque® ChemoGel and sterilised ChemoGel formulations

Release studies were carried out on drug Visipaque® ChemoGel and sterilised drug ChemoGel and drug Visipaque® ChemoGel as per Section 2.2.3.4. Release medium was analysed for paclitaxel content using HPLC, as per Section 2.2.3.1, and platinum content using ICP-MS, as per Section 2.2.3.2. All experiments were carried out in triplicate, for three independent batches. Each sample was analysed

in duplicate. Results are represented as the mean of the three independent experiments \pm SEM.

4.2.8 Statistical analysis

One-way ANOVA followed by Dunnett's multiple comparisons test was performed to determine statistical differences in Visipaque® release studies described in Section 4.2.1.3. Statistical differences between forces required to perform injections of ChemoGel solution as outlined in Section 4.2.2.2 were determined using two-way ANOVA with Sidak's multiple comparisons test or one-way ANOVA with Bonferroni's multiple comparisons test. Two-way ANOVA with Tukey's multiple comparisons was used to determine statistical differences between viability post-treatment *in vitro* as described in Section 4.2.3. All statistical tests were performed using GraphPad Prism v6. Error is reported as SEM, unless otherwise stated, and significance was determined using a probability value of $p \leq 0.05$.

4.3 Results

4.3.1 Assessment of the radiopacity of ChemoGel

4.3.1.1 Rheological assessment of thermoresponsivity of Visipaque® labelled ChemoGel

Addition of Visipaque® at a concentration up to 20% w/w to the ChemoGel formulation did not result in a substantial change to the sol-gel transition temperature or the G' at 37°C (Fig. 4.3). The incorporation of 30% w/w Visipaque® resulted in a significant lowering of the sol-gel transition temperature to 22°C, with a concomitant increase in the G' that was almost two fold higher than blank ChemoGel at 37°C.

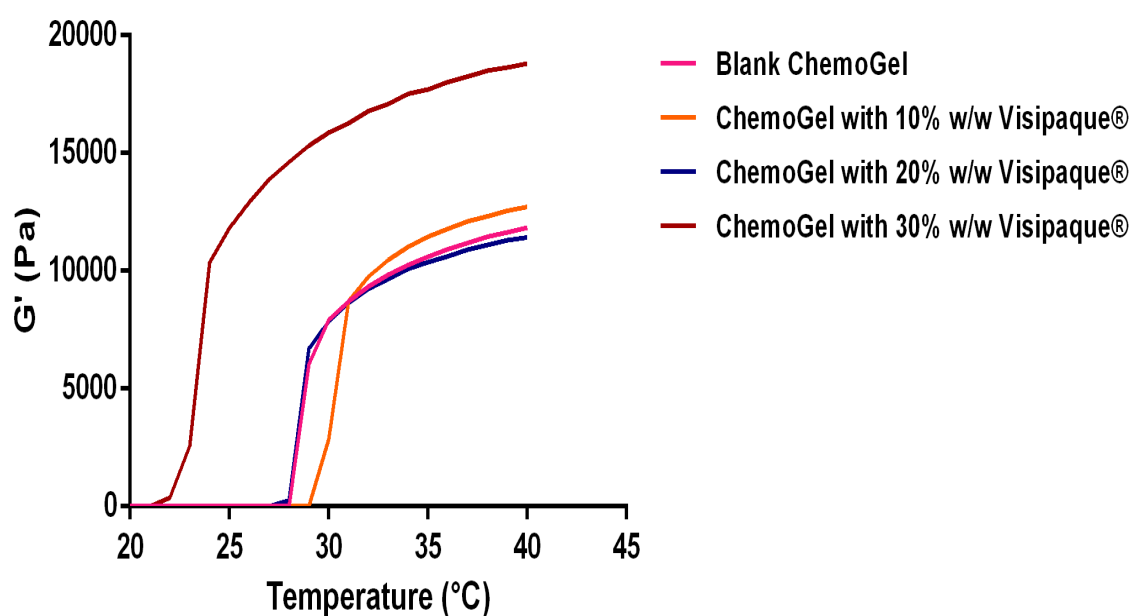

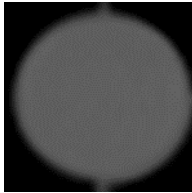
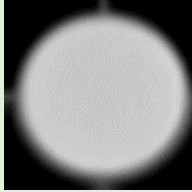
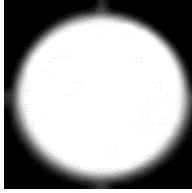



Figure 4.3 Addition of Visipaque® to the ChemoGel formulation impacted the rheological properties of the thermoresponsive hydrogel in a concentration dependant manner. Rheogram of the oscillatory temperature sweeps from 20°C - 40°C of ChemoGel formulations containing different concentrations of Visipaque® solution. Data shown is representative of the norm.

4.3.1.2 Measurement of radiopacity of Visipaque® labelled ChemoGel

Addition of Visipaque® to the ChemoGel formulation was seen to produce a homogenous formulation at all concentrations evaluated, as evidenced by CT imaging (Table 4.4). The radiopacity of ChemoGel with 0% w/w Visipaque® (unlabelled ChemoGel) was 33.57 ± 2.34 HU, and increased with increasing Visipaque® concentration (Table 4.4). Gelation reduced radiopacity in all three Visipaque® labelled ChemoGel groups, but radiopacity was still within clinically acceptable limits (Table 4.4).

Table 4.4 Addition of Visipaque® to the ChemoGel formulation increased radiopacity in a concentration dependent manner. Data shown is represented as the mean \pm SEM (n=3). HU, Hounsfield units.

Formulation	Radiopacity (HU)		Representative image
	Liquid	Gelled	
20% w/w Visipaque® solution	1523.7 ± 4.09	N/A	
ChemoGel with 0% w/w Visipaque®	33.57 ± 1.35	22.4 ± 1.19	
ChemoGel with 10% w/w Visipaque®	900.03 ± 2.97	697.11 ± 11.13	
ChemoGel with 20% w/w Visipaque®	1666.23 ± 4.02	1586.0 ± 6.95	
ChemoGel with 30% w/w Visipaque®	2428.83 ± 10.98	2378.7 ± 8.02	

Due to favourable rheological and radiopacity characteristics, ChemoGel with 20% w/w Visipaque® was selected for further assessment. Time-lapsed imaging revealed approximately 45% of iodinated contrast was released from the gelled ChemoGel with 20% w/w Visipaque® after 24 h. A statistically significant decrease in the radiopacity of ChemoGel with 20% w/w Visipaque® was observed after 4 and 24 h. (Fig. 4.4).

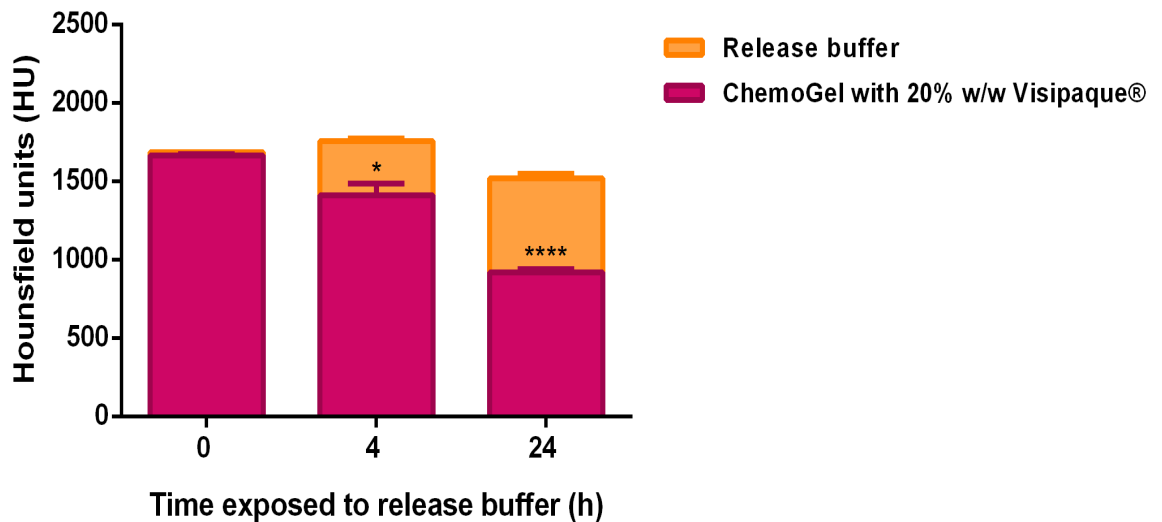


Figure 4.4 Visipaque® was released from ChemoGel with 20% w/w Visipaque® over 24 h as determined by quantification of the radiopacity of the remaining ChemoGel formulation and the release buffer at each timepoint. Data shown is represented as the mean + SEM (n=3). Significance was determined using a one-way ANOVA of ChemoGel with 20% w/w Visipaque® radiopacity, with $p < 0.05$, **** = $p < 0.0001$ compared to 0 h ChemoGel with 20% w/w Visipaque® radiopacity.

Injection into *ex vivo* calves tissue demonstrated that ChemoGel with 20% w/w Visipaque® was readily injectable, and moulded to the shape of the target tissue. On US, the radiopaque ChemoGel was found to be clearly visualised, anechoic and without speckling (Fig. 4.5 A & B). ChemoGel with 20% w/w Visipaque® demonstrated satisfactory radiopacity on CT (Fig. 4.5 C & D), and was seen to both pool in parenchyma, and spread along vascular and biliary channels when punctured, before undergoing gelation and remaining localised (Fig. 4.5 E).

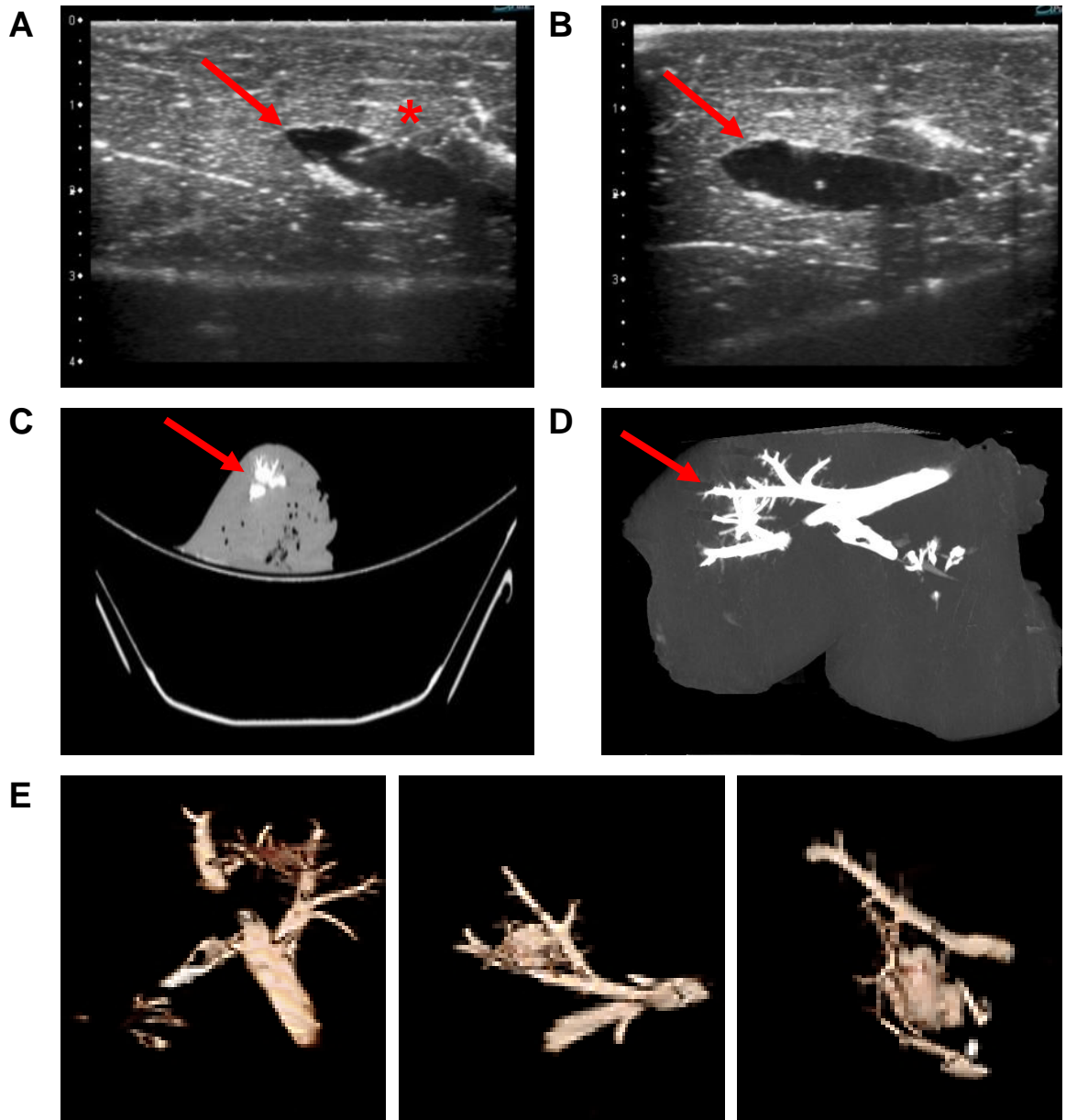


Figure 4.5 *Ex vivo* tissue administration of ChemoGel with 20% w/w Visipaque® was visualised using CT and US. Representative (A&B) US and (C&D) CT images of ChemoGel with 20%w/w Visipaque® distribution in an *ex vivo* tissue model. Arrows indicate pooling of radiopaque ChemoGel (E) CT images of radiopaque ChemoGel spreading through vascular and biliary channels. * indicates needle in US images.

4.3.2 Injectability of ChemoGel

Rheological measurement of the viscosity of the ChemoGel formulations in response to increasing shear rate determined the flow characteristics of each formulation, to predict how they would respond to the increased shear during injection. Both blank and drug ChemoGel were determined to undergo shear thinning at 20°C, with increasing shear rate resulting in a decrease in viscosity for both hydrogels (Fig. 4.6). Subsequently, the Visipaque® labelled hydrogels underwent the same flow procedure, and all three formulations demonstrated shear

thinning properties, with higher viscosities than the unlabelled ChemoGel. 30% w/w Visipaque® labelled ChemoGel was determined to have the highest viscosity, and remained the highest over the range of shear stresses applied (Fig. 4.6).

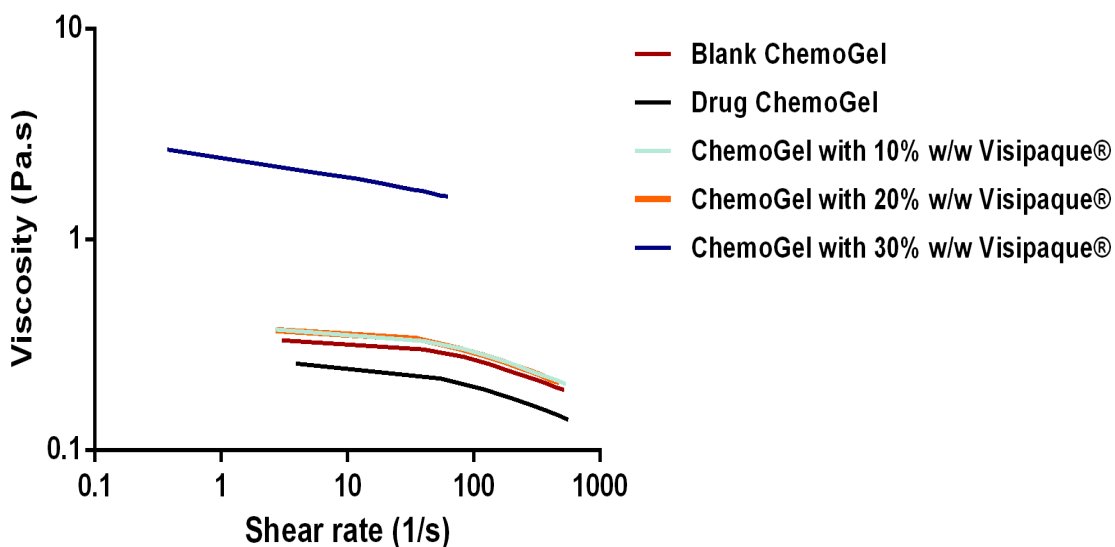


Figure 4.6 All ChemoGel formulations were capable of undergoing shear thinning in response to increasing applied stress. Rheograms of steady state flow procedure on blank and drug ChemoGel and ChemoGel with Visipaque® (0 . 30% w/w) demonstrating that formulations underwent a decrease in viscosity in response to increasing shear rate. Data shown is representative of the norm.

An average maximum force of $3.21 \text{ N} \pm 0.54 \text{ N}$ was required to inject $500 \mu\text{L}$ of blank ChemoGel through a 18G needle (7 cm length) at a speed of 2 ml/min (Fig. 4.7 A). The maximum force required to inject blank ChemoGel through a catheter was significantly higher than that required to inject the same hydrogel through the needle ($86.53 \text{ N} \pm 0.47 \text{ N}$, $p = < 0.0001$). A reduction in the speed of injection to 1 ml/min caused reduction in the maximum force to $61.5 \text{ N} \pm 1.89 \text{ N}$, however both speeds required a maximum force which surpasses the 50 N limit defined as hand injectable with ease.

A maximum force of 3.9 N was required to inject ChemoGel with 20% w/w Visipaque® through an 18G, 7 cm needle, which did not vary significantly from the force required to inject blank ChemoGel under the same conditions (Fig. 4.7 B). Further injectability assessment revealed that ChemoGel with 20% w/w Visipaque was injectable through various needles and catheters below 23G. The highest average maximum force recorded was 67.9 N required to inject the contrast labelled ChemoGel through a 23G needle of 9cm length (Fig. 4.7 C).

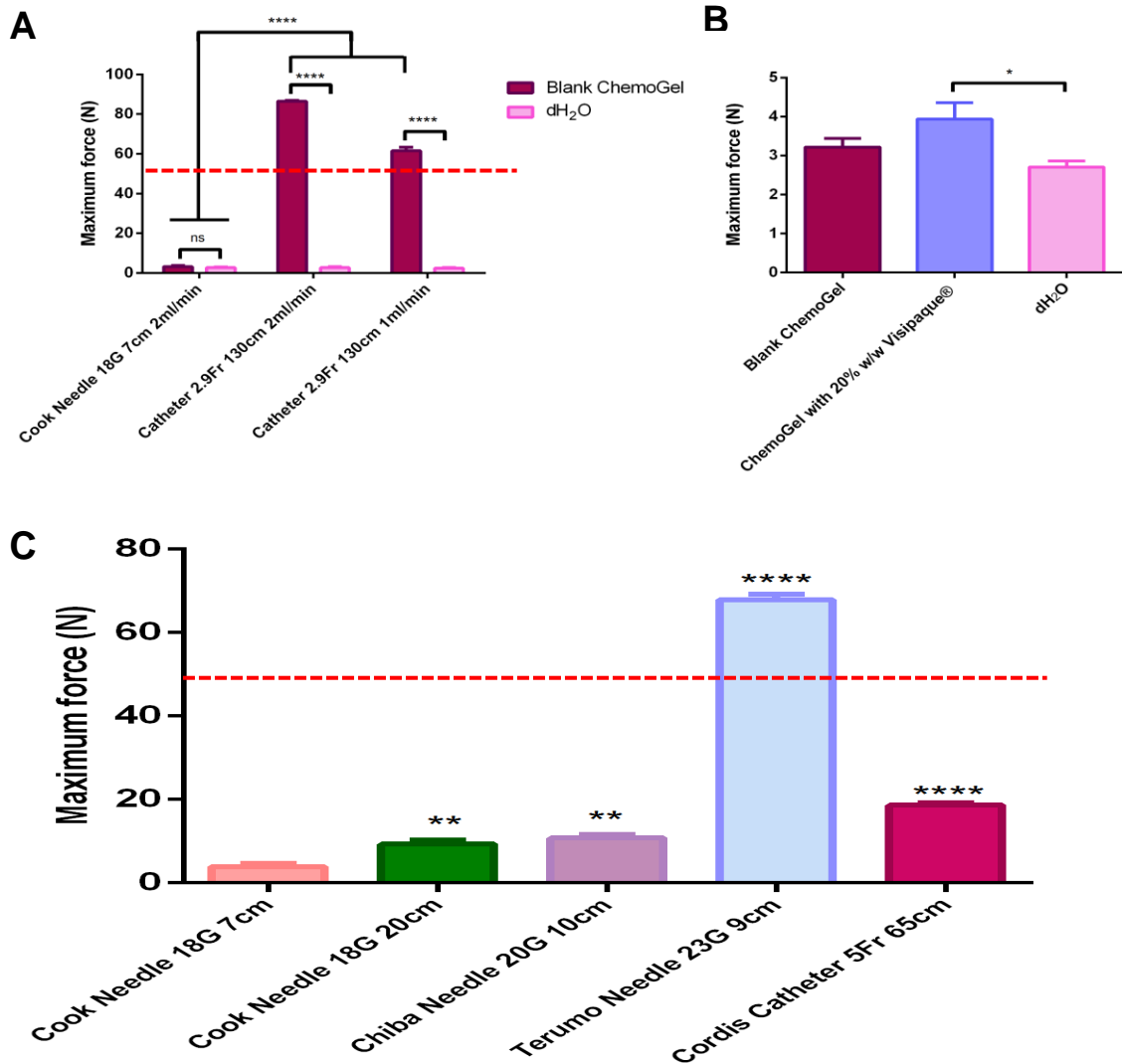


Figure 4.7 Maximum force required to inject various ChemoGel formulations was dependent on the length of the needle, the gauge of the needle, the speed of injection and the formulation injected. Determination of the maximum force required to inject 500 μ L of (A) blank ChemoGel or dH₂O through an 18G needle of 7cm length or 2.9Fr catheter of 130cm length at 2 ml/min or 1 ml/min and (B) blank ChemoGel, ChemoGel with 20% w/w Visipaque® and dH₂O through an 18G needle of 7cm length at a rate of 2 ml/min. (C) ChemoGel with 20% w/w Visipaque® through a range of clinically relevant needles/catheters at a rate of 2 ml/min. Data shown is represented as the mean + SEM (n=3 minimum). Significance was determined using a two-, χ^2 or Fisher's exact test for (A) and a one-, χ^2 or Fisher's exact test for (B) and (C). * = $p < 0.05$, **** = $p < 0.0001$ in (A) & (B). ** = $p < 0.01$, **** = $p < 0.0001$ compared to Cook Needle 18G 7cm in (C). Dashed line indicates maximum force of 50 N, which is deemed to be the threshold below which a product is hand injectable and above which is hand injectable with difficulty.

4.3.3 Assessment of the cytotoxicity of blank and drug Visipaque® ChemoGel in a 3D model of lung cancer

Treatment of A549-seeded scaffolds with blank and drug ChemoGel with 20% w/w Visipaque® (hereafter referred to as blank Visipaque® ChemoGel and drug Visipaque® ChemoGel) resulted in a significant decrease in viability at all timepoints over 14 days compared to medium treated control (Fig. 4.8 A). No significant difference was observed between blank Visipaque® ChemoGel and drug Visipaque® ChemoGel at any timepoint, although drug Visipaque® ChemoGel reduced viability to a greater extent at day 5, 7 and 14. Live/Dead staining confirmed these results with less live cells (green) and a greater amount of dead cells (red) observed in both the Visipaque® ChemoGel and drug Visipaque® ChemoGel treated A549-seeded scaffolds at all timepoints (Fig. 4.8 B).

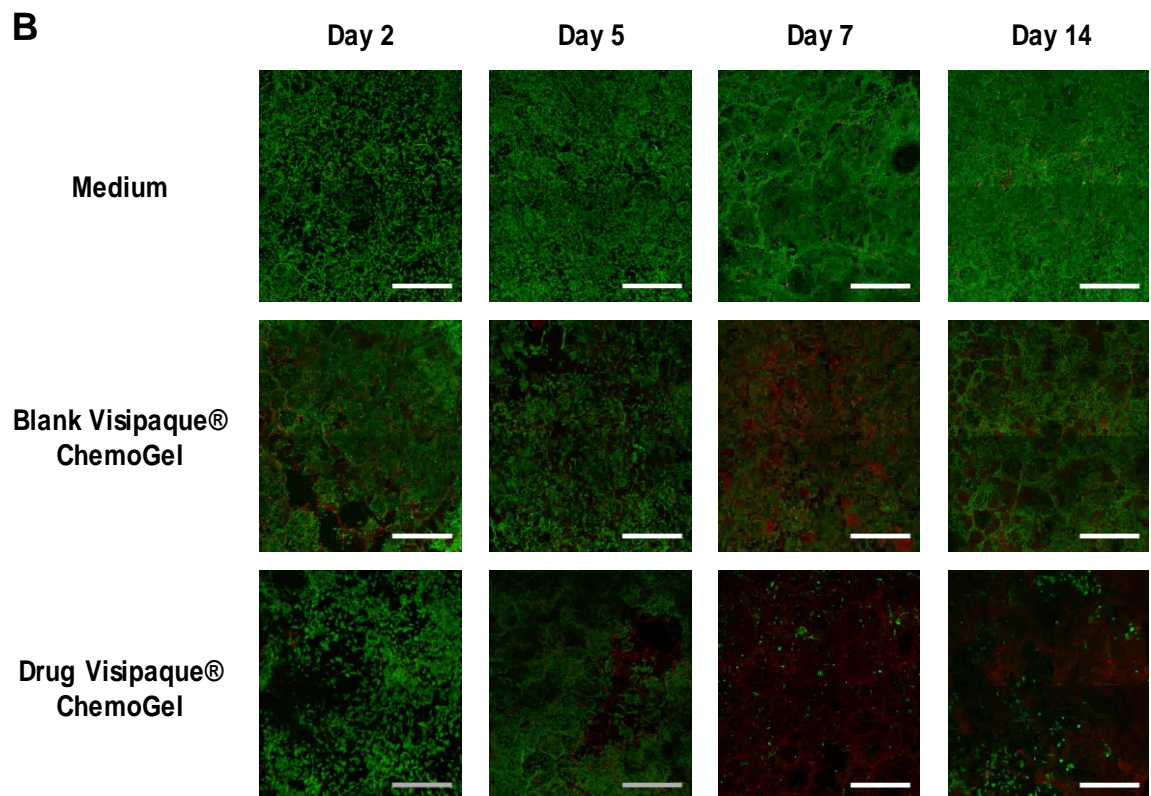
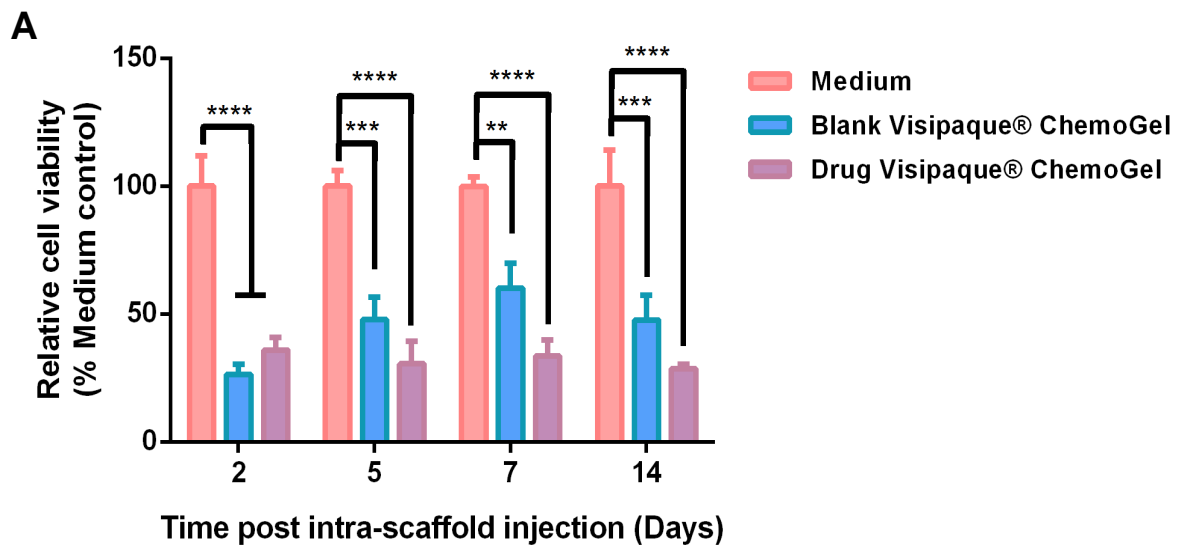


Figure 4.8 Blank Visipaque® ChemoGel and drug Visipaque® ChemoGel significantly reduced viability of A549 cells cultured in 3D on a collagen scaffold over 14 days compared to Medium treated control. **(A)** Relative viability of A549 cells cultured on a 3D scaffold following intra-scaffold injection of Medium, blank Visipaque® ChemoGel or drug Visipaque® ChemoGel. Data shown is represented as the mean + SEM (n=4 replicates). Significance was determined using a two-way ANOVA. ** = $p < 0.01$, *** = $p < 0.001$, **** = $p < 0.0001$. **(B)** Live/Dead staining of A549-seeded scaffolds post treatment with Medium, blank Visipaque® ChemoGel or drug Visipaque® ChemoGel over time. Live cells are stained green and dead cells are stained red. Scale bar, 500 μ m.

4.3.4 Assessment of freeze-drying and sterilisation on the material properties of ChemoGel formulations

4.3.4.1 Freeze-drying and rehydration of ChemoGel

The freeze-drying of blank ChemoGel produced a brittle, white wafer (Fig. 4.9 A), which could be rehydrated with an appropriate amount of dH₂O to restore the thermoresponsive hydrogel to its original state. This process did not negatively impact the sol-gel transition temperature of the formulation or the G' at 37°C, compared to the original ChemoGel formulation (Fig. 4.9 B).

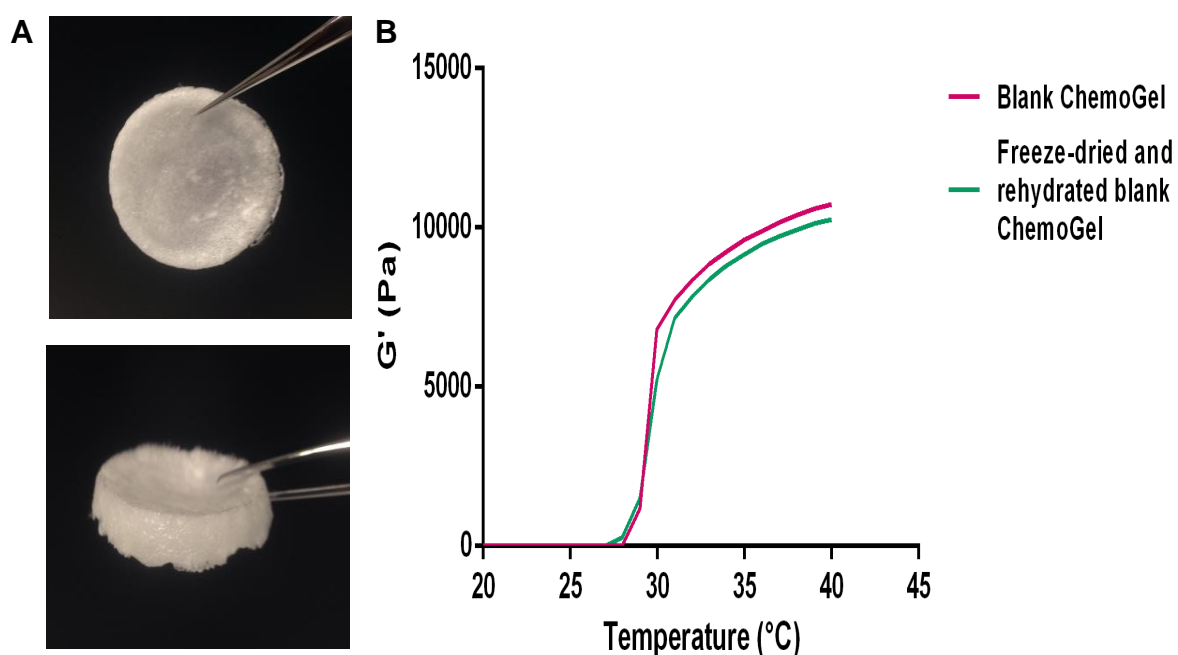


Figure 4.9 Freeze-drying and rehydration of ChemoGel did not adversely affect thermoresponsivity. (A) Representative image of front (top) and side (bottom) view of ChemoGel wafer produced after freeze-drying. (B) Rheogram of oscillatory temperature sweep from 20°C - 40°C of ChemoGel pre- and post-freeze-drying and rehydration. Data shown is representative of the norm.

4.3.4.2 Sterilisation of ChemoGel

Dry heat sterilisation of the freeze-dried ChemoGel wafer produced a brown solid, which would not rehydrate to form a solution (Table 4.5). Following gamma-irradiation of the freeze-dried ChemoGel wafer, the powder was rehydrated to produce a yellow liquid, with variable consistency. The thermoresponsive nature of ChemoGel was lost during the process; the liquid did not undergo gelation over an oscillatory temperature sweep from 20°C – 40°C (Table 4.5). Filtration of the powder was not feasible. Rehydration of the ChemoGel wafer after EtO sterilisation

produced a homogeneous liquid, which demonstrated a similar thermoresponsive profile as the original ChemoGel formulation (Fig. 4.10).

Table 4.5 Evaluation of the effect of compendial sterilisation methods on thermoresponsivity of blank ChemoGel.

Sterilisation method	Thermoresponsivity of blank ChemoGel maintained post-sterilisation
Dry Heat	No
Gamma Irradiation	No
Microbial Retentive Filter	N/A
Ethylene Oxide	Yes

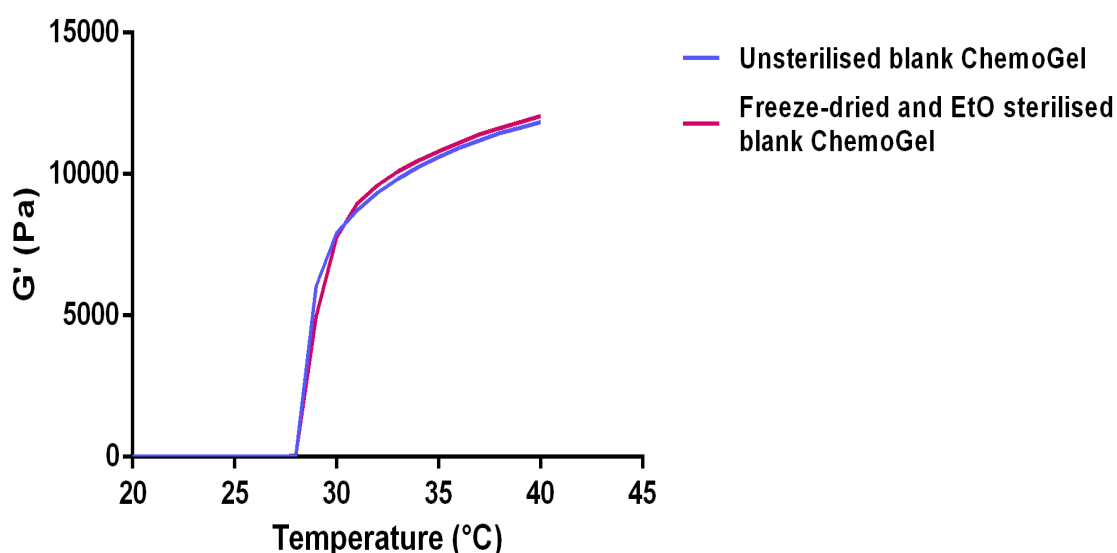


Figure 4.10 Ethylene oxide (EtO) sterilisation did not adversely affect thermoresponsivity of the rehydrated ChemoGel wafer. Rheogram of oscillatory temperature sweep from 20°C - 40°C of ChemoGel pre- and post- EtO sterilisation. Data shown is representative of the norm.

Following the initial screen of sterilisation methods, a complete comparison of all lead ChemoGel formulations before, and after, EtO sterilisation was conducted (Table 4.6). EtO sterilisation did not substantially alter the rheological profile of any of the thermoresponsive hydrogels formulated as per protocol. ChemoGel, drug ChemoGel and blank Visipaque® ChemoGel all demonstrated a 1°C reduction in thermoresponse temperature, with a modestly increased G' at 37°C. No change to

thermoreponse temperature or G' at 37°C was observed for drug Visipaque® ChemoGel.

Table 4.6 Sol-gel transition temperature and G' at 37°C of paclitaxel-loaded Visipaque® ChemoGel formulations before and after pre- and post- ethylene oxide sterilisation. Data shown is representative of the norm.

Formulation	Sol-gel transition temperature (°C)		G' at 37°C (Pa)	
	Pre-sterilisation	Post-sterilisation	Pre-sterilisation	Post-sterilisation
Blank ChemoGel	29	28	11,190	11,423
Drug ChemoGel	32	31	7,663	8,895
Blank Visipaque® ChemoGel	28	27	10,910	12,236
Drug Visipaque® ChemoGel	28	28	11,320	11,501

Freeze-drying and EtO sterilisation of the paclitaxel-loaded Visipaque® ChemoGel, and addition of cisplatin at point of rehydration produced a thermoresponsive hydrogel with a favourable viscosity profile, which demonstrated shear thinning behaviour (Fig. 4.11). Sterilised Visipaque® containing formulations demonstrated higher viscosity than the non-radiopaque formulations, which was also seen in non-sterilised formulations (Fig. 4.6).

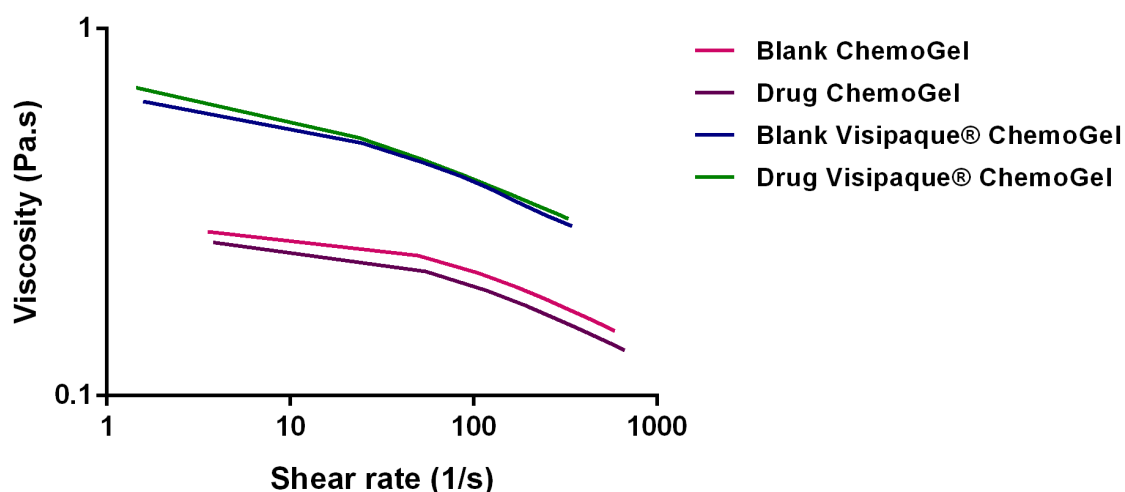


Figure 4.11 All ChemoGel formulations were capable of undergoing shear thinning in response to increasing applied stress post-sterilisation. Rheogram of steady state flow procedure demonstrating that viscosity of all formulations decreased with increasing shear rate. Data shown is representative of the norm.

4.3.5 Disintegration studies

Non-sterilised blank and drug Visipaque® ChemoGel underwent similar disintegration patterns as non-radiopaque blank and drug ChemoGel (Fig. 4.12 A & 2.14 A respectively). Initial loss in mass was observed at 4 h, which was recovered by 24 h, followed by a steady decrease in mass until 24.69% \pm 1.37% and 23.02% \pm 4.15% of blank and drug Visipaque® ChemoGel was remaining respectively at 240 h. After this point mass loss slowed, and the mass of hydrogel remaining remained constant until the end of study. More variable disintegration profiles were observed for all ChemoGel formulations after sterilisation (Fig. 4.12 B). Blank and drug Visipaque® ChemoGel post-sterilisation underwent the greatest mass loss with 35.2% \pm 1.45% and 41.49% \pm 19.93% remaining respectively by the end of the study. Sterilised drug ChemoGel underwent slower disintegration up to 240 h at which point a 30% reduction in mass occurred over 116 h to bring the remaining mass to 40.24% \pm 0.92% at 336 h. Blank ChemoGel post-sterilisation demonstrated the slowest disintegration, with 67.72% \pm 2.6% remaining by the end of the study.

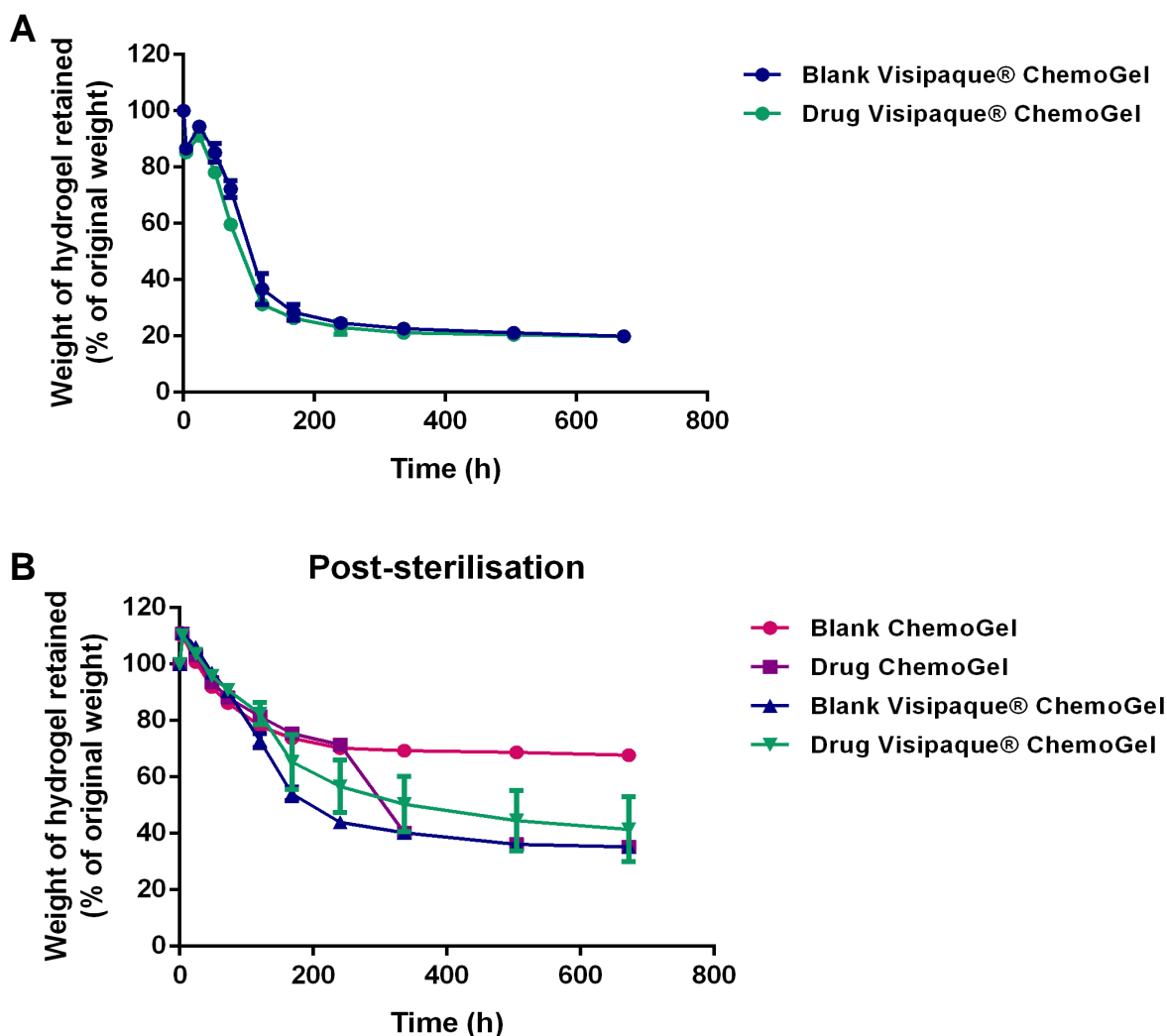


Figure 4.12 Disintegration profile of (A) unsterilised blank or drug Visipaque® ChemoGel and (B) blank or drug ChemoGel or Visipaque® ChemoGel post-ethylene oxide sterilisation over 28 days. Disintegration determined by measuring loss in mass (% of original weight of hydrogel) per timepoint. Data shown is representative of the mean of three independent experiments \pm SEM ($n=3$).

4.3.6 Release studies

Release of both chemotherapeutics from drug Visipaque® ChemoGel was observed over a 10 day period. $53.19\% \pm 4.52\%$ of loaded Pt and $71.65\% \pm 6.21\%$ of loaded paclitaxel was detected in the release buffer over the 10 day period (Fig. 4.13 A). An initial burst release of both drugs was observed, with the cumulative amount of Pt detected levelling off at an earlier timepoint (120 h) than paclitaxel (168 h), indicating that Pt release ceased after 72 h. This was confirmed when the quantities of each chemotherapeutic detected were analysed at each timepoint (Fig. 4.13 B, left). Over the course of the release study, the same quantity of both Pt ($69.18 \mu\text{g/ml} \pm 10.18 \mu\text{g/ml}$) and paclitaxel ($71.70 \mu\text{g/ml} \pm 10.7 \mu\text{g/ml}$) was detected in the release buffer (Fig. 4.13 B, right).

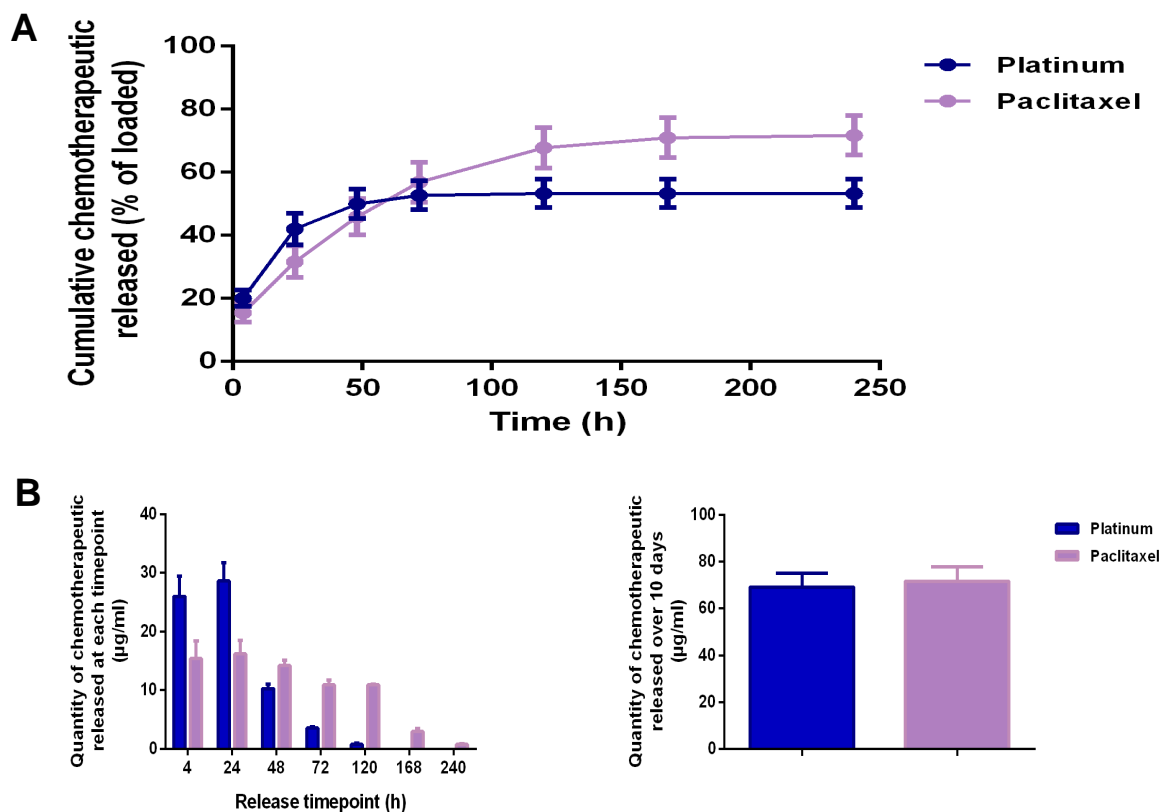


Figure 4.13 Drug Visipaque® ChemoGel demonstrated sustained release of loaded chemotherapeutics for up to 14 days. **(A)** Cumulative amount of platinum and paclitaxel detected in release buffer over 10 days as a percent of original quantity of platinum and paclitaxel respectively loaded in drug Visipaque® ChemoGel. **(B)** Quantity of platinum and paclitaxel detected in release buffer at each timepoint measured up to 10 days (left) and total quantity of platinum and paclitaxel detected in release buffer over 10 days (right). Data shown is representative of the mean of three independent experiments \pm SEM ($n=3$).

The study was repeated under the same experimental conditions following EtO sterilisation of drug ChemoGel and drug Visipaque® ChemoGel to determine if the sterilisation process had any impact on the release profile of the chemotherapeutics. $42.02\% \pm 1.55\%$ and $44.13\% \pm 1.22\%$ of the loaded Pt and $53.7\% \pm 6.32\%$ and $46.97\% \pm 10.27\%$ of the loaded paclitaxel was detected in release over 10 days from EtO sterilised drug ChemoGel and drug Visipaque® ChemoGel respectively (Fig. 4.14 A & C). The amount of Pt released was determined to slow after 120 h, in comparison to paclitaxel, which was detected up to the end of the study (Fig. 4.14 B & D, left). Similar quantities of Pt and paclitaxel were detected over the 10 day study for EtO sterilised drug ChemoGel ($54.65 \mu\text{g/ml} \pm 2.02 \mu\text{g/ml}$ and $55.82 \mu\text{g/ml} \pm 6.73 \mu\text{g/ml}$ respectively) (Fig. 4.14 B, right). Analysis of release buffer from drug Visipaque® ChemoGel revealed that less paclitaxel was detected over 10 days than Pt ($48.44 \mu\text{g/ml} \pm 6.52 \mu\text{g/ml}$ and $57.39 \mu\text{g/ml} \pm 0.91 \mu\text{g/ml}$ respectively) (Fig. 4.14 D, right).

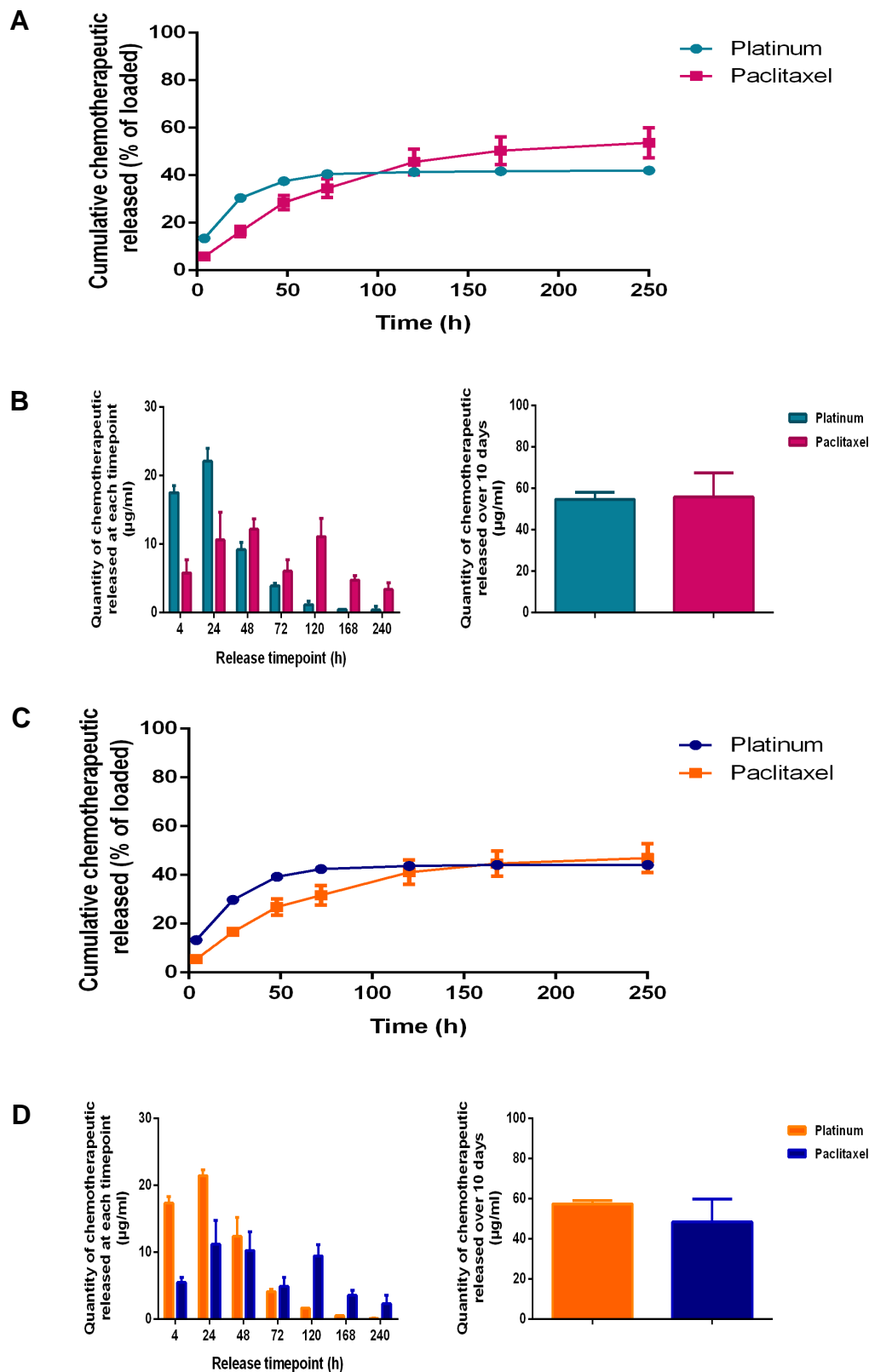


Figure 4.14 Ethylene oxide (EtO) sterilisation of drug ChemoGel and drug Visipaque® ChemoGel does not adversely affect sustained release profile. **(A & C)** Cumulative amount of platinum and paclitaxel detected in release buffer over 10 days as a percent of original quantity of platinum and paclitaxel respectively loaded in EtO sterilised drug ChemoGel and drug Visipaque® ChemoGel respectively. **(B & D)** Quantity of platinum and paclitaxel detected in release buffer at each timepoint measured up to 10 days (left) and total quantity of platinum and paclitaxel detected in release buffer over 10 days (right) in EtO sterilised drug ChemoGel and drug Visipaque® ChemoGel respectively. Data shown is representative of the mean of three independent experiments \pm SEM (n=3).

4.4 Discussion

The early stage development of the ChemoGel formulation was undertaken with a view to anticipating some of the common barriers to clinical translation of this technology (6). Collaboration with clinicians identified intra-procedural imaging as a key priority to ensure ChemoGel was compatible with the key aspects of an interventional procedure, thereby improving chances of clinical adoption of the technology. Intra-procedural imaging is critical in ensuring accuracy of delivery and patient safety. As a defining trait of IO procedures, it is important that administration of ChemoGel can be visualised using currently available imaging technology, e.g. CT or US. It is also essential that delivery through commercially available devices is feasible and adaptable to the current expertise of clinicians. Finally, the development of a portable and sterile version of the ChemoGel was developed as a preliminary effort to address some of the manufacturing and regulatory challenges associated with thermoresponsive hydrogels.

As a key aspect of IO procedures, intra-procedural imaging of ChemoGel administration will facilitate accurate delivery selectively to the tumour site, and allow for a reduction in the amount of ChemoGel delivered to off target, healthy tissue. The inherent radiopacity of blank ChemoGel was determined to be $33.6 \text{ HU} \pm 4$ and $22.4 \text{ HU} \pm 3.6$ at room and body temperature respectively. This is intermediate between water (0 HU) and non-enhanced liver (approximately 60 HU) (336). It would be challenging for interventional oncologists to track administration of the radiolucent ChemoGel, and therefore, addition of a radiopaque contrast agent to the formulation was warranted.

To this end, a commercial and commonly used iodinated contrast agent, Visipaque® was incorporated into the ChemoGel formulation at a variety of concentrations. Labelling of ChemoGel with Visipaque® at 10% w/w and 20% w/w did not have a significant effect on the thermoresponsive behaviour. However, at a concentration of 30% w/w Visipaque®, the sol-gel transition temperature of the formulation dropped to 22°C (Fig. 4.3). The final Visipaque® formulation contains salts, and it is hypothesised that at this concentration the level of salts in the formulation resulted in a reduction in sol-gel transition temperature, which has been previously demonstrated to occur in Ploxamer-based hydrogels (195, 337). Previously reported CS-based thermoresponsive hydrogels labelled with Visipaque® also underwent changes in their thermoresponsive profiles following

addition of the iodinated contrast agent (338). As expected, CT imaging of unlabelled and labelled ChemoGel revealed that radiopacity increased as Visipaque® concentration increased (Table. 4.4). Taken together, the rheological and radiopacity characteristics of ChemoGel with 20% w/w Visipaque® led to it being selected as the lead radiopaque candidate.

Visipaque® is a non-ionic contrast medium, and rapid release was observed due to the lack of ionic or covalent bonding retaining the iodixanol within the ChemoGel structure (Fig. 4.4). Similar rates of release from CS thermoresponsive hydrogels containing Visipaque® have been reported (318, 338).

As previously discussed in Section 4.1.1, US and CT are widely used during IO procedures to monitor the intervention in real time and post procedure. During US imaging, internal structures are visualised due to the different interactions of structures with the US waves, which gives rise to different strengths of US waves transmitted or reflected back, called echogenicity (339). ChemoGel with 20% w/w Visipaque® was seen to be anechoic on US, without speckling (Fig. 4.5 A & B). Anechoic images on US are those which do not allow the US waves to penetrate through them, and thus show up as black on the image (339). Speckling is one the main disadvantages of US imaging as it can result in poor image quality and interferes with automated diagnostic techniques (340). CT imaging of ChemoGel with 20% w/w Visipaque® showed clear definition on CT images of the injected hydrogel in the *ex vivo* model (Fig. 4.5 C & D). This study established the feasibility of real time intra-procedural monitoring of the radiopaque ChemoGel, with post-procedural assessment also achievable using CT imaging, thereby presenting it as a suitable candidate for IO procedures.

In a clinical setting, a balance between adequate tissue distribution and rapid *in situ* gelation post administration of ChemoGel will be of critical importance. While rapid gelation is called for to prevent indiscriminate spread of the thermoresponsive polymer solution, it would be preferable to have a system which could distribute in a defined manner throughout the tissue prior to gelation. Conversely, if gelation is too slow then the administered ChemoGel could spread in an uncontrolled fashion throughout the tissue, resulting in ablation of both tumour tissue and surrounding healthy tissue. *Ex vivo* administration of ChemoGel with 20% w/w Visipaque® was technically feasible and no gelation was observed to occur within the needle following introduction into the tissue. The envisaged route of IT administration for ChemoGel to lung tumours in a clinical setting is via the currently established biopsy

techniques, using a needle or catheter in a transthoracic or bronchoscopic approach. Clinician adoption of a new technology is one of the critical factors in successful translation to the clinic, so by implementation of previously established methods, it is hoped that the uptake of a new treatment modality will be increased (341).

ChemoGel with 20% w/w Visipaque® demonstrated the ability to flow from the needle, through the parenchyma of the *ex vivo* model, before undergoing gelation. The three injections carried out demonstrated a similar distribution profile, which suggests that the distribution is controlled and repeatable, although a larger sample size would be required to confirm this. Different needle types could also be employed to further influence distribution. Vogl *et al.* (2002) used a 19.5G needle with six side holes (SOMATEX, Berlin Germany) in a clinical trial, administering Intradose® Injectable Gel. The authors of this study noted that several needle positionings were required to ensure complete distribution within the tumour tissue, without encroaching on healthy tissue (62).

While preliminary evidence to support the technical feasibility of ChemoGel injection was established, it is essential to ensure that the ChemoGel formulations can be delivered through a range of clinically relevant needles and catheters, in order to increase the scope of applications. The viscosity and flow behaviour of the material are both central to achieving delivery. All ChemoGel and Visipaque® ChemoGel formulations, were shown to have shear thinning behaviour, which is beneficial to delivery as viscosity will reduce in response to increasing shear stress. (Fig 4.6 B) (328). However, the viscosity of the formulations was increased following labelling with Visipaque®, with the greatest increase seen at the 30% w/w concentration. As viscosity increases, so too does the force required for injection (327). This further confirmed the selection of ChemoGel with 20% w/w Visipaque® as the lead radiopaque thermoresponsive hydrogel.

It should be noted that most conventional rheometers cannot achieve the high shear rates that occur within the syringe barrel and needle during injection. Shear rates within the device can reach up to $200,000 \text{ s}^{-1}$ and above, depending of factors such as needle gauge and flow rate (342). Additionally, areas at the edge of the devices experience the highest shear stress, with the lowest shear stresses recorded in the centre, this makes viscosity prediction of shear thinning fluids highly complex (343).

The force required to inject a liquid through a needle is affected by the area of the plunger, diameter of the syringe barrel, needle gauge, flow rate and viscosity of the fluid. As outlined in Section 4.1.2, a force of 0 – 10 N may be defined as “easy to inject”, and forces up to 50 N can be defined as “injectable” (330). It was also noted that if the injectability force measured was less than 10 N, a needle with a smaller internal diameter could be used. The feasibility of IT administration of ChemoGel to LC tumours using currently employed biopsy methods was assessed by selecting needles and catheters of clinically relevant gauges and lengths for a transthoracic or bronchoscopic approach.

An 18G needle is commonly used in transthoracic core biopsy of NSCLC and this needle gauge was selected for initial evaluation of injectability (344). This was compared to a longer catheter with a thinner gauge (2.9Fr = 19.6G) that would be used in a bronchoscopic procedure. This determined that the maximum force required to inject the same volume of blank ChemoGel increased from 3.2 N to 86.5 N between the two injection devices (Fig. 4.7 A). Forces between 51 – 100N are defined as “injectable with difficulty” (330). A slower injection rate has been shown to reduce the force required for injection (330, 345), and therefore the maximum force required to inject blank ChemoGel through the catheter was reduced at an injection rate of 1 ml/min. At this rate, the force required was still above 50 N, but had reduced compared to 2 ml/min injection, indicating that should a longer, thinner medical device be required for administration of ChemoGel, modification of injection rate can compensate for the increased force required for injection in these medical devices. It is also of note that complete injection without failure was achieved at both speeds (Fig. 4.7 A).

Injectability of ChemoGel with 20% w/w Visipaque® was first assessed against unlabelled ChemoGel. No significant differences were found between the two thermoresponsive hydrogels when injected through an 18G, 7 cm needle (Fig. 4.7 B). The Visipaque® labelled ChemoGel was then injected through a variety of needles and catheters, which would be used in core biopsy (up to 18G) and FNAB (up to 25G) (323, 324). ChemoGel with 20% w/w Visipaque® was determined to be injectable across all devices evaluated, only the 23G device required a force greater than 50 N to achieve injection. From this data set it can be determined that both gauge and length of device can be tailored to suit the type of access required to treat the lung tumour, and still maintain injectability.

Addition of Visipaque® to the ChemoGel formulation called for a review of the cytotoxicity of the drug delivery platform to determine if the change to the formulation had an impact on the previously established cytotoxicity profiles (Fig. 4.8). Drug Visipaque® ChemoGel demonstrated a similar pattern of sustained reduction in viability across the 14 day study period, with a higher viability observed at Day 14 compared to drug ChemoGel (28.72% ± 3.28% vs 11.44% ± 2.51% respectively). Blank Visipaque® ChemoGel reduced viability to a greater extent at Day 2 (26.47% ± 7.61%) compared to blank ChemoGel at the same time point (52.83% ± 3.76%). This may be due to the initial release of Visipaque® from the labelled ChemoGel (Fig. 4.4) formulation having a negative impact on viability. Following medium change, and subsequent removal of released Visipaque®, the blank Visipaque® ChemoGel had a reduced cytotoxic effect, with levels comparable to that of blank ChemoGel observed at Day 14 (47.65% ± 19.611% vs 39.04% ± 3.43% respectively). Fatimi *et al.* (2016) assessed the toxicity of the released Visipaque®, and found that extracts of the 20% w/w and 30% w/w Visipaque® labelled hydrogels incubated for 24 h were significantly more toxic than 0% w/w hydrogels at 24 h. Viability was restored to 100% when treated with the hydrogel extracts taken in the following 24 h (338).

Attention was next directed to how the formulation can be prepared in a format that would be acceptable for end users and address regulatory requirements. Two main aspects were identified as initial development priorities; (i) preparation of a product that could be easily transported, stored and prepared at point of administration, and (ii) sterilisation of this final product.

Freeze-drying of the fully formulated, hydrated ChemoGel into a wafer would circumvent the need for aseptic compounding of ChemoGel from individual excipients in the hospital pharmacy. The one-step rehydration process is easier to execute, decreases risk of compounding errors, and reduces the cost associated with complicated extemporaneous compounding, thereby improving the path to translation. It is also of note that hydrated thermoresponsive hydrogel solutions would require refrigeration to prevent unintended gelation on storage, which on an industrial production scale would require specialised equipment and quality control processes, ultimately adding to the cost of the final product, and increasing risk of process failure. Transport and storage of a solid is widely accepted as easier than the same for a liquid.

To this end, production of a wafer that could be hydrated at the point of use was determined to be the preferred option for transport and storage of the final product in a commercial setting. The freeze-drying and rehydration process did not adversely affect the thermoresponsivity of blank ChemoGel (Fig. 4.9). Schuetz *et al.* (2008) compared three methods of storage of CS-based thermoresponsive hydrogels; refrigeration at 4°C, freezing at -80°C, and freeze-drying and rehydration. The freeze-drying and rehydration method was found to be the optimal method for storage and recovery of the gelation properties of the original thermoresponsive hydrogel (346).

Sterility assurance of pharmaceutical products for human use is a regulatory prerequisite, but sterilisation of hydrogels presents significant challenges to translation to the clinic. The impact of sterilisation has on the rheological and mechanical properties of the hydrogel, which becomes particularly complex when dealing with thermoresponsive hydrogels, is not commonly dealt with at a pre-clinical research stage of development (331, 347). Implementation of the EMA decision tree to guide the stepwise assessment of the various sterilisation methods was conducted with translation to clinic and regulatory hurdles in mind (Fig. 4.1). Terminal sterilisation is the preferred method, from both a regulatory and cost-saving perspective, compared to point of use compounding of individually sterilised excipients (332).

Terminal sterilisation of the ChemoGel wafer using the methods proposed in the EMA sterilisation decision tree was deemed to be unsuccessful. While dry heat sterilisation physically destroyed the wafer, gamma-irradiation of the freeze-dried ChemoGel was seen to destroy the thermoresponsive nature upon rehydration (Table 4.5). It was originally hypothesised that the low heat associated with gamma-irradiation sterilisation would be preferable, however, no consensus exists in the literature as to the suitability of this sterilisation method for thermoresponsive hydrogels. Some studies have indicated that gamma-irradiation is a suitable sterilisation method for P407 and P407-CS hydrogels (348, 349). Yang *et al.* (2007) suggested that main chain scission occurs in CS following exposure to gamma irradiation above 10kGy, and this may have negatively impacted the properties of the overall formulation (350). The individualised behaviour of different thermoresponsive hydrogel formulations is once again highlighted by these conflicting reports.

Thermoresponsivity of the ChemoGel formulations was not negatively impacted following EtO sterilisation (Table 4.5 & 4.6, Fig. 4.11), which is a gas sterilisation

method commonly employed in sterilisation of medical devices (350). This method is not included in the EMA sterilisation decision tree (Fig. 4.1), but it is included in the BP appendix of approved sterilisation methods (Table 4.2). EtO sterilisation of CS flakes has been previously shown to not degrade CS, in comparison to significant degradation demonstrated in gamma irradiation of same (351). This study noted that EtO sterilisation was only suitable for sterilisation of CS in dried form, and would not be applicable to CS hydrogels, an issue which is overcome in ChemoGel due to the freeze-drying process. Other studies also confirm that EtO sterilisation does not negatively impact the structure and chemical properties of CS (350, 352). Oscillatory temperature sweeps confirmed that all sterilised ChemoGel formulations retained thermoresponsivity and shear thinning (Table 4.6, Fig. 4.11).

The disintegration of blank and drug Visipaque® ChemoGel was observed to follow a similar temporal pattern to the non-radiopaque blank and drug ChemoGel (Fig. 4.12 A and Fig. 2.14 A respectively). CS-GP crosslinking was observed to proceed in much the same manner as the non-radiopaque formulations, and thus was not affected by the presence of Visipaque® in the formulation (data not shown). The disintegration profiles of all sterilised formulations determined that sterilisation retards the rate of disintegration, as up to $70\% \pm 2.8\%$ of the sterilised blank ChemoGel was retained after 240 h (Fig. 4.12 B), compared to $25.4\% \pm 3.45\%$ retained at the same timepoint for the unsterilised formulation (Fig. 2.14 A). The sterilised radiopaque formulations also demonstrated a slower rate of disintegration than non-sterilised formulations of the same, with $44\% \pm 1.89\%$ and $24.69\% \pm 1.37\%$ of the sterilised and non-sterilised blank formulations respectively remaining after 240 h exposure to PBS (Fig. 4.12). While no literature could be found reporting the disintegration rates of P407 or CS hydrogels post EtO sterilisation, studies investigating the effects of EtO sterilisation of collagen and silk sericin scaffolds demonstrated retarded disintegration rates, which was attributed to increased crosslinking in the scaffolds following the sterilisation process (353, 354).

No significant change in the pattern of release of the loaded chemotherapeutics was observed from non-sterile drug Visipaque® ChemoGel, as compared to the non-radiopaque formulation (Fig. 4.13 & 2.15 respectively). As previously suggested in Chapter 2, the curing and disintegration of the ChemoGel formulation may have been responsible for the pattern of release observed, and as such due to the similarities in disintegration profiles it is reasonable to expect a similar pattern to be seen in release studies. A reduced amount of chemotherapeutics was

released per timepoint in both drug ChemoGel and drug Visipaque® ChemoGel following sterilisation at the 4 h timepoint. This may be as result of the slower rate of disintegration in the sterilised hydrogels at this timepoint compared to the non-sterilised (Fig. 2.14 A & 4.12). The reduced disintegration rate of the sterilised hydrogels may have also caused a slower release rate of both chemotherapeutics, which impacted the final quantity of chemotherapeutic released by the end of the 14 day study by reducing it by 15 – 20 µg after sterilisation (Fig. 4.14 B & D).

4.5 Conclusion

Presented in this Chapter, was a preliminary review of the clinical and regulatory acceptability of the ChemoGel technology. This was undertaken early in the development process, in order to identify aspects of the formulation which could be modified to improve rates of translation to the clinic. In conclusion, a number of key considerations emerged as critical to the translational reality of ChemoGel, which required modification and re-characterisation of the formulation, including:

- ◁ the development of a radiopaque, thermoresponsive ChemoGel to assist with intraoperative monitoring of the delivery to the tumour site, which was
 - successfully imaged under CT and US guidance *in vitro* and *ex vivo*
 - assessed across a range of commercially available delivery devices, and its “injectable range” has been preliminarily defined by gauge and length of the device
- ◁ the development of a storage and sterilisation method, which
 - would be acceptable to both the product end user and regulatory authorities
 - did not negatively impact the thermoresponsive, chemoablative or sustained release capacity of ChemoGel

In all, the focus on the translation of ChemoGel to the clinic at this early research stage has sought to pre-emptively address the pitfalls often encountered by drug delivery technologies at a later stage of the product development lifecycle. In order to continue the progression of the ChemoGel technology through the development cycle an *in vivo* evaluation will be carried out in Chapter 5.

5.1 Introduction	189
5.1.1 Pre-clinical murine cancer models	189
5.1.2 In vivo imaging of animal models	192
5.1.3 Aim and Objectives	194
5.2 Materials and Methods	195
5.2.1 Blank and drug Visipaque® ChemoGel preparation	195
5.2.2 Cell culture	195
5.2.3 Animal procedures	196
5.2.3.1 <i>Animal maintenance</i>	196
5.2.3.2 <i>Anaesthesia</i>	196
5.2.3.3 <i>Tumour xenograft establishment</i>	196
5.2.3.4 <i>Intratumoural injection</i>	197
5.2.4 Xenograft monitoring	198
5.2.4.1 <i>Physical tumour volume measurement</i>	198
5.2.4.2 <i>Bioluminescence monitoring</i>	198
5.2.4.3 <i>Fluorescence monitoring</i>	199
5.2.5 Post-experiment analysis	200
5.2.5.1 <i>Ex vivo analysis of blood serum</i>	200
5.2.5.2 <i>Ex vivo analysis of tumour and organs</i>	201
5.2.6 Statistical analysis	201
5.3 Results	202
5.3.1 <i>In vitro</i> evaluation of fluorescent Visipaque® ChemoGel	202
5.3.2 <i>In vitro</i> and <i>in vivo</i> evaluation of bioluminescent A549-luc cell line	202
5.3.3 Assessment of localisation and retention of blank and drug Visipaque® ChemoGel following intratumoural administration	203
5.3.4 <i>Ex vivo</i> analysis of retention of blank and drug Visipaque® ChemoGel	204
5.3.5 Assessment of effect of intratumoural administration of blank and drug Visipaque® ChemoGel on tumour volume	206
5.3.6 Assessment of effect of blank or drug Visipaque® ChemoGel on tumour bioluminescence	207
5.3.7 Assessment of acute off-site toxicity following intratumoural administration of blank and drug Visipaque® ChemoGel	209
5.4 Discussion	211
5.5 Conclusion	217

5.1 Introduction

IT delivery of thermoresponsive hydrogels is an area of pre-clinical research that has become increasingly popular over the last number of years, with successful translation to the clinic lagging behind (6). Chapters 2 – 4 were dedicated to the pharmaceutical and cytotoxic assessment of the various ChemoGel formulations *in vitro*. This Chapter details the pre-clinical evaluation of the efficacy and off-site toxicity of the lead Visipaque® ChemoGel formulations to confirm the *in vitro* evidence obtained thus far, and to progress the Visipaque® ChemoGel platform along the product development pathway.

5.1.1 Pre-clinical murine cancer models

A significant amount of pre-clinical evidence to support claims of safety and efficacy must be gathered prior to clinical testing of a drug delivery platform for any disease treatment (355). Murine models are the most commonly employed pre-clinical models of cancer (356). A variety of approaches can be used to induce tumourigenesis in mice, with varying degrees of similarity to the human condition, as shown in Figure 5.1.

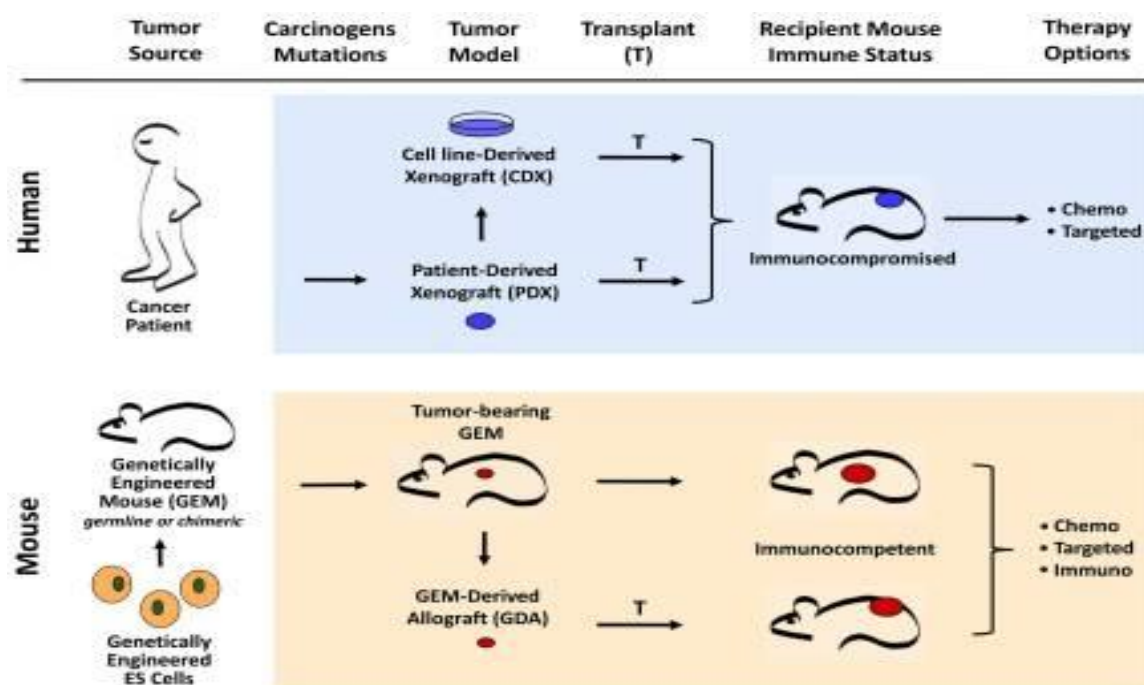


Figure 5.1 Murine models of cancer can be derived from human or murine sources using a variety of methods. Taken from (356).

Xenograft models can be derived from cell lines or primary patient sources, and can be implanted heterotopically or orthotopically. Heterotopic cell line derived xenograft models were first reported in the immunocompromised nu/nu mouse model in the early 1970's, and are perhaps the most commonly employed murine model of cancer (357). An immunocompromised strain of mouse can be inoculated with a human cancer cell line via SC, IV, IM or IP injection at a site distant from the origin of the tumour, such as the flank or hind leg (358). This results in a rapidly grown tumour, which can be physically measured without the need for advanced imaging machinery. The complex inter- and intra- tumour heterogeneity associated with human cancer is, however, lost in this model as the typical TME interactions do not occur at the distant site of inoculation. In addition, the lack of immune involvement in these models is not truly biomimetic, as evidenced by limited invasion and metastatic processes (359). Their reproducibility, and comparative cost and time effectiveness compared to more advanced murine models sees heterotopic xenografts ideally placed in early stage research as an initial screen for *in vivo* efficacy.

Orthotopic tumours are those which are grown at the site of tumour origin. The subsequent involvement of the TME makes this model more representative of the clinical reality. However, this technique requires greater operator skill, and is more time consuming than heterotopic xenografts. Moreover, as the tumour is not palpable, advanced imaging is required to ascertain tumour measurements throughout the experimental procedure (358).

Other types of xenograft murine models can make use of patient derived tumours, which are taken from fresh explanted human tumour tissue and grown at heterotopic or orthotopic sites to produce more representative models of human cancer. Development of these models is more time- and cost- demanding, with increased variability of successful implantation and response (359).

The use of immunocompetent mice gives a more representative picture of the off-site toxicity of treatment, and a greater appreciation of the influence of the immune system on tumourigenesis, but due to high rate of rejection of xenograft human tumours by immunocompetent mice, syngeneic tumour models must be employed. These models develop an allograft using murine tumour cell lines, which are less representative of human tumours (360). Recent reports of sensitising murine foetuses to human tumour cells has demonstrated successful tumour engraftment of human derived xenografts (361). Genetically engineered murine models can also

be used, which involves breeding of carcinogenesis-prone immunocompetent mice. These *de novo* developed tumours are more representative of tumour development in humans, but as with syngeneic mice xenografts, treatment response may be altered due to the murine origin of the tumour (362). Carcinogen-induced murine models can also be used, but this requires greater time and cost, with increasing variability (358).

A number of murine models of LC are employed in pre-clinical research. While orthotopic models of LC can be established, increased technical expertise is required for the endobronchial inoculation of the tumours, resulting in variable rates of engraftment success in this model. Lewis lung carcinoma cells in C57BL mice have been used to develop a syngeneic murine LC model, but this process is challenging and associated with the limitations of using murine-derived tumours to predict human tumour response (360). Patient derived xenograft models have also been established in NSCLC research at heterotopic and orthotopic sites, and are proposed as a possible tool for personalised medicine selection. This would involve screening a number of possible treatment options on a patient-specific murine xenograft model. A number of barriers remain before translation of this technique to the clinic, including technical feasibility and ethical considerations (363). For early pharmaceutical research, heterotopic xenograft models of LC are rapidly and reliably developed. A wide range of NSCLC cell lines have been successfully used in heterotopic xenograft models, including A549, H1299, NCI-H460, H1975, NCI-H226 and HCC4006 cell lines (60, 364-368). Methods for engraftment commonly involve SC injection of cells into the hind flank. The cells are often suspended in Matrigel to improve retention of tumour cells at site of inoculation (359). The *in vivo* study reported in this Chapter utilised A549 cells suspended in Matrigel, for SC injection into the hind flank of immunocompromised athymic nude mice to produce xenograft adenocarcinoma LC tumours.

It should also be borne in mind that mice are 3,000 times smaller than humans, with significantly shorter life cycles. Although this infers many advantages, such as increased ease of handling and housing in a laboratory setting, murine models represent an approximation of the human condition, and due consideration should be given to inter-species variation. On the whole as relevance to human tumours increases in murine models of cancer, so too do the associated time and cost requirements, and therefore, these more advanced models are usually restricted to late stage pre-clinical research. Other animals used in pre-clinical cancer research

include rats, zebrafish, rabbits, dogs, cats and pigs, with rare case-reports of non-human primate cancer models also available (369).

5.1.2 *In vivo* imaging of animal models

While heterotopic xenograft models of LC grown on the hind flank can facilitate physical measurement of tumour dimensions, efforts have been directed towards developing non-invasive imaging methods to determine tumour burden in murine models. Advanced imaging techniques available for murine models of disease include MRI, US, CT, PET and SPECT. Optical imaging techniques using fluorescent and bioluminescent imaging are relatively cheaper than the advanced imaging techniques, and are commonly used to determine tumour burden in animal models (370). As mammalian tissue is not fully opaque, the transmission of fluorescent or bioluminescent light through tissues is possible (371, 372). A charge-coupled device camera is required to detect the weak bioluminescent or fluorescent signals emitted from *in vivo* models. Pseudo-coloured images are generated to represent signal intensity, and are superimposed over a greyscale image of the animal.

Bioluminescent imaging (BLI) involves the use of an enzyme, luciferase (luc), which is genetically inserted into the cancer cell. As the tumour grows the signal also propagates, and is therefore representative of the size of the tumour. In the presence of oxygen, luciferin (substrate) is oxidised by the luc (enzyme) on the tagged cells to emit light in a characteristic region (373). In small animals, luciferin is usually injected IP or IV, and allowed to circulate around the body, before imaging the light emitted as a result of the enzymatic reaction with the luc tagged cells. One of the benefits of BLI is that, although the light signal emitted is relatively weak, the background noise in small animals is virtually non-existent, as light is not naturally emitted from mammalian tissue without excitation (374). This relatively large signal to noise ratio means that BLI is highly specific to the luc tagged cells. Luc can come from a number of biological sources, and this determines the emission wavelength. Firefly-luc is the most commonly used source, and emits light at the far end of the spectrum (approximately 612nm), which further improves its specificity (375).

Fluorescent imaging (FLI) is also employed in small animal imaging. Fluorescent tags require excitation at shorter wavelengths in order to emit light at longer wavelengths. The majority of traditional fluorescent probes are in the blue and green region of the visible spectrum, which is also absorbed by mammalian

haemoglobin, and as such considerable non-specific excitation and emission can occur in *in vivo* models resulting in higher levels of background autofluorescence (375). Recent fluorescent probes developed have focused on those that are in the far red or near infrared regions of the visible spectrum in order to increase the signal to noise ratio (374). Fluorescent probes can be conjugated to cancer cells for *in vivo* quantification of tumour burden, but are also commonly used as tags on drug delivery platforms, to track biodistribution and retention in real time (376, 377).

5.1.3 Aim and Objectives

The overall aim of this Chapter was to evaluate the effect of the IT administration of lead Visipaque® ChemoGel formulations in an A549 xenograft murine model of LC.

The specific objectives of this chapter were to:

- ◁ Develop a bioluminescent murine xenograft model of LC using A549-luc cells
- ◁ Assess retention of fluorescently tagged Visipaque® ChemoGel formulations at the site of injection over 14 days following IT administration
- ◁ Determine the efficacy of IT administration of lead Visipaque® ChemoGel formulations on reducing tumour burden, using physical and bioluminescent measurements over 14 days
- ◁ Evaluate off-site toxicity of lead Visipaque® ChemoGel formulations following IT administration

5.2 Materials and Methods

An A549 cell line expressing firefly luc with puromycin resistance (SC043-luc) was purchased from AMS Biotechnology (Abingdon, UK). 6-Deoxy-6-[(5/6)-Fluoresceinylthioureido]-HP- β -CD was purchased from Cycloab (Budapest, Hungary). Matrigel® Basement Membrane Matrix, Phenol Red-Free, *LDEV-Free (356237) was purchased from Corning® Life Sciences (MA, USA). All syringes and needles were obtained from Medguard Healthcare (Co. Meath, Ireland). All sterile surgical instruments and digital callipers were purchased from Harvard Apparatus (MA, USA). XenoLight D-Luciferin - K+ Salt Bioluminescent Substrate (122799) was purchased from Perkin Elmer (MA, USA). Controlled medicinal products required for animal anaesthesia and analgesia, Ketamine (Narketan-10 100 mg/ml solution for injection, Vetoquinol UK Limited, UK), Xylazine (Chanazine 2% w/v solution for injection, Chanelle Pharmaceuticals Manufacturing Ltd., Ireland), Isoflurane (Isoflurin 100 mg/g Inhalation vapour, liquid, Vetpharma Animal Health, S.L., Spain) were obtained under prescription from the designated RCSI veterinarian, and kept in accordance with controlled drug legislation. Aspartate Aminotransferase Activity Assay Kit (MAK055), Urea Assay Kit (MAK006), NBF 10% v/v were all obtained from Sigma Aldrich (MO, USA).

5.2.1 Blank and drug Visipaque® ChemoGel preparation

Sterilised blank and drug Visipaque® ChemoGel formulations were prepared as per Section 4.2.5.3. Fluorescently tagged ChemoGel formulations were prepared by replacing 0.01% w/w of the original HP- β -CD content with the same concentration of 6-Deoxy-6-[(5/6)-Fluoresceinylthioureido]-HP- β -CD, which contained one fluorescent unit per CD ring.

5.2.2 Cell culture

In vitro subculture of A549-luc cell line was carried out using aseptic technique as per Section 3.2.1. The A549-luc cells were maintained in DMEM:F12 supplemented with 10% v/v FBS, 1% v/v Pen/Strep solution. Polymerase Chain Reaction-based murine pathogen testing of the cell line was carried out prior to use *in vivo* to ensure that the cells were free from contamination (IMPACT-1 test, IDEXX Bioresearch, ME, USA).

5.2.3 Animal procedures

5.2.3.1 Animal maintenance

All animal experiments were approved by the Animal Research Ethics Committee, Royal College of Surgeons in Ireland (REC no. 1389) and by the national scientific animal regulatory authority, the Health Products Regulatory Authority (HPRA) (Project authorisation: AE19127/P040), and were conducted in accordance with European Union legislation (Directive 2010/63/EU) on the subject of animal rights. All animal handling and procedures were performed by Ms Seóna Rossi and Dr Ben Ryan in accordance with their respective individual authorisations.

Female Hsd:Athymic Nude-Foxn1nu mice (20 – 25 g weight) were purchased from Envigo (Huntingdon, UK), and group housed, four per cage, in the Biomedical Research Facility, RCSI. Due to their immunocompromised nature, the mice were housed under specific pathogen free (SPF) conditions in a Scantainer (Scanbur, Copenhagen, Denmark) with controlled temperature of between 20 – 24°C, humidity between 45 – 65%, and 12 h light/dark cycle. All animal handling outside the Scantainer was conducted in a dedicated SPF facility under laminar airflow using aseptic procedures. All mice were maintained on autoclaved water and food available *ad libitum*. Regular welfare checks were conducted on all mice as per project authorisation, including body weight measurements, and physical and behavioural observations.

5.2.3.2 Anaesthesia

Inhalation-based anaesthesia was induced using 4% v/v isoflurane and oxygen in an induction chamber, with 2% v/v isoflurane used as maintenance anaesthesia in induction chamber or nose cone. If a systemic anaesthetic regimen was required, ketamine (90 mg/kg) and xylazine (10 mg/kg) were administered IP using a 25G needle and 1 ml luer-lock syringe. In all cases, absence of pedal withdrawal reflex was confirmed prior to commencement of the procedure to ensure deep anaesthesia was achieved.

5.2.3.3 Tumour xenograft establishment

A549-luc cells were trypsinised as per protocol at 80 – 90% confluency, and resuspended in a PBS:Matrigel mixture (1:1) at a density of 1×10^7 cells/ml, and kept on ice until use, based on methods by Fridman *et al.* (2012) (378). Once anaesthesia had been induced via inhalation as per Section 5.2.3.2, 100 μ L of cell suspension (1×10^6 cells) was injected SC into the flank of the mouse in the lower

right hand quadrant, using a 29G insulin syringe (Romed, Utrecht, Netherlands). The needle was left in place for 30 sec after injection, rotated and removed slowly to prevent leakage of cell suspension from injection site. While under anaesthesia, mice were also ear clipped to allow for later identification. Animals were then placed into a clean recovery cage adjacent to a heat lamp, and allowed to fully recover from anaesthesia before being returned to their home cage.

5.2.3.4 Intratumoural injection

IT administration of sterile blank or drug Visipaque® ChemoGel or saline was undertaken once tumour volume had reached $250\text{mm}^3 \pm 50\text{mm}^3$. 100 μL of the appropriate ChemoGel formulation or saline for injection was loaded into a 1 ml luer-lock syringe with 22G needle and kept on ice prior to administration. Inhalation anaesthesia was induced as per Section 5.2.3.2. Tumours were stabilised using forceps and secured from beneath to minimise risk of needle piercing through tumour. The needle was inserted into the tumour, and the entire volume of required formulation was expelled slowly (Fig. 5.2). The needle remained in place for 30 sec following completion of injection to allow for gelation of ChemoGel formulations to occur, rotated and removed slowly to prevent backflow of injected material. Animals were then placed into a clean recovery cage adjacent to a heat lamp and allowed to fully recover from anaesthesia before being returned to their home cage.



Figure 5.2 *Example of intratumoural injection on anaesthetised mouse.*

An overview of the experimental procedure and subsequent monitoring is detailed in Figure 5.3.

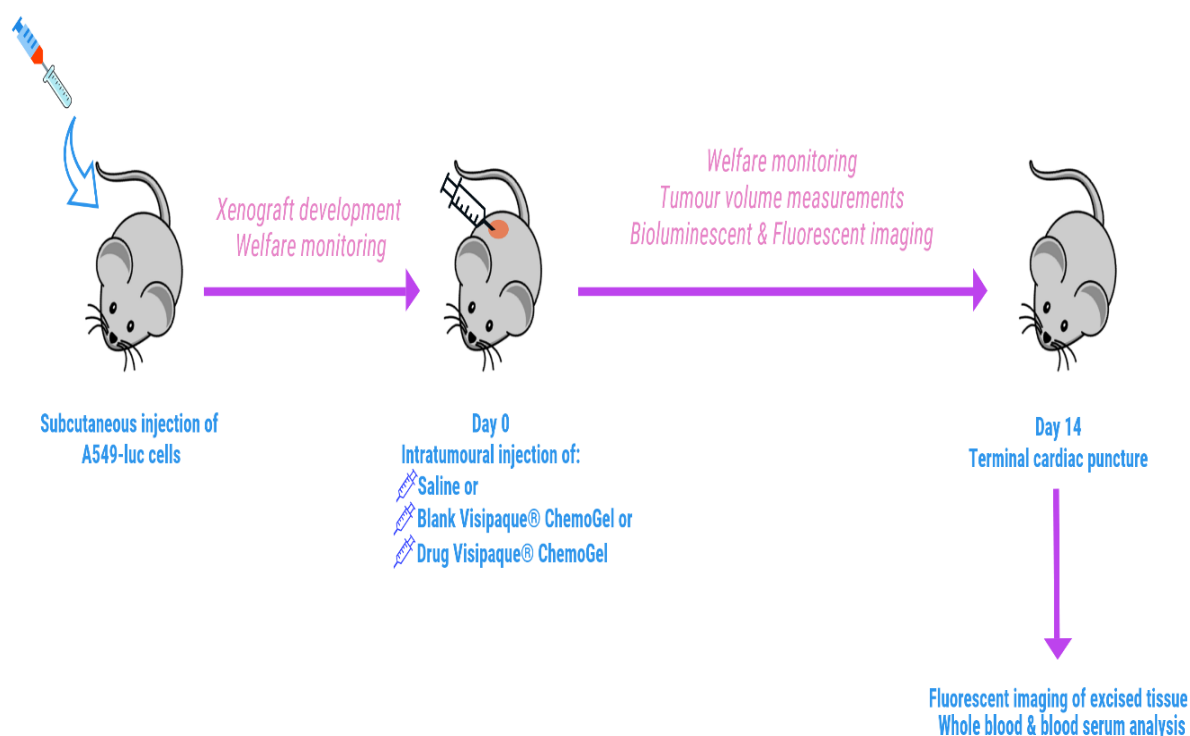


Figure 5.3 Schematic of experimental set up for *in vivo* experiments in Chapter 5.

5.2.4 Xenograft monitoring

5.2.4.1 Physical tumour volume measurement

Once tumours were palpable, dimensions of the tumour were taken externally using digital callipers to measure the length (l) and width (w). Tumour volume was derived using Equation 7 (379). Post-IT administration of treatment or control, tumour volume was measured at 2 h, Day 2, Day 7, Day 9 and Day 14 to monitor disease progression.

(Equation 7)

5.2.4.2 Bioluminescence monitoring

To confirm bioluminescence of A549-luc cells, they were first evaluated *in vitro* prior to *in vivo* administration. A549-luc cells were seeded in supplemented medium into 96-well black plates (Perkin Elmer, MA, USA) at a density of 64,000 cells per well in triplicate. Serial dilutions of cells were also plated to a final cell density of 2,000 cells per well. After 4 h, medium was aspirated from the wells, and replaced with

100 μL of freshly prepared D-Luciferin solution (150 $\mu\text{g}/\text{ml}$). Following a 10 min incubation period, bioluminescent signal was imaged using an IVIS® Spectrum In Vivo Imaging System (Perkin Elmer, MA, USA) using parameters outlined in Table 5.1.

In vivo BLI was conducted when tumours had reached a volume of $250 \text{ mm}^3 \pm 50 \text{ mm}^3$, measured as per Section 5.2.4.1. Animals were injected IP with freshly prepared D-Luciferin solution in PBS (150 mg/kg) and anaesthetised via inhalation as per Section 5.2.3.2. Visualisation of the bioluminescent light emitted from the A549-luc cells using an IVIS® Spectrum In Vivo Imaging System was conducted using the parameters in Table 5.1.

An initial kinetic curve of bioluminescence of A549-luc cells *in vivo* was to determine optimal imaging time post-D-Luciferin administration, as per manufacturer's instructions (380). Images were acquired, commencing at 10 min post-D-Luciferin administration, every 5 min for up to 30 min.

BLI of tumour progression post-IT administration of treatment or control was undertaken at 2 h and Day 14 after treatment. Images were acquired between 10-12 min post-D-Luciferin administration as determined by kinetic curve.

Following image capture, mice were removed from the IVIS machine, and returned to a recovery cage adjacent to a heating lamp until sedation was removed, at which point they were returned to the home cage.

Pseudo-coloured images of bioluminescent cells were generated and superimposed on greyscale images of the well plate or whole animal by the Living Image software (Perkin Elmer, MA, USA). Total flux (photons/s) of the light emitted by the A549-luc cells was quantified by the Living Image software following identification of a region of interest (ROI) around the bioluminescent signal.

5.2.4.3 Fluorescence monitoring

In vitro confirmation of fluorescence was conducted on fluorescently tagged Visipaque® ChemoGel. 100 μL of the fluorescently tagged Visipaque® ChemoGel was added to wells in a black 96-well plate in triplicate and allowed to gel for 15 min. Fluorescent signals emitted were recorded using an IVIS® Spectrum In Vivo Imaging System according to the parameters in Table 5.1.

For *in vivo* imaging, animals were anaesthetised via inhalation as per Section 5.2.3.2, and the fluorescently tagged Visipaque® ChemoGel formulations were

imaged using an IVIS® Spectrum In Vivo Imaging System using the fluorescent parameters outlined in Table 5.1. Saline treated animals were also fluorescently imaged to act as a control. Images were acquired at Day 0 and Day 14 while still under anaesthesia from BLI, as outlined outline in Section 5.2.4.2.

For *ex vivo* analysis, FLI of the excised tumour, liver and kidney was carried out using the parameters outlined in Table 5.1 immediately following excision.

Pseudo-coloured images of fluorescent signal were generated and superimposed on greyscale images of the well plate, whole animal or excised tissue by the Living Image software. Images were used for qualitative confirmation of ChemoGel localisation and retention only, and quantification of signal was not undertaken.

Table 5.1 *Imaging parameters used for bioluminescent and fluorescent image acquisition on the IVIS® Spectrum In Vivo Imaging System.*

Signal	Exposure	Binning	F/stop	Excitation (nm)	Emission (nm)	Field of view
Bioluminescent	Auto	Medium	1	Block	Open	D
Fluorescent	Auto	Medium	2	500	540	D

5.2.5 Post-experiment analysis

5.2.5.1 *Ex vivo* analysis of blood serum

Following IVIS imaging on Day 14 post-IT injection, animals were immediately administered systemic anaesthesia as outlined in Section 5.2.3.2. Under deep anaesthesia, terminal cardiac puncture was performed, using a 1 ml luer-slip syringe (B Braun, Melsungen, Germany) and 21G needle. The animal was placed securely on its back, and the needle was inserted at a 45° angle into the heart. The plunger was slowly withdrawn to collect the circulating blood, and needle was repositioned if required to complete blood collection, with due care given to prevent coagulation of blood in needle or syringe during procedure. 300 µL of the collected blood was then expelled into a K₃EDTA anti-coagulation tube (Microvette 500 K3E, Sarstedt, Nümbrecht, Germany) and the remainder was expelled into a 2 ml Eppendorf tube (Eppendorf, Hamburg, Germany).

The anti-coagulated blood sample in the K₃EDTA tube was analysed immediately for white blood cell count using a Sysmex KX-21N haematology analyser (Sysmex Corp., Kobe, Japan).

The remaining blood sample was allowed to stand for approximately 30 min to coagulate. Samples were then centrifuged at 4,700 rpm for 5 min using a Minispin® centrifuge (Eppendorf, Hamburg, Germany) to separate out the blood serum. Serum was carefully removed from the centrifuged tube and transferred to a CryoPure Tube (Sarstedt, Nümbrecht, Germany) and frozen at -80°C until analysis. Serum was analysed using Aspartate Aminotransferase (AST) and Urea assay kits according to manufacturer's instructions. Absorbance was read at 450 nm and 570 nm respectively using a Victor² 1420 plate reader (Perkin Elmer, MA, USA).

5.2.5.2 Ex vivo analysis of tumour and organs

Following terminal cardiac puncture, death of the animal was confirmed using cervical dislocation. Liver and kidneys were identified and removed using a sharp scissors. The tumour was then removed from the lower right hand quadrant of the flank. Excess tissue and fascia were carefully removed from excised organs and tumour. Visual images of the excised tumour were taken, and all excised tissue was fluorescently imaged as outlined in Section 5.2.4.3.

5.2.6 Statistical analysis

Two-way ANOVA with repeated measures was used to determine statistically significant differences between tumour volumes measurements made as per Section 5.2.4.1. One-way ANOVA was performed to determine statistically significant differences in bioluminescent signal in the kinetic curve study emitted post-IP administration of D-Luciferin and differences in blood chemistry between treatment groups as outlined in Section 5.2.4.2 and 5.2.5.1 respectively. Bioluminescent signal fold change post-treatment at Day 14 as outlined in Section 5.2.4.2 was evaluated for statistical significance using the non-parametric Mann-Whitney test. All statistical tests were performed using GraphPad Prism v6 (GraphPad Software Inc., CA, USA). Error is reported as SEM and statistical significance was determined using a probability value of $p \leq 0.05$

5.3 Results

5.3.1 *In vitro* evaluation of fluorescent Visipaque® ChemoGel

Due to the lack of inherent fluorescence associated with the ChemoGel (data not shown) a fluorescent tag was added into the formulation. *In vitro* assessment of fluorescently labelled Visipaque® ChemoGel revealed that it was amenable to FLI (Fig. 5.4 left). Bioluminescent imaging of the same wells demonstrated that no cross-over occurred in the bioluminescent range, indicating that fluorescently labelled ChemoGel formulations would not interfere with the bioluminescent signal emitted from A549-luc cells (Fig. 5.4 right).

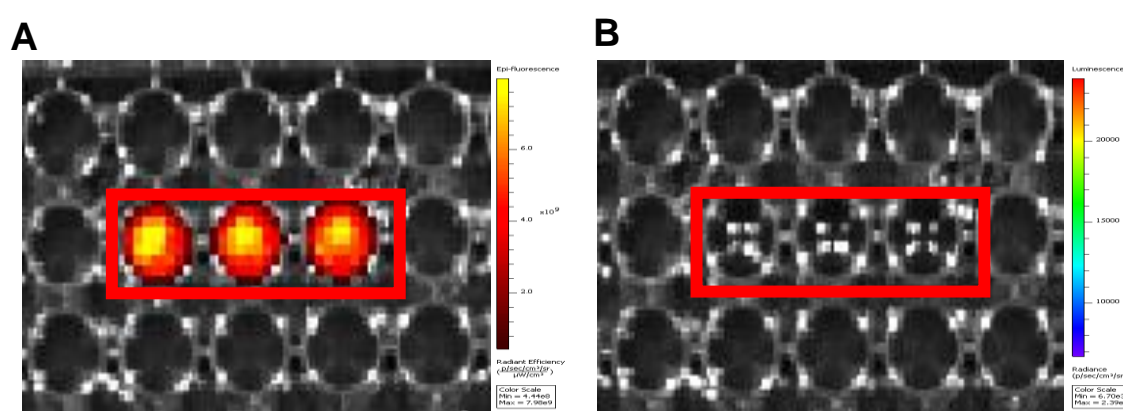


Figure 5.4 Fluorescently tagged Visipaque® ChemoGel formulations was fluorescently imaged *in vitro*, with no cross-over bioluminescent signal. Representative *in vitro* (A) fluorescent and (B) bioluminescent images of fluorescently labelled Visipaque® ChemoGel. Red box indicates filled wells.

5.3.2 *In vitro* and *in vivo* evaluation of bioluminescent A549-luc cell line

In vitro assessment of the A549-luc cells demonstrated linearity between cell number seeded and bioluminescent signal emitted, within a range of 2,000 to 64,000 cells (Fig. 5.5 A & B), supporting the use of this cell line for bioluminescent quantification of tumour burden. A kinetic curve was established *in vivo* to determine an acceptable time window for bioluminescent image acquisition post-administration of the D-Luciferin solution. The bioluminescent signals emitted between 10 and 30 min after D-Luciferin administration were determined not to be statistically significant, indicating that images could be acquired at any point within this time frame, without impacting the validity of the results (Fig. 5.5 C). An image

acquisition time of 10 – 12 min after D-Luciferin administration was utilised for all subsequent *in vivo* bioluminescent experiments, in order to minimise variability.

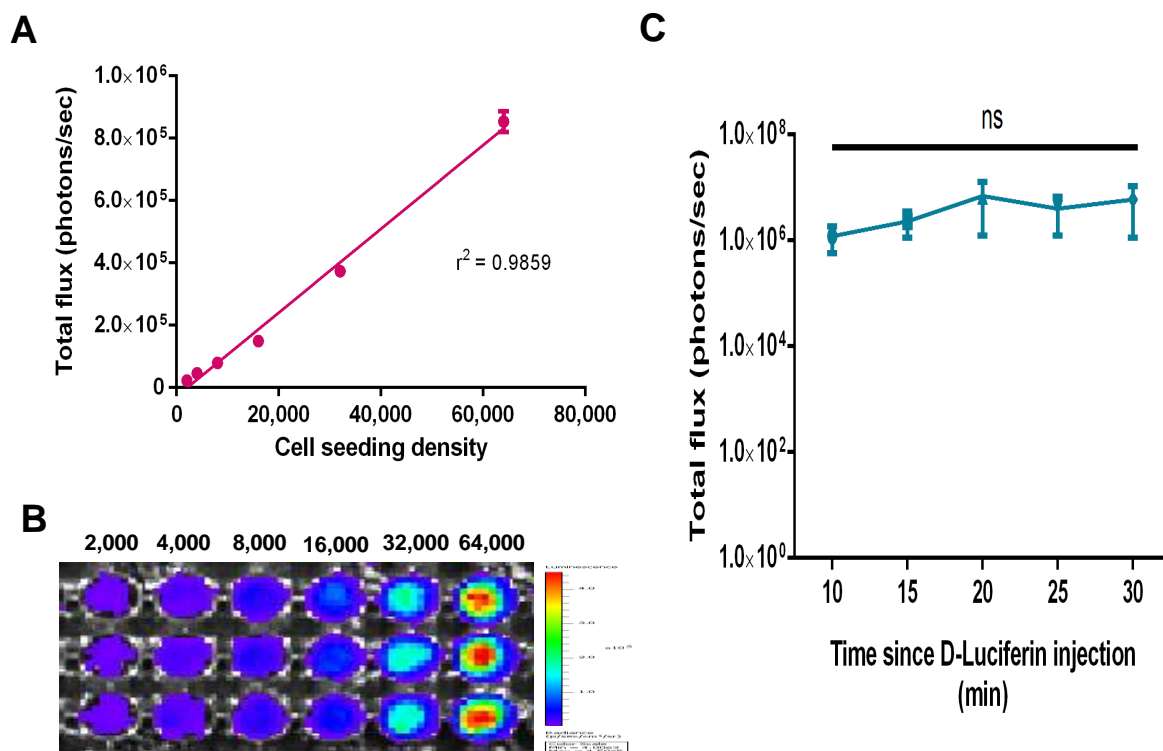


Figure 5.5 Bioluminescent imaging of A549-luc cells was feasible *in vitro* and *in vivo*. **(A & B)** A549-luc cells *in vitro* demonstrate a linear bioluminescent signal between 2,000 and 64,000 cells. **(C)** *In vivo* bioluminescent imaging of A549-luc tumours 10 . 30 min after D-Luciferin administration. Data shown is represented as the mean \pm SEM ($n=3$ wells for A & B, $n=3$ mice for C). r^2 was determined using linear regression. Significance was determined using a repeated measures one-way ANOVA. $ns = p > 0.05$

5.3.3 Assessment of localisation and retention of blank and drug Visipaque® ChemoGel following intratumoural administration

Localisation of blank and drug Visipaque® ChemoGel was confirmed 2 h after IT injection by creating an overlay image of the bioluminescent signal from the A549-luc cells and the fluorescent signal from the fluorescently tagged formulation. IT administration was considered successful if the fluorescent signal was in the region of the bioluminescent signal (Fig. 5.6 A). All injected formulations were successfully fluorescently imaged at 2 h post-IT administration, with *in vivo* imaging of retention at Day 14 also observed (Fig. 5.6 B).

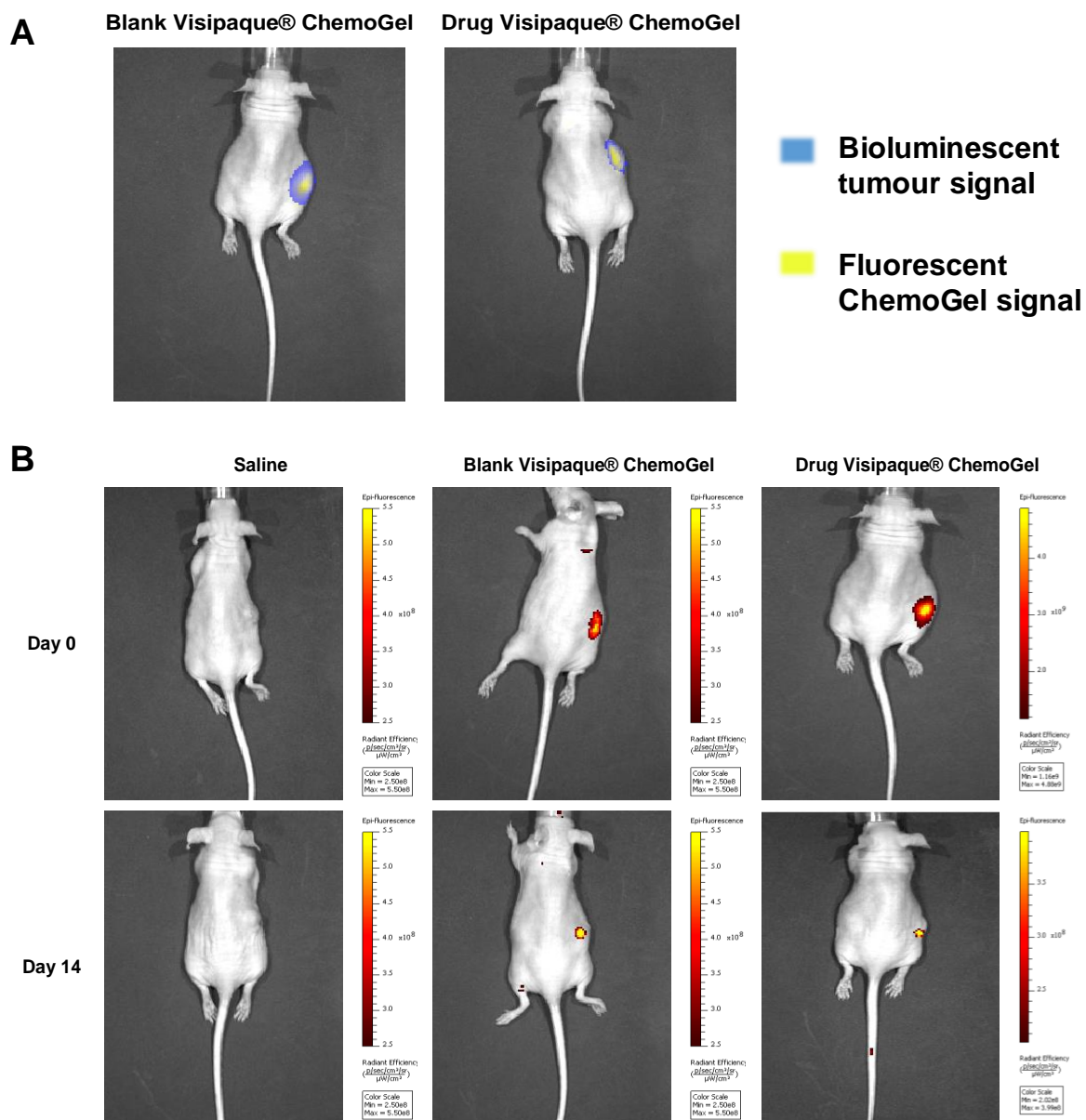


Figure 5.6 Blank and drug Visipaque® ChemoGel was retained at site of injection for 14 days *in vivo*. **(A)** Representative overlay images of bioluminescent A549-luc cells post-intratumoural administration of 100 µL of fluorescently tagged blank Visipaque® ChemoGel (left) or drug Visipaque® ChemoGel (right) at Day 0. Blue represents bioluminescent signal from A549-luc cells, Yellow represents fluorescent signal from blank or drug Visipaque® ChemoGel. **(B)** Representative fluorescent images at Day 0 (top) and Day 14 (bottom) post-intratumoural administration of Saline (left), blank Visipaque® ChemoGel (centre) or drug Visipaque® ChemoGel (right).

5.3.4 *Ex vivo* analysis of retention of blank and drug Visipaque® ChemoGel

Blank and drug Visipaque® ChemoGel formulations were qualitatively observed *ex vivo* to be retained in all treated tumours at Day 14 (Fig. 5.7 A). Saline was used as a control to ensure no fluorescence was emitted from the tumour mass. Excised liver and kidney were also fluorescently imaged to determine if any fluorescently

tagged blank or drug Visipaque® ChemoGel was observed in these excretory organs, with none noted in any treatment group (Fig. 5.7 B).

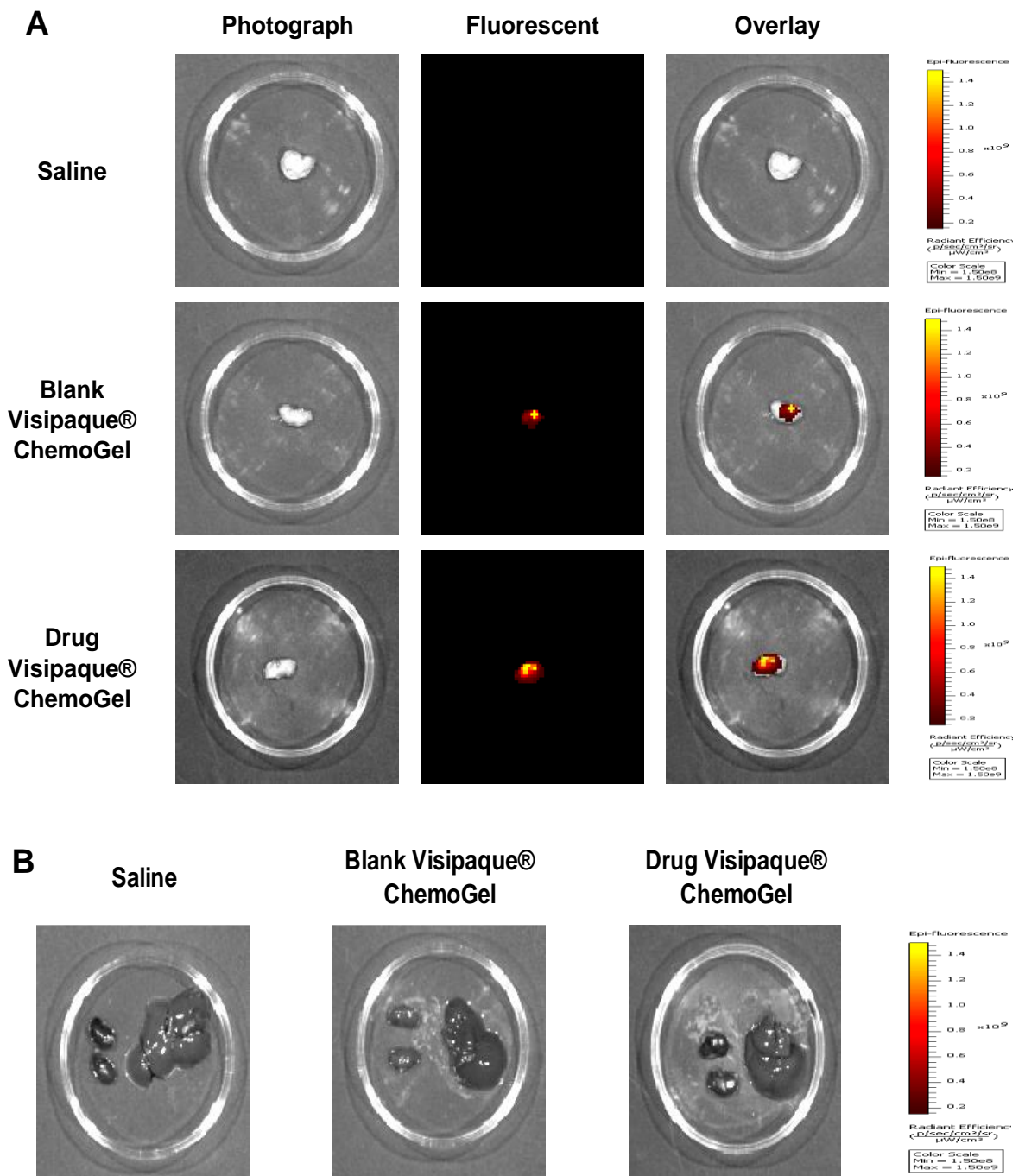


Figure 5.7 Fluorescent signals were only observed in blank and drug Visipaque® ChemoGel treated excised tumours at 14 days post-intratumoural administration. **(A)** Representative images (greyscale photograph [left], fluorescent signal [centre] and overlay [right]) of Saline (top), blank Visipaque® ChemoGel (centre) or drug Visipaque® ChemoGel (bottom) treated tumours excised on Day 14 post-intratumoural administration. **(B)** Representative images of kidneys (left hand side of image) and liver (right hand side of image) excised at Day 14 from mice treated with Saline (left), blank Visipaque® ChemoGel (centre) or drug Visipaque® ChemoGel (right).

5.3.5 Assessment of effect of intratumoural administration of blank and drug Visipaque® ChemoGel on tumour volume

Blank Visipaque® ChemoGel and drug Visipaque® ChemoGel significantly reduced tumour volume increase compared to saline treated control 14 days after IT administration (Fig. 5.8 A). The final volume of saline treated tumours was recorded as $429.34 \text{ mm}^3 \pm 12.87 \text{ mm}^3$. Blank Visipaque® ChemoGel treated tumours increased in volume by 18.99% on average after 14 days (final tumour volume $282.52 \text{ mm}^3 \pm 43.02 \text{ mm}^3$, $p = 0.026$), compared to drug Visipaque® ChemoGel tumours which increased by 5.2% on average (final tumour volume $246.16 \text{ mm}^3 \pm 20.77 \text{ mm}^3$, $p = < 0.0022$). Macroscopic inspection of excised tumours at Day 14, visually supported the quantitative results (Fig. 5.8 B).

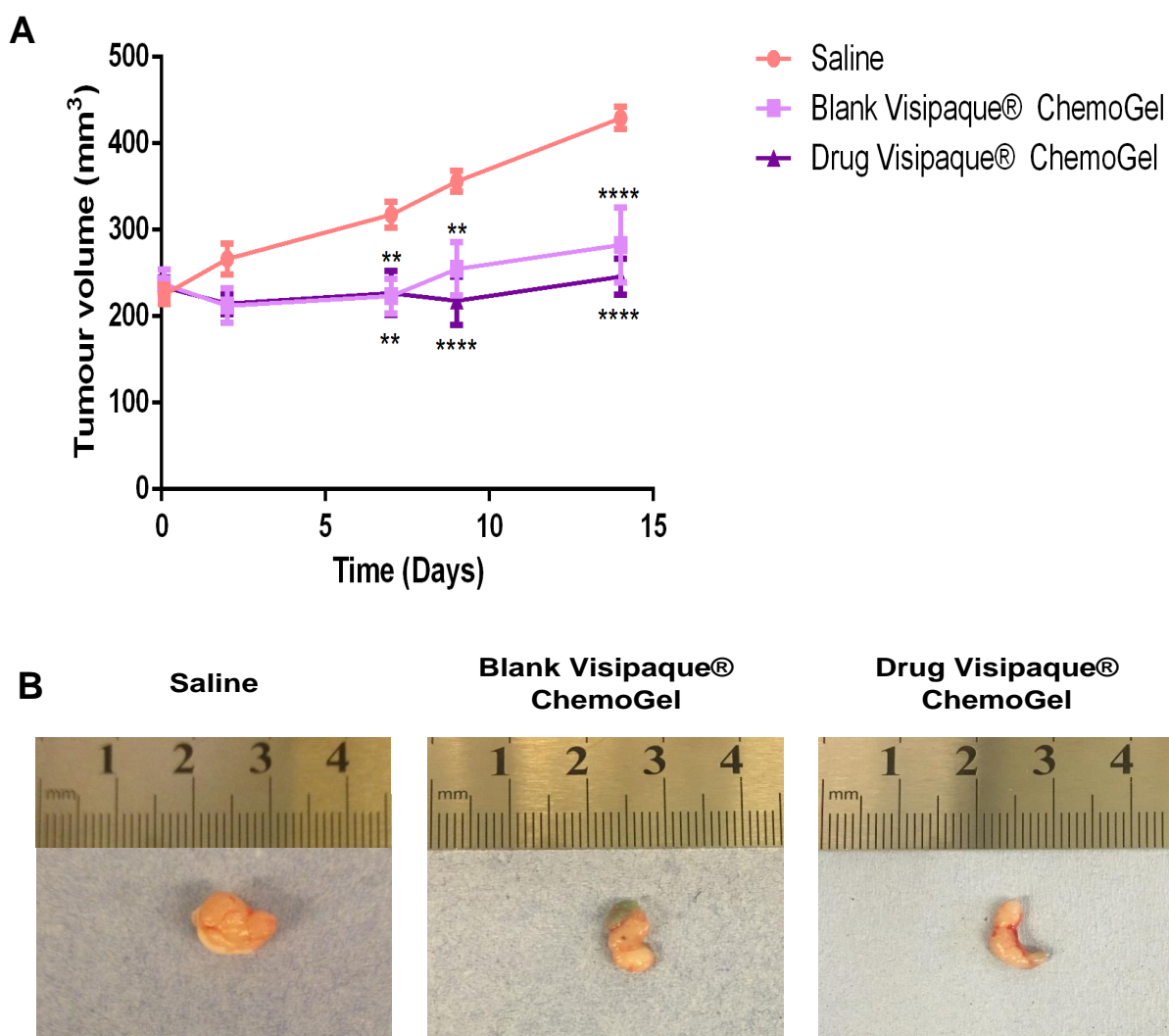


Figure 5.8 Intratumoural administration of blank or drug Visipaque® ChemoGel formulations significantly reduced tumour volume increase. **(A)** Tumour volume (mm³) following intratumoural administration of 100 µL of Saline, blank Visipaque® ChemoGel or drug Visipaque® ChemoGel at Day 0. Data shown is represented as the mean ± SEM (n=6 mice per group). Significance was determined using a repeated measures two-way ANOVA. ** = $p < 0.01$, **** = $p < 0.0001$ compared to volume of blank or drug Visipaque® ChemoGel tumour volume at the same timepoint. **(B)** Representative images of excised tumours at Day 14 following intratumoural administration of Saline (left), blank Visipaque® ChemoGel (centre) or drug Visipaque® ChemoGel (right).

5.3.6 Assessment of effect of blank or drug Visipaque® ChemoGel on tumour bioluminescence

Quantification of the fold change of the bioluminescent signal emitted from A549-luc tumour bearing mice treated at Day 14 post-IT administration did not reveal statistically significant differences (Fig. 5.9 A). However, the trend was similar to the tumour volume measurements at Day 14 (Fig. 5.8), with the greatest reduction in signal fold change induced by drug Visipaque® ChemoGel (Fig. 5.9 A & B).

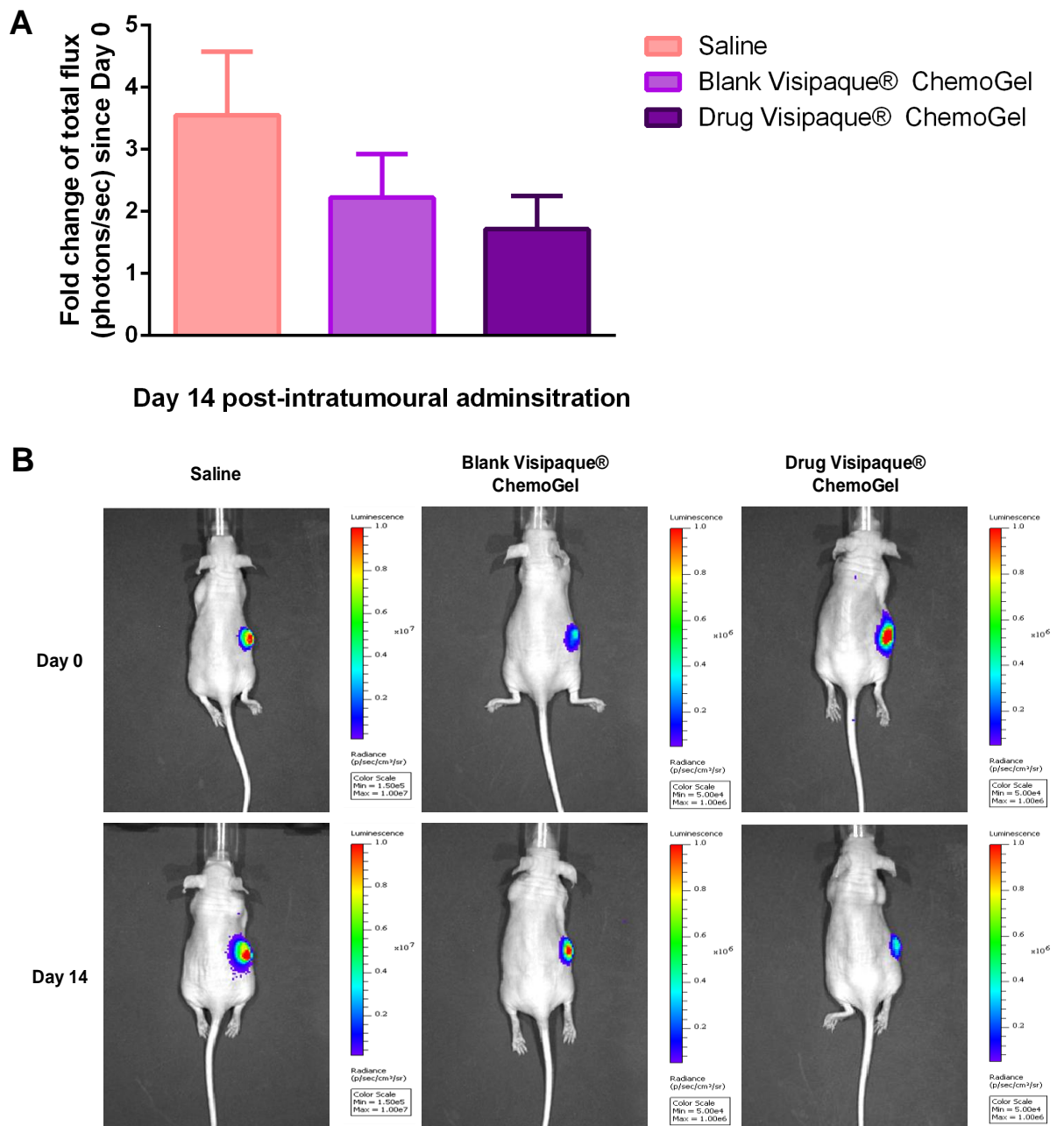


Figure 5.9 Intratumoural administration of blank or drug Visipaque® ChemoGel reduced bioluminescent signal of A549-luc tumours *in vivo* for up to 14 days. **(A)** Fold change in bioluminescent signal (total flux, photons/s) since Day 0, at Day 14 post-intratumoural administration of saline ($n=6$), blank Visipaque® ChemoGel ($n=5$) or drug Visipaque® ChemoGel ($n=6$). Data shown is represented as the mean + SEM. Significance was determined using a Mann-Whitney test. **(B)** Representative images of bioluminescent signal from A549-luc tumours *in vivo* at Day 0 (left) and Day 14 (right) following intratumoural administration of Saline (top), blank Visipaque® ChemoGel (centre) or drug Visipaque® ChemoGel (bottom).

5.3.7 Assessment of acute off-site toxicity following intratumoural administration of blank and drug Visipaque® ChemoGel

Off-site toxicity was monitored throughout the study using a welfare scoring system approved by the RCSI Animal Research Ethics Committee and the HPRA. This did not reveal any treatment associated toxicity (data not shown). 100% survival by Day 14 was achieved for all treatment groups. A reduction in body weight of 20% or greater was pre-determined to require a humane end point due to unacceptable toxicity. While the drug Visipaque® ChemoGel treated group demonstrated the largest decrease in body weight, this was only a transient 4% decrease between Day 7 and Day 9, and weight increased thereafter (Fig. 5.10 A). White blood cell count was quantified from whole blood samples extracted during terminal cardiac puncture, and no statistically significant differences were determined between any of the groups ($p= 0.9722$ and $p = 0.5957$ for saline vs. blank Visipaque® ChemoGel and drug Visipaque® ChemoGel respectively) (Fig. 5.10 B). AST and Urea were quantified from serum separated from whole blood extracted during terminal cardiac puncture, and also revealed no statistically significant difference between any of the treatment groups (Fig. 5.10 C).

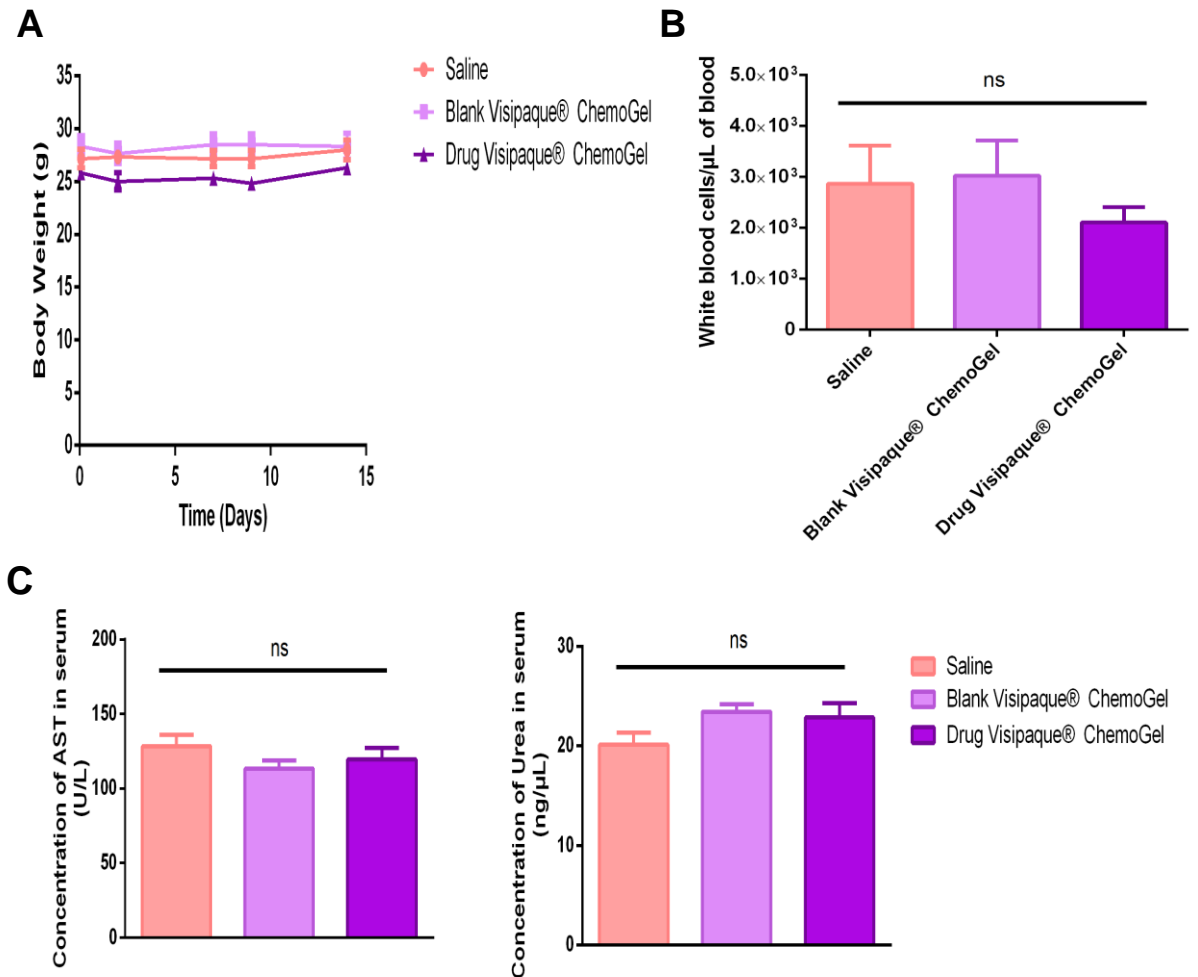


Figure 5.10 Intratumoural administration of blank or drug Visipaque® ChemoGel did not cause acute off site toxicity for up to 14 days. A549-luc tumour bearing mice treated with Saline, blank Visipaque® ChemoGel or drug Visipaque® ChemoGel did not show any significant alterations in **(A)** body weight, **(B)** white blood cell count or **(C)** blood serum levels of Aspartate transaminase (AST) (left) and Urea (right). Data shown is represented as the mean + SEM (n=6 mice per group). Significance was determined using a one-way ANOVA for (B) and (C). ns = $p > 0.05$.

5.4 Discussion

This *in vivo* study brought forward the lead blank and drug Visipaque® ChemoGel formulations, which were developed and characterised throughout Chapters 2 – 4 of this thesis, to perform a preliminary *in vivo* assessment on the acute efficacy and off-site toxicity of treatment. The overall goal of the ChemoGel technology is to employ the chemoablative properties of the formulation and its drug delivery functions in a locoregional manner to reduce tumour burden in LC. To this end, an *in vivo* xenograft tumour model of LC was developed to evaluate the IT administration of blank and drug Visipaque® ChemoGel, compared to saline treatment of LC.

A heterotopic, SC murine xenograft model of LC was used for the preliminary *in vivo* assessment of retention, efficacy and off-site toxicity of blank and drug Visipaque® ChemoGel. The A549 cell line was used to develop this xenograft model in order to facilitate comparison with previously generated *in vitro* data (Chapter 3 & 4). Adenocarcinoma is the most commonly used murine model used in LC research (381, 382), with SC, hind flank administration the method of choice for heterotopic implantation (360). The athymic nude mouse is a hairless, immunodeficient mouse, characterised by lack of T-cell production resulting from a dysfunctional, rudimentary thymus. The immunodeficient status of the mouse enables xenograft tumour growth from injected cancer cell lines. Matrigel, a commercially available basement membrane matrix protein, was used in this study to further improve rates of tumour establishment, since it has been shown to improve cancer cell growth and tumour development *in vivo* (378). For the purposes of this study, IT administration was technically simpler to achieve as the tumours were easily accessible and could be secured using a forceps (Fig. 5.2) in the heterotopic, SC xenografts. This technique would not be feasible in a clinical setting, as lung tumours are embedded in the lung tissue, and not amenable to physical stabilisation, thereby necessitating the use of advanced imaging techniques such as US or CT to guide needle placement and track administration (131, 314).

In vivo imaging of the Visipaque® ChemoGel technology was employed throughout this study to track *in vivo* disintegration. As previously discussed in Chapter 4, it was proposed that the inclusion of the iodinated contrast agent, Visipaque®, would facilitate intra-procedural monitoring in the clinical setting. Due to lack of pre-clinical

CT imaging machinery available, utilisation of FLI was proposed as a surrogate marker to monitor biodistribution post-IT administration. Visipaque® ChemoGel formulations were first evaluated for autofluorescence, as it was hypothesised that the GP content in the Visipaque® ChemoGel formulation could act as an autofluorescent marker. It has previously been demonstrated that GP autofluorescence was detectable at various wavelengths, such as 490 nm/ 520 nm em/ex or 590 nm/ 620 nm em/ex (383, 384). However, the concentrations of GP used in the ChemoGel formulations (0.1% w/w) were much lower than those employed in previous studies, which may account for the lack of autofluorescent signal. Substitution of 0.01% w/w of the original HP- β -CD with a commercially available fluorescently tagged HP- β -CD facilitated FLI of the ChemoGel formulation, with no cross over emission in the bioluminescent spectrum. This is important as any interference between the two signals may lead to incorrect conclusions being drawn as to the efficacy of treatment (Fig. 5.4).

Overlay imaging was employed 2 h post-IT administration of blank or drug Visipaque® ChemoGel to confirm localisation of treatment (Fig. 5.6 A). This technique of simultaneous FLI/BLI has previously been reported to confirm localisation and retention of fluorescently tagged drug-loaded NPs in the treatment of an A549-luc NSCLC murine xenograft model (385). The retention of blank and drug Visipaque® ChemoGel was subsequently tracked *in vivo* over the course of the 14 day study (Fig. 5.6 B), in order to qualitatively confirm the *in vitro* disintegration profiles established in Chapter 4 (Fig. 4.12). Real time FLI is commonly cited as a powerful tool to track hydrogel retention in a minimally invasive manner, with many studies employing fluorescent markers to determine *in vivo* disintegration profiles (386-389). Several other studies have used FITC-labelled nanoparticles or drugs to track distribution of treatment *in vivo* (390-393). Kim *et al.* (2014) utilised FITC-tagged dextran loaded into P407 hydrogels to monitor *in vivo* drug distribution using IVIS® imaging following intravesical instillation to nude mice. They determined that the P407 increased retention time of the drug compared to the free drug solution administered under same conditions (394). While this study monitored retention of drug, rather than the injected hydrogel, it further confirms the validity of employing FLI to achieve minimally invasive *in vivo* monitoring, and also underscores the improved pharmacokinetics associated with IT delivery using thermoresponsive hydrogels.

FLI was also used to confirm the retention of blank and drug Visipaque® ChemoGel at site of administration *ex vivo* (Fig. 5.7 A). All excised tumours treated with blank or drug Visipaque® ChemoGel were qualitatively confirmed to have retained the thermoresponsive hydrogel. Retention at site of injection indicates that the ChemoGel technology demonstrates *in vivo* robustness and resistance to rapid disintegration. This is of clinical significance because a major limitation of IT instillation of chemotherapeutic solutions is the rapid clearance of from the tumour site (395). As previously discussed in Chapter 2, the poor mechanical strength associated with Poloxamer hydrogels has been reported to result in rapid *in vivo* disintegration (396, 397), and therefore it can be confirmed that the inclusion of CS and GP in the formulation infers increased resistance to disintegration *in vivo*. Longer *in vivo* studies are required to determine the total retention time of blank and drug Visipaque® ChemoGel at the site of administration.

Retention time of drug-loaded thermoresponsive hydrogels at site of administration has previously been shown to have a significant effect on anti-cancer efficacy. A P407 hydrogel was used as the faster disintegrating hydrogel, and a poly(ethylene glycol)-*b*-poly(caprolactone-co-lactide) diblock copolymer hydrogel was used as the slower disintegrating hydrogel. The slower disintegrating hydrogel prolonged drug retention time IT, compared to P407 and drug solution. Both thermoresponsive hydrogels significantly reduced tumour volume growth over the study period, with the slow disintegrating hydrogel also determined to significantly reduce the growth rate of the tumour compared to the fast degrading hydrogel (176). Localisation of the drug delivery platform at site of injection is hypothesised to facilitate the sustained release of chemotherapeutics over a longer timeframe than administration of a chemotherapeutic solution. In the case of drug Visipaque® ChemoGel, the release of chemotherapeutics was demonstrated to occur *in vitro* for up to 10 days post-sterilisation (Fig. 4.14 C). Retention of the thermoresponsive hydrogel for the duration of this sustained release is, therefore, of critical importance.

Additionally, FLI of the excretory organs did not reveal the presence of either blank or drug Visipaque® ChemoGel (Fig. 5.7 B). Quantitative analysis of fluorescent signals from *ex vivo* tissue is cautioned, due to the significant impact tissue size and density has on fluorescent signal (398). Instead, FLI of *ex vivo* organs has been recommended as a valuable qualitative comparison to determine distribution to

distant organs, and is a technique commonly employed when assessing retention of drug delivery platforms in pre-clinical studies (399, 400).

The purpose of the *in vivo* efficacy study presented in this thesis was to establish the baseline characteristics of blank and drug Visipaque® ChemoGel treatment over an acute treatment timeframe of 14 days. The chemoablative properties of blank Visipaque® ChemoGel observed in the *in vitro* cytotoxicity studies (Chapter 4) were confirmed in the *in vivo* efficacy studies (Fig. 5.8). Blank Visipaque® ChemoGel significantly reduced the tumour volume increase compared to saline after 14 days of treatment.

Pre-clinical assessments of IT-administered thermoresponsive hydrogels generally focus specifically on their use for drug delivery, rather than their inherent cytotoxicity. Several studies have demonstrated that delivering cisplatin or paclitaxel, or a combination of both, in thermoresponsive hydrogels can improve therapeutic outcomes in mice models of cancer. A novel cisplatin-loaded thermoresponsive hydrogel was combined with paclitaxel-loaded micelles to form a dual drug-loaded thermoresponsive hydrogel. IT administration of this hydrogel to an A549 xenograft murine model of LC resulted in a reduction in tumour growth and prolonged survival time, compared to control (gel alone and cisplatin and paclitaxel alone) (60). This highlights that direct IT administration of “gold-standard” chemotherapeutics in solution is not as effective as IT administration of the same chemotherapeutics using a thermoresponsive hydrogel. In this study the thermoresponsive hydrogel demonstrated no cytotoxic properties, and therefore differences between blank and drug-loaded groups were easier to elicit compared to the Visipaque® ChemoGel studies contained in this Chapter. A similar thermoresponsive hydrogel was prepared by Jiang *et al.* (2016) using a modified CS-based hydrogel loaded with a paclitaxel-CD complex for IT administration to a mouse hepatoma xenograft model (H22 cells). A statistically significant reduction in tumour volume was observed over 10 days following IT administration of the drug-loaded hydrogel, compared to the paclitaxel-CD complex alone, hydrogel alone, Taxol solution and saline control. Improved survival time was also observed for the drug-loaded hydrogel compared to all other treatment groups (401).

Chemoablative hydrogels have been reported in the literature as drug-free methods of cancer treatment. Morhard *et al.* (2017) demonstrated the ability of a chemotherapeutic-free IT-administered gel to act as a chemoablative treatment *in*

vivo. The chemoablative nature of this gel was based on ethanol, which is currently used as chemoablative solution in locoregional treatment of solid tumours (402).

It was hypothesised that the loading of chemotherapeutics into the chemoablative blank Visipaque® ChemoGel, as outlined in Chapter 4, would facilitate a multi-faceted treatment approach. It was previously reported by Oun *et al.* (2014) that low dose cisplatin (30 µg cisplatin/mouse) encapsulated in a gelatin/polyvinyl (alcohol) was more effective *in vivo* than IP administered free cisplatin at five times the dose (150 µg/mouse) (403). This is underscored by the fact that IT administration of chemotherapeutics has been cited as delivering 10 – 30 times the concentration of chemotherapeutics to the tumour site, compared to systemic administration (57). Although no significant difference was observed between blank and drug Visipaque® ChemoGel treatment, drug Visipaque® ChemoGel was successful at reducing tumour volume increase throughout the study. Blank Visipaque® ChemoGel treated tumours began to increase in volume from Day 7, whereas increased volume was only observed in drug Visipaque® ChemoGel at Day 14. It is hypothesised that the sustained release of chemotherapeutics from drug Visipaque® ChemoGel may have been responsible for the delayed tumour growth. The lack of statistically significant difference between treatments may be attributed to the relatively low dose of chemotherapeutics loaded into the drug Visipaque® ChemoGel formulation. In relation to drug Visipaque® ChemoGel it was proposed that low dose chemotherapy delivered directly to the tumour, in combination with the inherent chemoablative nature of the blank Visipaque® ChemoGel formulation, would be sufficient to halt tumour growth. This was confirmed in this study, but in order to determine the effect of drug-loading, additional research is required. Extending the duration of the study or increasing the chemotherapeutic dose may elicit differences in tumour response between blank and drug Visipaque® ChemoGel.

Bioluminescence measurements were also used to assess tumour burden. While statistical significance was not determined between any groups in the bioluminescence measurements, a similar trend to the physical measurements was observed in the fold change of bioluminescence since Day 0. Bioluminescent signal emitted from the tumour cells was decreased following blank and drug Visipaque® ChemoGel treatment (Fig. 5.9). Drug Visipaque® ChemoGel reduced the fold change in bioluminescent signal to the greatest extent. Additionally, BLI provides

an opportunity to qualitatively confirm tumour establishment and localisation, and track the trends in tumour growth across the course of the study.

Finally, acute off-site toxicity was reviewed using a number of indicators of animal health. Body weight is commonly used as real time indicator of animal well-being, with a sudden loss of weight indicating potential toxicity of treatment, or disease progression (404). All mice in this study maintained a stable weight over the course of the 14 days, thereby suggesting that treatment was not inducing widespread toxicity. WBC counts from whole blood samples of all mice were also evaluated, given that myelosuppression is a side effect of cisplatin and paclitaxel treatment (97). The inoculation of tumour cells in immunocompromised mice has previously been shown to induce an increase in WBC (405), which can then be significantly reduced due to off-site toxicity associated with cytotoxic treatment (406). Although drug Visipaque® ChemoGel treated mice had the lowest WBC count, this was determined to not be statistically significantly different to saline or blank Visipaque® ChemoGel treated mice (Fig. 5.10 B). It is hypothesised that locoregional delivery of chemotherapeutics in thermoresponsive hydrogels reduces off-site toxicity, due to the reduced chemical payload administered directly to the tumour site, and increased retention of drug at site of administration. Blood serum markers of liver and kidney damage were also assessed post-mortem to determine whether elimination of the drugs and/or Visipaque® ChemoGel had a detrimental effect on the function of these excretory organs. In particular, cisplatin treatment is associated with severe nephrotoxicity (97), and P407 has also been suggested to induce renal toxicity (32). No significant difference in levels of either AST or Urea compared to saline treatment were observed, indicating that the liver and kidneys were functioning to the same capacity following blank or drug Visipaque® ChemoGel (Fig. 5.10 C). Taken together, in conjunction with the positive general welfare scoring, these results indicate that treatment with blank or drug Visipaque® ChemoGel did not induce off-site toxicity following IT administration over a 14 day period.

5.5 Conclusion

This Chapter presents preliminary evidence to support the retention, efficacy and off-site toxicity of IT administration of either blank or drug Visipaque® ChemoGel in an A549 xenograft murine model of LC. In conclusion, these results indicate that both blank and drug Visipaque® ChemoGel:

- ◁ Facilitate localised gelation at site of administration, with retention for at least 14 days
- ◁ Demonstrate efficacy in significantly reducing tumour volume increase over 14 days
- ◁ Do not induce acute off-site toxicity

Establishment of these initial treatment parameters will enable design and execution of further *in vivo* studies to investigate variations in dose and administration schedules, with a view to determining optimal ChemoGel-based treatment regimens. These results indicate that blank Visipaque® ChemoGel has localised chemoablative properties. Modification of drug-loading or longer study timeframes may illicit significant differences between blank and drug Visipaque® ChemoGel, but these results confirm the feasibility and preliminary efficacy of IT treatment with a dual drug-loaded thermoresponsive hydrogel.

„Šťáň“®

„Šťáň“ „Šťáň“

6.1 Overview	220
6.2 Chapter 2: Development and optimisation of a thermoresponsive hydrogel as a drug delivery platform	222
6.3 Chapter 3: <i>In vitro</i> evaluation of ChemoGel formulations.....	223
6.4 Chapter 4: Translational reality of ChemoGel – assessment of relevant factors	225
6.5 Chapter 5: <i>In vivo</i> assessment of Visipaque® ChemoGel formulations in a murine xenograft model of Lung Cancer.....	227
6.6 Future work	230
6.7 Overall conclusion	232

6.1 Overview

The overall objective of this thesis was to develop and characterise a dual drug-loaded thermoresponsive hydrogel, which would be suitable for the locoregional treatment of LC in IO procedures. The principal hypothesis was that a thermoresponsive hydrogel could be loaded with a hydrophilic and hydrophobic drug to enable local delivery directly to the tumour site in a sustained release manner.

Thermoresponsive hydrogels consist of hydrophilic polymers, which can undergo a sharp conformational change in response to temperature (24). Clinically relevant LCST polymers undergo a phase transition from liquids at room temperature to gels at body temperature. Drug-loading of thermoresponsive hydrogels to create sustained release drug depots has been extensively evaluated in the preclinical setting (49, 407, 408). These “smart” hydrogels are ideally situated as platforms for minimally invasive, locoregional drug delivery to a wide range of disease states. The translation to the clinical setting has, nonetheless, proven to be challenging. Rationale design and end-user focused development of thermoresponsive hydrogels from an early stage is required in order to improve the translational strength of new technologies (6). To that end, ChemoGel was developed, with the patient, and the clinical and regulatory practicalities, central to the process.

LC was selected as the lead clinical indication for the ChemoGel technology as it currently represents the leading cause of cancer-related death worldwide (83). Specifically, NSCLC was chosen as this is the most common histological subtype of LC patients. Current treatment strategies revolve around the systemic administration of traditional chemotherapy, with the option of employing targeted therapies if the tumour is of the appropriate molecular subtype (125). The gruelling treatment regimens, and significant off-site toxicity, associated with systemic chemotherapy is well documented, with co-administration of other medications required to offset these side-effects (97). Conflicting reports surrounding the efficacy of newer targeted therapies exists, and while they are generally regarded as improving the side-effect profile, their superiority over traditional chemotherapy has yet to be firmly established (110).

Several small scale clinical studies have established the feasibility and safety of IT administration to LC. Delivery of “gold-standard” chemotherapeutics using the ChemoGel technology will enable sustained local concentrations, with reduced

systemic exposure, thereby mitigating side-effects. Additionally, the anatomical location of LC means that locoregional delivery via IT administration is feasible, with current expertise in biopsy techniques suitable for adaption to ChemoGel delivery. Clinical application of the ChemoGel technology may be suited to early stage NSCLC patients, with non-metastatic lesions, who are not suitable candidates for surgery due to poor performance status or co-morbidities. Additionally, the ChemoGel technology may also be suitable for palliation of late stage NSCLC patients in the debulking of larger tumours to improve quality of life.

Throughout this thesis, careful consideration was given to the application of ChemoGel in the clinical setting. Increasing attention is directed at utilising advanced drug delivery platforms, such as DEB-TACE, in conjunction with image-guided technology in IO. Advanced imaging capability and minimally invasive device compatibility is critical to improve rates of translation to the clinic. Assessment of the impact of manufacturing processes on the formulation behaviour is also important to ensure that large scale production for human use is feasible.

Development and characterisation of the blank and dual drug-loaded thermoresponsive hydrogel was undertaken in *Chapter 2* of this thesis, which identified the lead blank and drug ChemoGel formulations. These formulations were selected for *in vitro* efficacy assessment in 2D and 3D models of NSCLC in *Chapter 3*. Screening of off-site toxicity was also conducted *in vitro* in a non-cancerous cell line to determine if ChemoGel had cancer-cell directed cytotoxicity. *Chapter 4* sought to build on the promising physicochemical and biological properties of the ChemoGel technology demonstrated in the previous two Chapters, by modifying the blank and drug-loaded formulations to produce radiopaque thermoresponsive hydrogels suitable for minimally invasive IO procedures. An appropriate storage and sterilisation method for the end product was also identified. This thesis culminated in the *in vivo* assessment of the lead blank and drug Visipaque® thermoresponsive formulations in *Chapter 5*, to further strengthen the pre-clinical evidence supporting the use of the ChemoGel technology as a chemoablative, drug delivery platform for LC applications.

This Chapter will summarise the key findings and conclusions drawn from the work detailed in this thesis, with due recognition given to outstanding research questions and future directions to be explored in the development of ChemoGel.

6.2 Chapter 2: Development and optimisation of a thermoresponsive hydrogel as a drug delivery platform

Chapter 2 detailed the thorough optimisation process undertaken to identify the optimal formulation for the blank and dual drug-loaded thermoresponsive hydrogel. This Chapter introduced the four key excipients used in ChemoGel, and their anticipated role in the physicochemical and biological characteristics of the final formulation. It is of note that three of the four excipients used are listed as GRAS by the FDA, indicating their compatibility with regulatory requirements for new medicinal products. The only non-GRAS excipient, GP, is commonly used in traditional Chinese medicine, and is coming to prominence in the western world, with small scale clinical trials for GP-containing products indicating preliminary safety in humans (313).

Cisplatin and paclitaxel were selected for inclusion in the ChemoGel formulation as they represent one of the current first line systemic treatment options in NSCLC (97, 125). From a physicochemical perspective, they offer the opportunity to evaluate the capacity of ChemoGel to simultaneously carry, and deliver, a hydrophilic and hydrophobic small molecule drug. Hydrophobic drug delivery is one of the major challenges facing the pharmaceutical industry, and there has been extensive research directed at improving solubility of these drugs. Clinically, integration of ChemoGel as a drug delivery platform into standard-of-care is proposed to be more achievable using a well-defined drug regimen, with safety and efficacy firmly established.

Results detailed in this Chapter defined the effect exerted by each excipient on the material properties of blank and drug ChemoGel. P407 was employed as the thermoresponsive base of ChemoGel, with concentration affecting the sol-gel transition temperature, as well the G' at 37°C. HP- β -CD was utilised as the paclitaxel-solubiliser, and modulator of sol-gel transition temperature of the final formulations. CS acted as the interpenetrating net, which facilitated GP-based crosslinking. Challenges achieving clinically relevant sol-gel transition temperatures in the single and dual drug-loaded formulations were surmounted by manipulation of the excipient concentration. Rheological characterisation of all formulations demonstrated the complexity of formulating multi-excipient thermoresponsive hydrogels.

Ploxamer-based hydrogels are noted for their physical instability when exposed to an aqueous medium (25). Therefore, disintegration testing was conducted to evaluate the robustness of the gelled hydrogel following exposure to PBS *in vitro*. The importance of GP in the formulation was confirmed at this point, as evidenced by the rapid disintegration of the non-crosslinked group, which occurred at a similar rate to P407 alone. This indicates that CS alone, acting as the interpenetrating net, is not sufficient to retard disintegration, and highlights the critical nature of both CS and the GP in the overall formulation. Complete disintegration of blank and drug ChemoGel had not occurred by Day 28 of exposure to PBS *in vitro*, indicating robustness of the formulations, as compared to P407 alone. The prolonged disintegration profile positions ChemoGel to act as a sustained release platform, and it was determined that release of chemotherapeutics from drug ChemoGel was feasible over a 10 day period *in vitro*. Taken together the *in vitro* disintegration and release profiles suggest that ChemoGel holds potential to circumvent the rapid clearance from the tumour site witnessed after IT administration of chemotherapeutic solutions.

6.3 Chapter 3: *In vitro* evaluation of ChemoGel formulations

Following assessment of the effects of the individual excipients on the material properties of the overall formulation in Chapter 2, the aim of Chapter 3 was to determine the *in vitro* cytotoxicity of ChemoGel. A 2D model of NSCLC using A549 cells was established to conduct an initial *in vitro* cytotoxicity screen on both formulations. Balb/c 3T3 clone A31 cells were employed as a non-cancerous cell line to evaluate cytotoxicity of ChemoGel in a 2D *in vitro* model of healthy cells. Evaluation of thermoresponsive hydrogels for drug delivery to solid tumours is almost exclusively conducted in 2D *in vitro* models, using either direct or indirect contact methods. As previously outlined, 2D *in vitro* models of cancer do not accurately represent the *in vivo* reality of the TME, due to their organised, monolayer growth patterns (274). Despite the lack of biorelevant conditions, 2D cytotoxicity testing provides a quick, simple, cheap, and standardised screen for potential anti-cancer candidates or drug delivery platforms. Throughout the 48 h study, both blank and drug ChemoGel had significantly reduced viability at all doses evaluated. Comparison with a chemotherapeutic solution of cisplatin/paclitaxel did not reveal any statistically significant difference between treatments. Drug ChemoGel was determined to induce more cell death in the late apoptotic stage/necrotic phase, however, 2D evaluation did not facilitate determination of

differences between treatments. Additionally, ISO *in vitro* cytotoxicity testing for medical devices is recommended to be carried out in 2D cell culture, using Balb/c 3T3 clone A31 (269). While it is acknowledged that murine cell lines are not wholly representative of the *in vivo* reality, they provide an opportunity for comparison with an extensive range of alternative drug delivery platforms, and satisfy regulatory requirements. Blank ChemoGel was determined to be non-toxic at low doses evaluated in the fibroblast cell line, but toxicity was evident at higher doses, indicating that cancer-cell directed cytotoxicity of ChemoGel may occur at lower doses.

The cytotoxicity tests contained in Chapter 3 sought to evaluate ChemoGel and drug ChemoGel at doses which could facilitate gelation, to better approximate the clinical scenario. As 2D *in vitro* cell culture is flat, however, the injection of both formulations into the culture saw gelation occur in a segmented fashion. 3D *in vitro* models of cancer have been developed in an effort to bridge the gap between the *in vitro* and *in vivo* environment of cancer (276). In particular, when dealing with advanced drug delivery platforms, the delivery of the drug is not the only factor that impacts on efficacy of the whole system; spread of the hydrogel within the tumour, subsequent interaction with tumour tissue following gelation, embolic actions, and drug delivery all act to bring about the overall treatment effect. While all these mechanisms may not be recapitulated in the *in vitro* environment, 3D models offer an opportunity to better approximate this multifaceted approach to treatment.

The 3D *in vitro* model developed in this thesis was specifically designed to accommodate a volume of thermoresponsive hydrogels via intra-scaffold injection to mimic the IT injection process. The subsequent gelation and retention of the thermoresponsive hydrogel within the scaffold further mimicked the post-administration behaviour in *in vivo* tumours. Validation of the model was undertaken to determine the differences in cellular behaviour between 2D and 3D *in vitro* cell culture, and the optimal seeding density for the 3D studies. Migration analysis determined that a 3D environment had, in fact, been established, as cells were no longer arranged in a monolayer, but were dispersed throughout the scaffold. Cytotoxicity evaluation of treatment was subsequently facilitated over a prolonged period of 14 days, which is a further improvement over 2D cell culture. The cytotoxic capacity of blank and drug ChemoGel in a NSCLC cell line *in vitro* over 14 days was confirmed.

The results contained in this Chapter provided convincing evidence to warrant further development of the ChemoGel technology in order to ensure that the formulation was fit for the intended clinical purpose in IO procedures.

6.4 Chapter 4: Translational reality of ChemoGel – assessment of relevant factors

It is well established that the volume of pre-clinical research directed towards the development of advanced drug delivery platforms does not match the level of clinical translation (6). Various reasons have been identified at all stages of the product development lifecycle to account for this, including inappropriate excipient selection or overly complex formulation processes, poor biorelevance of *in vitro* and pre-clinical *in vivo* models, and challenges associated with selecting relevant clinical trial endpoints in locoregional drug delivery (6, 187, 276). The research outlined in this thesis was directed at developing a clinically relevant thermoresponsive hydrogel for drug delivery to LC. Chapter 4, in particular, sought to identify weaknesses in the translational process, and address them at an early development stage.

Central to IO procedures is the use of imaging modalities to track the delivery of treatment, whether it be energy- or chemical- based ablation or embolisation (154). With a particular focus on integrating the ChemoGel technology into IO procedures, it was determined that a radiopaque formulation was required in order to facilitate intra-procedural imaging. To this end, a commercially available iodinated contrast agent, Visipaque®, was incorporated into the formulation, and the rheological characteristics were re-evaluated. At the highest concentration of Visipaque®, 30% w/w, the sol-gel transition temperature was found to be reduced to a clinically unsuitable temperature. All formulations were found to have increased radiopacity compared to the original ChemoGel formulation. Taken together, ChemoGel with 20% w/w Visipaque® was selected, as this formulation presented a similar rheological profile to the unlabelled ChemoGel, with a clinically suitable level of radiopacity on CT (338).

In order to evaluate the behaviour of blank Visipaque® ChemoGel post-administration, an *ex vivo* tissue model was employed to assess distribution and imaging characteristics. Both US and CT imaging were determined to be compatible for use in intra-procedural monitoring of Visipaque® ChemoGel administration.

Clearly defined imaging capability is of critical importance to accurately monitor delivery in real time. Repositioning of the needle, and recommencing administration, can facilitate adequate tumour coverage, all of which can be confirmed using image-guidance. Post-procedure, CT imaging of ChemoGel localisation in the tumour area would provide further confirmation of accurate delivery. Visipaque® ChemoGel demonstrated excellent resolution on both imaging modalities, which would not have been possible with unlabelled ChemoGel due to its inherent radiolucent properties.

Injection of ChemoGel formulations through a range of needles and catheters currently used in clinical practice was conducted. Increasing device length and gauge resulted in an increased force required for injection, and all devices were able to complete injection of the ChemoGel formulations. Injectability is critically important to ensure that the ChemoGel technology can be delivered in a minimally invasive manner, without the need for surgical intervention, thereby conferring reduced risk to the patient. Additionally, direct IT injection to lung tumours has been conducted under local anaesthetic and mild sedation, which offers considerable advantages in terms of patient safety, procedure duration and post-procedure hospital stay times (170). Together this reduces the overall cost of the procedure, resulting in more competitive reimbursement pricing of the product.

Confirmation that blank Visipaque® ChemoGel retained the chemoablative properties demonstrated in Chapter 3 was undertaken to ensure that the alteration to the formulation did not affect the *in vitro* efficacy. The 3D *in vitro* model of NSCLC was selected for this assessment to improve the biorelevance of testing, as outlined in Chapter 3. The transient increased cytotoxicity of blank Visipaque® ChemoGel may be attributed to the release of Visipaque® from the thermoresponsive hydrogel, as compared to blank ChemoGel. Otherwise the trend in cytotoxic profile was similar to that observed for blank and drug ChemoGel in Chapter 3, indicating that Visipaque® did not adversely affect the cytotoxic capacity of either thermoresponsive hydrogel.

Storage and transport of a refrigerated item is associated with increased cost and risk of compromising the integrity of the product. The challenges and costs associated with maintenance of an uninterrupted cold chain from manufacturing site to point of administration are well established (409). Additionally, a product requiring complete aseptic compounding by pharmacists at point of administration carries increased risk, and makes products less favourable, compared to “off-the-shelf”

products. Therefore, it was an objective of Chapter 4 to present the fully formulated hydrogel as a dry product, which could be rehydrated at point of administration. This would be comparative to the preparation process required for current commercially available products such as DC Bead. Freeze-drying of the ChemoGel formulation produced a wafer, which could be rehydrated to return it to its original thermoresponsive state.

Ensuring sterility of the final product is another hurdle facing translation of thermoresponsive hydrogels. Compendial sterility methods were assessed, with EtO sterilisation determined to be the most suitable. Following EtO sterilisation, the material properties of all ChemoGel formulations were maintained, as confirmed by rheological and disintegration testing. In fact, sterilisation of ChemoGel formulations prolonged their disintegration profiles *in vitro*. Drug release from the EtO sterilised formulations was also feasible, with release of chemotherapeutics observed *in vitro* for up to 10 days.

Taken together, the results presented in this Chapter reflect the in-depth consideration given to the translational reality of the ChemoGel technology. Efforts directed at improving clinical adoption and securing regulatory approval were undertaken early in the development process to attempt to mitigate against the high rate of attrition seen in the pharmaceutical industry.

6.5 Chapter 5: *In vivo* assessment of Visipaque® ChemoGel formulations in a murine xenograft model of Lung Cancer

Establishing safety and efficacy of a new drug delivery platform in a pre-clinical disease model is a pre-requisite of clinical studies. Although not an exact recapitulation of the human condition, murine models of cancer offer an opportunity to assess the drug delivery platform in a living animal. Xenograft heterotopic models of LC are most frequently used due to their relative ease of establishment and lower cost than orthotopic models (357). In particular, with respect to IT administration, the physical accessibility of a heterotopic tumour increases ease of administration. The aim of this Chapter was to assess three main endpoints following IT administration of blank and drug Visipaque® ChemoGel - retention, efficacy and off-site toxicity.

In vivo imaging was employed throughout this study to monitor both the thermoresponsive hydrogel and the tumour development in a minimally invasive

manner. In a clinical setting, this would be facilitated by US or CT imaging of the radiopaque formulations, however, these imaging modalities were not available in this pre-clinical setting. Therefore, a fluorescent probe was included in the formulation, and localisation and retention was subsequently monitored over the 14 day study. Co-localisation of the fluorescent signal from the IT administered blank and drug Visipaque® ChemoGel and the bioluminescent signal confirmed successful locoregional administration. Follow-up *in vivo* FLI revealed that the fluorescently labelled blank and drug Visipaque® ChemoGel was retained at the tumour site for the duration of the study, which was further confirmed by *ex vivo* FLI of excised tumours. The clinical significance of this is underlined when considering that one of the major limitations associated with IT administration of chemotherapeutic solutions is poor retention at the tumour site. Retention of ChemoGel enables more sustained exposure to its chemoablative bolus, with a concomitant release of chemotherapeutics over this time frame, as evidenced by data contained in Chapter 2 and 4.

Blank and drug Visipaque® ChemoGel statistically significantly reduced tumour volume increase at Day 14 post-IT administration, which confirmed previous *in vitro* assessments of efficacy in Chapter 4. BLI of tumours at Day 14 *in vivo* revealed a similar trend, although statistical significance between treatment groups was not established. The inherent efficacy of the ChemoGel technology presents as an attractive clinical treatment option, as this would reduce the concentration of chemotherapeutics required for administration. While no statistically significant difference was observed between the blank and drug Visipaque® ChemoGel groups in this study, longer studies or increased drug-loading may reveal the true potential of this drug-loaded chemoablative thermoresponsive hydrogel in the locoregional treatment of LC.

Assessment of the off-site toxicity of IT administration of blank and drug Visipaque® ChemoGel was the final endpoint to be assessed in this study. Feasibility of procedure and safety of treatment are often used as primary endpoints in Phase 1 clinical trials. A number of regulatory approvals are driven by achieving a similar efficacy rate, in tandem with an improved side-effect profile, compared to the current standard-of-care. In the case of ChemoGel, it was of significant importance to establish preliminary evidence of pre-clinical treatment safety due to the chemoablative nature of the blank treatment. Analysis of body weight and blood chemistries provided preliminary evidence to support the hypothesis that treatment

with blank or drug Visipaque® ChemoGel does not result in widespread off-site toxicity. The functional capacity of excretory organs is often compromised during chemotherapeutic treatment, but liver and kidney markers assessed in this study demonstrated no statistically significant difference in serum levels between treatment groups.

Taken together the results contained in this Chapter support the hypothesis that Visipaque® ChemoGel holds potential as a safe and effective dual drug-loaded chemoablative, thermoresponsive hydrogel for the treatment of LC in IO procedures.

6.6 Future work

The results contained in this thesis have provided sufficient evidence to support continued research into the ChemoGel technology.

Dose and administration schedule optimisation: Loading and release of a hydrophilic and hydrophobic chemotherapeutic drug as a proof of concept for the utility of ChemoGel as a dual drug-loaded thermoresponsive hydrogel was established in Chapter 2 and 4 of this thesis. To build on the preliminary efficacy data established in the *in vivo* study contained in Chapter 5, the following modifications could be implemented to further evaluate the efficacy of the ChemoGel technology:

- ◁ A higher concentration of chemotherapeutics could be evaluated in order to establish a difference in efficacy between blank and drug-loaded formulations
- ◁ Definition of an optimal administration schedule is required, with comparison of multiple IT injections over a period of time.
- ◁ *In vivo* pharmacokinetic studies would provide information on the release of chemotherapeutics from drug Visipaque® ChemoGel and the subsequent tumour and off-site distribution.
- ◁ A further *in vivo* study is underway to evaluate the effects of treatment over a longer timeframe to determine if time of treatment differentiates between blank and drug Visipaque® ChemoGel treatment

Following these optimisation studies, comparison with an IV and IT administered chemotherapeutic solution at the same dose would facilitate comparison of the ChemoGel technology to current “gold-standard” treatment options, and locoregional delivery without advanced drug delivery platforms respectively.

Characterisation of chemoablative effects of ChemoGel: Further *in vitro* studies could be conducted to identify the mechanism by which ChemoGel exerts its chemoablative function. Additional *in vivo* studies are planned to assess the contribution of HP- β -CD in the overall cytotoxicity of blank ChemoGel.

Assessment of *in vivo* biocompatibility following SC injection into non-tumour site: Blank and drug Visipaque® ChemoGel did not induce any off-site toxicity following IT injection, however, it would be prudent to conduct biocompatibility studies in healthy tissue. This is commonly conducted as a SC

injection in a non-disease rat model, with subsequent H & E analysis of excised tissue in contact with the injected hydrogel. This study would also determine if the chemoablative effects associated with ChemoGel treatment *in vivo* were cancer cell-directed.

Large animal studies: Following successful completion of the above additional pre-clinical studies, assessment of ChemoGel in a large animal model of cancer could be conducted. Canine models of spontaneously occurring cancer and genetically modified porcine cancer models have been used as large animal models of cancer (369, 410). This would allow for establishment of efficacy and safety in an animal of similar weight to humans to further strengthen the evidence supporting clinical use. Additionally, non-disease large animal models could be used to evaluate the feasibility of procedure, and biocompatibility with non-target tissue.

Alternative applications: Initial work has been conducted on the evaluation of ChemoGel in ovarian and pancreatic cell lines *in vitro*, with similar cytotoxicity profiles established. ChemoGel has also been loaded with doxorubicin, and gemcitabine and paclitaxel as a single and dual drug-loaded thermoresponsive hydrogel respectively, thereby further indicating its flexibility as a drug delivery platform technology. Further *in vitro* assessment of ChemoGel in a panel of cell lines could be conducted to identify an increased number of solid tumours amenable to ChemoGel treatment. Loading and assessment of new targeted therapies or immune-oncology drugs could also expand the functionality of the ChemoGel technology.

6.7 Overall conclusion

Collectively, the research presented in this thesis has demonstrated that a chemoablative, thermoresponsive hydrogel with the capacity to be dual drug-loaded was developed and characterised. *In vitro* and *in vivo* efficacy in NSCLC, in tandem with requisite characteristics for integration into clinical IO practice, was detailed. ChemoGel presents as an attractive candidate for further development as a clinically feasible method of minimally invasive, image-guided, locoregional drug delivery to solid tumours.

„Šťáňí®

° ťťíª ŸŸe-

Appendix 1. High-performance liquid chromatography determination of paclitaxel

Calibration curves were generated by HPLC analysis of paclitaxel (0.25 µg/ml – 12.5 µg/ml), as described in Section 2.2.3.1 (Fig. A.1).

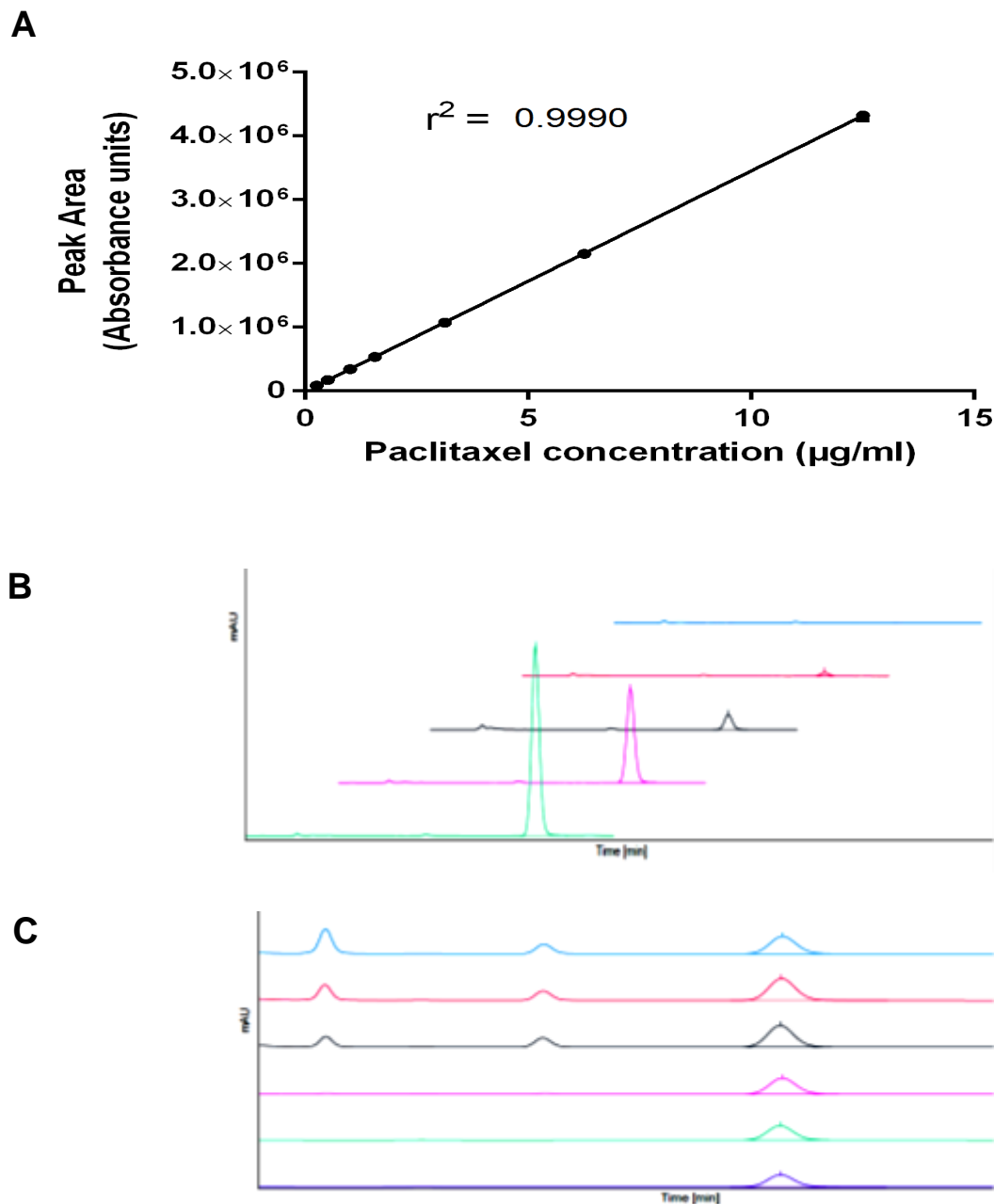


Figure A.1 (A) Paclitaxel calibration curve determined by high-performance liquid chromatography. Data shown is representative of the mean of three independent repeats \pm SEM ($n=3$). r^2 was determined using linear regression. **(B)** Representative peaks of calibration curve. Peaks displaced along x- and y- axis for better visualisation. Data shown from 12.5 µg/ml to 0 µg/ml of paclitaxel (left to right). **(C)** Representative HPLC peaks from release study at different time points. Peaks displaced along the y-axis for better visualisation. Data shown from 4 h to Day 7.

Appendix 2. Inductively coupled plasma mass spectrometry determination of platinum

Calibration curves were generated by ICP-MS analysis of platinum (1 – 4 ppm), as described in Section 2.2.3.2 (Fig. A.2).

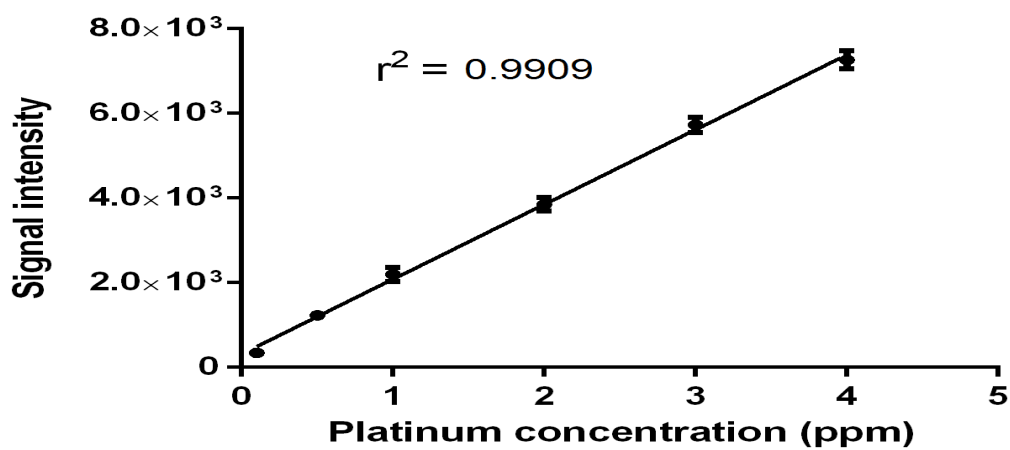


Figure A.2 (A) *Platinum calibration curve determined by inductively coupled plasma mass spectrometry. Data shown is representative of the mean of three independent repeats \pm SEM ($n=3$). r^2 was determined using linear regression.*

Appendix 3. Assessment of the effect of cisplatin-loading on thermoresponsive hydrogel

Individual components of the hydrogel were added to the formulation in a stepwise manner, with and without cisplatin at 0.02% w/w, initially excluding HP- β -CD (Table A.1). The thermoresponsivity of the hydrogel formulations was maintained following addition of cisplatin to P407 20% w/w alone and P407 20% w/w & CS 0.5% w/w (GF8 - 11). However, thermoresponsivity of GF13 was lost upon addition of GP at 0.3% w/w in the presence of cisplatin (Table A.1). Thermoresponsivity was restored to the cisplatin-loaded formulation following the reduction of the GP concentration to 0.1% w/w (GF15). GF15 had a reduced storage modulus at 37°C, of 6,377 Pa, compared to the same formulation without cisplatin (GF14). A reduction in the content of P407 to 17% w/w in the blank hydrogel (GF16) did not change the sol-gel transition temperature compared to the same formulation with higher P407 concentration (GF14). Addition of cisplatin to this formulation resulted in a reduction in thermoresponse by 1°C (GF17).

Table A.1 Formulation composition of preparations evaluated for thermoresponsivity. P407, Poloxamer 407; HP- β -CD, 2-Hydroxypropyl- β -Cyclodextrin; CS, Chitosan; GP, Genipin.

	Gel Formulation (GF)										
	8	9	10	11	12	13	14	15	16	17	
P407 (% w/w)	20	20	20	20	20	20	20	20	20	17	17
HP-β-CD (% w/w)	-	-	-	-	-	-	-	-	-	-	-
CS (% w/w)	-	-	0.5	0.5	0.5	0.5	0.5	0.5	0.5	0.5	0.5
GP (% w/w)	-	-	-	-	0.3	0.3	0.1	0.1	0.1	0.1	0.1
Cisplatin (% w/w)	-	0.02	-	0.02	-	0.02	-	0.02	-	0.02	0.02
Thermoresponse (°C)	22	23	23	23	23	<20	23	25	23	22	
G' @ 37°C (Pa)	19,847	16,510	14,020	15,020	15,480	17,550	14,340	6,377	16,160	17,190	

Appendix 4. Determination of the linear viscoelastic region of blank and drug ChemoGel

Oscillatory stress sweeps were performed to determine the LVR of the formulations at room and body temperature (Fig. A.3 A & B respectively). As previously discussed, the LVR is defined as the region in which the storage and loss modulus behave independent of the applied stress. This is important to establish to ensure that rheological tests conducted are not distorted due to deformation of sample as a result of stress applied. It also provides information on how the structure of the hydrogel performs over a range of oscillatory stresses applied (411). In all cases, the lead ChemoGel formulations did not demonstrate a phase transition over the range of stresses evaluated.

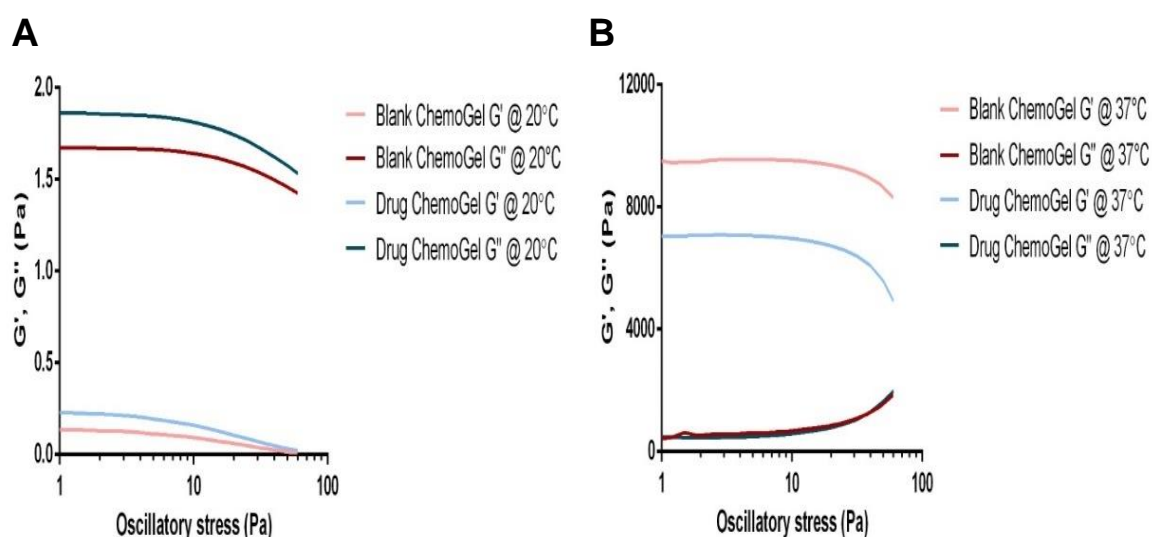


Figure A.3 Rheograms of oscillatory stress sweeps from 1 to 100 Pa at (A) 20°C (B) 37°C determined the linear viscoelastic region (LVR) of blank and drug ChemoGel. The LVR of blank and drug ChemoGel was determined to be over a range of oscillatory stresses up to 10 Pa, after which some deformation is observed to occur.

References

1. Hoffman AS. Hydrogels for biomedical applications. *Advanced drug delivery reviews*. 2002;54(1):3-12.
2. Hoare TR, Kohane DS. Hydrogels in drug delivery: Progress and challenges. *Polymer*. 2008;49(8):1993-2007.
3. Ahmed EM. Hydrogel: Preparation, characterization, and applications: A review. *Journal of Advanced Research*. 2015;6(2):105-21.
4. Caló E, Khutoryanskiy VV. Biomedical applications of hydrogels: A review of patents and commercial products. *European Polymer Journal*. 2015;65:252-67.
5. Peppas NA, Bures P, Leobandung W, Ichikawa H. Hydrogels in pharmaceutical formulations. *European Journal of Pharmaceutics and Biopharmaceutics*. 2000;50(1):27-46.
6. Lee SC, Kwon IK, Park K. Hydrogels for delivery of bioactive agents: A historical perspective. *Advanced drug delivery reviews*. 2013;65(1):17-20.
7. Buwalda SJ, Boere KWM, Dijkstra PJ, Feijen J, Vermonden T, Hennink WE. Hydrogels in a historical perspective: From simple networks to smart materials. *Journal of Controlled Release*. 2014;190:254-73.
8. Wolinsky JB, Colson YL, Grinstaff MW. Local Drug Delivery Strategies for Cancer Treatment: Gels, Nanoparticles, Polymeric Films, Rods, and Wafers. *Journal of controlled release : official journal of the Controlled Release Society*. 2012;159(1):10.1016/j.jconrel.2011.11.031.
9. Soppimath KS, Aminabhavi TM, Dave AM, Kumbar SG, Rudzinski WE. Stimulus-Responsive "Smart" Hydrogels as Novel Drug Delivery Systems. *Drug Development and Industrial Pharmacy*. 2002;28(8):957-74.
10. Thakral S, Thakral NK, Majumdar DK. Eudragit: a technology evaluation. *Expert opinion on drug delivery*. 2013;10(1):131-49.
11. Hibbins A, Kumar P, Choonara Y, Kondiah P, Marimuthu T, du Toit L, Pillay V. Design of a Versatile pH-Responsive Hydrogel for Potential Oral Delivery of Gastric-Sensitive Bioactives. *Polymers*. 2017;9(10):474.
12. Lubrizol. Carbopol® Polymer Products n.d. [cited 2017 13 February]. Available from: <https://www.lubrizol.com/en/Life-Sciences/Products/Carbopol-Polymer-Products>.
13. Kumar S, Himmelstein KJ. Modification of in situ gelling behavior of carbopol solutions by hydroxypropyl methylcellulose. *Journal of pharmaceutical sciences*. 1995;84(3):344-8.
14. Hoffman AS. Stimuli-responsive polymers: Biomedical applications and challenges for clinical translation. *Advanced drug delivery reviews*. 2013;65(1):10-6.
15. Zhao L, Zhu L, Liu F, Liu C, Shan D, Wang Q, Zhang C, Li J, Liu J, Qu X, Yang Z. pH triggered injectable amphiphilic hydrogel containing doxorubicin and paclitaxel. *International journal of pharmaceutics*. 2011;410(1-2):83-91.
16. Li Y, Huang G, Zhang X, Li B, Chen Y, Lu T, Lu TJ, Xu F. Magnetic Hydrogels and Their Potential Biomedical Applications. *Advanced Functional Materials*. 2013;23(6):660-72.
17. Zhang J, Huang Q, Du J. Recent advances in magnetic hydrogels. *Polymer International*. 2016;65(12):1365-72.
18. Jalili NA, Muscarello M, Gaharwar AK. Nanoengineered thermoresponsive magnetic hydrogels for biomedical applications. *Bioengineering & Translational Medicine*. 2016;1(3):297-305.
19. Häring M, Schiller J, Mayr J, Grijalvo S, Eritja R, Díaz DD. Magnetic gel composites for hyperthermia cancer therapy. *Gels*. 2015;1(2):135-61.
20. Peppas NA, Bures CD. Glucose-Responsive Hydrogels. 2006.

21. Volkan Y, J. WM, A. AE, Colin G, Robert L, G. AD. Injectable Self Healing Glucose Responsive Hydrogels with pH Regulated Mechanical Properties. *Advanced Materials*. 2016;28(1):86-91.
22. Ward MA, Georgiou TK. Thermoresponsive Polymers for Biomedical Applications. *Polymers*. 2011;3(4):1215-42.
23. Sood N, Bhardwaj A, Mehta S, Mehta A. Stimuli-responsive hydrogels in drug delivery and tissue engineering. *Drug delivery*. 2014:1-23.
24. Li Z, Guan J. Thermosensitive hydrogels for drug delivery. *Expert opinion on drug delivery*. 2011;8(8):991-1007.
25. Klouda L, Mikos AG. Thermoresponsive hydrogels in biomedical applications - a review. *European journal of pharmaceutics and biopharmaceutics : official journal of Arbeitsgemeinschaft fur Pharmazeutische Verfahrenstechnik eV*. 2008;68(1):34-45.
26. Klouda L. Thermoresponsive hydrogels in biomedical applications: A seven-year update. *European Journal of Pharmaceutics and Biopharmaceutics*. 2015;97:338-49.
27. Volkmer E, Leicht U, Moritz M, Schwarz C, Wiese H, Milz S, Matthias P, Schloegl W, Friess W, Goettlinger M, Augat P, Schieker M. Poloxamer-based hydrogels hardening at body core temperature as carriers for cell based therapies: in vitro and in vivo analysis. *Journal of materials science Materials in medicine*. 2013;24(9):2223-34.
28. Shin SC, Cho CW. Physicochemical characterizations of piroxicam-poloxamer solid dispersion. *Pharmaceutical development and technology*. 1997;2(4):403-7.
29. Gratieri T, Gelfuso GM, Rocha EM, Sarmiento VH, de Freitas O, Lopez RF. A poloxamer/chitosan in situ forming gel with prolonged retention time for ocular delivery. *Eur J Pharm Biopharm*. 2010;75(2):186-93.
30. Ricci EJ, Bentley MVLB, Farah M, Bretas RES, Marchetti JM. Rheological characterization of Poloxamer 407 lidocaine hydrochloride gels. *European Journal of Pharmaceutical Sciences*. 2002;17(3):161-7.
31. Cabana A, Ait-Kadi A, Juhasz J. Study of the Gelation Process of Polyethylene Oxidea -Polypropylene Oxideb -Polyethylene Oxidea Copolymer (Poloxamer 407) Aqueous Solutions. *Journal of colloid and interface science*. 1997;190(2):307-12.
32. Dumortier G, Grossiord JL, Agnely F, Chaumeil JC. A Review of Poloxamer 407 Pharmaceutical and Pharmacological Characteristics. *Pharmaceutical Research*. 2006;23(12):2709-28.
33. Schmolka IR. Artificial skin. I. Preparation and properties of pluronic F-127 gels for treatment of burns. *J Biomed Mater Res*. 1972;6(6):571-82.
34. Seuring J, Bayer FM, Huber K, Agarwal S. Upper Critical Solution Temperature of Poly(N-acryloyl glycinamide) in Water: A Concealed Property. *Macromolecules*. 2012;45(1):374-84.
35. Schmaljohann D. Thermo- and pH-responsive polymers in drug delivery. *Advanced drug delivery reviews*. 2006;58(15):1655-70.
36. Barnes HA, Hutton JF, Walters K. Chapter 1 - Introduction. In: Barnes HA, Hutton JF, Walters K, editors. *Rheology Series*. 3: Elsevier; 1989. p. 1-10.
37. Franck A, Germany TI. Viscoelasticity and dynamic mechanical testing.
38. Roylance D. *Engineering Viscoelasticity* 2001.
39. Mezger TG. *The rheology handbook: for users of rotational and oscillatory rheometers*: Vincentz Network GmbH & Co KG; 2006.
40. Matanović MR, Kristl J, Grabnar PA. Thermoresponsive polymers: Insights into decisive hydrogel characteristics, mechanisms of gelation, and promising biomedical applications. *International journal of pharmaceutics*. 2014;472(1):262-75.

41. Quattrone A, Czajka A, Sibilla S. Thermosensitive Hydrogel Mask Significantly Improves Skin Moisture and Skin Tone; Bilateral Clinical Trial. *Cosmetics*. 2017;4(2):17.
42. Cheng Y-H, Tsai T-H, Jhan Y-Y, Chiu AW-h, Tsai K-L, Chien C-S, Chiou S-H, Liu CJ-I. Thermosensitive chitosan-based hydrogel as a topical ocular drug delivery system of latanoprost for glaucoma treatment. *Carbohydrate Polymers*. 2016;144:390-9.
43. Nazar H, Fatouros DG, van der Merwe SM, Bouropoulos N, Avgouropoulos G, Tsibouklis J, Roldo M. Thermosensitive hydrogels for nasal drug delivery: the formulation and characterisation of systems based on N-trimethyl chitosan chloride. *European journal of pharmaceutics and biopharmaceutics : official journal of Arbeitsgemeinschaft fur Pharmazeutische Verfahrenstechnik eV*. 2011;77(2):225-32.
44. Taurin S, Almomen AA, Pollak T, Kim SJ, Maxwell J, Peterson CM, Owen SC, Janát-Amsbury MM. Thermosensitive hydrogels a versatile concept adapted to vaginal drug delivery. *Journal of Drug Targeting*. 2018;26(7):533-50.
45. Supper S, Anton N, Seidel N, Riemenschnitter M, Curdy C, Vandamme T. Thermosensitive chitosan/glycerophosphate-based hydrogel and its derivatives in pharmaceutical and biomedical applications. *Expert opinion on drug delivery*. 2014;11(2):249-67.
46. Zhang K, Shi X, Lin X, Yao C, Shen L, Feng Y. Poloxamer-based in situ hydrogels for controlled delivery of hydrophilic macromolecules after intramuscular injection in rats. *Drug delivery*. 2015;22(3):375-82.
47. Ruel-Gariépy E, Leroux J-C. In situ-forming hydrogels—review of temperature-sensitive systems. *European Journal of Pharmaceutics and Biopharmaceutics*. 2004;58(2):409-26.
48. Hastings CL, Kelly HM, Murphy MJ, Barry FP, O'Brien FJ, Duffy GP. Development of a thermoresponsive chitosan gel combined with human mesenchymal stem cells and desferrioxamine as a multimodal pro-angiogenic therapeutic for the treatment of critical limb ischaemia. *Journal of Controlled Release*. 2012;161(1):73-80.
49. Jeong B, Kim SW, Bae YH. Thermosensitive sol–gel reversible hydrogels. *Advanced drug delivery reviews*. 2002;54(1):37-51.
50. Bajpai AK, Shukla SK, Bhanu S, Kankane S. Responsive polymers in controlled drug delivery. *Progress in Polymer Science*. 2008;33(11):1088-118.
51. Lin C-C, Metters AT. Hydrogels in controlled release formulations: Network design and mathematical modeling. *Advanced drug delivery reviews*. 2006;58(12):1379-408.
52. Xu S, Wang W, Li X, Liu J, Dong A, Deng L. Sustained release of PTX-incorporated nanoparticles synergized by burst release of DOX HCl from thermosensitive modified PEG/PCL hydrogel to improve anti-tumor efficiency. *European Journal of Pharmaceutical Sciences*. 2014;62(Supplement C):267-73.
53. Larsen C, Larsen SW, Jensen H, Yaghmur A, Ostergaard J. Role of in vitro release models in formulation development and quality control of parenteral depots. *Expert opinion on drug delivery*. 2009;6(12):1283-95.
54. United States Food and Drug Administration. FDA ODAC Briefing Document for NDA 21-236. IntraDose® (cisplatin/epinephrine) Injectable Gel for Recurrent Squamous Cell Carcinoma of the Head and Neck. 2001.
55. DeWitt JM, Murthy SK, Ardhanari R, DuVall GA, Wallner G, Litka P, Daugherty C, Fowers K. EUS-guided paclitaxel injection as an adjunctive therapy to systemic chemotherapy and concurrent external beam radiation before surgery for localized or locoregional esophageal cancer: a multicenter prospective randomized trial. *Gastrointestinal Endoscopy*. 2016.

56. Jonsson Comprehensive Cancer Center. Compassionate Use of MitoGel in Upper Tract Urothelial Carcinoma (NCT02701023) Bethesda (MD): National Library of Medicine (US). 2000-2016 [Available from: <https://clinicaltrials.gov/ct2/show/NCT02701023>].
57. Celikoglu F, Celikoglu SI, Goldberg EP. Techniques for intratumoral chemotherapy of lung cancer by bronchoscopic drug delivery. *Cancer Ther.* 2008;6:545-52.
58. Ma H, He C, Cheng Y, Li D, Gong Y, Liu J, Tian H, Chen X. PLK1shRNA and doxorubicin co-loaded thermosensitive PLGA-PEG-PLGA hydrogels for osteosarcoma treatment. *Biomaterials.* 2014;35(30):8723-34.
59. Chen YY, Wu HC, Sun JS, Dong GC, Wang TW. Injectable and thermoresponsive self-assembled nanocomposite hydrogel for long-term anticancer drug delivery. *Langmuir : the ACS journal of surfaces and colloids.* 2013;29(11):3721-9.
60. Wu Z, Zou X, Yang L, Lin S, Fan J, Yang B, Sun X, Wan Q, Chen Y, Fu S. Thermosensitive hydrogel used in dual drug delivery system with paclitaxel-loaded micelles for in situ treatment of lung cancer. *Colloids and surfaces B, Biointerfaces.* 2014;122:90-8.
61. Donin NM, Duarte S, Lenis AT, Caliliw R, Torres C, Smithson A, Strauss-Ayali D, Agmon-Gerstein Y, Malchi N, Said J, Raman SS, Holden S, Pantuck A, Beldegrun AS, Chamie K. Sustained-release Formulation of Mitomycin C to the Upper Urinary Tract Using a Thermosensitive Polymer: A Preclinical Study. *Urology.* 2017;99:270-7.
62. Vogl TJ, Engelmann K, Mack MG, Straub R, Zangos S, Eichler K, Hochmuth K, Orenberg E. CT-guided intratumoural administration of cisplatin/epinephrine gel for treatment of malignant liver tumours. *British Journal of Cancer.* 2002;86(4):524-9.
63. Tyler BF, Kirk D.; Li, Khan W.; Renard Recinos, Violette; Caplan, Justin M.; Hdeib, Alia; Grossman, Rachel; Basaldella, Luca; Bekelis, Kimon; Pradilla, Gustavo; Legnani, Federico; Brem, Henry. A thermal gel depot for local delivery of paclitaxel to treat experimental brain tumors in rats. *Journal of Neurosurgery.* 2010;113(2):210-7.
64. Rahib L, Smith BD, Aizenberg R, Rosenzweig AB, Fleshman JM, Matrisian LM. Projecting Cancer Incidence and Deaths to 2030: The Unexpected Burden of Thyroid, Liver, and Pancreas Cancers in the United States. *Cancer Research.* 2014;74(11):2913-21.
65. Waschke JP, Friedrich. Sobotta - Atlas of Human Anatomy. Internal Organs. Elsevier UF, editor2013.
66. Weibel ER. Principles and methods for the morphometric study of the lung and other organs. *Laboratory investigation; a journal of technical methods and pathology.* 1963;12:131-55.
67. Hsia CC, Hyde DM, Weibel ER. Lung Structure and the Intrinsic Challenges of Gas Exchange. *Comprehensive Physiology.* 2016;6(2):827-95.
68. de Sousa VML, Carvalho L. Heterogeneity in Lung Cancer. *Pathobiology.* 2018;85(1-2):96-107.
69. Trédan O, Galmarini CM, Patel K, Tannock IF. Drug Resistance and the Solid Tumor Microenvironment. *Journal of the National Cancer Institute.* 2007;99(19):1441-54.
70. Joyce JA, Pollard JW. Microenvironmental regulation of metastasis. *Nat Rev Cancer.* 2009;9(4):239-52.
71. Wood SL, Pernemalm M, Crosbie PA, Whetton AD. The role of the tumor-microenvironment in lung cancer-metastasis and its relationship to potential therapeutic targets. *Cancer treatment reviews.* 2014;40(4):558-66.

72. Graves EE, Maity A, Le Q-T. The Tumor Microenvironment in Non-Small-Cell Lung Cancer. *Seminars in Radiation Oncology*. 2010;20(3):156-63.
73. Pugh CW, Ratcliffe PJ. Regulation of angiogenesis by hypoxia: role of the HIF system. *Nat Med*. 2003;9(6):677-84.
74. Popper HH. Progression and metastasis of lung cancer. *Cancer Metastasis Reviews*. 2016;35:75-91.
75. Fais S, Venturi G, Gatenby B. Microenvironmental acidosis in carcinogenesis and metastases: new strategies in prevention and therapy. *Cancer Metastasis Reviews*. 2014;33(4):1095-108.
76. Ferlay J, Islami M, Ervik M, Dikshit R, Eser S, Mathers C, Rebelo M, Parkin DM, Forman D, Bray F. GLOBOCAN 2012 v1.0, Cancer Incidence and Mortality Worldwide: IARC CancerBase No. 11 Lyon, France: International Agency for Research on Cancer; 2013.; 2012 [cited 2017 12 March]. Available from: <http://globocan.iarc.fr>.
77. Allemani C, Matsuda T, Di Carlo V, Harewood R, Matz M, Nikšić M, Bonaventure A, Valkov M, Johnson CJ, Estève J, Ogunbiyi OJ, Azevedo e Silva G, Chen W-Q, Eser S, Engholm G, et al. Global surveillance of trends in cancer survival 2000 - 14 (CONCORD-3): analysis of individual records for 37 513 025 patients diagnosed with one of 18 cancers from 322 population-based registries in 71 countries. *The Lancet*. 2018;391(10125):1023-75.
78. Jemal A, Bray F, Center MM, Ferlay J, Ward E, Forman D. Global cancer statistics. *CA: a cancer journal for clinicians*. 2011;61(2):69-90.
79. Islami F, Torre LA, Jemal A. Global trends of lung cancer mortality and smoking prevalence. *Translational Lung Cancer Research*. 2015;4(4):327-38.
80. Lortet-Tieulent J, Soerjomataram I, Ferlay J, Rutherford M, Weiderpass E, Bray F. International trends in lung cancer incidence by histological subtype: Adenocarcinoma stabilizing in men but still increasing in women. *Lung cancer*. 2014;84(1):13-22.
81. Baldwin DRP, Sanjay. Non-Small Cell Cancer 2017 [cited 2018 22 April]. Available from: <http://bestpractice.bmj.com/topics/en-gb/1082>.
82. de Groot P, Munden RF. Lung Cancer Epidemiology, Risk Factors, and Prevention. *Radiologic Clinics of North America*. 2012;50(5):863-76.
83. Siegel RL, Miller KD, Jemal A. Cancer statistics, 2017. *CA: a cancer journal for clinicians*. 2017;67(1):7-30.
84. Crinò L, Weder W, van Meerbeeck J, Felip E, Group ObotEGW. Early stage and locally advanced (non-metastatic) non-small-cell lung cancer: ESMO Clinical Practice Guidelines for diagnosis, treatment and follow-up. *Annals of Oncology*. 2010;21(suppl 5):v103-v15.
85. Detterbeck FC, Mazzone PJ, Naidich DP, Bach PB. Screening for Lung Cancer: Diagnosis and Management of Lung Cancer, 3rd ed: American College of Chest Physicians Evidence-Based Clinical Practice Guidelines. *Chest*. 2013;143(5 Suppl):e78S-e92S.
86. Rivera MP, Mehta AC, Wahidi MM. Establishing the diagnosis of lung cancer: Diagnosis and management of lung cancer, 3rd ed: american college of chest physicians evidence-based clinical practice guidelines. *Chest*. 2013;143(5_suppl):e142S-e65S.
87. Lemjabbar-Alaoui H, Hassan OUI, Yang Y-W, Buchanan P. Lung cancer: Biology and treatment options. *Biochimica et Biophysica Acta (BBA) - Reviews on Cancer*. 2015;1856(2):189-210.
88. Andrews T, Wallace W. Pathology of lung tumours. *Surgery (Oxford)*. 2011;29(5):204-11.
89. McMullan DM, Wood DE. Pulmonary carcinoid tumors. *Seminars in Thoracic and Cardiovascular Surgery*. 2003;15(3):289-300.

90. Cogen A, Dockx Y, Cheung KJ, Meulemans E, Lauwers P, Nia PS, Hendriks JM, Van Schil PE. TNM-classification for lung cancer: from the 7th to the 8th edition. *Acta chirurgica Belgica*. 2011;111(6):389-92.
91. Detterbeck FC, Boffa DJ, Kim AW, Tanoue LT. The Eighth Edition Lung Cancer Stage Classification. *Chest*.151(1):193-203.
92. Shim HS, Choi Y-L, Kim L, Chang S, Kim W-S, Roh MS, Kim T-J, Ha SY, Chung J-H, Jang SJ, Lee GK, The Korean Cardiopulmonary Pathology Study G, The Korean Molecular Pathology Study G. Molecular Testing of Lung Cancers. *Journal of Pathology and Translational Medicine*. 2017;51(3):242-54.
93. Sundar R, Chénard-Poirier M, Collins DC, Yap TA. Imprecision in the Era of Precision Medicine in Non-Small Cell Lung Cancer. *Frontiers in Medicine*. 2017;4(39).
94. Tsao AS, Scagliotti GV, Bunn PA, Jr., Carbone DP, Warren GW, Bai C, de Koning HJ, Yousaf-Khan AU, McWilliams A, Tsao MS, Adusumilli PS, Rami-Porta R, Asamura H, Van Schil PE, Darling GE, et al. Scientific Advances in Lung Cancer 2015. *Journal of Thoracic Oncology*.11(5):613-38.
95. DeVita VT, Chu E. A History of Cancer Chemotherapy. *Cancer Research*. 2008;68(21):8643-53.
96. Siddik ZH. Cisplatin: mode of cytotoxic action and molecular basis of resistance. *Oncogene*. 2003;22(47):7265-79.
97. Joint Formulary Committee. *British National Formulary (online) 75th ed.* London: BMJ Group and Pharmaceutical Press; 2018.
98. Dasari S, Tchounwou PB. Cisplatin in cancer therapy: molecular mechanisms of action. *European journal of pharmacology*. 2014;0:364-78.
99. Zhang D, Yang R, Wang S, Dong Z. Paclitaxel: new uses for an old drug. *Drug design, development and therapy*. 2014;8:279-84.
100. Gelderblom H, Verweij J, Nooter K, Sparreboom A. Cremophor EL: the drawbacks and advantages of vehicle selection for drug formulation. *European journal of cancer (Oxford, England : 1990)*. 2001;37(13):1590-8.
101. Yuan Dm, Lv Yl, Yao Yw, Miao Xh, Wang Q, Xiao Xw, Yin J, Shi Y, Shi Mq, Zhang Xw, Song Y. Efficacy and safety of Abraxane in treatment of progressive and recurrent non small cell lung cancer patients: A retrospective clinical study. *Thoracic Cancer*. 2012;3(4):341-7.
102. Horwitz SB. Taxol (paclitaxel): mechanisms of action. *Annals of oncology : official journal of the European Society for Medical Oncology / ESMO*. 1994;5 Suppl 6:S3-6.
103. Del Rivero J, Enewold L, Thomas A. Metastatic lung cancer in the age of targeted therapy: improving long-term survival. *Translational Lung Cancer Research*. 2016;5(6):727-30.
104. Patel JN, Ersek JL, Kim ES. Lung cancer biomarkers, targeted therapies and clinical assays. *Translational Lung Cancer Research*. 2015;4(5):503-14.
105. Baumgart M, Pandya K. The use of biomarkers in the treatment of non-small cell lung cancer. *Expert Review of Precision Medicine and Drug Development*. 2016;1(1):25-36.
106. Greenhalgh J, Dwan K, Boland A, Bates V, Vecchio F, Dundar Y, Jain P, Green JA. First-line treatment of advanced epidermal growth factor receptor (EGFR) mutation positive non-squamous non-small cell lung cancer. *Cochrane Database of Systematic Reviews*. 2016(5).
107. Camidge DR, Doebele RC. Treating ALK-positive lung cancer—early successes and future challenges. *Nature Reviews Clinical Oncology*. 2012;9:268.
108. Mahoney KM, Freeman GJ, McDermott DF. The Next Immune-Checkpoint Inhibitors: PD-1/PD-L1 Blockade in Melanoma. *Clinical Therapeutics*. 2015;37(4):764-82.

109. Creelan BC. Update on immune checkpoint inhibitors in lung cancer. *Cancer control : journal of the Moffitt Cancer Center*. 2014;21(1):80-9.
110. Remon J, Besse B, Soria J-C. Successes and failures: what did we learn from recent first-line treatment immunotherapy trials in non-small cell lung cancer? *BMC Medicine*. 2017;15(1):55.
111. Hellmann MD, Ciuleanu T-E, Pluzanski A, Lee JS, Otterson GA, Audigier-Valette C, Minenza E, Linardou H, Burgers S, Salman P, Borghaei H, Ramalingam SS, Brahmer J, Reck M, O'Byrne KJ, et al. Nivolumab plus Ipilimumab in Lung Cancer with a High Tumor Mutational Burden. *New England Journal of Medicine*. 2018;378(22):2093-104.
112. Kaufman J, Stinchcombe TE. Treatment of kras-mutant non-small cell lung cancer: The end of the beginning for targeted therapies. *JAMA*. 2017;317(18):1835-7.
113. Yu HA, Riely GJ. Second Generation Epidermal Growth Factor Receptor Tyrosine Kinase Inhibitors In Lung Cancers. *Journal of the National Comprehensive Cancer Network : JNCCN*. 2013;11(2):161-9.
114. Bollinger MK, Agnew AS, Mascara GP. Osimertinib: A third-generation tyrosine kinase inhibitor for treatment of epidermal growth factor receptor-mutated non-small cell lung cancer with the acquired Thr790Met mutation. *Journal of oncology pharmacy practice : official publication of the International Society of Oncology Pharmacy Practitioners*. 2017;1078155217712401.
115. Liao BC, Lin CC, Lee JH, Yang JC. Optimal management of EGFR-mutant non-small cell lung cancer with disease progression on first-line tyrosine kinase inhibitor therapy. *Lung cancer*. 2017;110:7-13.
116. Tan C-S, Kumarakulasinghe NB, Huang Y-Q, Ang YLE, Choo JR-E, Goh B-C, Soo RA. Third generation EGFR TKIs: current data and future directions. *Molecular Cancer*. 2018;17:29.
117. Thai AA, Solomon BJ. Treatment of ALK-positive nonsmall cell lung cancer: recent advances. *Current Opinion in Oncology*. 2018;30(2):84-91.
118. Mok TSK, Crino L, Felip E, Salgia R, De Pas T, Tan DSW, Chow LQM. The accelerated path of ceritinib: Translating pre-clinical development into clinical efficacy. *Cancer treatment reviews*. 2017;55:181-9.
119. Sgambato A, Casaluca F, Maione P, Gridelli C. Targeted therapies in non-small cell lung cancer: a focus on ALK/ROS1 tyrosine kinase inhibitors. *Expert Review of Anticancer Therapy*. 2018;18(1):71-80.
120. Kazandjian D, Suzman DL, Blumenthal G, Mushti S, He K, Libeg M, Keegan P, Pazdur R. FDA Approval Summary: Nivolumab for the Treatment of Metastatic Non-Small Cell Lung Cancer With Progression On or After Platinum-Based Chemotherapy. *The Oncologist*. 2016;21(5):634-42.
121. Peters S, Kerr KM, Stahel R. PD-1 blockade in advanced NSCLC: A focus on pembrolizumab. *Cancer treatment reviews*. 2018;62:39-49.
122. Weinstock C, Khozin S, Suzman D, Zhang L, Tang S, Wahby S, Goldberg KB, Kim G, Pazdur R. U.S. Food and Drug Administration Approval Summary: Atezolizumab for Metastatic Non-Small Cell Lung Cancer. *Clinical cancer research : an official journal of the American Association for Cancer Research*. 2017;23(16):4534-9.
123. Antonia SJ, Villegas A, Daniel D, Vicente D, Murakami S, Hui R, Yokoi T, Chiappori A, Lee KH, de Wit M, Cho BC, Bourhaba M, Quantin X, Tokito T, Mekhail T, et al. Durvalumab after Chemoradiotherapy in Stage III Non-Small-Cell Lung Cancer. *New England Journal of Medicine*. 2017;377(20):1919-29.
124. Melosky B. Current Treatment Algorithms for Patients with Metastatic Non-Small Cell, Non-Squamous Lung Cancer. *Frontiers in oncology*. 2017;7:38.
125. National Institute for Health and Care Excellence. Lung cancer: The diagnosis and treatment of lung cancer. : National Institute for Health and Care

- Excellence; 2011 [cited 2015 03 December]. Available from: <https://www.nice.org.uk/guidance/cg121/chapter/1-guidance#treatment>
126. Luengo-Fernandez R, Leal J, Gray A, Sullivan R. Economic burden of cancer across the European Union: a population-based cost analysis. *The Lancet Oncology*. 2013;14(12):1165-74.
 127. Kantarjian HM, Fojo T, Mathisen M, Zwelling LA. Cancer Drugs in the United States: Justum Pretium—The Just Price. *Journal of Clinical Oncology*. 2013;31(28):3600-4.
 128. Carelle N, Piotto E, Bellanger A, Germanaud J, Thuillier A, Khayat D. Changing patient perceptions of the side effects of cancer chemotherapy. *Cancer*. 2002;95(1):155-63.
 129. Ramazani F, van Nostrum CF, Storm G, Kiessling F, Lammers T, Hennink WE, Kok RJ. Locoregional cancer therapy using polymer-based drug depots. *Drug Discovery Today*. 2016;21(4):640-7.
 130. van den Bosch MA, Prevoe W, van der Linden EM, Meijerink MR, van Delden OM, Mali WP, Reekers JA. [The radiologist as the treating physician for cancer: interventional oncology]. *Nederlands tijdschrift voor geneeskunde*. 2009;153:A532.
 131. Solomon SB, Silverman SG. Imaging in interventional oncology. *Radiology*. 2010;257(3):624-40.
 132. Duka E, Ierardi AM, Floridi C, Terrana A, Fontana F, Carrafiello G. The Role of Interventional Oncology in the Management of Lung Cancer. *Cardiovascular and interventional radiology*. 2017;40(2):153-65.
 133. Dempsey PJ, Ridge CA, Solomon SB. Advances in Interventional Oncology: Lung Cancer. *Cancer J*. 2016;22(6):393-400.
 134. Lencioni R, Cioni D, Crocetti L, Bartolozzi C. Percutaneous ablation of hepatocellular carcinoma: State-of-the-art. *Liver Transplantation*. 2004;10(S2):S91-S7.
 135. Shiina S. Image-guided percutaneous ablation therapies for hepatocellular carcinoma. *Journal of gastroenterology*. 2009;44 Suppl 19:122-31.
 136. Ahmed M, Solbiati L, Brace CL, Breen DJ, Callstrom MR, Charboneau JW, Chen M-H, Choi BI, de Baère T, Dodd GD, Dupuy DE, Gervais DA, Gianfelice D, Gillams AR, Lee FT, et al. Image-guided Tumor Ablation: Standardization of Terminology and Reporting Criteria—A 10-Year Update. *Radiology*. 2014;273(1):241-60.
 137. de Baere T, Tselikas L, Pearson E, Yevitch S, Boige V, Malka D, Ducreux M, Goere D, Elias D, Nguyen F, Deschamps F. Interventional oncology for liver and lung metastases from colorectal cancer: The current state of the art. *Diagnostic and Interventional Imaging*. 2015;96(6):647-54.
 138. Chow DS, Itagaki MW. Interventional Oncology Research in the United States: Slowing Growth, Limited Focus, and a Low Level of Funding. *Radiology*. 2010;257(2):410-7.
 139. Fernando HC. Radiofrequency Ablation to Treat Non-Small Cell Lung Cancer and Pulmonary Metastases. *The Annals of Thoracic Surgery*. 2008;85(2):S780-S4.
 140. Jones GC, Kehrer JD, Kahn J, Koneru BN, Narayan R, Thomas TO, Camphausen K, Mehta MP, Kaushal A. Primary Treatment Options for High-Risk/Medically Inoperable Early Stage NSCLC Patients. *Clinical Lung Cancer*. 2015;16(6):413-30.
 141. Brace CL. Radiofrequency and microwave ablation of the liver, lung, kidney, and bone: what are the differences? *Current problems in diagnostic radiology*. 2009;38(3):135-43.
 142. Lencioni R, Crocetti L, Cioni R, Suh R, Glenn D, Regge D, Helmberger T, Gillams AR, Frilling A, Ambrogi M, Bartolozzi C, Mussi A. Response to

radiofrequency ablation of pulmonary tumours: a prospective, intention-to-treat, multicentre clinical trial (the RAPTURE study). *The Lancet Oncology*. 2008;9(7):621-8.

143. Matsuoka T, Okuma T. CT-guided radiofrequency ablation for lung cancer. *International journal of clinical oncology*. 2007;12(2):71-8.

144. Lu Q, Cao W, Huang L, Wan Y, Liu T, Cheng Q, Han Y, Li X. CT-guided percutaneous microwave ablation of pulmonary malignancies: Results in 69 cases. *World journal of surgical oncology*. 2012;10:80.

145. Carrafiello G, Mangini M, Fontana F, Di Massa A, Ierardi AM, Cotta E, Piacentino F, Nocchi Cardim L, Pellegrino C, Fugazzola C. Complications of microwave and radiofrequency lung ablation: personal experience and review of the literature. *La Radiologia medica*. 2012;117(2):201-13.

146. Okuma T, Matsuoka T, Yamamoto A, Oyama Y, Toyoshima M, Nakamura K, Inoue Y. Frequency and risk factors of various complications after computed tomography-guided radiofrequency ablation of lung tumors. *Cardiovascular and interventional radiology*. 2008;31(1):122-30.

147. Inoue M, Nakatsuka S, Jinzaki M. Cryoablation of early-stage primary lung cancer. *Biomed Res Int*. 2014;2014:521691.

148. Niu L, Chen J, Yao F, Zhou L, Zhang C, Wen W, Bi X, Hu Y, Piao X, Jiang F, Zeng J, Liu W, Li J, He L, Mu F, Zuo J, Xu K. Percutaneous cryoablation for stage IV lung cancer: a retrospective analysis. *Cryobiology*. 2013;67(2):151-5.

149. National Institute for Health and Care Excellence. Irreversible electroporation for treating primary lung cancer and metastases in the lung 2013 [cited 2017 27 February]. Available from: <https://www.nice.org.uk/guidance/IPG441/chapter/2-The-procedure>.

150. Wagstaff PGK, Buijs M, van den Bos W, de Bruin DM, Zondervan PJ, de la Rosette JJ, Laguna Pes MP. Irreversible electroporation: state of the art. *OncoTargets and therapy*. 2016;9:2437-46.

151. Angiodynamics. NanoKnife® System 2017 [cited 2017 27 February]. Available from: <http://www.angiodynamics.com/products/nanoknife>.

152. Okada M, Nishio W, Sakamoto T, Uchino K, Yuki T, Nakagawa A, Tsubota N. Effect of tumor size on prognosis in patients with non-small cell lung cancer: The role of segmentectomy as a type of lesser resection. *The Journal of Thoracic and Cardiovascular Surgery*. 2005;129(1):87-93.

153. Oliveri RS, Wetterslev J, Gluud C. Transarterial (chemo)embolisation for unresectable hepatocellular carcinoma. *The Cochrane database of systematic reviews*. 2011(3):Cd004787.

154. Neill SBC, Owen J, Ryan, Max F, Maher, Michael M. *Interventional Radiology and the Care of the Oncology Patient*. Radiology Research and Practice. 2011;2011.

155. Lee EP, HL. Sarpel, U. Hepatic Arterial Embolization for the Treatment of Metastatic Neuroendocrine Tumors. *International Journal of Hepatology*. 2012;2012.

156. Gaba RC. Chemoembolization practice patterns and technical methods among interventional radiologists: results of an online survey. *AJR American journal of roentgenology*. 2012;198(3):692-9.

157. Lewis AL, Gonzalez MV, Lloyd AW, Hall B, Tang Y, Willis SL, Leppard SW, Wolfenden LC, Palmer RR, Stratford PW. DC Bead: In Vitro Characterization of a Drug-delivery Device for Transarterial Chemoembolization. *Journal of Vascular and Interventional Radiology*. 2006;17(2, Part 1):335-42.

158. Varela M, Real M, Burrel M, Forner A, Sala M, Brunet M, Ayuso C, Castells L, Montañá X, Llovet JM, Bruix J. Chemoembolization of hepatocellular carcinoma with drug eluting beads: Efficacy and doxorubicin pharmacokinetics. *Journal of hepatology*. 2007;46(3):474-81.

159. Lencioni R, de Baere T, Burrel M, Caridi JG, Lammer J, Malagari K, Martin RC, O'Grady E, Real MI, Vogl TJ, Watkinson A, Geschwind JF. Transcatheter treatment of hepatocellular carcinoma with Doxorubicin-loaded DC Bead (DEBDOX): technical recommendations. *Cardiovascular and interventional radiology*. 2012;35(5):980-5.
160. Lewis AL, Dreher MR, O'Byrne V, Grey D, Caine M, Dunn A, Tang Y, Hall B, Fowers KD, Johnson CG, Sharma KV, Wood BJ. DC BeadM1™: towards an optimal transcatheter hepatic tumour therapy. *Journal of materials science Materials in medicine*. 2016;27:13.
161. Poon RTP, Tso WK, Pang RWC, Ng KKC, Woo R, Tai KS, Fan ST. A Phase VII Trial of Chemoembolization for Hepatocellular Carcinoma Using a Novel Intra-Arterial Drug-Eluting Bead. *Clinical Gastroenterology and Hepatology*. 2007;5(9):1100-8.
162. Reyes DK, Vossen JA, Kamel IR, Azad NS, Wahlin TA, Torbenson MS, Choti MA, Geschwind J-FH. Single-Center Phase II Trial of Transarterial Chemoembolization With Drug-Eluting Beads for Patients With Unresectable Hepatocellular Carcinoma: Initial Experience in the United States. *Cancer journal (Sudbury, Mass)*. 2009;15(6):526-32.
163. Franklin JM, GebSKI V, Poston GJ, Sharma RA. Clinical trials of interventional oncology[mdash]moving from efficacy to outcomes. *Nat Rev Clin Oncol*. 2015;12(2):93-104.
164. Vogl TJ, Wetter A, Lindemayr S, Zangos S. Treatment of Unresectable Lung Metastases with Transpulmonary Chemoembolization: Preliminary Experience. *Radiology*. 2005;234(3):917-22.
165. Baylatry M-T, Pelage J-P, Wassef M, Ghegediban H, Joly A-C, Lewis A, Lacombe P, Fernandez C, Laurent A. Pulmonary artery chemoembolization in a sheep model: Evaluation of performance and safety of irinotecan eluting beads (DEB-IRI). *Journal of Biomedical Materials Research Part B: Applied Biomaterials*. 2011;98B(2):351-9.
166. Celikoglu SI, Celikoglu F, Goldberg EP. Endobronchial intratumoral chemotherapy (EITC) followed by surgery in early non-small cell lung cancer with polypoid growth causing erroneous impression of advanced disease. *Lung cancer*. 2006;54(3):339-46.
167. Celikoglu F, Celikoglu SI, York AM, Goldberg EP. Intratumoral administration of cisplatin through a bronchoscope followed by irradiation for treatment of inoperable non-small cell obstructive lung cancer. *Lung cancer*. 2006;51(2):225-36.
168. Ghazaly HE, Mohammed T, Madkour A, Koraa E. The efficacy of bronchoscopic intratumoral chemotherapy in palliation of inoperable lung cancer. *Journal of Clinical Oncology*. 2012;30(15_suppl):e17556-e.
169. Hohenforst-Schmidt W, Zarogoulidis P, Darwiche K, Vogl T, Goldberg EP, Huang H, Simoff M, Li Q, Browning R, Turner FJ, Le Pivert P, Spyrtatos D, Zarogoulidis K, Celikoglu SI, Celikoglu F, Brachmann J. Intratumoral chemotherapy for lung cancer: re-challenge current targeted therapies. *Drug design, development and therapy*. 2013;7:571-83.
170. Celikoglu F, Celikoglu SI, Goldberg EP. Bronchoscopic intratumoral chemotherapy of lung cancer. *Lung cancer*. 2008;61(1):1-12.
171. Niu Q, Wang W, Li Q, Li Y, Ruden DM, He B. Percutaneous Fine-Needle 5% Ethanol-Cisplatin Intratumoral Injection Combined with Second-Line Chemotherapy Improves On the Standard of Care in Patients with Platinum-Pretreated Stage IV Non-Small Cell Lung Cancer. *Translational Oncology*. 2014;7(2):303-8.
172. Li S-y, Li Q, Guan W-j, Huang J, Yang H-p, Wu G-m, Jin F-g, Hu C-p, Chen L-a, Xu G-l, Liu S-z, Wu C-g, Han B-h, Xiang Y, Zhao J-p, Wang J, Zhou X, Li H-p, Zhong N-s. Effects of para-toluenesulfonamide intratumoral injection on non-small

- cell lung carcinoma with severe central airway obstruction: A multi-center, non-randomized, single-arm, open-label trial. *Lung cancer*. 2016;98:43-50.
173. Lee JMM, Lee M-H, Garon E, Goldman JW, Salehi-rad R, Baratelli FE, Schae D, Wang G, Rosen F, Yanagawa J, Walser TC, Lin Y, Park SJ, Adams S, Marincola FM, et al. Phase I trial of intratumoral injection of CCL21 gene modified dendritic cells in lung cancer elicits tumor-specific immune responses and CD8+ T cell infiltration. *Clinical Cancer Research*. 2017.
174. Fujiwara T, Tanaka N, Kanazawa S, Ohtani S, Saijo Y, Nukiwa T, Yoshimura K, Sato T, Eto Y, Chada S, Nakamura H, Kato H. Multicenter Phase I Study of Repeated Intratumoral Delivery of Adenoviral p53 in Patients With Advanced Non-Small-Cell Lung Cancer. *Journal of Clinical Oncology*. 2006;24(11):1689-99.
175. Goldberg EP, Hadba AR, Almond BA, Marotta JS. Intratumoral cancer chemotherapy and immunotherapy: opportunities for nonsystemic preoperative drug delivery. *The Journal of pharmacy and pharmacology*. 2002;54(2):159-80.
176. Kim DY, Kwon DY, Kwon JS, Park JH, Park SH, Oh HJ, Kim JH, Min BH, Park K, Kim MS. Synergistic anti-tumor activity through combinational intratumoral injection of an in-situ injectable drug depot. *Biomaterials*. 2016;85:232-45.
177. Jhan HJ, Liu JJ, Chen YC, Liu DZ, Sheu MT, Ho HO. Novel injectable thermosensitive hydrogels for delivering hyaluronic acid-doxorubicin nanocomplexes to locally treat tumors. *Nanomedicine (London, England)*. 2015;10(8):1263-74.
178. Sheu M-T, Jhan H-J, Su C-Y, Chen L-C, Chang C-E, Liu D-Z, Ho H-O. Codelivery of doxorubicin-containing thermosensitive hydrogels incorporated with docetaxel-loaded mixed micelles enhances local cancer therapy. *Colloids and Surfaces B: Biointerfaces*. 2016;143:260-70.
179. Li T, Zhang M, Wang J, Wang T, Yao Y, Zhang X, Zhang C, Zhang N. Thermosensitive Hydrogel Co-loaded with Gold Nanoparticles and Doxorubicin for Effective Chemoradiotherapy. *The AAPS journal*. 2016;18(1):146-55.
180. Kang YM, Kim GH, Kim JI, Kim DY, Lee BN, Yoon SM, Kim JH, Kim MS. In vivo efficacy of an intratumorally injected in situ-forming doxorubicin/poly(ethylene glycol)-b-polycaprolactone diblock copolymer. *Biomaterials*. 2011;32(20):4556-64.
181. Seo HW, Kim DY, Kwon DY, Kwon JS, Jin LM, Lee B, Kim JH, Min BH, Kim MS. Injectable intratumoral hydrogel as 5-fluorouracil drug depot. *Biomaterials*. 2013;34(11):2748-57.
182. Liang Y, Dong C, Zhang J, Deng L, Dong A. A reconstituted thermosensitive hydrogel system based on paclitaxel-loaded amphiphilic copolymer nanoparticles and antitumor efficacy. *Drug Development and Industrial Pharmacy*. 2017;43(6):972-9.
183. Wu Z, Zou X, Yang L, Lin S, Fan J, Yang B, Sun X, Wan Q, Chen Y, Fu S. Thermosensitive hydrogel used in dual drug delivery system with paclitaxel-loaded micelles for in situ treatment of lung cancer. *Colloids and Surfaces B: Biointerfaces*. 2014;122:90-8.
184. Elstad NL, Fowers KD. OncoGel (ReGel/paclitaxel)--clinical applications for a novel paclitaxel delivery system. *Advanced drug delivery reviews*. 2009;61(10):785-94.
185. DuVall GA, Tarabar D, Seidel RH, Elstad NL, Fowers KD. Phase 2: a dose-escalation study of OncoGel (ReGel/paclitaxel), a controlled-release formulation of paclitaxel, as adjunctive local therapy to external-beam radiation in patients with inoperable esophageal cancer. *Anti-cancer drugs*. 2009;20(2):89-95.
186. Urogen Pharma Ltd. UroGen Pharma urology product candidate pipeline » Upper Tract Urothelial Carcinoma New York, USA2016 [cited 2017 02 March]. Available from: <http://www.urogen.com/pipeline/utuc/>.

187. Franklin JM, Gebiski V, Poston GJ, Sharma RA. Clinical trials of interventional oncology - moving from efficacy to outcomes. *Nat Rev Clin Oncol*. 2015;12(2):93-104.
188. Yeo Y, Kim BK. Drug Carriers: Not an Innocent Delivery Man. *The AAPS journal*. 2015;17(5):1096-104.
189. BASF. Kolliphor® P Grades. Technical information. 2013 [cited 2018 07 June]. Available from: <https://pharmaceutical.basf.com/en/Drug-Formulation/Kolliphor-P407.html>
190. Singh-Joy SD, McLain VC. Safety assessment of poloxamers 101, 105, 108, 122, 123, 124, 181, 182, 183, 184, 185, 188, 212, 215, 217, 231, 234, 235, 237, 238, 282, 284, 288, 331, 333, 334, 335, 338, 401, 402, 403, and 407, poloxamer 105 benzoate, and poloxamer 182 dibenzoate as used in cosmetics. *International journal of toxicology*. 2008;27 Suppl 2:93-128.
191. Bodratti AM, Alexandridis P. Formulation of Poloxamers for Drug Delivery. *Journal of functional biomaterials*. 2018;9(1).
192. Ur-Rehman T, Tavelin S, Grobner G. Chitosan in situ gelation for improved drug loading and retention in poloxamer 407 gels. *International journal of pharmaceutics*. 2011;409(1-2):19-29.
193. Chung T-W, Liu D-Z, Yang J-S. Effects of interpenetration of thermo-sensitive gels by crosslinking of chitosan on nasal delivery of insulin: In vitro characterization and in vivo study. *Carbohydrate Polymers*. 2010;82(2):316-22.
194. Sosnik A, Cohn D. Ethoxysilane-capped PEO–PPO–PEO triblocks: a new family of reverse thermo-responsive polymers. *Biomaterials*. 2004;25(14):2851-8.
195. Desai PR, Jain NJ, Sharma RK, Bahadur P. Effect of additives on the micellization of PEO/PPO/PEO block copolymer F127 in aqueous solution. *Colloids and Surfaces A: Physicochemical and Engineering Aspects*. 2001;178(1–3):57-69.
196. Pandit NK, Wang D. Salt effects on the diffusion and release rate of propranolol from poloxamer 407 gels. *International journal of pharmaceutics*. 1998;167(1–2):183-9.
197. Batrakova EV, Kabanov AV. Pluronic Block Copolymers: Evolution of Drug Delivery Concept from Inert Nanocarriers to Biological Response Modifiers. *Journal of controlled release : official journal of the Controlled Release Society*. 2008;130(2):98-106.
198. Pitto-Barry A, Barry NP. Pluronic® block-copolymers in medicine: from chemical and biological versatility to rationalisation and clinical advances. *Polymer Chemistry*. 2014;5(10):3291-7.
199. Parnaud G, Tache S, Peiffer G, Corpet DE. Pluronic F68 block polymer, a very potent suppressor of carcinogenesis in the colon of rats and mice. *Br J Cancer*. 2001;84(1):90-3.
200. Li C, Palmer WK, Johnston TP. Disposition of poloxamer 407 in rats following a single intraperitoneal injection assessed using a simplified colorimetric assay. *Journal of pharmaceutical and biomedical analysis*. 1996;14(5):659-65.
201. United States Food & Drug Administration. Summary of Safety and Effectiveness. LeGoo®. 2011 [cited 2016 07 March]. Available from: https://www.accessdata.fda.gov/cdrh_docs/pdf11/P110003b.pdf.
202. Loftsson T, Brewster ME. Cyclodextrins as Functional Excipients: Methods to Enhance Complexation Efficiency. *Journal of pharmaceutical sciences*. 2012;101(9):3019-32.
203. Brewster ME, Loftsson T. Cyclodextrins as pharmaceutical solubilizers. *Advanced drug delivery reviews*. 2007;59(7):645-66.
204. Loftsson T, Jarho P, Másson M, Järvinen T. Cyclodextrins in drug delivery. *Expert opinion on drug delivery*. 2005;2(2):335-51.
205. Sharma N, Baldi A. Exploring versatile applications of cyclodextrins: an overview. *Drug delivery*. 2016;23(3):729-47.

206. Bonacucina G, Spina M, Misici-Falzi M, Cespi M, Pucciarelli S, Angeletti M, Palmieri GF. Effect of hydroxypropyl β -cyclodextrin on the self-assembling and thermogelation properties of Poloxamer 407. *European Journal of Pharmaceutical Sciences*. 2007;32(2):115-22.
207. Malanga M, Szeman J, Fenyvesi E, Puskas I, Csabai K, Gyemant G, Fenyvesi F, Szente L. "Back to the Future": A New Look at Hydroxypropyl Beta-Cyclodextrins. *Journal of pharmaceutical sciences*. 2016;105(9):2921-31.
208. Yokoo M, Kubota Y, Motoyama K, Higashi T, Taniyoshi M, Tokumaru H, Nishiyama R, Tabe Y, Mochinaga S, Sato A, Sueoka-Aragane N, Sueoka E, Arima H, Irie T, Kimura S. 2-Hydroxypropyl- β -Cyclodextrin Acts as a Novel Anticancer Agent. *PLOS ONE*. 2015;10(11):e0141946.
209. Gould S, Scott RC. 2-Hydroxypropyl- β -cyclodextrin (HP- β -CD): A toxicology review. *Food and Chemical Toxicology*. 2005;43(10):1451-9.
210. Gidwani B, Vyas A. A Comprehensive Review on Cyclodextrin-Based Carriers for Delivery of Chemotherapeutic Cytotoxic Anticancer Drugs. *BioMed Research International*. 2015;2015:198268.
211. Szymanska E, Winnicka K. Stability of chitosan-a challenge for pharmaceutical and biomedical applications. *Marine drugs*. 2015;13(4):1819-46.
212. Baldrick P. The safety of chitosan as a pharmaceutical excipient. *Regulatory Toxicology and Pharmacology*. 2010;56(3):290-9.
213. Younes I, Rinaudo M. Chitin and Chitosan Preparation from Marine Sources. Structure, Properties and Applications. *Marine drugs*. 2015;13(3):1133.
214. Zhang H, Neau SH. In vitro degradation of chitosan by a commercial enzyme preparation: effect of molecular weight and degree of deacetylation. *Biomaterials*. 2001;22(12):1653-8.
215. Berger J, Reist M, Mayer JM, Felt O, Peppas NA, Gurny R. Structure and interactions in covalently and ionically crosslinked chitosan hydrogels for biomedical applications. *European journal of pharmaceutics and biopharmaceutics : official journal of Arbeitsgemeinschaft fur Pharmazeutische Verfahrenstechnik eV*. 2004;57(1):19-34.
216. Ur-Rehman T, Tavelin S, Gröbner G. Chitosan in situ gelation for improved drug loading and retention in poloxamer 407 gels. *International journal of pharmaceutics*. 2011;409(1-2):19-29.
217. Cheung RCF, Ng TB, Wong JH, Chan WY. Chitosan: An Update on Potential Biomedical and Pharmaceutical Applications. *Marine drugs*. 2015;13(8):5156-86.
218. Dhawan S, Singla AK, Sinha VR. Evaluation of mucoadhesive properties of chitosan microspheres prepared by different methods. *AAPS PharmSciTech*. 2004;5(4):122-8.
219. Sogias IA, Williams AC, Khutoryanskiy VV. Why is Chitosan Mucoadhesive? *Biomacromolecules*. 2008;9(7):1837-42.
220. Wimardhani YS, Suniarti DF, Freisleben HJ, Wanandi SI, Siregar NC, Ikeda M-A. Chitosan exerts anticancer activity through induction of apoptosis and cell cycle arrest in oral cancer cells. *Journal of oral science*. 2014;56(2):119-26.
221. Qi L-F, Xu Z-R, Li Y, Jiang X, Han X-Y. In vitro effects of chitosan nanoparticles on proliferation of human gastric carcinoma cell line MGC803 cells. *World Journal of Gastroenterology : WJG*. 2005;11(33):5136-41.
222. Gibot L, Chabaud S, Bouhout S, Bolduc S, Auger FA, Moulin VJ. Anticancer properties of chitosan on human melanoma are cell line dependent. *International Journal of Biological Macromolecules*. 2015;72:370-9.
223. Qi L, Xu Z. In vivo antitumor activity of chitosan nanoparticles. *Bioorganic & Medicinal Chemistry Letters*. 2006;16(16):4243-5.
224. Wang C, Lau TT, Loh WL, Su K, Wang DA. Cytocompatibility study of a natural biomaterial crosslinker--Genipin with therapeutic model cells. *Journal of biomedical materials research Part B, Applied biomaterials*. 2011;97(1):58-65.

225. Koo H-J, Song YS, Kim H-J, Lee Y-H, Hong S-M, Kim S-J, Kim B-C, Jin C, Lim C-J, Park E-H. Antiinflammatory effects of genipin, an active principle of gardenia. *European Journal of Pharmacology*. 2004;495(2–3):201-8.
226. Butler MF, Ng Y-F, Pudney PDA. Mechanism and kinetics of the crosslinking reaction between biopolymers containing primary amine groups and genipin. *Journal of Polymer Science Part A: Polymer Chemistry*. 2003;41(24):3941-53.
227. Yoo JS, Kim YJ, Kim SH, Choi SH. Study on Genipin: A New Alternative Natural Crosslinking Agent for Fixing Heterograft Tissue. *The Korean Journal of Thoracic and Cardiovascular Surgery*. 2011;44(3):197-207.
228. Tsai C-C, Huang R-N, Sung H-W, Liang HC. In vitro evaluation of the genotoxicity of a naturally occurring crosslinking agent (genipin) for biologic tissue fixation. *Journal of Biomedical Materials Research*. 2000;52(1):58-65.
229. Cheng NC, Estes BT, Young TH, Guilak F. Genipin-crosslinked cartilage-derived matrix as a scaffold for human adipose-derived stem cell chondrogenesis. *Tissue engineering Part A*. 2013;19(3-4):484-96.
230. Mailloux RJ, Adjeitey CN-K, Harper M-E. Genipin-Induced Inhibition of Uncoupling Protein-2 Sensitizes Drug-Resistant Cancer Cells to Cytotoxic Agents. *PLoS ONE*. 2010;5(10):e13289.
231. Deng S, Yang Y, Han Y, Li X, Wang X, Li X, Zhang Z, Wang Y. UCP2 Inhibits ROS-Mediated Apoptosis in A549 under Hypoxic Conditions. *PLoS ONE*. 2012;7(1):e30714.
232. Ayyasamy V, Owens KM, Desouki MM, Liang P, Bakin A, Thangaraj K, Buchsbaum DJ, LoBuglio AF, Singh KK. Cellular Model of Warburg Effect Identifies Tumor Promoting Function of UCP2 in Breast Cancer and Its Suppression by Genipin. *PLoS ONE*. 2011;6(9):e24792.
233. Liu B-S, Huang T-B. Nanocomposites of Genipin-Crosslinked Chitosan/Silver Nanoparticles - Structural Reinforcement and Antimicrobial Properties. *Macromolecular Bioscience*. 2008;8(10):932-41.
234. Lee S-y, Kim HJ, Oh SC, Lee D-H. Genipin inhibits the invasion and migration of colon cancer cells by the suppression of HIF-1 α accumulation and VEGF expression. *Food and Chemical Toxicology*. 2018;116:70-6.
235. Tan H-Y, Wang N, Tsao S-W, Che C-M, Yuen M-F, Feng Y. IRE1 α inhibition by natural compound genipin on tumour associated macrophages reduces growth of hepatocellular carcinoma. *Oncotarget*. 2016;7(28):43792-804.
236. Muzzarelli R, El Mehtedi M, Bottegoni C, Aquili A, Gigante A. Genipin-Crosslinked Chitosan Gels and Scaffolds for Tissue Engineering and Regeneration of Cartilage and Bone. *Marine drugs*. 2015;13(12):7068.
237. Bouquet W, Ceelen W, Fritzing B, Pattyn P, Peeters M, Remon JP, Vervaet C. Paclitaxel/ β -cyclodextrin complexes for hyperthermic peritoneal perfusion – Formulation and stability. *European Journal of Pharmaceutics and Biopharmaceutics*. 2007;66(3):391-7.
238. Choi SG, Lee SE, Kang BS, Ng CL, Davaa E, Park JS. Thermosensitive and mucoadhesive sol-gel composites of paclitaxel/dimethyl-beta-cyclodextrin for buccal delivery. *PLoS One*. 2014;9(9):e109090.
239. Kraitzer A, Ofek L, Schreiber R, Zilberman M. Long-term in vitro study of paclitaxel-eluting bioresorbable core/shell fiber structures. *Journal of controlled release : official journal of the Controlled Release Society*. 2008;126(2):139-48.
240. Danhier F, Lecouturier N, Vroman B, Jérôme C, Marchand-Brynaert J, Feron O, Préat V. Paclitaxel-loaded PEGylated PLGA-based nanoparticles: In vitro and in vivo evaluation. *Journal of Controlled Release*. 2009;133(1):11-7.
241. Lim Soo P, Cho J, Grant J, Ho E, Piquette-Miller M, Allen C. Drug release mechanism of paclitaxel from a chitosan-lipid implant system: effect of swelling, degradation and morphology. *European journal of pharmaceutics and*

- biopharmaceutics : official journal of Arbeitsgemeinschaft fur Pharmazeutische Verfahrenstechnik eV. 2008;69(1):149-57.
242. Kalepu S, Nekkanti V. Insoluble drug delivery strategies: review of recent advances and business prospects. *Acta Pharmaceutica Sinica B*. 2015;5(5):442-53.
243. Buwalda SJ, Vermonden T, Hennink WE. Hydrogels for Therapeutic Delivery: Current Developments and Future Directions. *Biomacromolecules*. 2017;18(2):316-30.
244. Jones DS, Bruschi ML, de Freitas O, Gremião MPD, Lara EHG, Andrews GP. Rheological, mechanical and mucoadhesive properties of thermoresponsive, bioadhesive binary mixtures composed of poloxamer 407 and carbopol 974P designed as platforms for implantable drug delivery systems for use in the oral cavity. *International journal of pharmaceutics*. 2009;372(1-2):49-58.
245. Touyama R, Takeda Y, Inoue K, Kawamura I, Yatsuzuka M, Ikumoto T, Shingu T, Yokoi T, Inouye H. Studies on the Blue Pigments Produced from Genipin and Methylamine. I. Structures of the Brownish-Red Pigments, Intermediates Leading to the Blue Pigments. *CHEMICAL & PHARMACEUTICAL BULLETIN*. 1994;42(3):668-73.
246. Mi F-L, Sung H-W, Shyu S-S, Su C-C, Peng C-K. Synthesis and characterization of biodegradable TPP/genipin co-crosslinked chitosan gel beads. *Polymer*. 2003;44(21):6521-30.
247. Moura MJ, Faneca H, Lima MP, Gil MH, Figueiredo MM. In Situ Forming Chitosan Hydrogels Prepared via Ionic/Covalent Co-Cross-Linking. *Biomacromolecules*. 2011;12(9):3275-84.
248. Baloglu E, Karavana SY, Senyigit ZA, Guneri T. Rheological and mechanical properties of poloxamer mixtures as a mucoadhesive gel base. *Pharmaceutical development and technology*. 2011;16(6):627-36.
249. Yu Z, Guo F, Guo Y, Zhang Z, Wu F, Luo X. Optimization and evaluation of astragalus polysaccharide injectable thermoresponsive in-situ gels. *PLOS ONE*. 2017;12(3):e0173949.
250. Abdel-Bar HM, Abdel-Reheem AY, Osman R, Awad GA, Mortada N. Defining cisplatin incorporation properties in thermosensitive injectable biodegradable hydrogel for sustained delivery and enhanced cytotoxicity. *International journal of pharmaceutics*. 2014;477(1-2):623-30.
251. Singla AK, Garg A, Aggarwal D. Paclitaxel and its formulations. *International journal of pharmaceutics*. 2002;235(1-2):179-92.
252. Yared JA, Tkaczuk KH. Update on taxane development: new analogs and new formulations. *Drug design, development and therapy*. 2012;6:371-84.
253. Sobhani Z, Dinarvand R, Atyabi F, Ghahremani M, Adeli M. Increased paclitaxel cytotoxicity against cancer cell lines using a novel functionalized carbon nanotube. *International Journal of Nanomedicine*. 2011;6:705-19.
254. Kong Y, Zhang J, Wang T, Qiu X, Wang Y. Preparation and characterization of paclitaxel-loaded poly lactic acid-co-glycolic acid coating tracheal stent. *Chinese medical journal*. 2014;127(12):2236-40.
255. Miro A, Quaglia F, Sorrentino U, La Rotonda MI, D'Emmanuele Di Villa Bianca R, Sorrentino R. Improvement of gliquidone hypoglycaemic effect in rats by cyclodextrin formulations. *European Journal of Pharmaceutical Sciences*. 2004;23(1):57-64.
256. Xu S, Wang W, Li X, Liu J, Dong A, Deng L. Sustained release of PTX-incorporated nanoparticles synergized by burst release of DOXHCl from thermosensitive modified PEG/PCL hydrogel to improve anti-tumor efficiency. *European journal of pharmaceutical sciences : official journal of the European Federation for Pharmaceutical Sciences*. 2014;62:267-73.

257. Sun KH, Sohn YS, Jeong B. Thermogelling Poly(ethylene oxide-b-propylene oxide-b-ethylene oxide) Disulfide Multiblock Copolymer as a Thiol-Sensitive Degradable Polymer. *Biomacromolecules*. 2006;7(10):2871-7.
258. Delmar K, Bianco-Peled H. The dramatic effect of small pH changes on the properties of chitosan hydrogels crosslinked with genipin. *Carbohydrate Polymers*. 2015;127:28-37.
259. Li J, Mooney DJ. Designing hydrogels for controlled drug delivery. *Nature Reviews Materials*. 2016;1:16071.
260. de Graaf AJ, Azevedo Próspero dos Santos II, Pieters EHE, Rijkers DTS, van Nostrum CF, Vermonden T, Kok RJ, Hennink WE, Mastrobattista E. A micelle-shedding thermosensitive hydrogel as sustained release formulation. *Journal of Controlled Release*. 2012;162(3):582-90.
261. Petit A, Sandker M, Müller B, Meyboom R, van Midwoud P, Bruin P, Redout EM, Versluijs-Helder M, van der Lest CHA, Buwalda SJ, de Leede LGJ, Vermonden T, Kok RJ, Weinans H, Hennink WE. Release behavior and intra-articular biocompatibility of celecoxib-loaded acetyl-capped PCLA-PEG-PCLA thermogels. *Biomaterials*. 2014;35(27):7919-28.
262. Hanahan D, Weinberg RA. The hallmarks of cancer. *Cell*. 2000;100(1):57-70.
263. Hanahan D, Weinberg RA. Hallmarks of Cancer: The Next Generation. *Cell*. 2011;144(5):646-74.
264. American Type Culture Collection. Human Lung Cancer Cell Lines 2015 [cited 2015 09 Dec]. Available from: http://www.lgcstandards-atcc.org/Search_Results.aspx?dsNav=Ntk:PrimarySearch%7chuman+lung+cancer%7c3%7c,Ny:True,N:1000552-1000578-4294963778&searchTerms=human+lung+cancer&redir=1.
265. American Type Culture Collection. A549 (ATCC® CCL-185™) 2018 [Available from: https://www.lgcstandards-atcc.org/Products/All/CCL-185?geo_country=ie#culturemethod].
266. Shoemaker RH. The NCI60 human tumour cell line anticancer drug screen. *Nature Reviews Cancer*. 2006;6:813.
267. American Type Culture Collection. BALB/3T3 clone A31 (ATCC® CCL-163™) 2017 [Available from: https://www.lgcstandards-atcc.org/Products/All/CCL-163.aspx?geo_country=ie].
268. International Workshop Organized by the Interagency Coordinating Committee on the Validation of Alternative Methods (ICCVAM). Guidance Document on Using In Vitro Data to Estimate In Vivo Starting Doses for Acute Toxicity Based on Recommendations from an International Workshop Organized by ICCVAM and NICEATM 2001 [Available from: https://ntp.niehs.nih.gov/iccvam/docs/acutetox_docs/guidance0801/iv_guide.pdf].
269. International Organization for Standardization. Biological evaluation of medical devices. Part 5: Tests for in vitro cytotoxicity (ISO 10993-5:2009). Geneva, Switzerland 2009.
270. Wu Z, Guan R, Tao M, Lyu F, Cao G, Liu M, Gao J. Assessment of the toxicity and inflammatory effects of different-sized zinc oxide nanoparticles in 2D and 3D cell cultures. *RSC Advances*. 2017;7(21):12437-45.
271. Ekert JE, Johnson K, Strake B, Pardinias J, Jarantow S, Perkinson R, Colter DC. Three-Dimensional Lung Tumor Microenvironment Modulates Therapeutic Compound Responsiveness In Vitro – Implication for Drug Development. *PLoS ONE*. 2014;9(3):e92248.
272. Antoni D, Burckel H, Josset E, Noel G. Three-Dimensional Cell Culture: A Breakthrough in Vivo. *International Journal of Molecular Sciences*. 2015;16(3):5517-27.

273. Alemany-Ribes M, Semino CE. Bioengineering 3D environments for cancer models. *Advanced drug delivery reviews*. 2014;79–80:40-9.
274. Kim JB. Three-dimensional tissue culture models in cancer biology. *Seminars in Cancer Biology*. 2005;15(5):365-77.
275. Pampaloni F, Reynaud EG, Stelzer EHK. The third dimension bridges the gap between cell culture and live tissue. *Nature Reviews Molecular Cell Biology*. 2007;8:839.
276. Fitzgerald KA, Malhotra M, Curtin CM, FJ OB, CM OD. Life in 3D is never flat: 3D models to optimise drug delivery. *Journal of controlled release : official journal of the Controlled Release Society*. 2015;215:39-54.
277. Breslin S, O'Driscoll L. Three-dimensional cell culture: the missing link in drug discovery. *Drug Discovery Today*. 2013;18(5–6):240-9.
278. Zanoni M, Piccinini F, Arienti C, Zamagni A, Santi S, Polico R, Bevilacqua A, Tesei A. 3D tumor spheroid models for in vitro therapeutic screening: a systematic approach to enhance the biological relevance of data obtained. *Scientific Reports*. 2016;6:19103.
279. Lv D, Hu Z, Lu L, Lu H, Xu X. Three-dimensional cell culture: A powerful tool in tumor research and drug discovery. *Oncology Letters*. 2017;14(6):6999-7010.
280. Li X, Valadez AV, Zuo P, Nie Z. Microfluidic 3D cell culture: potential application for tissue-based bioassays. *Bioanalysis*. 2012;4(12):1509-25.
281. Godugu C, Patel AR, Desai U, Andey T, Sams A, Singh M. Algimatrix™ Based 3D Cell Culture System as an In-Vitro Tumor Model for Anticancer Studies. *PLoS ONE*. 2013;8(1):e53708.
282. Hao R, Wei Y, Li C, Chen F, Chen D, Zhao X, Luan S, Fan B, Guo W, Wang J, Chen J. A Microfabricated 96-Well 3D Assay Enabling High-Throughput Quantification of Cellular Invasion Capabilities. *Scientific Reports*. 2017;7:43390.
283. Prina-Mello A, Jain N, Liu B, Kilpatrick JI, Tutty MA, Bell AP, Jarvis SP, Volkov Y, Movia D. Culturing substrates influence the morphological, mechanical and biochemical features of lung adenocarcinoma cells cultured in 2D or 3D. *Tissue and Cell*. 2018;50:15-30.
284. Mishra DK, Sakamoto JH, Thrall MJ, Baird BN, Blackmon SH, Ferrari M, Kurie JM, Kim MP. Human Lung Cancer Cells Grown in an Ex Vivo 3D Lung Model Produce Matrix Metalloproteinases Not Produced in 2D Culture. *PLoS ONE*. 2012;7(9):e45308.
285. Ruppen J, Wildhaber FD, Strub C, Hall SR, Schmid RA, Geiser T, Guenat OT. Towards personalized medicine: chemosensitivity assays of patient lung cancer cell spheroids in a perfused microfluidic platform. *Lab on a chip*. 2015;15(14):3076-85.
286. Amann A, Zwierzina M, Koeck S, Gamerith G, Pechriggl E, Huber JM, Lorenz E, Kelm JM, Hilbe W, Zwierzina H, Kern J. Development of a 3D angiogenesis model to study tumour – endothelial cell interactions and the effects of anti-angiogenic drugs. *Scientific Reports*. 2017;7(1):2963.
287. Mas C, Boda B, CaulFuty M, Huang S, Wiszniewski L, Constant S. Antitumour efficacy of the selumetinib and trametinib MEK inhibitors in a combined human airway–tumour–stroma lung cancer model. *Journal of Biotechnology*. 2015;205:111-9.
288. Dojindo Molecular Technologies Inc. Cell Counting Kit-8 2017 [Available from: <http://www.dojindo.com/store/p/456-Cell-Counting-Kit-8.html>].
289. Invitrogen. LIVE/DEAD® Viability/Cytotoxicity Kit for Mammalian Cells Protocol 2004 [Available from: <https://www.thermofisher.com/ie/en/home/references/protocols/cell-and-tissue-analysis/protocols/live-dead-viability-cytotoxicity-kit-for-mammalian-cells.html>].
290. National Cancer Institute; Division of Cancer Treatment & Diagnosis NCIH. Discovery & Development Services; NCI-60 Human Cancer Cell Line Screen

- Maryland, USA2015 [Available from: https://dtp.cancer.gov/discovery_development/nci-60/methodology.htm.]
291. BioLegend. APC Annexin V Apoptosis Detection Kit with PI San Diego, CA2017 [Available from: <https://www.biolegend.com/en-us/products/apc-annexin-v-apoptosis-detection-kit-with-pi-9788>.]
292. Matsiko A, Levingstone TJ, O'Brien FJ, Gleeson JP. Addition of hyaluronic acid improves cellular infiltration and promotes early-stage chondrogenesis in a collagen-based scaffold for cartilage tissue engineering. *Journal of the Mechanical Behavior of Biomedical Materials*. 2012;11:41-52.
293. Invitrogen. Quant-iT™ PicoGreen® dsDNA Reagent and Kits Protocol 2008 [Available from: <https://tools.thermofisher.com/content/sfs/manuals/mp07581.pdf>.]
294. Matsiko A, Levingstone TJ, Gleeson JP, O'Brien FJ. Incorporation of TGF-beta 3 within collagen-hyaluronic acid scaffolds improves their chondrogenic potential. *Adv Healthc Mater*. 2015;4(8):1175-9.
295. Li W, Zhou J, Xu Y. Study of the in vitro cytotoxicity testing of medical devices. *Biomedical Reports*. 2015;3(5):617-20.
296. Elias PZ, Liu GW, Wei H, Jensen MC, Horner PJ, Pun SH. A functionalized, injectable hydrogel for localized drug delivery with tunable thermosensitivity: synthesis and characterization of physical and toxicological properties. *Journal of controlled release : official journal of the Controlled Release Society*. 2015;208:76-84.
297. Ma H, He C, Cheng Y, Yang Z, Zang J, Liu J, Chen X. Localized Co-delivery of Doxorubicin, Cisplatin, and Methotrexate by Thermosensitive Hydrogels for Enhanced Osteosarcoma Treatment. *ACS applied materials & interfaces*. 2015;7(49):27040-8.
298. Fan R, Tong A, Li X, Gao X, Mei L, Zhou L, Zhang X, You C, Guo G. Enhanced antitumor effects by docetaxel/LL37-loaded thermosensitive hydrogel nanoparticles in peritoneal carcinomatosis of colorectal cancer. *International Journal of Nanomedicine*. 2015;10:7291-305.
299. United States Food & Drug Administration. Inactive Ingredient Search for Approved Drug Products: Poloxamer 407 Maryland, USA2017 [Available from: <http://www.accessdata.fda.gov/scripts/cder/iig/getiigWEB.cfm>.]
300. Guo C, Zhang Y, Yang Z, Li M, Li F, Cui F, Liu T, Shi W, Wu X. Nanomicelle formulation for topical delivery of cyclosporine A into the cornea: in vitro mechanism and in vivo permeation evaluation. *Scientific Reports*. 2015;5:12968.
301. Hwang Y-S, Chiang P-R, Hong W-H, Chiao C-C, Chu IM, Hsiue G-H, Shen C-R. Study In Vivo Intraocular Biocompatibility of In Situ Gelation Hydrogels: Poly(2-Ethyl Oxazoline)-Block-Poly(ε-Caprolactone)-Block-Poly(2-Ethyl Oxazoline) Copolymer, Matrigel and Pluronic F127. *PLOS ONE*. 2013;8(7):e67495.
302. Thanou M, Verhoef JC, Junginger HE. Oral drug absorption enhancement by chitosan and its derivatives. *Advanced drug delivery reviews*. 2001;52(2):117-26.
303. Younes I, Frachet V, Rinaudo M, Jellouli K, Nasri M. Cytotoxicity of chitosans with different acetylation degrees and molecular weights on bladder carcinoma cells. *Int J Biol Macromol*. 2016;84:200-7.
304. Huang M, Khor E, Lim L-Y. Uptake and Cytotoxicity of Chitosan Molecules and Nanoparticles: Effects of Molecular Weight and Degree of Deacetylation. *Pharmaceutical Research*. 2004;21(2):344-53.
305. Ghajar CM, Bissell MJ. Tumor Engineering: The Other Face of Tissue Engineering. *Tissue engineering Part A*. 2010;16(7):2153-6.
306. Pampaloni F, Stelzer E. Three-dimensional cell cultures in toxicology. *Biotechnology & genetic engineering reviews*. 2010;26:117-38.
307. Curtin C, Nolan JC, Conlon R, Deneweth L, Gallagher C, Tan YJ, Cavanagh BL, Asraf AZ, Harvey H, Miller-Delaney S, Shohet J, Bray I, O'Brien FJ, Stallings

- RL, Piskareva O. A physiologically relevant 3D collagen-based scaffold-neuroblastoma cell system exhibits chemosensitivity similar to orthotopic xenograft models. *Acta biomaterialia*. 2018;70:84-97.
308. Stock K, Estrada MF, Vidic S, Gjerde K, Rudisch A, Santo VE, Barbier M, Blom S, Arundkar SC, Selvam I, Osswald A, Stein Y, Gruenewald S, Brito C, van Weerden W, et al. Capturing tumor complexity in vitro: Comparative analysis of 2D and 3D tumor models for drug discovery. *Scientific Reports*. 2016;6:28951.
309. Fitzgerald KA, Guo J, Tierney EG, Curtin CM, Malhotra M, Darcy R, O'Brien FJ, O'Driscoll CM. The use of collagen-based scaffolds to simulate prostate cancer bone metastases with potential for evaluating delivery of nanoparticulate gene therapeutics. *Biomaterials*. 2015;66:53-66.
310. Siddiqui M, Rajkumar SV. The High Cost of Cancer Drugs and What We Can Do About It. *Mayo Clinic Proceedings*. 2012;87(10):935-43.
311. Paul SM, Mytelka DS, Dunwiddie CT, Persinger CC, Munos BH, Lindborg SR, Schacht AL. How to improve R&D productivity: the pharmaceutical industry's grand challenge. *Nature Reviews Drug Discovery*. 2010;9:203.
312. Basavaraj S, Betageri GV. Can formulation and drug delivery reduce attrition during drug discovery and development—review of feasibility, benefits and challenges. *Acta Pharmaceutica Sinica B*. 2014;4(1):3-17.
313. Singh H, Racadio J, Brown M, Hedman T. P68 - Six-Month Safety and Efficacy of Genipin Crosslinking Treatment for Chronic Low Back Pain. *The Spine Journal*. 2017;17(10, Supplement):S206.
314. Kagadis GC, Katsanos K, Karnabatidis D, Loudos G, Nikiforidis GC, Hendeel WR. Emerging technologies for image guidance and device navigation in interventional radiology. *Medical physics*. 2012;39(9):5768-81.
315. Wile GE, Leyendecker JR, Krehbiel KA, Dyer RB, Zagoria RJ. CT and MR Imaging after Imaging-guided Thermal Ablation of Renal Neoplasms. *RadioGraphics*. 2007;27(2):325-39.
316. GE Healthcare AS. Summary of Product Characteristics. Visipaque 320 mg/ml Solution for Injection. 2010 [Available from: http://www.hpra.ie/img/uploaded/swedocuments/LicenseSPC_PA0735-009-013_02092016125242.pdf].
317. Lei K, Shen W, Cao L, Yu L, Ding J. An injectable thermogel with high radiopacity. *Chemical communications (Cambridge, England)*. 2015;51(28):6080-3.
318. Coutu JM, Fatimi A, Berrahmoune S, Soulez G, Lerouge S. A new radiopaque embolizing agent for the treatment of endoleaks after endovascular repair: influence of contrast agent on chitosan thermogel properties. *Journal of biomedical materials research Part B, Applied biomaterials*. 2013;101(1):153-61.
319. Fatimi A, Chabrot P, Berrahmoune S, Coutu JM, Soulez G, Lerouge S. A new injectable radiopaque chitosan-based sclerosing embolizing hydrogel for endovascular therapies. *Acta biomaterialia*. 2012;8(7):2712-21.
320. Huang L, Shen M, Li R, Zhang X, Sun Y, Gao P, Fu H, Liu H, He Y, Du Y, Cao J, Duan Y. Thermo-sensitive composite hydrogels based on poloxamer 407 and alginate and their therapeutic effect in embolization in rabbit VX2 liver tumors. *Oncotarget*. 2016;7(45):73280-91.
321. BTG announces CE Mark Certification for DC Bead LUMI™, the First commercially available Radiopaque Drug-Eluting Bead [press release]. UK2017.
322. Heerink WJ, de Bock GH, de Jonge GJ, Groen HJM, Vliegenthart R, Oudkerk M. Complication rates of CT-guided transthoracic lung biopsy: meta-analysis. *European Radiology*. 2017;27(1):138-48.
323. Winokur RS, Pua BB, Sullivan BW, Madoff DC. Percutaneous Lung Biopsy: Technique, Efficacy, and Complications. *Seminars in Interventional Radiology*. 2013;30(2):121-7.

324. Beslic S, Zukic F, Milisic S. Percutaneous transthoracic CT guided biopsies of lung lesions; fine needle aspiration biopsy versus core biopsy. *Radiology and Oncology*. 2012;46(1):19-22.
325. Harzheim D, Sterman D, Shah PL, Eberhardt R, Herth FJF. Bronchoscopic Transparenchymal Nodule Access: Feasibility and Safety in an Endoscopic Unit. *Respiration*. 2016;91(4):302-6.
326. Zaric B, Stojisic V, Sarcev T, Stojanovic G, Carapic V, Perin B, Zarogoulidis P, Darwiche K, Tsakiridis K, Karapantzos I, Kesisis G, Kougioumtzi I, Katsikogiannis N, Machairiotis N, Stylianaki A, Foroulis CN, Zarogoulidis K. Advanced bronchoscopic techniques in diagnosis and staging of lung cancer. *Journal of Thoracic Disease*. 2013;5(Suppl 4):S359-S70.
327. Cilurzo F, Selmin F, Minghetti P, Adami M, Bertoni E, Lauria S, Montanari L. Injectability Evaluation: An Open Issue. *AAPS PharmSciTech*. 2011;12(2):604-9.
328. Lee CH, Moturi V, Lee Y. Thixotropic property in pharmaceutical formulations. *Journal of Controlled Release*. 2009;136(2):88-98.
329. Rathore N, Pranay P, Eu B, Ji W, Walls E. Variability in syringe components and its impact on functionality of delivery systems. *PDA journal of pharmaceutical science and technology / PDA*. 2011;65(5):468-80.
330. Rungseevijitprapa W, Bodmeier R. Injectability of biodegradable in situ forming microparticle systems (ISM). *European Journal of Pharmaceutical Sciences*. 2009;36(4-5):524-31.
331. Galante R, Pinto T, Colaço R, Serro A. Sterilization of hydrogels for biomedical applications: A review: STERILIZATION OF HYDROGELS 2017.
332. British Pharmacopoeia Commission. *British Pharmacopoeia: Appendix XVIII Methods of Sterilisation*. London, England 2017.
333. International Organization for Standardization. *ISO 17665-1:2006(en): Sterilization of health care products — Moist heat — Part 1: Requirements for the development, validation and routine control of a sterilization process for medical devices*. Geneva, Switzerland 2006.
334. International Organization for Standardization. *ISO 20857:2010(en): Sterilization of health care products — Dry heat — Requirements for the development, validation and routine control of a sterilization process for medical devices*. Geneva, Switzerland 2010.
335. European Medicines Agency. *Decision trees for selection of sterilisation methods (Annex to note for guidance on development pharmaceuticals)*. London, England 2000.
336. Terrier F, Grossholz M, D. Becker C. *Spiral CT of the Abdomen* 2000.
337. Seo HJ, Kim J-C. Effects of additives on phase transitions of Poloxamer 407/Poloxamer 188 mixture and release property of monoolein cubic phase containing the poloxamers. *Journal of Industrial and Engineering Chemistry*. 2012;18(1):88-91.
338. Fatimi A, Zehtabi F, Lerouge S. Optimization and characterization of injectable chitosan-iodixanol-based hydrogels for the embolization of blood vessels. *Journal of Biomedical Materials Research Part B: Applied Biomaterials*. 2016;104(8):1551-62.
339. Ihnatsenka B, Boezaart AP. Ultrasound: Basic understanding and learning the language. *International Journal of Shoulder Surgery*. 2010;4(3):55-62.
340. Zhang J, Lin G, Wu L, Cheng Y. Speckle filtering of medical ultrasonic images using wavelet and guided filter. *Ultrasonics*. 2016;65:177-93.
341. Fudge N, Sadler E, Fisher HR, Maher J, Wolfe CDA, McKevitt C. Optimising Translational Research Opportunities: A Systematic Review and Narrative Synthesis of Basic and Clinician Scientists' Perspectives of Factors Which Enable or Hinder Translational Research. *PLOS ONE*. 2016;11(8):e0160475.

342. RheoSense. Accurate Estimate of Injectability (Syringeability) from High Shear Viscosity Measurement. San Ramon, CA; 2016.
343. Aguado BA, Mulyasasmita W, Su J, Lampe KJ, Heilshorn SC. Improving Viability of Stem Cells During Syringe Needle Flow Through the Design of Hydrogel Cell Carriers. *Tissue engineering Part A*. 2012;18(7-8):806-15.
344. Medford ARL, Bennett JA, Free CM, Agrawal S. Endobronchial ultrasound-guided transbronchial needle aspiration (EBUS-TBNA): Applications in chest disease. *Respirology*. 2010;15(1):71-9.
345. Vo A, Doumit M, Rockwell G. The Biomechanics and Optimization of the Needle-Syringe System for Injecting Triamcinolone Acetonide into Keloids. *Journal of Medical Engineering*. 2016;2016:5162394.
346. Schuetz YB, Gurny R, Jordan O. A novel thermoresponsive hydrogel based on chitosan. *European Journal of Pharmaceutics and Biopharmaceutics*. 2008;68(1):19-25.
347. Kikuchi IS, Cardoso Galante RS, Dua K, Malipeddi VR, Awasthi R, Ghisleni DDM, de Jesus Andreoli Pinto T. Hydrogel Based Drug Delivery Systems: A Review with Special Emphasis on Challenges Associated with Decontamination of Hydrogels and Biomaterials. *Current drug delivery*. 2017;14(7):917-25.
348. Al Kayal T, Panetta D, Canciani B, Losi P, Tripodi M, Burchielli S, Ottoni P, Salvadori PA, Soldani G. Evaluation of the effect of a gamma irradiated DBM-pluronic F127 composite on bone regeneration in Wistar rat. *PLoS One*. 2015;10(4):e0125110.
349. Leyva-Gómez G, Santillan-Reyes E, Lima E, Madrid-Martínez A, Kröttsch E, Quintanar-Guerrero D, Garcíadiego-Cázares D, Martínez-Jiménez A, Hernández Morales M, Ortega-Peña S, Contreras-Figueroa ME, Cortina-Ramírez GE, Abarca-Buis RF. A novel hydrogel of poloxamer 407 and chitosan obtained by gamma irradiation exhibits physicochemical properties for wound management. *Materials Science and Engineering: C*. 2017;74:36-46.
350. Yang Y-M, Zhao Y-H, Liu X-H, Ding F, Gu X-S. The effect of different sterilization procedures on chitosan dried powder. *Journal of Applied Polymer Science*. 2007;104(3):1968-72.
351. San Juan A, Montembault A, Gillet D, Say J, Rouif S, Bouet T, Royaud I, David L, editors. Degradation of chitosan-based materials after different sterilization treatments. *IOP Conference Series: Materials Science and Engineering*; 2012: IOP Publishing.
352. Marreco PR, da Luz Moreira P, Genari SC, Moraes AM. Effects of different sterilization methods on the morphology, mechanical properties, and cytotoxicity of chitosan membranes used as wound dressings. *Journal of biomedical materials research Part B, Applied biomaterials*. 2004;71(2):268-77.
353. Monaco G, Cholas R, Salvatore L, Madaghiele M, Sannino A. Sterilization of collagen scaffolds designed for peripheral nerve regeneration: Effect on microstructure, degradation and cellular colonization. *Materials science & engineering C, Materials for biological applications*. 2017;71:335-44.
354. Siritientong T, Srichana T, Aramwit P. The Effect of Sterilization Methods on the Physical Properties of Silk Sericin Scaffolds. *AAPS PharmSciTech*. 2011;12(2):771-81.
355. European Medicines Agency. A guideline on Summary of Product Characteristics (SmPC) 2009 [cited 2018 26th June]. Available from: https://ec.europa.eu/health/sites/health/files/files/eudralex/vol-2/c/smpc_guideline_rev2_en.pdf.
356. Day C-P, Merlino G, Van Dyke T. Preclinical Mouse Cancer Models: A Maze of Opportunities and Challenges. *Cell*. 2015;163(1):39-53.

357. Kelland LR. "Of mice and men": values and liabilities of the athymic nude mouse model in anticancer drug development. *European Journal of Cancer*. 2004;40(6):827-36.
358. Ruggeri BA, Camp F, Miknyoczki S. Animal models of disease: Pre-clinical animal models of cancer and their applications and utility in drug discovery. *Biochemical Pharmacology*. 2014;87(1):150-61.
359. Jung J. Human Tumor Xenograft Models for Preclinical Assessment of Anticancer Drug Development. *Toxicological Research*. 2014;30(1):1-5.
360. Kellar A, Egan C, Morris D. Preclinical Murine Models for Lung Cancer: Clinical Trial Applications. *BioMed Research International*. 2015;2015:17.
361. Basel MT, Narayanan S, Ganta C, Shreshta TB, Marquez A, Pyle M, Hill J, Bossmann SH, Troyer DL. Developing a xenograft human tumor model in immunocompetent mice. *Cancer Letters*. 2018;412:256-63.
362. Kersten K, de Visser KE, van Miltenburg MH, Jonkers J. Genetically engineered mouse models in oncology research and cancer medicine. *EMBO Molecular Medicine*. 2017;9(2):137-53.
363. Morgan KM, Riedlinger GM, Rosenfeld J, Ganesan S, Pine SR. Patient-Derived Xenograft Models of Non-Small Cell Lung Cancer and Their Potential Utility in Personalized Medicine. *Frontiers in oncology*. 2017;7:2.
364. Smith PW, Liu Y, Siefert SA, Moskaluk CA, Petroni GR, Jones DR. Breast cancer metastasis suppressor 1 (BRMS1) suppresses metastasis and correlates with improved patient survival in non-small cell lung cancer. *Cancer Letters*. 2009;276(2):196-203.
365. Rousalova I, Banerjee S, Sangwan V, Evenson K, McCauley J, Kratzke R, Vickers S, Saluja A, D'Cunha J. Minnelide: A Novel Therapeutic That Promotes Apoptosis in Non-Small Cell Lung Carcinoma In Vivo 2013. e77411 p.
366. Steiner P, Joynes C, Bassi R, Wang S, Tonra JR, Hadari YR, Hicklin DJ. Tumor Growth Inhibition with Cetuximab and Chemotherapy in Non-Small Cell Lung Cancer Xenografts Expressing Wild-type and Mutated Epidermal Growth Factor Receptor. *Clinical Cancer Research*. 2007;13(5):1540-51.
367. Pulford E, Hocking A, Griggs K, McEvoy J, Bonder C, Henderson DW, Klebe S. Vasculogenic mimicry in malignant mesothelioma: an experimental and immunohistochemical analysis. *Pathology*. 2016;48(7):650-9.
368. Luo H, England CG, Graves SA, Sun H, Liu G, Nickles RJ, Cai W. PET Imaging of VEGFR-2 Expression in Lung Cancer with (64)Cu-Labeled Ramucirumab. *Journal of nuclear medicine : official publication, Society of Nuclear Medicine*. 2016;57(2):285-90.
369. Schachtschneider KM, Schwind RM, Newson J, Kinachtchouk N, Rizko M, Mendoza-Elias N, Grippo P, Principe DR, Park A, Overgaard NH, Jungersen G, Garcia KD, Maker AV, Rund LA, Ozer H, Gaba RC, Schook LB. The OncoPig Cancer Model: An Innovative Large Animal Translational Oncology Platform. *Frontiers in oncology*. 2017;7(190).
370. O'Farrell AC, Shnyder SD, Marston G, Coletta PL, Gill JH. Non-invasive molecular imaging for preclinical cancer therapeutic development. *British Journal of Pharmacology*. 2013;169(4):719-35.
371. Cheong W-F, Prah SA, Welch AJ. A review of the optical properties of biological tissues. *IEEE journal of quantum electronics*. 1990;26(12):2166-85.
372. Jacques SL. Optical properties of biological tissues: a review. *Physics in Medicine & Biology*. 2013;58(11):R37.
373. Badr CE, Tannous BA. Bioluminescence imaging: progress and applications. *Trends in Biotechnology*. 2011;29(12):624-33.
374. Contag CH. In vivo pathology: seeing with molecular specificity and cellular resolution in the living body. *Annual review of pathology*. 2007;2:277-305.

375. Prescher JA, Contag CH. Guided by the light: visualizing biomolecular processes in living animals with bioluminescence. *Current Opinion in Chemical Biology*. 2010;14(1):80-9.
376. Yan W, Xiao D, Yao K. Combined bioluminescence and fluorescence imaging visualizing orthotopic lung adenocarcinoma xenograft in vivo. *Acta Biochimica et Biophysica Sinica*. 2011;43(8):595-600.
377. Vasquez KO, Casavant C, Peterson JD. Quantitative Whole Body Biodistribution of Fluorescent-Labeled Agents by Non-Invasive Tomographic Imaging. *PLoS ONE*. 2011;6(6):e20594.
378. Fridman R, Benton G, Aranoutova I, Kleinman HK, Bonfil RD. Increased initiation and growth of tumor cell lines, cancer stem cells and biopsy material in mice using basement membrane matrix protein (Cultrex or Matrigel) co-injection. *Nat Protoc*. 2012;7(6):1138-44.
379. Tomayko MM, Reynolds CP. Determination of subcutaneous tumor size in athymic (nude) mice. *Cancer chemotherapy and pharmacology*. 1989;24(3):148-54.
380. Perkin Elmer. Determining the Luciferin Kinetic Curve for Your Model 2016 [cited 2018 23 June]. Available from: http://www.perkinelmer.com/lab-solutions/resources/docs/SOP_Determine_Luciferin_Kinetic_Curve.pdf.
381. Farago AF, Snyder EL, Jacks T. SnapShot: Lung Cancer Models. *Cell*. 2012;149(1):246- e1.
382. de Seranno S, Meuwissen R. Progress and applications of mouse models for human lung cancer. *European Respiratory Journal*. 2010;35(2):426-43.
383. Turner PA, Thiele JS, Stegemann JP. Growth factor sequestration and enzyme-mediated release from genipin-crosslinked gelatin microspheres. *Journal of biomaterials science Polymer edition*. 2017;28(16):1826-46.
384. Matcham S, Novakovic K. Fluorescence imaging in genipin crosslinked chitosan-poly (vinyl pyrrolidone) hydrogels. *Polymers*. 2016;8(11):385.
385. Morton SW, Lee MJ, Deng ZJ, Dreaden EC, Siouve E, Shopsowitz KE, Shah NJ, Yaffe MB, Hammond PT. A Nanoparticle-Based Combination Chemotherapy Delivery System for Enhanced Tumor Killing by Dynamic Rewiring of Signaling Pathways. *Science Signaling*. 2014;7(325):ra44-ra.
386. Wang W, Liu J, Li C, Zhang J, Liu J, Dong A, Kong D. Real-time and non-invasive fluorescence tracking of in vivo degradation of the thermosensitive PEGlyated polyester hydrogel. *Journal of Materials Chemistry B*. 2014;2(26):4185-92.
387. Wang H, Mao D, Wang Y, Wang K, Yi X, Kong D, Yang Z, Liu Q, Ding D. Biocompatible fluorescent supramolecular nanofibrous hydrogel for long-term cell tracking and tumor imaging applications. *Scientific Reports*. 2015;5:16680.
388. Loebel C, Rodell CB, Chen MH, Burdick JA. Shear-thinning and self-healing hydrogels as injectable therapeutics and for 3D-printing. *Nature Protocols*. 2017;12:1521.
389. Dong X, Chen H, Qin J, Wei C, Liang J, Liu T, Kong D, Lv F. Thermosensitive porphyrin-incorporated hydrogel with four-arm PEG-PCL copolymer (II): doxorubicin loaded hydrogel as a dual fluorescent drug delivery system for simultaneous imaging tracking in vivo. *Drug delivery*. 2017;24(1):641-50.
390. Su Y, Huang N, Chen D, Zhang L, Dong X, Sun Y, Zhu X, Zhang F, Gao J, Wang Y, Fan K, Lo P, Li W, Ling C. Successful in vivo hyperthermal therapy toward breast cancer by Chinese medicine shikonin-loaded thermosensitive micelle. *Int J Nanomedicine*. 2017;12:4019-35.
391. Yu Q, Liu Y, Cao C, Le F, Qin X, Sun D, Liu J. The use of pH-sensitive functional selenium nanoparticles shows enhanced in vivo VEGF-siRNA silencing and fluorescence imaging. *Nanoscale*. 2014;6(15):9279-92.

392. Na K, Kim S, Woo DG, Sun BK, Yang HN, Chung HM, Park KH. Combination material delivery of dexamethasone and growth factor in hydrogel blended with hyaluronic acid constructs for neocartilage formation. *Journal of biomedical materials research Part A*. 2007;83(3):779-86.
393. Wang H, Wu Y, Ruifang Z, Nie G. Engineering the Assemblies of Biomaterial Nanocarriers for Delivery of Multiple Theranostic Agents with Enhanced Antitumor Efficacy 2013.
394. Kim SH, Kim SR, Yoon HY, Chang IH, Whang YM, Cho MJ, Kim MJ, Kim SY, Lee SJ, Choi YW. Poloxamer 407 Hydrogels for Intravesical Instillation to Mouse Bladder: Gel-Forming Capacity and Retention Performance. *Korean J Urol Oncol*. 2017;15(3):178-86.
395. Shuangxia R, Cuiyun L, Yu D, Ning L, Xin W, Fengjie T, Sufeng Z, Zhixia Q, Yang L, Di Z, Xijing C, Dingding C. Comparison of pharmacokinetics, tissue distribution and pharmacodynamics of liposomal and free doxorubicin in tumour bearing mice following intratumoral injection. *Journal of Pharmacy and Pharmacology*. 2014;66(9):1231-9.
396. Liu Y, Yang F, Feng L, Yang L, Chen L, Wei G, Lu W. In vivo retention of poloxamer-based in situ hydrogels for vaginal application in mouse and rat models. *Acta Pharmaceutica Sinica B*. 2017;7(4):502-9.
397. Hyun H, Kim YH, Song IB, Lee JW, Kim MS, Khang G, Park K, Lee HB. In Vitro and in Vivo Release of Albumin Using a Biodegradable MPEG-PCL Diblock Copolymer as an in Situ Gel-Forming Carrier. *Biomacromolecules*. 2007;8(4):1093-100.
398. McGowan JWD, Bidwell GL. The Use of Ex Vivo Whole-Organ Imaging and Quantitative Tissue Histology to Determine the Bio-distribution of Fluorescently-Labeled Molecules. *Journal of visualized experiments : JoVE*. 2016(118):10.3791/54987.
399. Zhang Y, Yang C, Wang W, Liu J, Liu Q, Huang F, Chu L, Gao H, Li C, Kong D, Liu Q, Liu J. Co-delivery of doxorubicin and curcumin by pH-sensitive prodrug nanoparticle for combination therapy of cancer. *Scientific Reports*. 2016;6:21225.
400. Lu L, Ding Y, Zhang Y, Ho RJY, Zhao Y, Zhang T, Guo C. Antibody-modified liposomes for tumor-targeting delivery of timosaponin AIII. *International Journal of Nanomedicine*. 2018;13:1927-44.
401. Jiang Y, Meng X, Wu Z, Qi X. Modified chitosan thermosensitive hydrogel enables sustained and efficient anti-tumor therapy via intratumoral injection. *Carbohydrate Polymers*. 2016;144:245-53.
402. Morhard R, Nief C, Barrero Castedo C, Hu F, Madonna M, Mueller JL, Dewhirst MW, Katz DF, Ramanujam N. Development of enhanced ethanol ablation as an alternative to surgery in treatment of superficial solid tumors. *Scientific Reports*. 2017;7(1):8750.
403. Oun R, Plumb JA, Wheate NJ. A cisplatin slow-release hydrogel drug delivery system based on a formulation of the macrocycle cucurbit[7]uril, gelatin and polyvinyl alcohol. *J Inorg Biochem*. 2014;134:100-5.
404. Workman P, Aboagye EO, Balkwill F, Balmain A, Bruder G, Chaplin DJ, Double JA, Everitt J, Farningham DAH, Glennie MJ, Kelland LR, Robinson V, Stratford IJ, Tozer GM, Watson S, Wedge SR, Eccles SA, An ad hoc committee of the National Cancer Research I. Guidelines for the welfare and use of animals in cancer research. *British Journal Of Cancer*. 2010;102:1555.
405. Kokolus KM, Capitano ML, Lee CT, Eng JW, Waight JD, Hylander BL, Sexton S, Hong CC, Gordon CJ, Abrams SI, Repasky EA. Baseline tumor growth and immune control in laboratory mice are significantly influenced by subthermoneutral housing temperature. *Proceedings of the National Academy of Sciences of the United States of America*. 2013;110(50):20176-81.

406. Yang K, Zhao N, Zhao D, Chen D, Li Y. The drug efficacy and adverse reactions in a mouse model of oral squamous cell carcinoma treated with oxaliplatin at different time points during a day. *Drug design, development and therapy*. 2013;7:511-7.
407. Bhattarai N, Gunn J, Zhang M. Chitosan-based hydrogels for controlled, localized drug delivery. *Advanced drug delivery reviews*. 2010;62(1):83-99.
408. Klouda L, Mikos AG. Thermoresponsive hydrogels in biomedical applications. *European Journal of Pharmaceutics and Biopharmaceutics*. 2008;68(1):34-45.
409. Prakash G, Renold AP, Venkatalakshmi B. RFID based Mobile Cold Chain Management System for Warehousing. *Procedia Engineering*. 2012;38:964-9.
410. Rowell JL, McCarthy DO, Alvarez CE. Dog Models of Naturally Occurring Cancer. *Trends in molecular medicine*. 2011;17(7):380-8.
411. Choi B, Loh XJ, Tan A, Loh CK, Ye E, Joo MK, Jeong B. Introduction to In Situ Forming Hydrogels for Biomedical Applications. In: Loh XJ, editor. *In-Situ Gelling Polymers: For Biomedical Applications*. Singapore: Springer Singapore; 2015. p. 5-35.